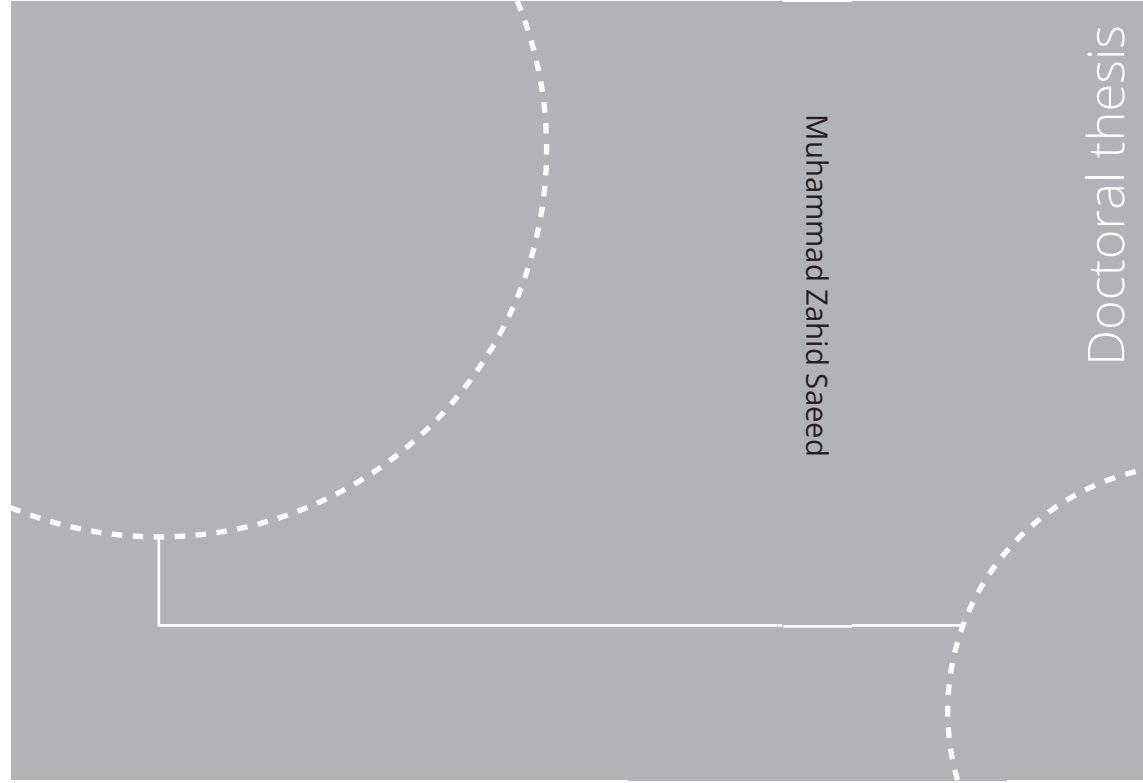


ISBN 978-82-326-8164-8 (printed ver.)
ISBN 978-82-326-8163-1 (electronic ver.)
ISSN 1503-8181 (printed ver.)
ISSN 2703-8084 (electronic ver.)



Doctoral theses at NTNU, 2024:286

Muhammad Zahid Saeed

Development and validation of CO₂ cooling systems with expansion work recovery

Doctoral theses at NTNU, 2024:286

NTNU
Norwegian University of
Science and Technology
Thesis for the degree of
Philosophiae Doctor
Faculty of Engineering
Department of Energy and Process Engineering

 **NTNU**
Norwegian University of
Science and Technology

 NTNU

 **NTNU**
Norwegian University of
Science and Technology

Muhammad Zahid Saeed

Development and validation of CO₂ cooling systems with expansion work recovery

Thesis for the degree of Philosophiae Doctor

Trondheim, July 2024

Norwegian University of Science and Technology
Faculty of Engineering
Department of Energy and Process Engineering



Norwegian University of
Science and Technology

NTNU

Norwegian University of Science and Technology

Thesis for the degree of Philosophiae Doctor

Faculty of Engineering
Department of Energy and Process Engineering

© Muhammad Zahid Saeed

ISBN 978-82-326-8164-8 (printed ver.)
ISBN 978-82-326-8163-1 (electronic ver.)
ISSN 1503-8181 (printed ver.)
ISSN 2703-8084 (electronic ver.)

Doctoral theses at NTNU, 2024:286



Printed by Skipnes Kommunikasjon AS

Preface

This doctoral dissertation is submitted in partial fulfilment of the criteria for obtaining the Philosophiae Doctor (PhD) degree from the Norwegian University of Science and Technology (NTNU). The duration of the PhD period spanned from September 2020 to December 2023, and the research was conducted at the Department of Energy and Process Engineering under the supervision of Professor Armin Hafner. The PhD work was assisted and co-supervised by Krzysztof Banasiak, Ángel Álvarez Pardiñas and Ignat Tolstorebrov. With financial support from the Norwegian Research Council, this PhD was funded jointly by cruiZE (308779) and HighEFF (257632) projects.

Muhammad Zahid Saeed
January 2024
Trondheim, Norway

Acknowledgements

I would like to express my profound gratitude to all individuals who played pivotal roles in providing assistance and guidance, contributing significantly to the successful completion of this doctoral thesis.

The unwavering support of my supervisor, Professor Armin Hafner, has been indispensable throughout this doctoral journey. I am forever grateful for the insightful discussions, motivation, trust, and encouragement. His enthusiasm for fostering innovation and exploring new ideas serves as a continual inspiration.

Special appreciation is extended to Dr. Ángel Álvarez Pardiñas, whose guidance was invaluable in navigating challenges during the experimental tests and the scientific publication process. Additionally, my deepest thanks go to Dr. Krzysztof Banasiak for his invaluable assistance in developing two novel ejectors. I also thank Associate Professor Ignat Tolstorebrov for engaging in coffee and lunch discussions.

I sincerely appreciate the Energy Recovery International California team, particularly Dr. Azam Thatte, for their invaluable contribution. Their provision of the Pressure Exchanger device and the sharing of technical knowledge played a crucial role in facilitating the testing conducted in the NTNU laboratory. I am very grateful to Mr Andres Hegglin and his company, E-jector AG, for developing and fabricating two ejectors.

I would also like to acknowledge Håvard Rekstad, Reidar Tellebon, and Stein Skånøy for their outstanding work in developing and retrofitting the SuperSmart test facility in the laboratory. Thanks to my fellow research group and department colleagues for the nice discussions and welcoming environment.

Finally, my heartfelt thanks go to my family for their kind support and love. I am thankful for everything you have done for me.

Abstract

The 2023 revised strategy of the International Maritime Organization (IMO) emphasises achieving net-zero greenhouse gas emissions within the shipping sector. Notably, nearly 40% of the energy demand in passenger ships is attributed to cooling and heating systems. Currently, these systems predominantly utilize R134a, a synthetic PFAS (per- and polyfluoroalkyl substances) chemical with a high global warming potential. In 2020, the European Union observed an approximate emission of 75,000 tonnes of PFAS into the environment. Subsequently, in 2023, a joint proposal was initiated by several member states of the EU aimed to prohibit the utilization of PFAS. If ratified, this proposition would lead to the ban of PFAS usage by either 2025 or 2026 [1, 2]. To align with existing and forthcoming environmental regulations, there is a critical need to transition towards zero-emission fuels and adopt natural refrigerants.

Within the realm of natural refrigerants, carbon dioxide (CO₂) stands out due to its non-toxic and non-flammable nature, addressing safety concerns onboard passenger ships. CO₂ refrigerants have gained widespread acceptance in sectors such as supermarkets, the hotel industry, process industries, and fishing vessels. Given its suitability and environmental advantages, adopting CO₂-based cooling and heating systems is anticipated to witness an upward trend in passenger ships, aligning with the evolving regulatory landscape and the IMO's overarching goal of achieving net-zero emissions.

Operating a CO₂ transcritical system in high ambient temperatures presents challenges, particularly expansion losses. Over the past decade, ejectors have been widely employed to recover expansion work, but with certain limitations. The pressure exchanger (PX) is a recent advancement gaining prominence, specifically designed for expansion work recovery.

The PX device is distinct in its capability to recover expansion work from the gas cooler to the receiver pressure and employ it to compress the flash gas. With its four ports and internal rotor, the PX seamlessly expands and compresses without requiring physical separation. A pressure lift is essential for the PX to propel the flash gas into its system, which is subsequently compressed to a pressure slightly lower than the gas cooler's. This underscores the PX's need for two low-pressure lift devices to effectively compress the flash gas from the receiver to the gas cooler pressure. The current practice involves employing two small booster compressors to fulfil this essential role in the CO₂ transcritical system.

This study investigates a novel integration concept incorporating a pressure exchanger (PX) with two innovative low-lift ejectors. Instead of relying on two booster compressors, the proposed approach leverages two ejectors to achieve the same objective. To enable the ejectors to compress flash gas from the PX compression outlet to the gas cooler pressure, a

prerequisite is to maintain a compressor discharge pressure higher than the gas cooler pressure.

A numerical analysis of this innovative PX integration concept is conducted, and its performance is compared with that of standard booster, parallel, and ejector configurations. The investigation findings indicate the viability of the PX integration concept, estimating a potential performance enhancement ranging from 2% to 6% when compared to the ejector configuration.

Following the theoretical investigation, an experimental setup was constructed in the Varmeteknisk NTNU laboratory to validate the conceptual findings. For this endeavour, a retrofit was performed on the SuperSmart CO₂ transcritical facility, integrating the pressure exchanger (PX), two newly introduced ejectors, and associated fittings and measuring instruments. A tailored control strategy was developed, and two PID controllers were incorporated into the existing control software to facilitate the operation of the PX mode.

Experiments were conducted to assess the cooling capacity of 70 kW with an evaporation temperature of 0 °C and gas cooler outlet temperatures of 33 °C, 35 °C, 37 °C, and 38 °C. The system maintained steady-state conditions for a duration of 10 minutes while recording data. The experimental outcomes have successfully validated the proof of concept, establishing a solid foundation for further exploration of the pressure exchanger (PX) and applying low-lift ejectors. Discrepancies observed between numerical predictions and experimental results are thoroughly discussed, with potential solutions highlighted for addressing these disparities.

The completion of the PhD thesis signifies the successful achievement of its objectives, encompassing the development of the pressure exchanger (PX) integration concept, numerical investigation, the establishment of an experimental setup, and the subsequent verification of the conceptual framework.

Table of contents

Preface	i
Acknowledgements	ii
Abstract	iii
Table of contents	v
List of Figures	vii
List of Tables	ix
Nomenclature	x
1 Introduction	1
1.1 Motivation	1
1.2 Research objectives	4
1.3 Thesis Structure	5
1.4 List of publications	5
1.4.1 Journal publications	5
1.4.2 Conference Publications	6
1.5 Co-supervision of Master students	7
2 Background and theory	8
2.1 CO ₂ refrigeration	8
2.2 CO ₂ expansion work recovery devices	11
2.2.1 Ejectors	11
2.2.2 Pressure exchanger	14
3 Experimental System	19
3.1 Experimental system description	19
3.2 Modification of the experimental system	21
3.3 Experimental control strategy of PX mode	26

4	Comparison of theoretical and experimental results.....	28
4.1	Boundary conditions	28
4.2	Ejectors.....	29
4.3	PX pressure lift.....	32
4.4	Temperatures around PX and expansion quality	33
4.5	Experimental results.....	37
4.6	Uncertainty analysis	39
5	Summary of the research work	40
5.1	Journal paper 1: Thermodynamic analysis of rotary pressure exchanger and ejectors for CO ₂ refrigeration	40
5.2	Journal paper 2: Experimental investigation of a transcritical CO ₂ refrigeration system incorporating rotary gas pressure exchanger and low lift ejectors.....	43
5.3	Journal paper 3: Ultra-Low-Temperature Refrigeration Systems: A Review and Performance Comparison of Refrigerants and Configurations	45
6	Conclusion and suggestions for further work.....	47
6.1	Conclusions.....	47
6.2	Suggestions for further work.....	48
	References	49
	Appendix	54
	A.1. PX calculation model EES	54
	A.2. Python script for Ejector uncertainty.....	59
	A.3. Dynamic simulation model Modelica	64
	A.4. Experimental results of Booster and parallel compression mode	65
	A.5. Experimental results of PX cases	66
	B. Collection of a publications	76

List of Figures

Figure 1.1: Different HFCs refrigerants for air conditioning in Swedish passenger ships (Adapted from Hafner et al. [6])	2
Figure 1.2: Different HFCs refrigerants for provision refrigeration in Swedish passenger ships (Adapted from Hafner et al. [6])	2
Figure 1.3: Research areas within Cruize project [2]	3
Figure 1.4: Pressure exchanger with two inlet and two outlet ports	4
Figure 2.1: CO ₂ subcritical cycle a (Ph diagram), b (TS diagram), transcritical cycle, c (Ph diagram), d (TS diagram).....	9
Figure 2.2: CO ₂ transcritical system performance improvement areas.....	10
Figure 2.3: Expansion loss on the TS diagram.....	11
Figure 2.4: Ejector layout	12
Figure 2.5: (a) Ejector configuration of the transcritical cycle (b) Pressure enthalpy diagram	13
Figure 2.6: PX inside mechanism (a) Cut section view (b) Four different PX ports.....	15
Figure 2.7: PX integration concept and with CO ₂ system (a) Schematic (b) Ph diagram	15
Figure 2.8: PX compression and expansion stages	16
Figure 3.1: Experimental system at the Varmeteknisk laboratory at NTNU before modification.	19
Figure 3.2: Retrofitted supersmart rack with integration of PX system.....	21
Figure 3.3: (a) Compressor discharge flow towards LP and HP ejectors motive (b) Outlet flow of HP ejector to gas cooler (c) Metering valve between a and b.....	22
Figure 3.4: (a) Flash gas flow towards LP ejector suction (b) Two-phase flow after expansion from PX (c) Gas cooler outlet flow towards ejector.....	22
Figure 3.5: (a) LP ejector (b) HP ejector with motor to control motive needle	23
Figure 3.6: (a) Pressure exchanger (PX) with four ports (b) VSD for PX motor and Flow meters transmitter	23

Figure 3.7: (a) Differential pressure sensor (b) Energy meter for PX motor	24
Figure 3.8: Schematic and state point diagram of the PX experimental configuration	25
Figure 3.9: Controlling of PX RPM and HP ejector needle. Manual controls (Left), PID controllers (Right)	26
Figure 4.1: Theoretical case entrainment ratio of LP and HP ejector	29
Figure 4.2: Experimental HP and LP ejectors efficiency and entrainment ratio	30
Figure 4.3: Experimental LP and HP ejectors pressure lift	31
Figure 4.4: Theoretical PX pressure lift of flash gas	32
Figure 4.5: Experimental PX pressure lift of flash gas	32
Figure 4.6: Theoretical temperatures around PX.....	33
Figure 4.7: Experimental PX ports (inside) temperatures of 35 °C case	34
Figure 4.8: Ph diagram showing the effect of PX low compression temperature	34
Figure 4.9: PX expansion quality (experimental points with orange stars)	35
Figure 4.10: Experiment in parallel compression mode with PX to verify PX expansion quality	36
Figure 5.1: Four configurations of CO ₂ transcritical system (a) Standard booster (b) Parallel compression (c) Ejector configuration (b) PX integration concept with two booster ejectors	41
Figure 5.2: COP comparison between air refrigeration cycle, two-stage refrigeration system, cascade refrigeration system using different refrigerants	46

List of Tables

Table 1.1: Properties of common natural refrigerants excluding hydrocarbons	3
Table 3.1: Compressors description of the experimental rig.....	20
Table 4.1: Compressor outlet and gas cooler pressure for theoretical work.....	28
Table 4.2: Sensitivity analysis of LP and HP ejector efficiency (2 bar lift) for theoretical cases at 35 °C GC outlet and 40 bar receiver pressure	29
Table 4.3: Sensitivity analysis of PX compression and expansion efficiency of theoretical cases	35
Table 4.4: Experimental results of PX 33 °C case for 10 Seconds	37
Table 4.5: Experimental results of PX 35 °C case for 10 Seconds	37
Table 4.6: Experimental results of PX 37 °C case for 10 Seconds	38
Table 4.7: Experimental results of PX 38 °C case for 10 Seconds	38

Nomenclature

Abbreviations

AC	Air conditioning
Aux	Auxiliary
CAM	Constant area mixing
CFD	Computation fluid dynamics
COP	Coefficient of performance
Com	compressor
CPM	Constant pressure mixing
DP	Differential pressure
ECHA	European Chemicals Agency
Ej	Ejector
Ejec	Ejector
EU	European union
ERI	Energy recovery international
Evap	Evaporator
FGBV	Flash gas bypass valve
FGV	Flash gas bypass valve
GC	Gas cooler
GHG	Green house gases
GWP	Global warming potential
HVAC	Heating ventilation and air conditioning
HFCS	Hydrofluorocarbons
HP	High pressure
HPV	High pressure valve
HPTD	High pressure travel distance
HX	Heat exchanger
IMO	International Maritime Organization

IHX	Internal heat exchanger
LT	Low temperature
LP	Low pressure
LPTD	Low pressure travel distance
LIQ	Liquid
MBR	Mass boost ratio
MT	Medium temperature
NBP	Normal boiling point
NTH	Norwegian institute of technology
PAR	Parallel
PFAS	Per- and polyfluoroalkyl substances
PX	Pressure exchanger
PXG	Pressure exchanger
PWS	Pressure wave supercharger
RO	Reverse osmosis
s	Supercritical
SEP	Separator
SHX	Suction heat exchanger
VSD	Variable speed drive

Variables and Symbols

E	exergy (kW)
h	specific enthalpy (kJ/kg)
m	mass flow (kg/s)
P	Pressure (bar)
Q	heat load (kW)
s	specific entropy (kJ/kg K)
T	temperature (°C)
W	power (kW)
x	vapour quality
ρ	density (kg/m ³)

η	efficiency
\emptyset	entrainment ratio

Subscripts

b	booster case
BR	boost ratio
com	compressor
D	destruction
e	evaporator
ej	ejector
exp	expansion
g	generation
GC	gascooler
HP	high pressure
in	inlet
is	isentropic
LP	low pressure
m	motive
o	ambient
out	outlet
par	parallel
px	pressure exchanger
rec	liquid receiver
s	suction
SHX	suction gas HX
tot	total

1 Introduction

1.1 Motivation

In 2023, the International Maritime Organization (IMO) adopted its revised strategy for greenhouse gas (GHG) emissions from the shipping sector. The amended IMO strategy incorporates an augmented collective aspiration to achieve carbon neutrality regarding GHG emissions emanating from global maritime activities by approximately 2050. There are four ambition levels for IMO 2023. First is the reduction of carbon intensity by enhancement of the energy efficiency of the ships. The second level is to reduce emissions by 40% by 2030 compared to 2008. The third level is a dedicated commitment to increase the use of alternative fuels by 5% (striving for 10%), which are zero or near zero GHG by 2030. The fourth level is to reach net zero GHG from the international shipping sector by 2050. The framework also outlines the two indicative milestones for assessment in 2030 (20% reduction in total GHG emissions compared to 2008, striving for 30%) and 2040 (70% reduction in total GHG emissions compared to 2008, striving for 80%) [3].

In passenger ships, the heating and cooling demand constitutes 40% of the ship's total energy/fuel requirements. Currently, a portion of this heating demand is covered by the waste heat recovery of combustion engines [4, 5]. However, with the development of modern propulsion systems, electric batteries and alternative fuels, the potential for waste heat recovery will decrease. This trend dramatically emphasizes the need for energy-efficient and environment-friendly heating and cooling systems, which aligns with IMO ambition level 1. Vapour compression systems are used to fulfil heating and cooling demands and use various working fluids called refrigerants. A significant number of refrigerants in use are synthesized from various chemicals, contributing to adverse environmental impacts, including GHG emissions, global warming potential (GWP) and PFAS pollution.

A survey study of the 30 Swedish passenger ships in the time periods of 2007-2012 and 2013-2016 shows the trend of different fluorinated refrigerants [6]. The report highlights the trend of refrigerants for Air Conditioning (AC) and provision refrigeration (Chilling and freezing of food). In these time periods, R134a was the dominant refrigerant for provision and air conditioning. R134a is a hydrofluorocarbon (HFC) refrigerant with a high global warming potential (1430 units), and it is not a long-term solution. The use of R22 in passenger ships has reduced from 10% in 2007 to 0% in 2016 [6]. The EU Council and parliament reached a revised provisional agreement in October 2023 to phase down HFCs completely by 2050 within the EU. The HFC production will be gradually reduced to a minimum of 15% by 2036 [7]. The Kigali Amendment to the Montreal Protocol, globally ratified in 2016, mandates phasedown schedules for HFCs across all nations. Anticipated to mitigate global warming by

as much as 0.4 °C, this amendment signifies the international effort to address the environmental impact of HFCs [8].

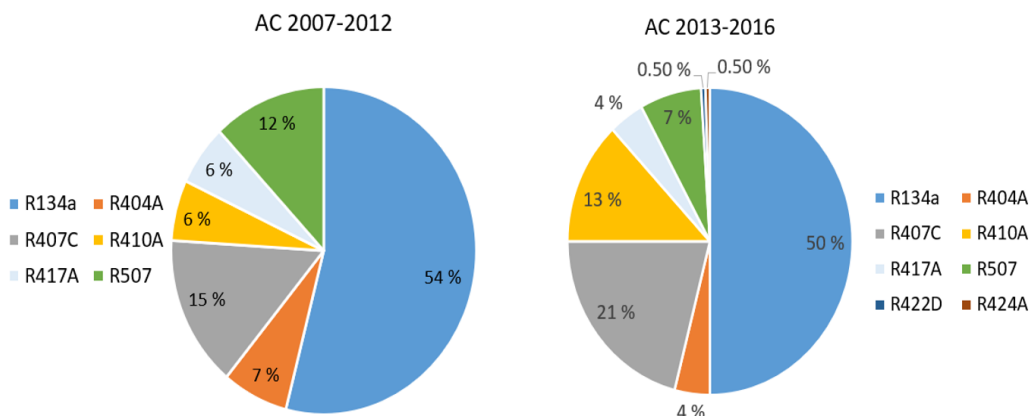


Figure 1.1: Different HFCs refrigerants for air conditioning in Swedish passenger ships (Adapted from Hafner et al. [6])

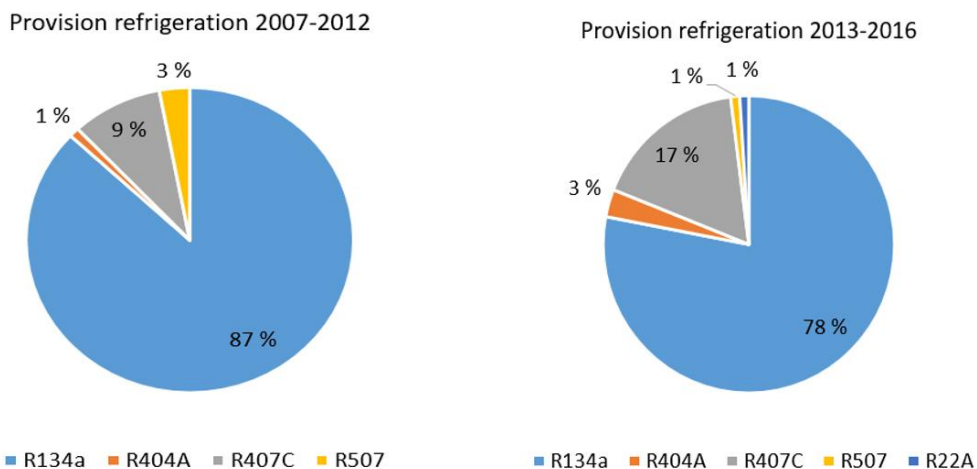


Figure 1.2: Different HFCs refrigerants for provision refrigeration in Swedish passenger ships (Adapted from Hafner et al. [6])

The sustainability of the ships' heating and cooling systems is in the utilization of natural refrigerants. They are evergreen solutions and will not be subject to any restrictions and regulations. The properties of common natural refrigerants are shown in Table 1.1 [9]. Among the natural refrigerants, there are few available options, and CO₂ possess a great potential to grow. Over 50 CO₂ units have been installed on the fishing vessels since 2016 [10]. This shows the wide acceptability of CO₂ refrigeration in the marine sector. However, efforts are ongoing

to enhance the acceptability of CO₂ systems for Air Conditioning on passenger ships. In 2019, a German manufacturer, GEA, installed a CO₂ system on the passenger ship to provide refrigeration; the trend is expected to increase [11].

Table 1.1: Properties of common natural refrigerants excluding hydrocarbons

Refrigerant	Molecular Mass (kg/kmol)	NBP (°C)	Critical Temperature (°C)	Critical Pressure (bar)	ODP	GWP
R-717	17	-33.32	132.4	113.6	0	0
R-744	44	-78.5	31	73.8	0	1
R-729	28.9	-213.4	-140.7	38.5	0	0
R-718	18	100	373.95	220.64	0	0

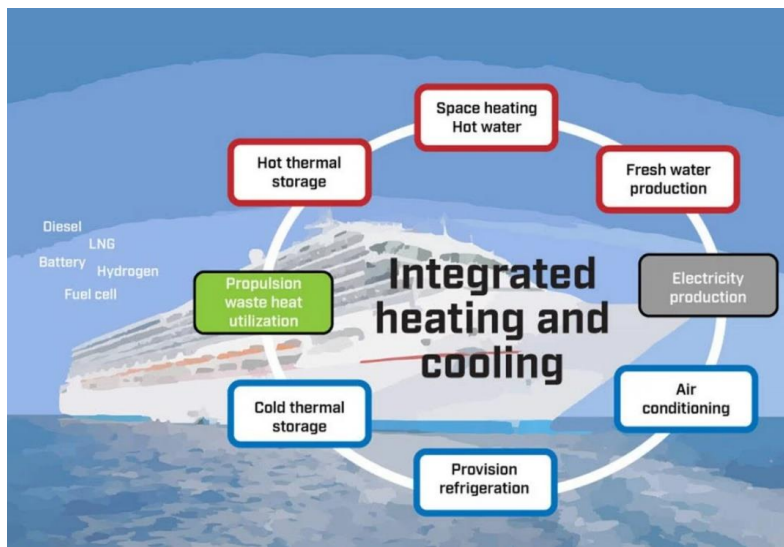


Figure 1.3: Research areas within CruIZE project [2]

The thesis work is part of the CruIZE project [4], whose objective is to introduce innovative and energy-efficient heating and cooling solutions to reduce passenger ships' overall energy usage. A comprehensive illustration of the CruIZE project is shown in Figure 1.3 [4].

In the initial year of the PhD work, the research primarily concentrated on utilising cold and heat recovery from the propulsion system and integrating it with the HVAC system. Furthermore, efforts were directed towards introducing CO₂ direct expansion evaporators into passenger ships' air handling units or cabins. This work is reported in the first conference paper. However, owing to various circumstances, a decision was made to shift the focus towards the theoretical and experimental investigation of the pressure exchanger (PX) device for CO₂ transcritical systems. This shift became the central focus and primary outcome of the thesis to scientifically document and validate the performance of this newly introduced

expansion work recovery device. PX is a device with four ports and a rotor, and it acts as a compression and expansion device. The PX is shown in Figure 1.4. It expands the gas cooler flow to the receiver pressure and compresses the flash gas from the receiver to the gas cooler pressure without physical separation within PX. The background and theory chapter will provide a detailed discussion of the PX.

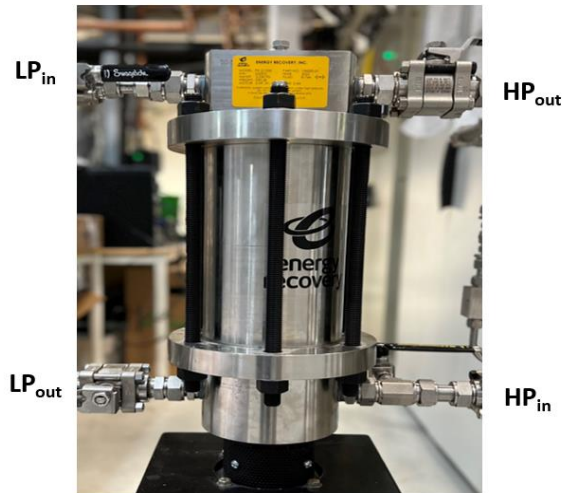


Figure 1.4: Pressure exchanger with two inlet and two outlet ports

1.2 Research objectives

The main objective of this PhD thesis is to develop a natural refrigerant CO₂ transcritical cooling system by integrating a pressure exchanger to improve energy efficiency when applied as an AC system. With the history of technical advancement of CO₂ transcritical systems in NTNU, this work aims to investigate theoretically and experimentally the new innovative PX device. This is to be done through the new PX integration concept and its verification through the experimental campaign in NTNU Varmeteknisk lab. It is essential to mention that the PX device was designed, fabricated, and provided for experiments by energy recovery international. The primary objectives and goals of this thesis are summarised as follows:

- Development of a PX integration concept with a CO₂ transcritical system.
- Numerically investigate the PX integration concept and comparison of system performance with the existing configurations.
- Development and integration of two novel ejectors for the PX based CO₂ AC system.

- Development of the experimental system by retrofitting of the existing CO₂ system (SuperSmart rack) in the NTNU Varmeteknisk lab.
- Verify the PX integration concept by experimental campaigns and document the findings compared to state-of-the-art configurations.

1.3 Thesis Structure

- **Chapter 1** highlights the motivation of the PhD research work. It also outlines the research objectives, thesis structure, and publication list.
- **Chapter 2** is about the background and theory of the research work. It includes the history of CO₂ refrigerant and the transition to synthetic refrigerants. The technicality of the ejector, the mechanism of the PX and the related thermodynamic equations are included in this chapter.
- **Chapter 3** describes the CO₂ transcritical system of the NTNU Varmeteknisk lab. The retrofitting process and integration of the PX, two new ejectors, related components and adjustment with the SuperSmart system are included. The PX experimental control strategy is also described in this chapter.
- **Chapter 4** provides the results of the experimental campaign and the comparison with the theoretical investigation.
- **Chapter 5** provides a summary of the research work by summarizing the articles.
- **Chapter 6** gives the conclusion and suggestions for further work.

1.4 List of publications

The author of this PhD research work has contributed to three journal articles and four conference papers on the subjects of pressure exchanger, refrigeration, and energy systems for ships. The journal articles and the conference papers with the main contribution are attached in the Appendix.

1.4.1 Journal publications

Journal article 1

M.Z. Saeed, Á.Á. Pardiñas, K. Banasiak, A. Hafner, A. Thatte, Thermodynamic analysis of rotary pressure exchanger and ejectors for CO₂ refrigeration system, Thermal Science and Engineering Progress, 51 (2024) 102643. <https://doi.org/10.1016/j.tsep.2024.102643>.

Authors contribution: Muhammad Zahid Saeed: Conceptualization, Methodology, Analysis, Software, Writing, Review & editing. Ángel Álvarez Pardiñas: Writing, Review & editing, Supervision. Krzysztof Banasiak: Technical discussion, Supervision. Armin Hafner: Conceptualization, Supervision, Technical discussion, Project administration, Funding acquisition. Azam Thatte: Technical discussion, Review & editing.

Journal article 2

M.Z. Saeed, A. Thatte, K. Banasiak, A. Hafner, Á.Á. Pardiñas. Experimental Investigation of Transcritical CO₂ Refrigeration System incorporating Rotary Gas Pressure Exchanger and Low Lift Ejectors. *Applied Thermal Engineering*. 2024. (In review process)

Authors contribution: Muhammad Zahid Saeed: Conceptualization, Methodology, Experiments, Analysis, Writing, Review & editing. Azam Thatte: Technical discussion, Experiments, Writing, Review & editing. Krzysztof Banasiak: Technical discussion, Review & editing, Supervision. Armin Hafner: Conceptualization, Supervision, Technical discussion, Project administration, Funding acquisition. Ángel Álvarez Pardiñas: Review & editing.

Journal article 3

M.Z. Saeed, L. Contiero, S. Blust, Y. Allouche, A. Hafner, T.M. Eikevik. Ultra-Low-Temperature Refrigeration Systems: A Review and Performance Comparison of Refrigerants and Configurations. *Energies* **2023**, *16*, 7274. <https://doi.org/10.3390/en16217274>

Authors contribution: Muhammad Zahid Saeed: Conceptualization, Methodology, Analysis, Software, Writing, Review & editing. Luca Contiero: Conceptualization, Methodology, Analysis, Software, Writing, Review & editing. Stefanie Blust: Conceptualization, Methodology, Analysis, Software, Writing, Review & editing. Yosr Allouche: Review & editing, Supervision. Armin Hafner: Conceptualization, Supervision, funding acquisition. Trygve Magne Eikevik: Conceptualization, Supervision, funding acquisition.

1.4.2 Conference Publications

1. **M.Z. Saeed**, A. Hafner, C.H. Gabriellii, I. Tolstorebrov, K.N. Widell. CO₂ refrigeration system design and optimization for LNG driven cruise ship. 9th IIR Conference on Ammonia and CO₂ Refrigeration Technologies. Proceedings: Ohrid, North Macedonia, 16-17 September 2021. <http://dx.doi.org/10.18462/iir.nh3-co2.2021.0015>
2. **M.Z. Saeed**, A. Hafner, A. Thatte, C.H. Gabriellii. Simultaneous implementation of rotary pressure exchanger and ejectors for CO₂ refrigeration system. 15th IIR-Gustav Lorentzen Conference on Natural Refrigerants. Proceedings. Trondheim, Norway, June 13-15th 2022. <http://dx.doi.org/10.18462/iir.gl2022.0130>

The following two papers have minor contributions from the author of this thesis.

3. Á.Á. Pardiñas, H. Selvnes, C.H. Gabriellii, **M.Z. Saeed**. Innovative refrigeration concept for passenger ships - combining CO₂ refrigerant, cold recovery, and cold storage. 15th IIR-Gustav Lorentzen Conference on Natural Refrigerants. Proceedings. Trondheim, Norway, June 13-15th 2022. <http://dx.doi.org/10.18462/iir.g|2022.0207>
4. H. Andersen. **M.Z. Saeed**. A. Hafner, C.H. Gabriellii. Investigation of CO₂ refrigeration system and thermal energy storage for passenger ships. 10th IIR Conference on Ammonia and CO₂ Refrigeration Technologies. Proceedings: Ohrid, North Macedonia, 27-29 April 2023. <http://dx.doi.org/10.18462/iir.nh3-co2.2023.0035>

1.5 Co-supervision of Master students

The following six students were Co-supervised during the doctoral work at NTNU.

1. Magnus Egerdahl. 2022. Integrated thermal system for hydrogen and ammonia driven cruise ship. <https://ntnuopen.ntnu.no/ntnu-xmlui/handle/11250/3025719>
2. Vanja Revold Olberg. 2022. Thermal energy recovery and storage for a hydrogen fuel cell and battery driven cruise ship. <https://ntnuopen.ntnu.no/ntnu-xmlui/handle/11250/3028968>
3. Henrik Andersen. 2022. Development of CO₂ refrigeration systems and thermal energy storage for cruise ships. <https://ntnuopen.ntnu.no/ntnu-xmlui/handle/11250/3024768>
4. Igor Koshelkov. 2022. Evaluation of mid-scale hydrogen distribution chains for compressed hydrogen. <https://ntnuopen.ntnu.no/ntnu-xmlui/handle/11250/3031492>
5. Matthias Ruppert. 2022. Integration of experimental setup for the experimental investigation of CO₂ chiller with expander versus ejector. <https://app.cristin.no/results/show.jsf?id=2206612>
6. Lene Dahl Jacobsen. 2023. Mid-scale hydrogen distribution chains. <https://ntnuopen.ntnu.no/ntnu-xmlui/handle/11250/3092535>

2 Background and theory

2.1 CO₂ refrigeration

The historical origins of the natural refrigerant CO₂ can be traced back to the 19th century. The first proposal for its use as a refrigerant was put forth in a British patent by Alexander Twining in 1850. During the initial years of the twentieth century, CO₂ was widely employed as a refrigerant, primarily in marine refrigeration systems [12]. The CO₂ was the prominent refrigerant until 1950 [13]. The introduction of chlorofluorocarbon (CFC) fluids in the 1930s and 1940s declined the use of natural refrigerants, including CO₂. The drop in the use of CO₂ cannot be linked to a single reason because multiple reasons likely influenced it. Some factors that influenced the use are reduced capacity and efficiency at elevated heat sink temperatures, intrusive marketing of CFCs, cost-effective tube assembly of synthetic refrigerants, and the insufficient commitment of CO₂ system manufacturers to enhance and modernize system and equipment designs [14].

The use of CFC refrigerants has been shown to have detrimental effects on the ozone layer and contribute to the intensification of the greenhouse effect. The severe threat posed by Ozone Depleting Substances (ODSs) to the ozone layer was formally recognised in the 1987 Montreal Protocol. It laid the groundwork for the gradual reduction and eventual abolition of ODS production and usage around the globe [15]. Consequently, investigating alternative refrigerants to replace CFCs emerged as a prominent area of focus in the refrigeration and heat pump sector. After the gradual reduction of CFCs, the subsequent development in refrigerant technology led to the emergence of the Hydrofluorocarbons (HFCs). These refrigerants possess zero ODP but have high global warming potential (GWP). In response to the growing apprehension about climate change and the release of greenhouse gases (GHGs) into the atmosphere, the Kigali Amendment to the Montreal Protocol was implemented in 2019. The agreement established a systematic reduction of HFC refrigerants with high GWP. The unsaturated HFCs, misleadingly called hydrofluoroolefins (HFOs), have emerged as another option for substituting high GWP HFCs. These kinds of HFCs are a class of synthetic chemicals that are now being advocated by several industries as promising options for future use in cooling equipment. However, unsaturated HFCs may exhibit reduced climatic impact. Their atmospheric degradation results in the production of significant quantities of trifluoroacetic acid (TFA), which has the potential to cause substantial damage to both human health and the environment. The Norwegian Environment Agency published a study in 2017 highlighting the lack of knowledge surrounding TFA and its potential effects on human health and the environment [16]. PFAS is another classification of synthetic chemicals that are widely used in society. They are considered environmental pollutants commonly observed in groundwater, surface water, and soil. PFAS compounds have carbon-fluorine bonds, which are known for their strong stability in organic chemistry. This means they do not easily break down

during use or in nature. Moreover, many PFAS can travel long distances in the environment, spreading far from where they were initially released [17]. Refrigerants like HFC (R134a) and HFO (1234yf) are in the category of PFAS. In January 2023, a proposal was initiated by Germany, Denmark, the Netherlands, Sweden, and Norway and submitted to the European Chemicals Agency (ECHA) to reduce PFAS emissions. Currently, ECHA is clarifying the steps to restrict the use of PFAS in Europe [18].

The refrigeration sector began looking for appropriate refrigerant substitutes when the CFC issue became a serious concern in the late 1980s. Professor Gustav Lorentzen, the founder of the Refrigeration institute at NTH in 1951, now the Norwegian University of Science and Technology, proposed the revival of CO₂ refrigerant. Lorentzen described a 'transcritical' CO₂ cycle system in a 1989 international patent application [19], which included a throttling valve to control the high-side pressure [20, 21]. This technology was developed for automobile air conditioning systems and water heaters [14]. Subsequently, several potential applications were introduced in the market.

There are several benefits of CO₂, which have led to its widespread use in many different system architectures in recent years. It is environmentally friendly, non-toxic, non-flammable, and has negligible GWP and zero ODP [22]. The higher volumetric refrigeration capacity leads to a compact system than other refrigerants [23]. Compressor efficiencies are better due to lower compression ratios. The lower critical temperature posed challenges earlier in the regions with elevated temperatures, but Gustav Lorentzen solved the issue satisfactorily in his CO₂ revival with transcritical operation.

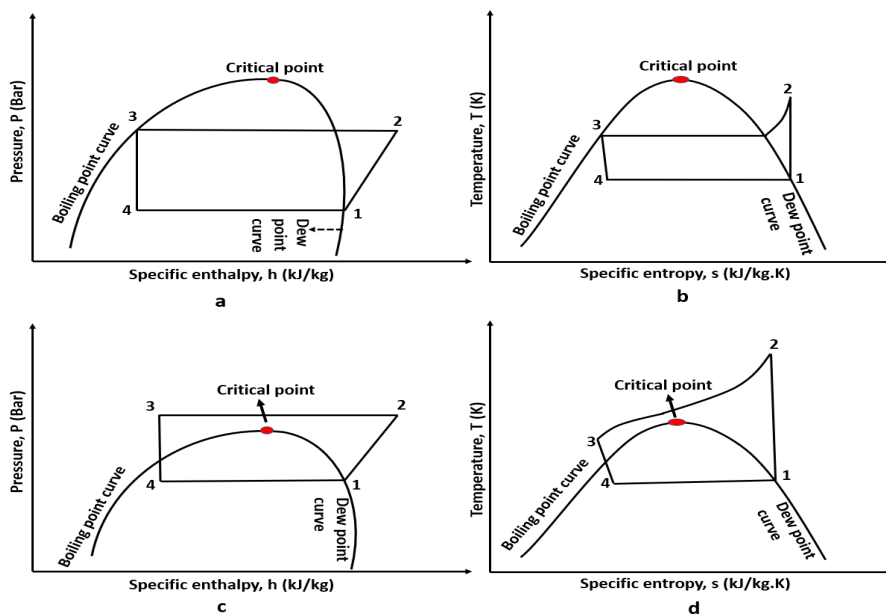


Figure 2.1: CO₂ subcritical cycle a (Ph diagram), b (TS diagram), transcritical cycle, c (Ph diagram), d (TS diagram)

In the subcritical operation, the heat rejection temperatures are below the critical temperature, and the refrigerant becomes liquid isothermally after heat rejection in the condenser. The transcritical operation is in the supercritical region (above critical temperature and pressure), and after heat rejection in the gas cooler, the refrigerant remains in the dense gaseous state. The Ph and TS diagrams of the subcritical and transcritical systems are shown in Figure 2.1. The numbers depicted in Figure 2.1 include four processes, which are the compression (1-2), Condensing/Gas cooling (2-3), expansion (3-4) and evaporation/heat absorption (4-1). The system's performance is termed a coefficient of performance (COP), the ratio of heat removed during evaporation to the work supplied to the compression process.

The innovation and research of CO₂ systems performance enhancement have played a vital role in the industry's extended applications and broader acceptance in the last decade. The innovation areas of the CO₂ can be divided into three categories. The first is consolidating all thermal functions in one unit [24]. These so-called integrated CO₂ systems can provide cooling and heating at different freezing, chilling, Air Conditioning, and hot water heating temperatures. It eliminates the need for several independent systems and makes it suitable for various applications, such as hotels, supermarkets, fishing vessels, passenger ships, and the process industries.

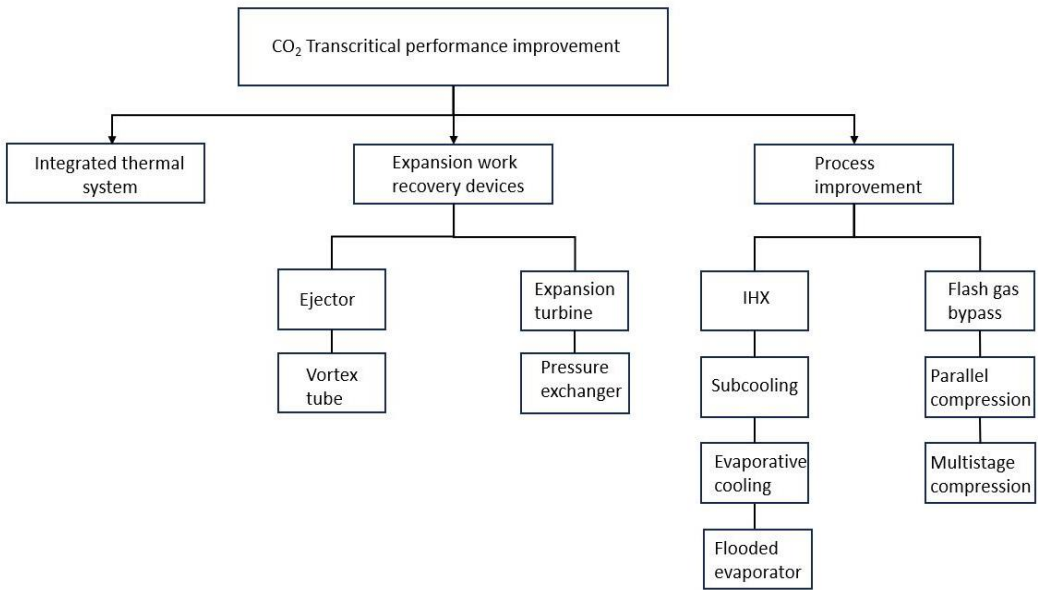


Figure 2.2: CO₂ transcritical system performance improvement areas

The second category is to recover the expansion work of the transcritical system by work recovery devices, such as ejectors, expansion turbines, vortex tubes, and pressure exchangers. Third is the process improvement by internal heat exchanger (IHX), subcooling, flash gas bypass, evaporative cooling, flooded evaporator, parallel compression, and multistage compression. Expansion work recovery devices can also be considered in the process

improvement category. However, they are in a separate category, distinguishing between expansion and non-expansion devices. These three categories are shown in Figure 2.2.

2.2 CO₂ expansion work recovery devices

In transcritical operations, expansion losses occur when high-pressure supercritical CO₂ expands in the expansion/HP valve. The expansion loss in the TS diagram is shown in Figure 2.3. This expansion loss can be recovered with the expansion work recovery devices. These devices can reduce the compression work and ultimately increase the system's performance. The main emphasis in this work is given to the ejector and pressure exchanger.

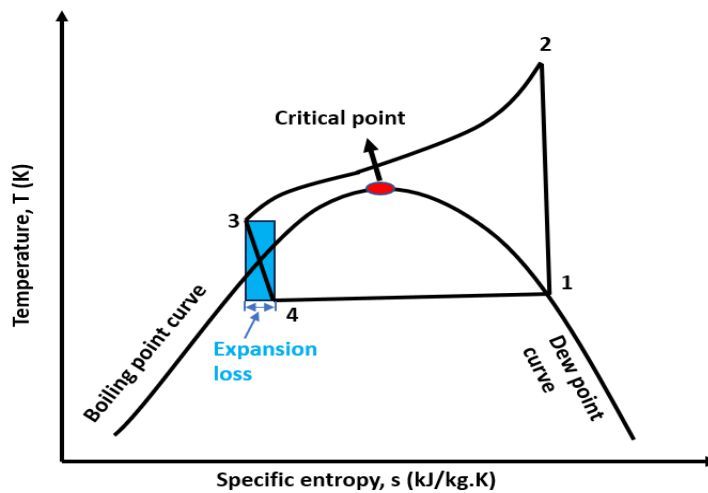


Figure 2.3: Expansion loss on the TS diagram

2.2.1 Ejectors

The ejector is a component with two inlets and one outlet stream. The motive flow from the high-pressure side enters the motive nozzle, accelerates, and expands, entraining a suction flow from the low-pressure side. Both flows mix in the mixing zone, and a diffuser elevates the discharge pressure of the total stream, leaving the device (Figure 2.4). The ejectors can be divided into three categories: motive nozzle position, nozzle design, and phases (vapour, liquid). Constant pressure mixing (CPM) and constant area mixing (CAM) are the two configurations of the motive nozzle positions. In CPM, the nozzle end is within the suction chamber; in CAM, it is in the constant area section. CPM ejectors are often used for their ability to perform at higher back pressures.

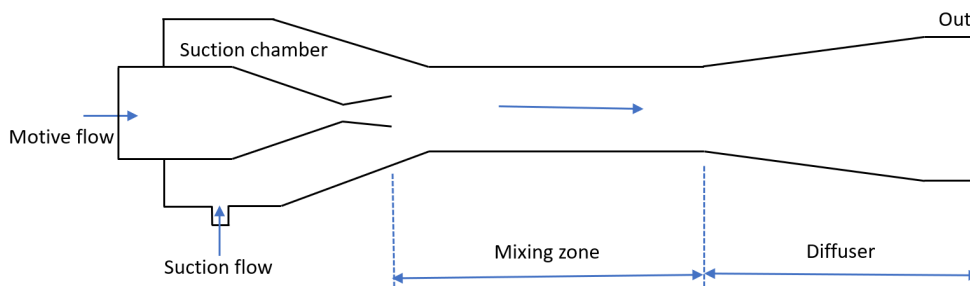


Figure 2.4: Ejector layout

Even though CAM ejectors can provide higher mass flow rates, CPM ejectors frequently outperform CAM ejectors [25, 26]. The design of the motive nozzle influences ejector performance. There are two motive nozzle designs. Convergent, which means the ejector functions in a subsonic condition and can only reach a sonic state at the outlet, and convergent-divergent, which means the flow through the ejector may reach supersonic speeds. The specific characteristics of the end application are crucial in deciding between the two kinds of ejectors. The motive and suction flow conditions decide the number of phases involved, which can be a single phase (Vapour or liquid) or two-phase [25].

The ejector was invented by Henry Giffard in 1858 for the intended application of steam engines as a replacement for mechanical pumps to feed liquid water to the boiler [27]. Later, ejector applications increased due to several advantages, e.g., low maintenance cost and no restriction for working fluids. Several researchers have performed comprehensive research and reviewed the use of ejectors in vapour compression systems. Elbel addressed ejectors' historical and recent (2011) development and their use in refrigeration and air conditioning systems [28]. His work summarized ejector cycles, expansion work recovery by two-phase ejectors, and analytical and experimental results of two-phase ejectors to identify performance enhancement areas. The advance developments of ejector technology were reviewed in 2016 by Elbel and Lawrence [29]. In this work, they covered the developments of ejectors after their first review in 2011. They discussed the alternative ejector cycles, low-pressure ejectors, control strategies, and commercialized systems and suggested further work to improve the suitability of ejectors for more applications. Similarly, several authors have done review work on ejector technology: Besagni et al. 2016 [25] (comprehensive review in four parts, description of ejector technology, refrigerant effect on ejector performance, cycles and the ejector systems), Gullo et al. 2019 [30] (Multi-ejector concept and development review), Tashtoush et al. 2019 [31] (Ejector performance, design and applications review), Besagni 2019 [32] (Ejectors past and present perspective review), Gullo et al. 2020 [33] (Two-phase ejectors capacity control strategies review), Ringstad et al. 2020 [34] (flow modelling of two-phase ejectors review), Song et al. 2020 [35] (Review of simulation models of two-phase ejectors), Barta et al. 2021 [36] (Review of transport and stationary air conditioning and

refrigeration including ejectors) and Zheng et al. 2022 [37] (Experimental, modelling and optimization review of ejectors). In the last decade, remarkable research has been performed on ejectors by notable authors, Banasiak and Hafner 2011 [38] (Two-phase computation model of ejector), Banasiak et al. 2012 [39] (Numerical and experimental investigation of ejector), Banasiak and Hafner 2013 [40] (Converging and diverging nozzle modelling of ejector), Lawrence and Elbel 2013 [41] (Practical and theoretical comparison of two-phase ejector cycles), Hafner et al. 2014 [42] (Concept of multi-ejector for supermarket refrigeration), Banasiak et al. 2014 [43] (Two-phase ejector CFD investigation), Lawrence and Elbel 2014 [44] (Two-phase ejector cycle experimental investigation for low pressure working fluids), Haida et al. 2016 [45] (Experimental investigation of multi-ejector equipped compressor rack) and Ringstad et al. 2021 [46] (CFD and machine learning for ejectors optimization and mapping).

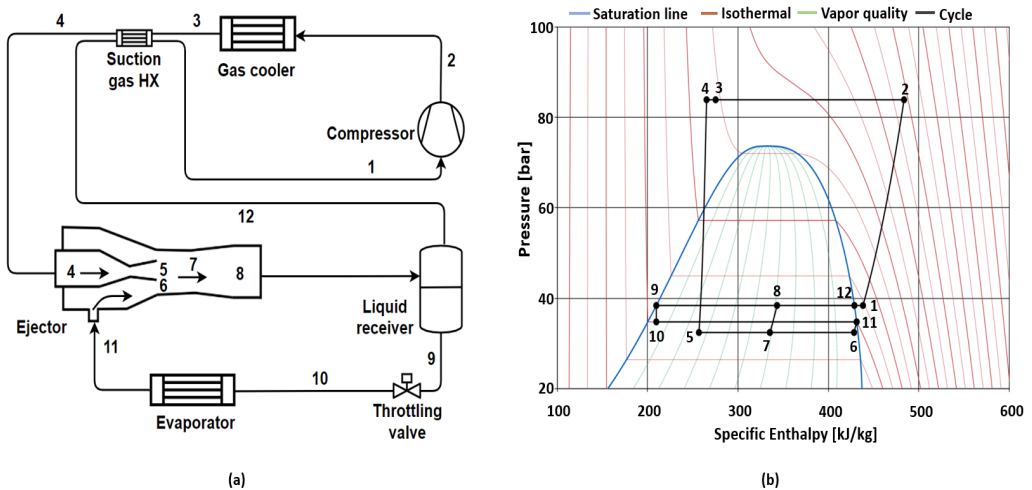


Figure 2.5: (a) Ejector configuration of the transcritical cycle (b) Pressure enthalpy diagram

The typical CO₂ ejector refrigeration cycle is shown in Figure 2.5. The high-pressure CO₂ flow enters the ejector primary/motive nozzle (point 4) and accelerates to a sonic condition in the converging section at the throat. It further accelerates in the diverging section to super-sonic condition. A two-phase process initiates at this point, and the pressure reduction is coupled with acceleration. At the end of the motive nozzle divergent part, the flow moves out and creates a low-pressure region (point 5), which initiates the suction of secondary flow (point 11) in the suction chamber (point 6). Both streams (motive and suction) mix in the mixing section (point 7). In the diffuser section (point 8), the flow deaccelerates, and the pressure increase occurs due to the conversion of the portion of kinetic energy. In this way, the pressure lift of the suction flow is achieved by recovering the energy lost while the motive flow expands [34]. The ejector expansion work recovery performance is usually indicated by four parameters: pressure lift, pressure ratio, mass entrainment ratio, and ejector efficiency. The

suction pressure ratio, pressure lift, mass entrainment ratio and ejector efficiency are shown in equations 1,2,3 and 4, adapted from Elbel and Hrnjak 2008 [47].

$$\Pi = \frac{P_{\text{diffuser outlet}}}{P_{\text{suction inlet}}} \quad (1)$$

$$P_{\text{lift}} = P_{\text{diffuser outlet}} - P_{\text{suction inlet}} \quad (2)$$

$$\phi = \frac{m_{\text{suction}}}{m_{\text{motive}}} \quad (3)$$

$$\eta_{\text{ejector}} = \frac{W_{\text{recovered}}}{W_{\text{max_recovered}}} = \phi \cdot \frac{h(P_{\text{diffuser outlet}}, S_{\text{suction inlet}}) - h_{\text{suction inlet}}}{h_{\text{motive inlet}} - h(P_{\text{diffuser outlet}}, S_{\text{motive inlet}})} \quad (4)$$

2.2.2 Pressure exchanger

A pressure exchanger, comprising a cylindrical rotor with numerous channels arranged around its central axis, is supported by two stationary end plates. These plates feature ports directing fluid flow into and out of the rotor channels. As the rotor revolves, the channel ends cyclically and comes into contact with various port pressures, leading to compression and expansion within the rotor channels. As a result, the pressure of a high-pressure stream can be transferred to a low-pressure stream, simultaneously raising the pressure of the latter while reducing the pressure of the former. A modified version of this PX, CO₂-PX, is designed for energy recovery in CO₂ systems. It recovers expansion work and directly compresses the flash gas. High-pressure CO₂ enters from the lower right port (HP_{in}) and, after a pressure reduction, exits through the lower-left port (LP_{out}). The flash gas from the phase separator enters from the top left port (LP_{in}) and departs through the top right port (HP_{out}) following compression inside the PX. The energy required for this compression is harnessed from the work expansion during the HP_{in} fluid stream's expansion to the LP_{out} pressure [48]. The comprehensive explanation of PX is described in the literature by Azam [49-51] and the 2D CFD model by Elatar et al. 2021 [52]. A PX integration concept of this PhD work is shown in Figure 2.7. The PX integration needs two booster devices due to friction losses in the pipes and the gas cooler. More details about this will be discussed in Chapter 3.

Over several years, Pressure Exchanger (PX) technology applications have been well-established in reverse osmosis (RO) desalination units. Its primary function in this context is the recovery of pressure work from the high-pressure reject concentrate, followed by its efficient transfer to the low-pressure feed stream. The fundamental objective behind the development of the PX device was to enable direct pressure transmission from the high-pressure to low-pressure feed stream of the RO system, ultimately enhancing the system's overall performance [53]. Early research and development efforts concerning incorporating PX in desalination units yielded projections of power savings above 60% [54]. Subsequent operational results obtained from desalination plants equipped with PX have demonstrated a noteworthy reduction in the energy demand of the RO unit, typically achieving energy savings

ranging from 25% to 30%, thus surpassing the performance of alternative energy recovery devices [55].

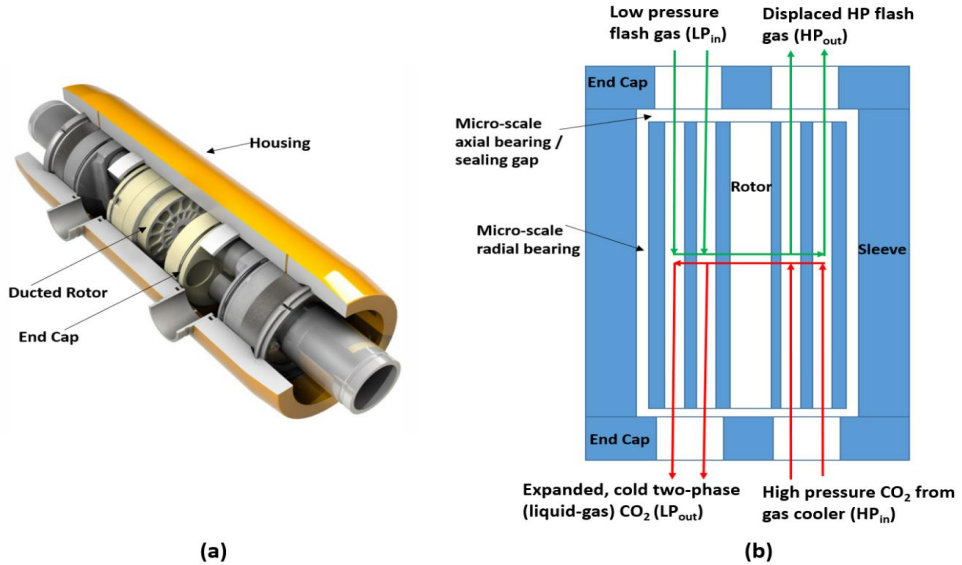


Figure 2.6: PX inside mechanism (a) Cut section view (b) Four different PX ports

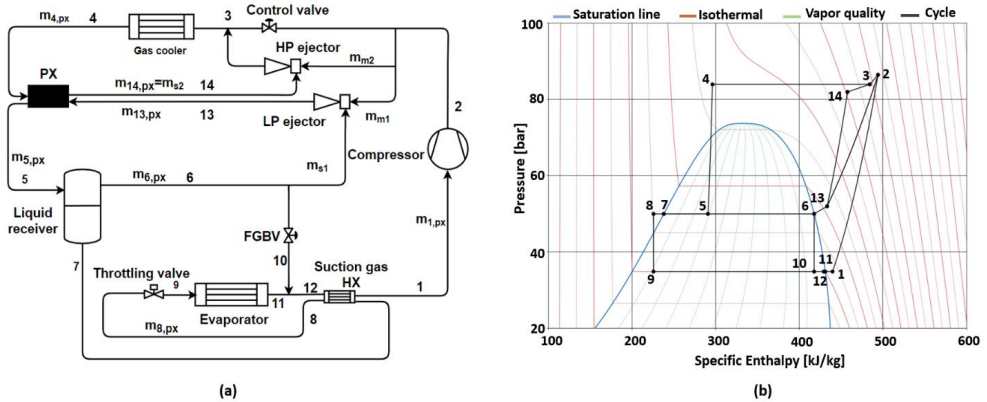


Figure 2.7: PX integration concept and with CO₂ system (a) Schematic (b) Ph diagram

Notably, PX shares the same operating principle with pressure-wave superchargers (PWS). In the context of compression ignition engines, PWS elevates the pressure of the incoming fresh air by leveraging exhaust gas pressure, accomplished through the rotation of the PWS rotor. This process leads to air intake compression while the exhaust gas undergoes expansion. PWS operation is based on the fact that pressure equalization occurs at a faster rate than the mixing of gas streams [56, 57]. It is essential to underscore that while the fundamental working

principle remains consistent, CO₂-PX stands out as a distinctive technology as it works with dense, high-pressure, and two-phase CO₂.

The four stages of PX are shown in Figure 2.8. In the initial phase (Stage 1), the low-pressure flash gas is directed from the liquid receiver tank into the PX via the LP_{in} port. This stream then fills the duct up to the level determined by the low-pressure travel distance (LPTD), a non-dimensional number dependent on factors such as the rotor duct volume, rotational speed, and the volumetric flow rate (LPTD= LP_{in} volumetric flow rate/(Total duct volume*rotational speed)). The LP_{in} flow displaces the LP_{out} flow from the preceding cycle. The two fluids may mix within the buffer zone but are contained within the designated duct as part of the design.

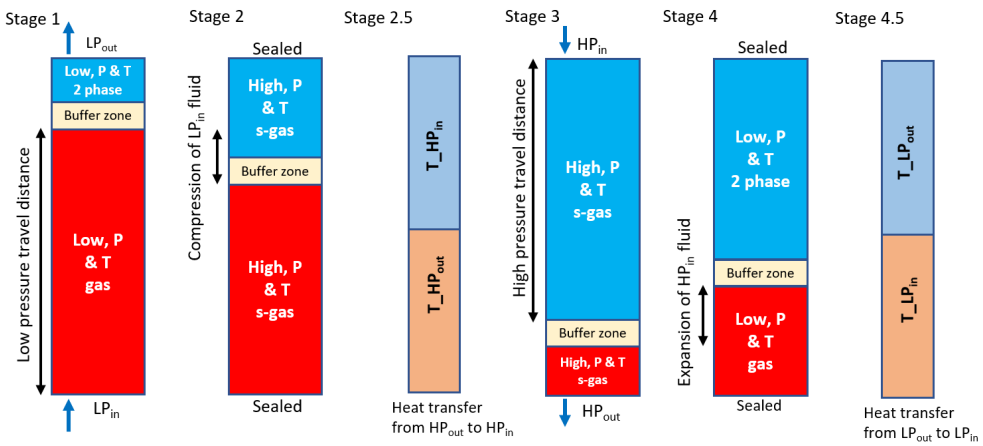


Figure 2.8: PX compression and expansion stages

Subsequently (Stage 2), as the duct rotates, the two fluids become sealed, transitioning into Stage 2.5. Upon exposure to the HP_{in} port, a pressure wave forms, elevating the LP_{in} stream's pressure to the HP_{in} level with a certain isentropic efficiency. The density of the LP_{in} increases, occupying a reduced volume while maintaining a constant mass within the duct.

During Stage 2.5, heat exchange occurs between the hot and cold streams, the extent of which relies on several factors, including heat transfer coefficient, density, thermal conductivity, specific heat capacity, and, notably, the available time (determined by rotational speed) before the subsequent stage.

In Stage 3, the duct aligns entirely with the HP_{in} and HP_{out} ports. The gas exiting the gas cooler enters through the HP_{in} port, occupying the duct per the HP travel distance. As HP_{in} enters, it displaces the LP_{in} (now HP_{out}) at an identical volumetric flow rate out of the duct. The density difference between HP_{out} and the preceding LP_{in} and HP_{in} determines the outflow state in a supercritical condition.

Continuing with the rotation, Stage 4 commences. The duct is sealed at high pressure, and upon exposure to LP_{in} and LP_{out} ports, an expansion wave occurs, reducing the duct pressure with a certain isentropic efficiency. This wave causes the supercritical CO₂ in the HP_{in} flow to transition to a low-pressure two-phase CO₂ state. The vapour quality of the LP_{out} stream is contingent upon the isentropic efficiency.

During Stage 4.5, the two-phase CO₂ engages in a brief heat exchange with LP_{in}, potentially vaporizing a minute fraction of the LP_{out} stream. Subsequently, this two-phase CO₂ exits through the LP_{out} port and is directed into the liquid receiver tank.

The following equations are utilized to calculate the PX efficiency curves. The kinetic energy terms in the energy balance are negligible compared to the specific enthalpy terms, and they are opted out.

$$m_{LP_{in}} \cdot h_{LP_{in}} + m_{HP_{in}} \cdot h_{HP_{in}} - m_{LP_{out}} \cdot h_{LP_{out}} - m_{HP_{out}} \cdot h_{HP_{out}} = 0 \quad (5)$$

The ideal operation of PX postulated that fluids are not mixed between compression and expansion sections. Thus, the relationship between mass flow rates at the four ports becomes:

$$m_{LP_{out}} = m_{HP_{in}} \quad (6)$$

$$m_{HP_{out}} = m_{LP_{in}} \quad (7)$$

In the context of the PX system, the mass boost ratio (MBR) is defined as the ratio between the mass flow rate at the low-pressure inlet, which can be compressed for each unit of mass flow entering the high-pressure inlet during the expansion process. The mass boost ratio can also be denoted in density ratio if the LP_{in}TD equals HP_{in}TD.

$$MBR = \frac{m_{LP_{in}}}{m_{HP_{in}}} \quad (8)$$

$$MBR = \frac{\rho_{LP_{in}}}{\rho_{HP_{in}}} \quad (9)$$

$$\frac{m_{LP_{in}}}{m_{HP_{in}}} = \frac{\rho_{LP_{in}}}{\rho_{HP_{in}}} \quad (10)$$

The efficiency of compression and expansion can be expressed mathematically as:

$$\eta_{com,PX} = \frac{h_{HP_{out, is}} - h_{LP_{in}}}{h_{HP_{out}} - h_{LP_{in}}} \quad (11)$$

$$\eta_{exp,PX} = \frac{h_{HP_{in}} - h_{LP_{out}}}{h_{HP_{in}} - h_{LP_{out, is}}} \quad (12)$$

The guessed efficiencies of compression and expansion must satisfy the mass boost ratio to get the real enthalpies of the following equation:

$$MBR = \frac{h_{LP_{out}} - h_{HP_{in}}}{h_{LP_{in}} - h_{HP_{out}}} = \frac{h_{HP_{in}} - h_{LP_{out}}}{h_{HP_{out}} - h_{LP_{in}}} \quad (13)$$

The volumetric flow rate at the four ports can be calculated as:

$$V_{\text{HP}_{\text{in}}} = \frac{m_{\text{HP}_{\text{in}}}}{\rho_{\text{HP}_{\text{in}}}} \quad (14)$$

$$V_{\text{HP}_{\text{out}}} = \frac{m_{\text{HP}_{\text{out}}}}{\rho_{\text{HP}_{\text{out}}}} \quad (15)$$

$$V_{\text{LP}_{\text{in}}} = \frac{m_{\text{LP}_{\text{in}}}}{\rho_{\text{LP}_{\text{in}}}} \quad (16)$$

$$V_{\text{LP}_{\text{out}}} = \frac{m_{\text{LP}_{\text{out}}}}{\rho_{\text{LP}_{\text{out}}}} \quad (17)$$

By using the Volumetric flow rates, the travel distance of the four ports can be calculated as:

$$\text{HP}_{\text{in}} \text{TD} = \frac{V_{\text{HP}_{\text{in}}}}{\text{Duct volume} \cdot \text{rotational speed}} \quad (18)$$

$$\text{HP}_{\text{out}} \text{TD} = \frac{V_{\text{HP}_{\text{out}}}}{\text{Duct volume} \cdot \text{rotational speed}} \quad (19)$$

$$\text{LP}_{\text{in}} \text{TD} = \frac{V_{\text{LP}_{\text{in}}}}{\text{Duct volume} \cdot \text{rotational speed}} \quad (20)$$

$$\text{LP}_{\text{out}} \text{TD} = \frac{V_{\text{LP}_{\text{out}}}}{\text{Duct volume} \cdot \text{rotational speed}} \quad (21)$$

The entropy generation (s_g) can be calculated by using the following energy balance.

$$m_{\text{LP}_{\text{in}}} \cdot s_{\text{LP}_{\text{in}}} + m_{\text{HP}_{\text{in}}} \cdot s_{\text{HP}_{\text{in}}} - m_{\text{LP}_{\text{out}}} \cdot s_{\text{LP}_{\text{out}}} - m_{\text{HP}_{\text{out}}} \cdot s_{\text{HP}_{\text{out}}} + s_g = 0 \quad (22)$$

$$s_g = \text{MBR} \cdot (s_{\text{HP}_{\text{out}}} - s_{\text{LP}_{\text{in}}}) + (s_{\text{LP}_{\text{out}}} - s_{\text{HP}_{\text{in}}}) \cdot m_{\text{HP}_{\text{in}}} \geq 0 \quad (23)$$

The proposed integration concept of CO₂-PX with ejectors represents an advancement of a previous approach. In the previous approach of PX integration, two booster compressors were used to lift flash gas from the liquid receiver to PX and from PX to the gas cooler. This eliminates the need for extra pressure lift by the primary compressor to make a pressure difference between the compressor discharge and the gas cooler. However, additional work is required for two booster compressors. Utilizing booster compressors for small pressure lift challenges cost, compressor performance, and complexity and replacing the booster compressors with ejectors simplifies the solution. Innovative ejectors offer a novel method to integrate the PX without introducing complexity and enhance the system's performance. However, the ejector performance and proper control are crucial to reduce the extra pressure lift. Lower ejector performance consequently increases the extra pressure lift by the primary compressor, and the performance gain diminishes.

3 Experimental System

3.1 Experimental system description

The SuperSmart rack, an experimental test facility in the NTNU/SINTEF varmeteknisk laboratory, is a versatile testing infrastructure designed to test and verify innovative concepts of medium-sized supermarkets. This system exhibits the capability to generate cooling at three distinct temperature levels, each designed for specific applications. The first level, dedicated to medium temperature (chilled products), operates with a robust capacity of 60 kW. The second level, tailored for low temperature (frozen products), offers a cooling capacity of 15 kW. Finally, the third level, intended for air conditioning, delivers a substantial cooling capacity of 45 kW.

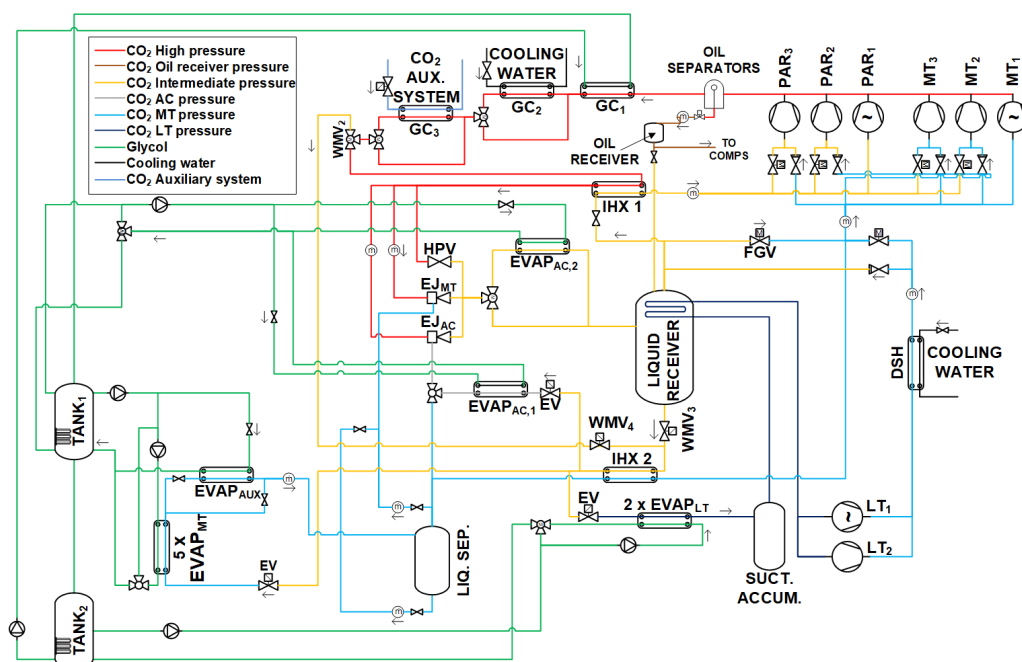


Figure 3.1: Experimental system at the Varmeteknisk laboratory at NTNU before modification.

The system comprises three compressor groups (MT, parallel, and LT compressors) responsible for regulating and maintaining desired pressures on the suction side. Depending on the specific experimental conditions, the flexibility exists to link two parallel compressors to the MT suction. To ensure superheat conditions for the suction stream of compressors, the system incorporates two internal heat exchangers (IHX 1 and IHX 2). Furthermore, the infrastructure features three gas coolers and heat dissipation is achieved through a secondary loop comprising glycol, water, and CO₂. The system has three expansion components: the High-

Pressure Valve (HPV) and two multi-ejector blocks. The system also includes three refrigerant accumulation tanks: a liquid receiver, a suction accumulator, and a liquid separator. In addition, the facility is equipped with five medium-temperature (MT) evaporators, two low-temperature (LT) evaporators, and two air conditioning (AC) evaporators.

Table 3.1: Compressors description of the experimental rig

Compressor group	Model	Displacement (m ³ /h) at 50 Hz
MT	4 MTC-10K-40S	6.5 (VSD)
	4 MTC-10K-40S	6.5 (VSD)
	4 JTC-15K-40P	9.2
Parallel	2 KTE-7K-40S	4.8 (VSD)
	2 KTE-7K-40S	4.8 (VSD)
	4 JTC-15K-40S	9.2
LT	2JME-3K	3.5 (VSD)
	2GME-4K	5

The system has a high level of flexibility and a history of serving as a testing ground for various innovations and configurations [58]. The experimental system can perform tests in three different modes: booster (1st generation), parallel (2nd generation), and ejector (3rd generation).

In the conventional CO₂ booster mode configuration, the flash gas bypass valve (FGV) bypasses the flash gas from the receiver tank to the MT evaporator pressure. The LT compressors lift the refrigerant gas from the LT evaporator pressure to the MT suction pressure. Before entering the LT compressors, the stream gets superheated by flowing through the liquid receiver tank. After an increment in pressure by LT compressors, the MT compressors lift the LT and flash gas flow to the gas cooler pressure. Typically, a HX is deployed after LT compressors to reduce the temperature of compressed gas before mixing with MT and flash gas stream.

In the parallel compression mode, instead of bypassing the flash gas with FGV to the MT pressure level, the parallel compressor group do this job. In this way, flash gas pressure will increase from liquid receiver pressure to the gas cooler pressure with the help of a parallel compressor. This shifts the compression load from the MT compressor group to the Parallel compressor group. However, it is necessary to have enough flash gas to keep the operation smooth. Depending on the amount of flash gas, the VSD compressor maintains the receiver pressure. The parallel compression mode is suitable for high ambient temperatures due to the high amount of flash gas after expansion.

In the ejector configuration, the ejector block replaces the HPV. The gas cooler flow enters the motive part of the ejector and suction flow from the evaporator outlet. In this way, the ejector

recovers the expansion work of high-pressure gas cooler flow and uses it to lift the pressure of evaporator flow to the receiver pressure. The compressors lift the flash gas and evaporator flow from the receiver pressure, reducing compression work. As there are two ejector blocks, other ejector configurations can also be tested in the SuperSmart rack. AC ejector block can completely lift the flow of the AC evaporator, while MT ejector block can partially lift the flow of MT evaporators to the receiver pressure.

3.2 Modification of the experimental system

The experimental facility was modified to incorporate the PX add-on and the related components to enable the testing of the PX configuration. The modified version of the P&ID is shown in Figure 3.2, and the black lines highlight the changes made in the original P&ID of Figure 3.1.

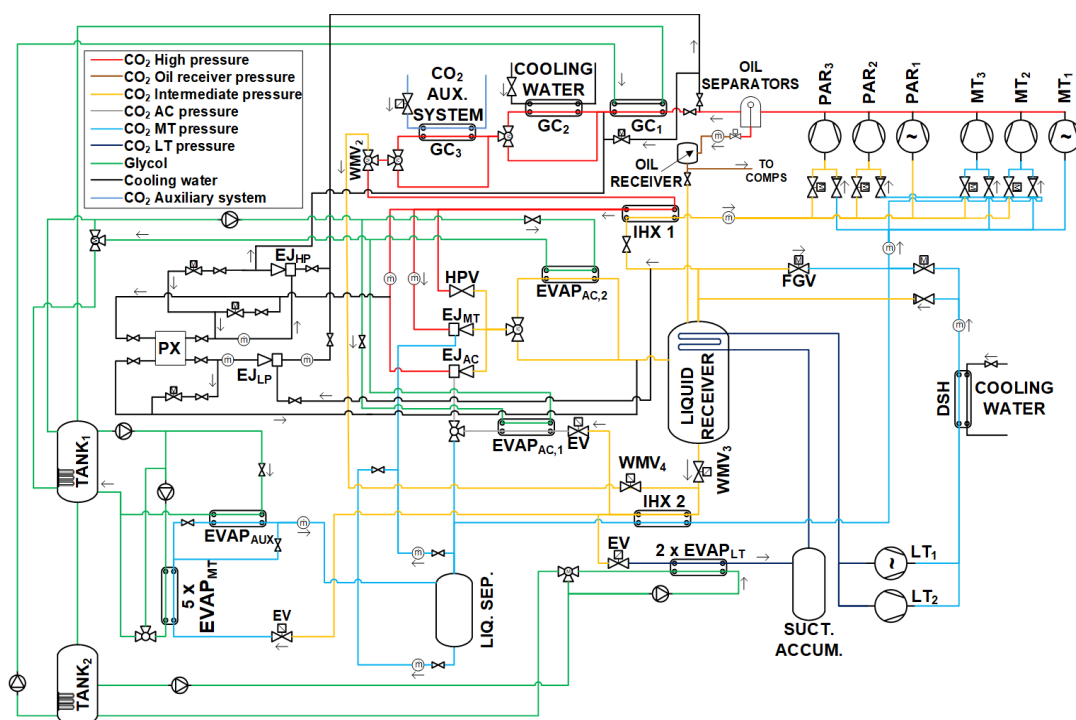


Figure 3.2: Retrofitted supersmart rack with integration of PX system

Five connections are established from the PX add-on to the main system. The first connection is after the oil separator takes out the flow after compression to the motives of LP and HP ejectors. A ball valve before GC₁ diverts the flow to the ejector's motive after compressors. The second connection is after the GC₁ to take the flow from the HP ejector outlet to the GC₂ for heat rejection. If required, a metering valve is deployed to bypass the flow between

connections one and two. The connections one (615F) and two (615G) and the metering valve are shown in Figure 3.3.

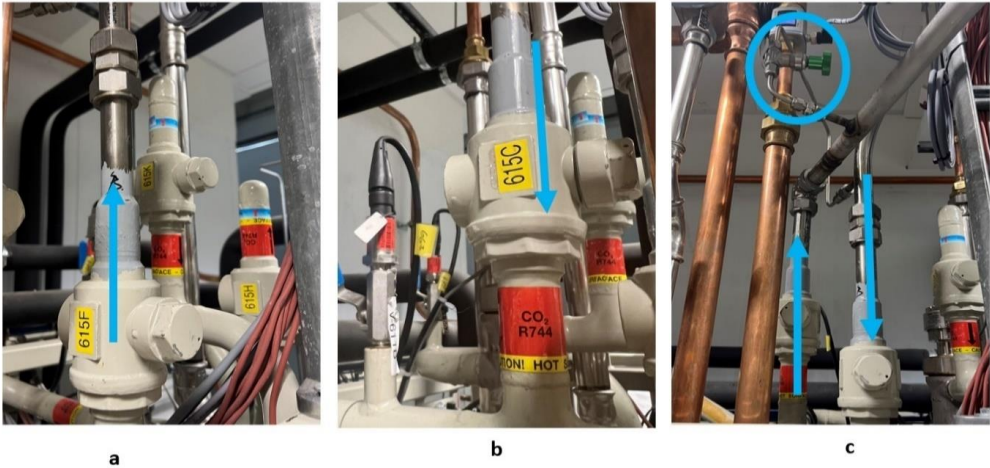


Figure 3.3: (a) Compressor discharge flow towards LP and HP ejectors motive (b) Outlet flow of HP ejector to gas cooler (c) Metering valve between a and b

The third and fourth connections are to and from the liquid receiver. In the third connection, the liquid receiver's flash gas flows towards the LP ejector suction. The fourth connection is for the two-phase CO₂ that PX expands and goes into the liquid receiver. The fifth connection is after the gas cooler and is taken out of the multi-ejector block. Inside the ejector block are the dummy cartridges, which work just like a pipe. The purpose of utilising the ejector block was to use the flow meter upstream. The third (a), fourth (b) and fifth (c) connections to the central system are shown in Figure 3.4.

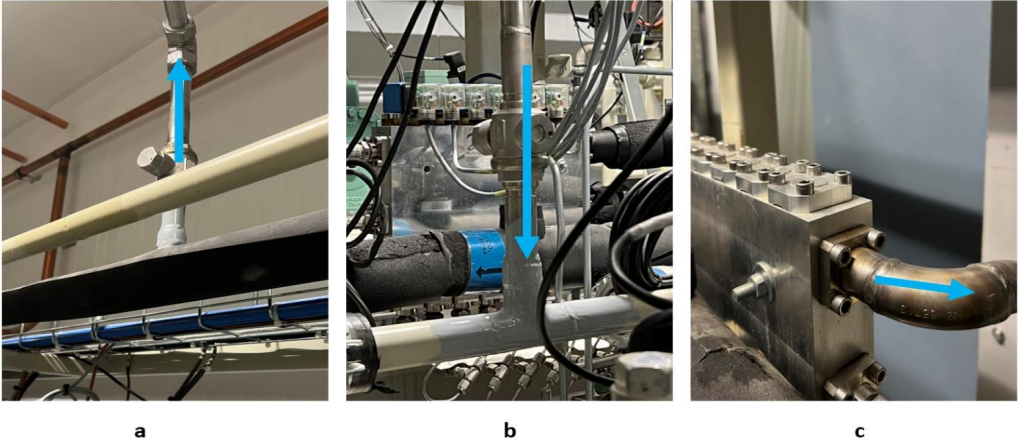


Figure 3.4: (a) Flash gas flow towards LP ejector suction (b) Two-phase flow after expansion from PX (c) Gas cooler outlet flow towards ejector

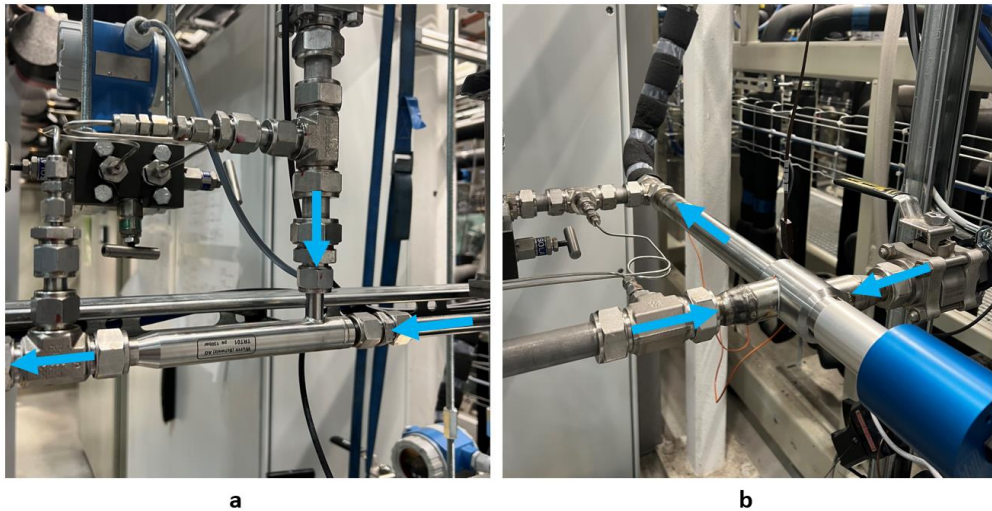


Figure 3.5: (a) LP ejector (b) HP ejector with motor to control motive needle

The LP and HP ejectors are shown in Figure 3.5. The arrows represent the directions, suction, motive, and outlet flow. The LP ejector is of fixed geometry, but the HP ejector has a motor which can control the motive flow.

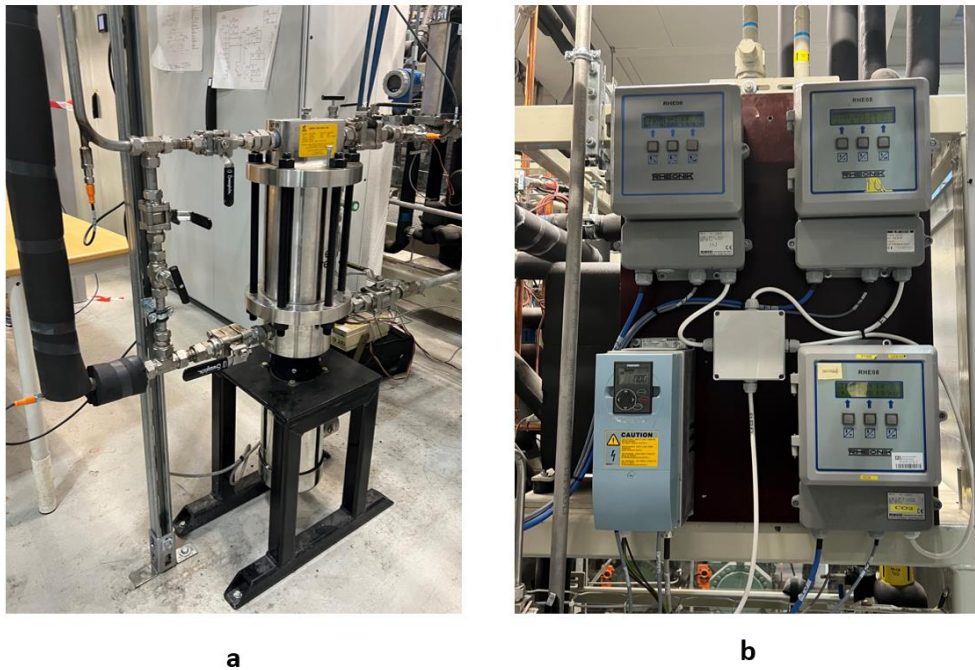


Figure 3.6: (a) Pressure exchanger (PX) with four ports (b) VSD for PX motor and Flow meters transmitter

The energy meter was utilised to obtain the power usage of the PX motor. The differential pressure sensor and energy meter are shown in Figure 3.7.

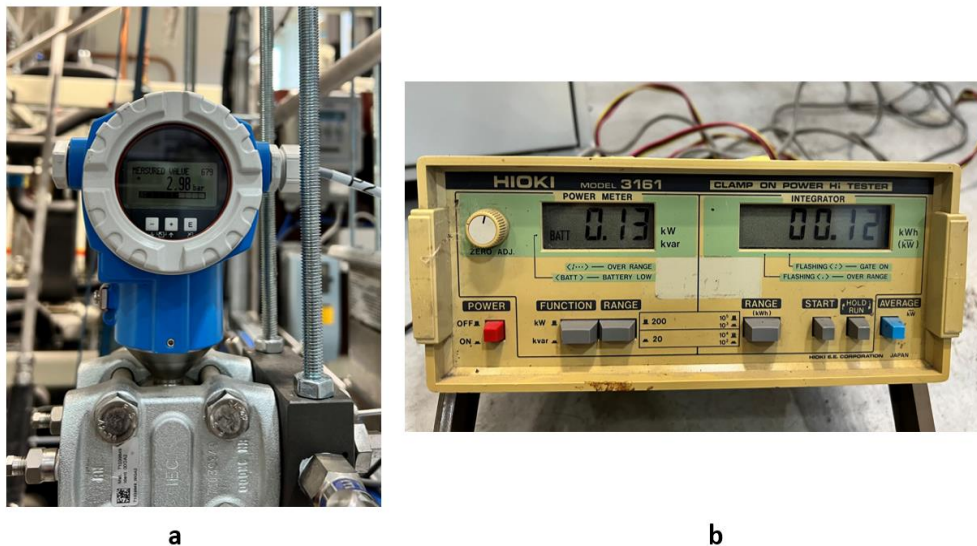


Figure 3.7: (a) Differential pressure sensor (b) Energy meter for PX motor

The simplified P&ID and state point diagram of the PX experimental configuration is shown in Figure 3.8. The components (LT evaporators, LT compressors, etc.) not used for testing are excluded from the P&ID. The evaporation happens from points 9 to 10 in $EVAP_{MT}$, and there are five MT evaporators in addition to $EVAP_{AC,1}$ (Figure 3.2). It can be linked to the MT section depending on the evaporation capacity. After gaining some superheat in IHX 2, it becomes point 11. As the FGV stream (point 12) mixes with the evaporator stream, it gives a new state point for compressor suction: point 1. After compression (point 2), the high-pressure and temperature CO_2 stream becomes the motive flow of EJ_{HP} and EJ_{LP} . The LP ejector suction (point 6) takes flash gas from the liquid receiver tank, and it combines with the LP ejector motive flow. The LP ejector increases the pressure of flash gas (point 13), becoming $PX_{LP,in}$. After gaining pressure inside PX, the stream comes out at higher pressure (point 14), which is the suction of the HP ejector. After combining with motive flow and increment in pressure, it becomes point 3 at the gas cooler pressure. The GC_2 maintains the set point temperature of CO_2 by adjusting the water flow; now, it is state point 4. There is no use of IHX1 because the flash gas does not flow on the other side of IHX1, and the main flow passes without any heat exchange. Point 4, after expansion inside PX, becomes a two-phase fluid and gets a state point 5.

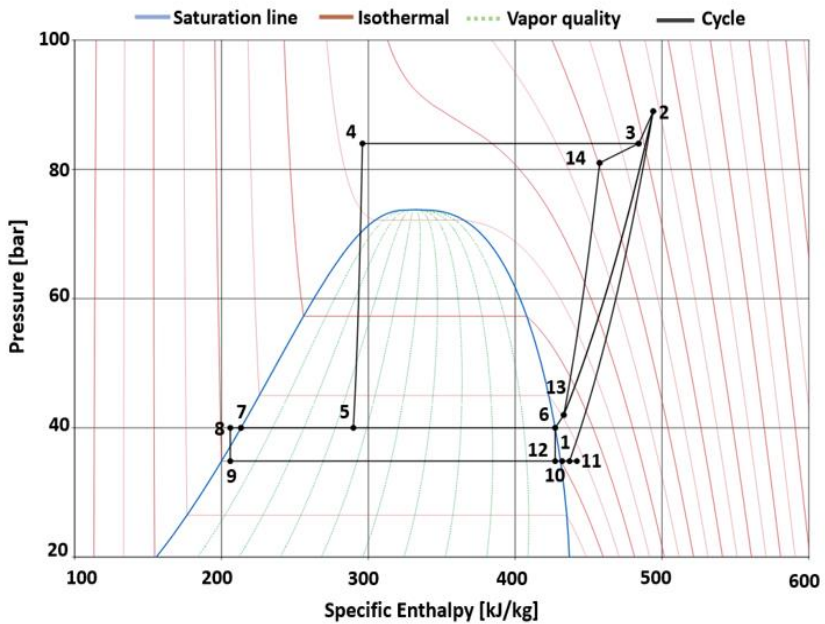
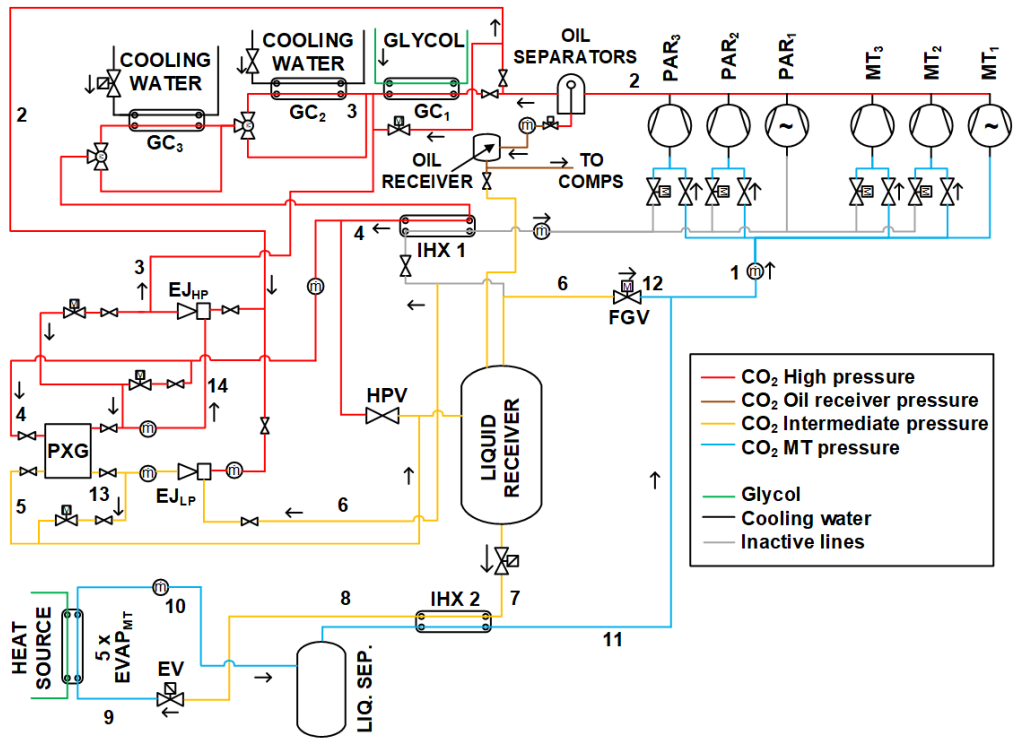


Figure 3.8: Schematic and state point diagram of the PX experimental configuration

3.3 Experimental control strategy of PX mode

Integrating the PX configuration with the main system is designed to seamlessly transition between standard booster and PX modes using the Danfoss controller settings. The system first operates in standard booster mode and is later adjusted to activate the PX mode. In Figure 3.2, the evaporator's heat source is a glycol loop, where GC_1 typically rejects heat into the glycol tanks. However, in PX mode, GC_1 remains inactive. To compensate, the two glycol tanks are equipped with eight electric heaters, totalling 48 kW. Ensuring the system operates in booster mode for an adequate duration is crucial to accumulate heat in the tanks, facilitating smooth PX mode operation with a 70 kW evaporation load. As the accumulated heat reduces, the glycol pump's flow rate increases to maintain a constant evaporation load until it reaches 96 l/min. Beyond this point, the load starts decreasing. During experiments, efforts were made to ensure the load remained consistent with the 70 kW set point.

After the tanks have accumulated sufficient heat, open the valve, directing the gas cooler flow towards PX HP_{in} . This action will result in the flow division between PX and HPV. Subsequently, the valves for LP ejector suction and HP and LP ejector motives are opened while the ball valve is partially closed upstream of GC_1 . It is crucial to allow a time margin for the GC_2 pump to adjust and dissipate the accumulated heat effectively. Enhancing this transitional period ensures a smoother operational shift.

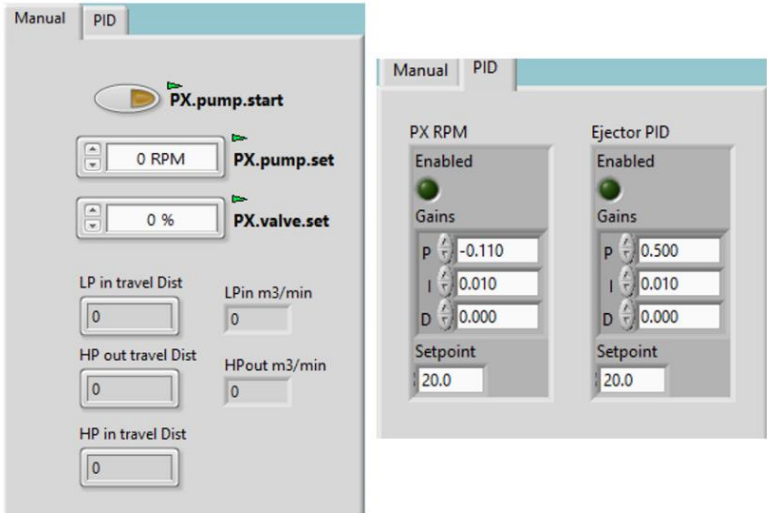


Figure 3.9: Controlling of PX RPM and HP ejector needle. Manual controls (Left), PID controllers (Right)

Initiate the RPM of the PX to shift the flow from HPV gradually. Subsequently, the ball valve must be fully closed upstream of GC₁, and the suction of the HP ejector must be opened. Activate the PID controller of the PX motor to regulate RPM and manually close the HPV using the Danfoss controller. This ensures that the entire GC flow is directed towards PX. The RPM of the PX motor serves as an equivalent to the opening of HPV, maintaining optimal gas cooler pressure by adjusting RPM based on GC outlet temperature input. The PID controller for PX motors follows the same optimum pressure curve (2 bar lower) as the Danfoss HPV controller.

Additionally, control over the motive needle opening percentage is achievable, as the HP ejector is equipped with a motorized motive needle. The manual and PID controls are illustrated in Figure 3.9. In the PX configuration, control over the compressor discharge pressure primarily lies with the HP ejector motive and the metering valve, establishing connections before and after GC₁. This setup ensures effective system management during the PX configuration.

The FGV and the LP ejector suction effectively regulated the liquid receiver pressure. Theoretical analysis revealed that the PX alone could not handle the flash gas efficiently, necessitating the inclusion of an FGV to facilitate its operation. The FGV and LP ejector combination proved effective in maintaining the required pressure in the liquid receiver tank. The compressors consistently maintained the evaporation suction pressure set point, showcasing their adaptability. The compressor group exhibited flexibility, with the capability of five compressors to operate in booster mode. Compressors could be selectively turned on or off to optimise system performance depending on factors such as GC outlet temperature, suction pressure, and cooling capacity.

4 Comparison of theoretical and experimental results

4.1 Boundary conditions

For the theoretical work, the constant evaporation capacity of 60 kW was investigated in all cases at an evaporating temperature of 0 °C. Gas cooler outlet temperatures are systematically adjusted within the range of 33 °C to 37 °C, with an incremental step size of 1 °C. Optimized gas cooler pressures are employed, aligning with the outlet temperature for each case. Notably, the compressor outlet pressure differs from the gas cooler pressure uniquely for the CO₂-PX configuration, a crucial aspect of this setup. This pressure differential facilitates the transfer of flash gas from the PX outlet to the gas cooler pressure through the HP ejector. The selection of the compressor discharge pressure is crucial to ensure the requisite motive flow for both ejectors, a parameter intricately linked to the flash gas handling capability of the PX. Deviation from the reported discharge pressure results in inadequate refrigerant flow for the motive flow of both ejectors if reduced or an excess of refrigerant flow that diminishes the COP if increased. Iterative processes were conducted to determine the optimal compressor discharge pressure and the percentage of flash gas bypassing through the Flash Gas Bypass Valve (FGBV) that satisfies the ejectors' motive flows and the PX's flash gas compression capacity.

Table 4.1: Compressor outlet and gas cooler pressure for theoretical work

Parameters	GC outlet (33 °C)	GC outlet (34 °C)	GC outlet (35 °C)	GC outlet (36 °C)	GC outlet (37 °C)
Compressor outlet pressure, PX cases (bar)	86.5	89.5	91.5	94.5	97.5
GC pressure all cases (bar)	84	87	89	92	95
LP ejector efficiency (%)	20	20	20	20	20
HP ejector efficiency (%)	20	20	20	20	20

The experimental work is performed at the GC outlet temperatures of 33 °C, 35 °C, 37 °C and 38 °C, evaporation temperature of 0 °C and liquid receiver pressure of 40 bar. PX device is mainly advocated for the transcritical operation to recover expansion work. For experimental

work, the minimum GC outlet temperature (33 °C) was selected to keep away from the critical point and the maximum (38 °C) was selected considering the operating capacity of the system. Initially, the experiments were performed at 60 kW evaporation capacity, but as the PX is typically designed for systems with 60 kW or higher capacity, the investigated capacity was raised to 70 kW.

4.2 Ejectors

The LP and HP ejectors for the PX theoretical cases were investigated for three different receiver pressures of 40, 45 and 50 bar and gas cooler outlets from 33 °C to 37 °C. Figure 4.1 shows the entrainment ratio of LP and HP ejectors. The entrainment ratio of the HP ejector is comparatively lower than the LP ejector and is similar to the typically employed ejectors for CO₂ refrigeration systems. The HP ejector entrainment ratio deviations are not prominent in various GC outlet and receiver cases. However, the LP ejector case shows prominent variations in various cases. The LP ejector entrainment ratio is very high because of the high-pressure difference between the suction and motive side, and the pressure lift is only 2 bar.

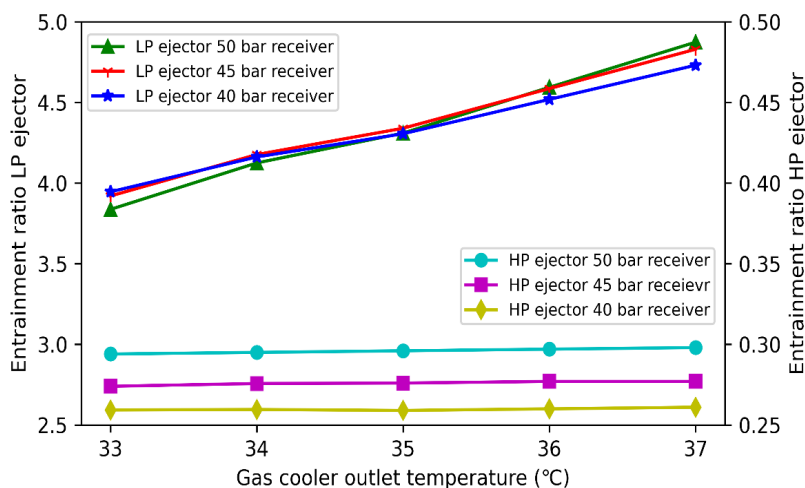


Figure 4.1: Theoretical case entrainment ratio of LP and HP ejector

Table 4.2: Sensitivity analysis of LP and HP ejector efficiency (2 bar lift) for theoretical cases at 35 °C GC outlet and 40 bar receiver pressure

	Original case	Case 2	Case 3
LP ejector efficiency (%)	20	10	30
HP ejector efficiency (%)	20	10	30
Compressor discharge pressure (bar)	91.5	94	90.7
COP	2.92	2.73	2.99

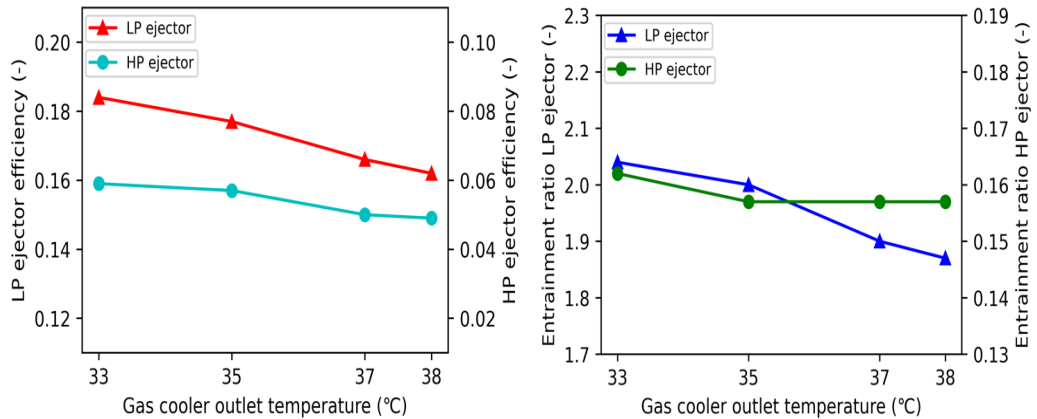


Figure 4.2: Experimental HP and LP ejectors efficiency and entrainment ratio

The sensitivity analysis of the HP and LP ejector efficiency for the theoretical cases is shown in Table 4.2. It shows that higher efficiency will reduce the compressor work and improve the COP. Figure 4.2 shows the experimental results of LP and HP ejectors. It shows that the ejector's efficiencies change with various GC outlet temperatures. The LP ejector efficiency is decreasing around 2% (18% to 16%) from GC outlet temperatures of 33 °C to 38 °C, contrary to the fixed assumed efficiency of 20% in theoretical investigations. It indicates a small difference between the assumed and experimental LP ejector efficiency. However, the difference in the entrainment ratio of the LP ejector is prominent for the LP ejector, which is correlated with the efficiency and geometry of the ejector. The HP ejector is not performing as expected, and its efficiency of 5% is very low. The HP ejector entrainment ratio is almost half that of the theoretical work, and the trend is similar to that of the LP ejector. However, both ejectors have successfully verified PX's concept and operation.

The pressure lift of the LP and HP ejectors is presented in Figure 4.3. The LP and HP case 1, 2, 3 and 4 shows the cases of GC outlet temperatures of 33 °C, 35 °C, 37 °C and 38 °C. The desired pressure lift for both ejectors is between 2 and 3 bar, but the experimental pressure lifts are higher. The LP ejector lift is between 3.5 and 4.2 bars, but the HP ejector lift is unexpectedly high (5.5 to 6.1 bar). The high-pressure lift of the HP ejector affects the other boundary conditions, especially the compressor discharge pressure, contrary to the 2.5 bar in the theoretical investigations. The high-pressure difference between the compressor and gas cooler leads to high compression work and ultimately reduces the COP of the system. The design of the HP ejector is crucial for improving performance in PX configuration. Using the motive needle and various motive nozzles, it has been observed that it is possible to mitigate pressure lift and reduce the pressure differential between the compressor discharge and the gas cooler. Simultaneously, the design of the diffuser emerges as a crucial factor in preventing reverse flow. A detailed CFD analysis focusing on individual components of the HP ejector becomes imperative to achieve the desired outcomes and optimize the system performance. Currently, the HP ejector is a compromise solution. Even the revised design used 'off the shelf'

components. This inevitably impacted its performance, as it was never intended for such atypical operating conditions. The most substantial enhancement in performance would come from a design supported by CFD. In this approach, all geometric components (flow channels) would be tailored specifically to the unique conditions imposed by the system, particularly the minimal pressure differential between the motive nozzle inlet and outlet.

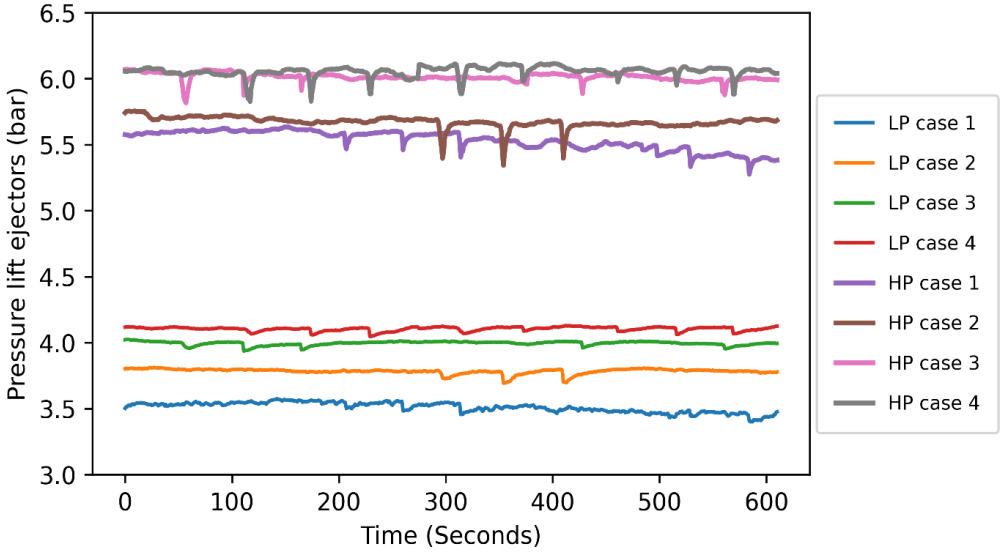


Figure 4.3: Experimental LP and HP ejectors pressure lift

As a general the experiments were stable, but some disturbances occurred. Most of the fluctuations in the experiments were attributed to the instability caused by PX, though some were related to the experimental system as well. PX was responsible for maintaining the GC pressure, and slight changes in RPM affected the GC pressure. This, in turn, influenced the compressor discharge pressure and the HP ejector pressure lift and suction flow. However, this issue might be resolved by introducing an appropriate bandwidth for the controller. Although the compressor maintained the evaporator pressure well, minor fluctuations were still observed.

4.3 PX pressure lift

The theoretical and experimental pressure lift of flash gas by PX is shown in Figure 4.4 and Figure 4.5, respectively. In theoretical and experimental cases, the PX successfully lifts the flash gas from the LP ejector outlet pressure to the HP ejector suction pressure.

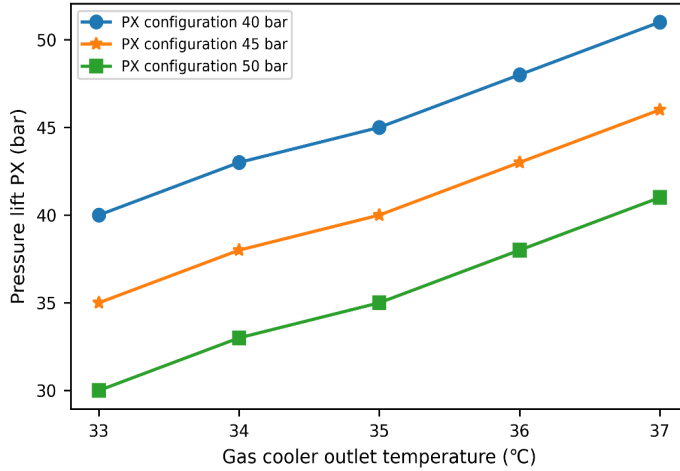


Figure 4.4: Theoretical PX pressure lift of flash gas

Following existing literature and CFD analyses of the PX, it has been determined that the PX pressure lift of the flash gas should range from the receiver pressure (1-2 bar higher) to the gas cooler pressure (1-2 bar lower) while maintaining the appropriate quantity of flash gas. It is crucial to note that exceeding the PX handling capacity can diminish the pressure lift, potentially leading to unmatched PX travel distances. Conversely, utilizing a flash gas amount below the PX handling capacity undermines the PX's performance potential.

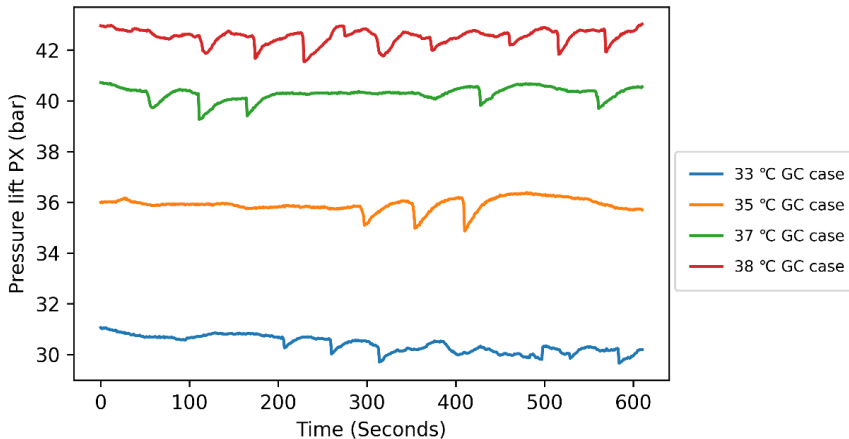


Figure 4.5: Experimental PX pressure lift of flash gas

Discrepancies between theoretical predictions and experimental results can be attributed to various factors. Firstly, an additional pressure loss occurs from the gas cooler outlet to the PX high-pressure inlet. The flow passed through unnecessary components, notably the multi-ejector block with dummy cartridges, introducing an extra pressure loss ranging from 1 to 2.5 bar, contingent on the flow rate or capacity. The second contributing factor is the restriction imposed on the correct amount of flash gas due to the fixed geometry of the low-pressure LP ejector. The third factor pertains to the compression performance of the PX, which will be discussed in the subsequent section. These identified reasons collectively contribute to the observed differences in pressure lift between theoretical predictions and experimental outcomes.

4.4 Temperatures around PX and expansion quality

The calculated and experimental temperature values are shown in Figure 4.6 and Figure 4.7, respectively. The LP ejector outlet temperature, which is the inlet temperature of PX LP_{in}, has a deviation of around 7 °C (between theoretical and experimental work), and the difference is the outcome of low efficiency and slightly higher motive temperature in the experimental work. The most significant deviation is for the PX compression temperature, which is very low compared to the theoretical estimation. The low temperature highlights the fact that there is heat or thermal transport within PX during flash gas compression. The compression heat dissipates within PX and affects the vapour quality of the PX expansion. Several experiments and verification scenarios have been performed with the current configuration to see the HP_{out} temperature. It is observed that this temperature is around 5 °C higher than the HP_{in} temperature.

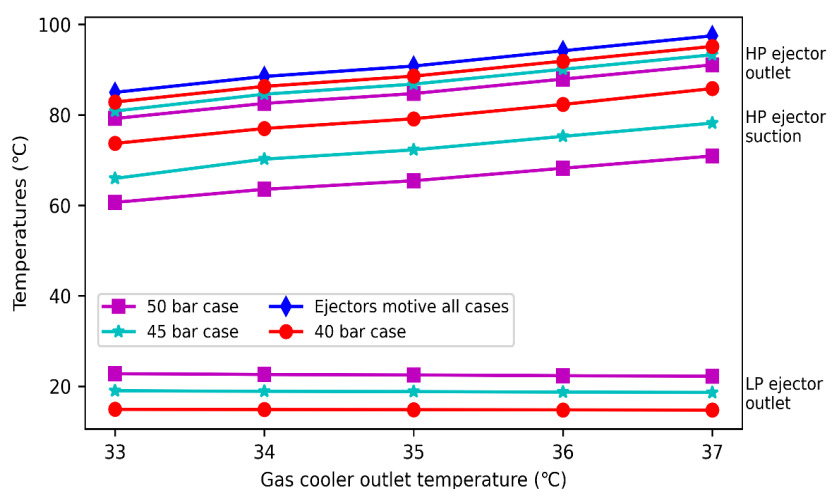


Figure 4.6: Theoretical temperatures around PX



Figure 4.7: Experimental PX ports (inside) temperatures of 35 °C case

The effect of the PX compression temperature is shown in Figure 4.8. As the compression temperature decreases, the compression line undergoes a leftward shift, deviating from the expected path of isentropic efficiency. This deviation directly impacts the expansion quality of two-phase CO_2 during the expansion process. Notably, the expansion line exhibits a deviation from the anticipated isentropic expansion behaviour, resembling more closely an isenthalpic expansion and, in some instances, displaying even worse behaviour. Despite these deviations, using a PX device remains advantageous due to the benefits associated with the free compression of flash gas.

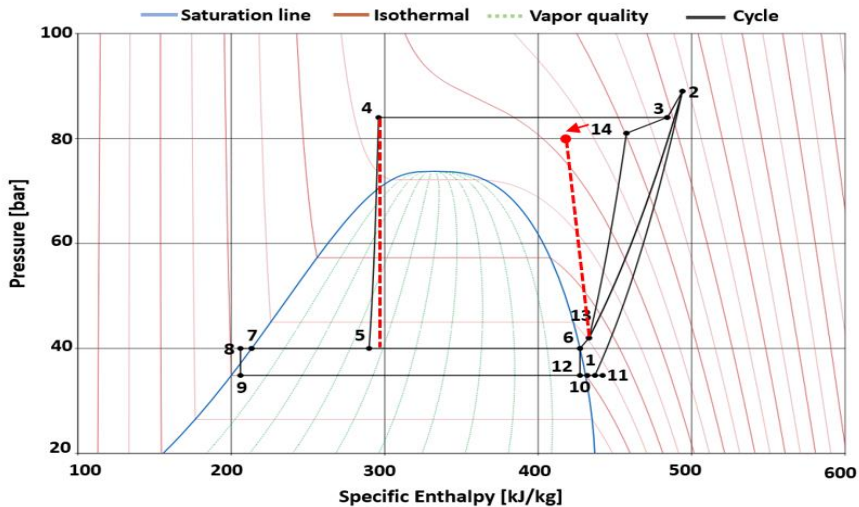


Figure 4.8: Ph diagram showing the effect of PX low compression temperature

Table 4.3: Sensitivity analysis of PX compression and expansion efficiency of theoretical cases

	Original case	Case 2	Case 3
PX compression efficiency (%)	70.4	100	58
PX expansion efficiency (%)	82.4	58	100
Compressor discharge pressure (bar)	91.5	91.3	91.7
COP	2.92	2.87	2.94

Table 4.3 presents a sensitivity analysis examining the impact of both PX compression and expansion efficiency. Notably, the findings underscore that a higher expansion efficiency holds more significance for COP improvement than a higher compression efficiency. Lower compression efficiency results in elevated PX compression discharge temperatures, necessitating a greater pressure difference for the HP ejector to lift an equivalent flow. Conversely, a higher PX expansion efficiency enhances vapour quality, increasing the liquid content and reducing the required refrigerant flow for the same evaporation capacity.

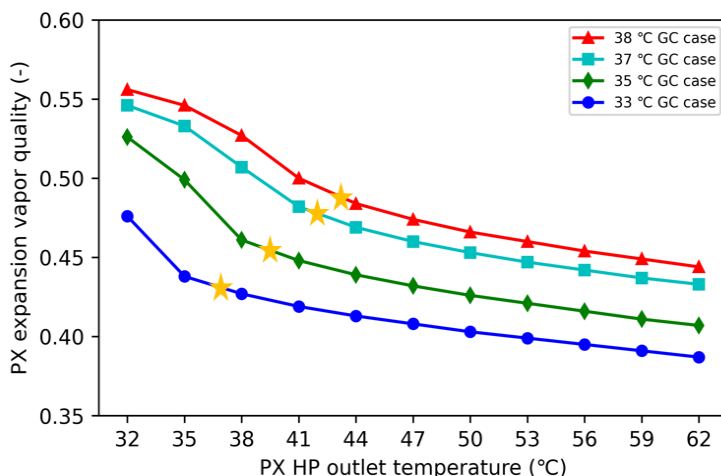


Figure 4.9: PX expansion quality (experimental points with orange stars)

Figure 4.9 illustrates the expansion quality of the PX expansion process. Notably, the expansion quality demonstrates a high sensitivity to slight increases in temperature, particularly in the initial few degrees Celsius above the gas cooler outlet temperatures. The orange stars on the graph represent experimental data points, while the remaining points are computed using the energy balance equation (Equation 5). All experimental parameters were

held constant throughout these calculations, except for the PX high-pressure outlet temperature, which served as the variable of interest. This approach facilitates a focused examination of the impact of varying PX high-pressure outlet temperatures on the expansion quality.

A parallel compression experiment was conducted concurrently with the PX system to validate the expansion quality of the PX. The upstream section of the parallel compressor was equipped with a flow meter, in contrast to the flash gas valve, which lacked a flow meter. In this experiment, the overall vapour flow was divided into the suction flow of the LP ejector and the flow through the parallel compressor. This division of total vapour flow indicated the expansion quality, thereby validating the expansion quality calculated theoretically. The flow rates from the verification experiment are depicted in Figure 4.10, offering a visual representation of the experimental findings.

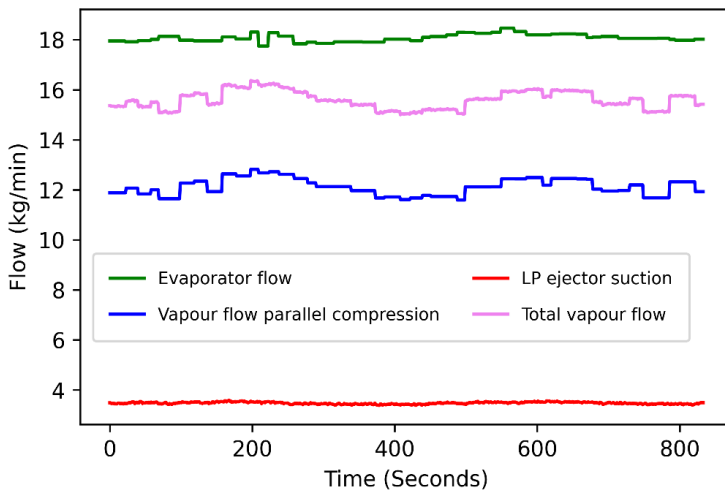


Figure 4.10: Experiment in parallel compression mode with PX to verify PX expansion quality

4.5 Experimental results

The experimental results of the four cases of PX experiments with relevant readings are shown in the following tables. Each of these experiments spanned a duration of 10 minutes, and additional readings are provided in Appendix A.5 for further reference and comprehensive analysis.

Table 4.4: Experimental results of PX 33 °C case for 10 Seconds

Time Seconds	Ejectors motive pressure bar	GC pressure bar	LP ejector DP bar	HP ejector DP bar	PX DP bar	PX HP _{out} C	PX LP _{in} flow kg/min	PX HP _{out} flow kg/min	PX RPM RPM
1	89.76	81.76	3.50	5.58	31.06	36.44	5.08	5.29	708.72
2	89.76	81.72	3.51	5.57	31.02	36.44	5.09	5.29	706.48
3	89.76	81.72	3.51	5.57	31.02	36.44	5.09	5.29	706.48
4	89.78	81.76	3.53	5.57	31.05	36.44	5.13	5.29	708.45
5	89.76	81.73	3.53	5.57	31.03	36.45	5.11	5.27	708.15
6	89.79	81.74	3.52	5.57	31.05	36.34	5.09	5.27	708.21
7	89.74	81.76	3.53	5.57	31.05	36.44	5.12	5.27	709.09
8	89.76	81.71	3.54	5.57	31.01	36.45	5.13	5.27	709.46
9	89.78	81.72	3.53	5.57	31.01	36.34	5.08	5.31	711.30
10	89.78	81.72	3.53	5.57	31.01	36.34	5.08	5.31	711.30

Table 4.5: Experimental results of PX 35 °C case for 10 Seconds

Time Seconds	Ejectors motive pressure bar	GC pressure bar	LP ejector DP bar	HP ejector DP bar	PX DP bar	PX HP _{out} °C	PX LP _{in} flow kg/min	PX HP _{out} flow kg/min	PX RPM RPM
1	95.39	87.09	3.80	5.74	36.00	39.72	5.36	5.62	696.85
2	95.38	87.12	3.81	5.75	36.02	39.72	5.31	5.65	696.77
3	95.35	87.08	3.80	5.75	35.98	39.72	5.31	5.66	696.87
4	95.36	87.11	3.80	5.75	36.01	39.71	5.29	5.65	696.99
5	95.36	87.11	3.80	5.75	36.01	39.71	5.29	5.65	696.99
6	95.39	87.11	3.81	5.75	36.02	39.65	5.38	5.67	697.17
7	95.39	87.10	3.81	5.75	36.00	39.65	5.36	5.66	695.82
8	95.37	87.10	3.81	5.75	36.00	39.65	5.36	5.66	695.82
9	95.39	87.10	3.80	5.75	36.01	39.65	5.26	5.66	695.72
10	95.38	87.12	3.80	5.76	36.02	39.65	5.29	5.67	696.09

Table 4.6: Experimental results of PX 37 °C case for 10 Seconds

Time Seconds	Ejectors motive pressure bar	GC pressure bar	LP ejector DP bar	HP ejector DP bar	PX DP bar	PX HP _{out} C	PX LP _{in} flow kg/min	PX HP _{out} flow kg/min	PX RPM RPM
1	100.99	92.32	4.02	6.07	40.72	42.13	5.46	5.59	624.22
2	101.01	92.31	4.02	6.07	40.71	42.03	5.41	5.59	624.33
3	100.98	92.32	4.02	6.07	40.72	42.03	5.43	5.59	624.24
4	100.96	92.28	4.02	6.07	40.68	42.03	5.39	5.60	624.32
5	100.96	92.28	4.02	6.07	40.68	42.03	5.39	5.60	624.32
6	100.95	92.28	4.02	6.06	40.70	42.02	5.41	5.59	624.40
7	100.96	92.28	4.02	6.07	40.69	41.94	5.40	5.59	623.96
8	100.96	92.27	4.02	6.07	40.68	41.94	5.44	5.61	624.23
9	100.95	92.25	4.02	6.07	40.66	41.94	5.46	5.60	624.58
10	100.94	92.25	4.02	6.07	40.66	41.94	5.45	5.60	624.21

Table 4.7: Experimental results of PX 38 °C case for 10 Seconds

Time Seconds	Ejectors motive pressure bar	GC pressure bar	LP ejector DP bar	HP ejector DP bar	PX DP bar	PX HP _{out} C	PX LP _{in} flow kg/min	PX HP _{out} flow kg/min	PX RPM RPM
1	103.26	94.64	4.12	6.06	42.96	43.01	5.52	5.75	617.18
2	103.27	94.63	4.12	6.05	42.94	43.02	5.48	5.70	618.13
3	103.27	94.63	4.12	6.05	42.94	43.02	5.48	5.70	618.13
4	103.25	94.65	4.12	6.06	42.96	43.01	5.46	5.69	617.76
5	103.24	94.60	4.12	6.06	42.92	43.01	5.46	5.71	618.40
6	103.27	94.61	4.12	6.06	42.92	43.01	5.48	5.70	618.27
7	103.27	94.61	4.12	6.06	42.92	43.01	5.48	5.70	618.27
8	103.28	94.63	4.12	6.06	42.94	43.01	5.46	5.73	618.68
9	103.29	94.66	4.12	6.06	42.96	43.01	5.48	5.76	618.13
10	103.29	94.65	4.12	6.06	42.96	43.14	5.43	5.73	618.05

4.6 Uncertainty analysis

The measuring instruments' experimental uncertainties were calculated using the following equation.

$$u(T, P, DP, m) = \sqrt{\frac{\sum_{i=1}^N (x_i - \bar{x})^2}{N-1}} \quad (24)$$

Where u is the uncertainty, x_i is the individual value in the measured data, \bar{x} is the mean value, and N is the number of measured points. The total measurement uncertainty is the root sum square of the sensor and steady-state deviation. The ejector's efficiency combined uncertainty was calculated using the propagation of uncertainty principle described by Apera et al. [59]. A coverage factor of 2 was used in the uncertainty propagation calculation, corresponding to the confidence level of 95%. The entrainment ratio uncertainty is written as follows:

$$u(\phi) = \sqrt{\left(\frac{\partial \phi}{\partial m_{suction}}\right)^2 u(m_{suction})^2 + \left(\frac{\partial \phi}{\partial m_{motive}}\right)^2 u(m_{motive})^2} \quad (25)$$

The complete equation of ejector uncertainty follows the same procedure described in equation 26. A complete python script for ejector efficiency uncertainty calculation is attached in Appendix A.

$$u(y) = \sqrt{\sum_{i=1}^N \left(\frac{\partial F}{\partial x_i}\right)^2 \cdot u(x_i)^2} \quad y = F(x_1, x_2, \dots) \quad (26)$$

5 Summary of the research work

This chapter comprehensively summarises the research conducted throughout the doctoral work. It is organised into distinct sections aligned with an individual article; each section highlights the key points extracted from its article. These articles contribute to achieving the research objective of the doctoral work. The first article is dedicated to the theoretical work and provides a foundational framework for laboratory work. The second article is completely focused on the experimental results. The third article reviews and compares the performance of natural refrigerants. The summary of the articles discussed in this chapter is meant to describe and discuss the key points briefly. Complete articles are attached in the appendix.

5.1 Journal paper 1: Thermodynamic analysis of rotary pressure exchanger and ejectors for CO₂ refrigeration

Abstract: *Natural refrigerant CO₂ has become a viable choice for refrigeration units for land-based and offshore applications due to its environment-friendly nature and compactness. The CO₂ transcritical cycle allows operating in colder climates and in elevated ambient temperature conditions and with significant heat recovery. However, the energy efficiency of the system suffers at higher heat rejection conditions mainly due to expansion losses. This work theoretically investigates and proposes the implementation of a new expansion work recovery device, a pressure exchanger (CO₂-PX), for the transcritical CO₂ cycle. The numerical models are developed in the Engineering Equation solver (EES) to compare the performance of CO₂-PX configuration with standard booster-, parallel-, and ejector- configurations for various conditions. The analysis is carried out for the evaporation temperature of 0 °C and the gas cooler outlet temperature of 33 °C to 37 °C. The results indicate that the coefficient of performance (COP) is improved by 17.7-23.5%, 16.3-20.3%, and 2.4-5.5% to the standard booster, parallel and ejector configurations, respectively, at the investigated conditions.*

This journal article is dedicated to the thermodynamic analysis of the standard booster, parallel and ejector configurations of the CO₂ transcritical system. The three investigated systems are compared with the newly introduced PX integration concept with two novel ejectors. The four investigated system layout and their Ph diagrams are shown in Figure 5.1.

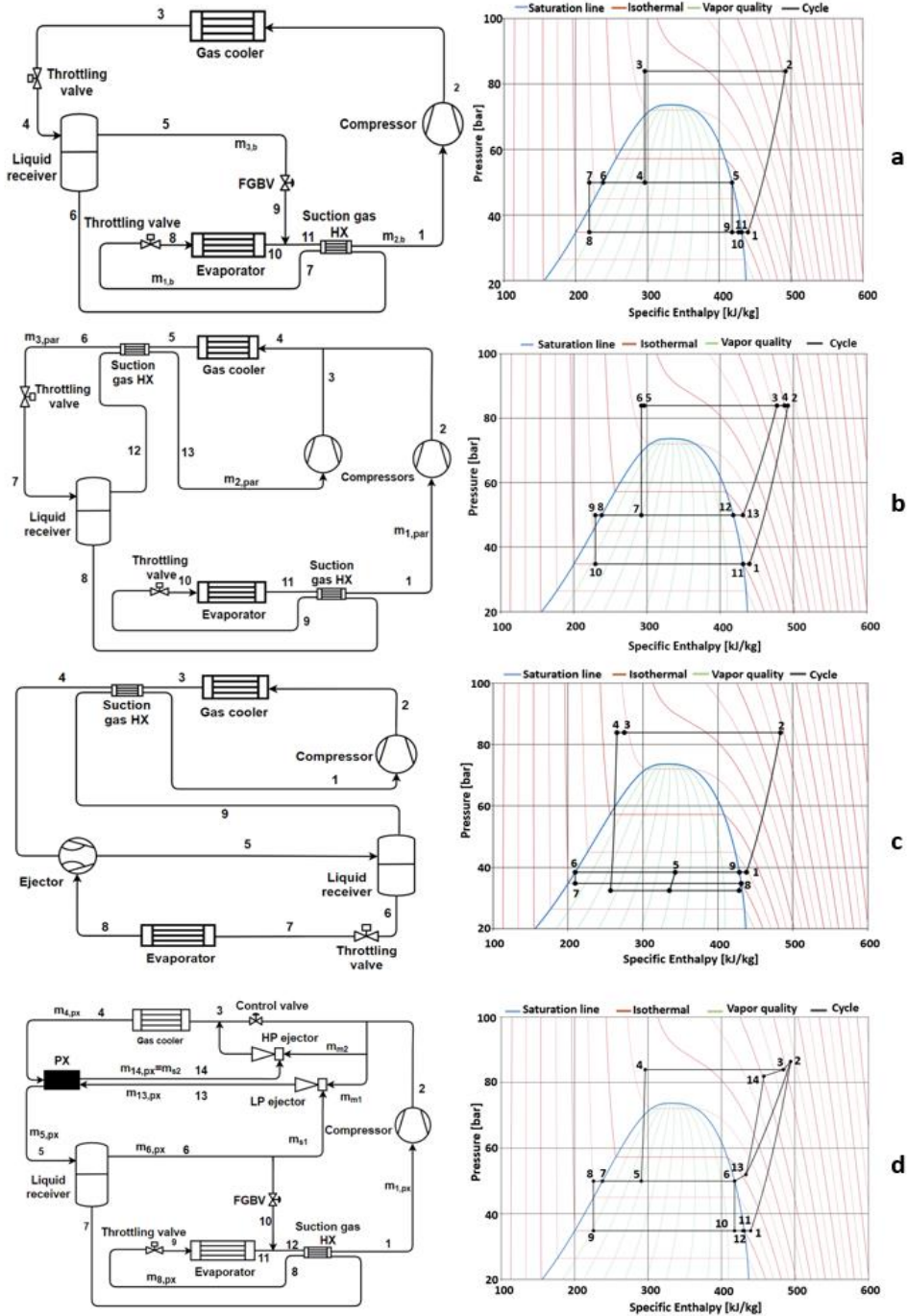


Figure 5.1: Four configurations of CO₂ transcritical system (a) Standard booster (b) Parallel compression (c) Ejector configuration (b) PX integration concept with two booster ejectors

The article's introduction section provides a review of the literature on CO₂ transcritical expansion work recovery methods. Subsequently, a detailed discussion of the PX's internal mechanism and working principle is presented. Towards the end of the introduction, a novel PX integration concept is introduced, visually represented in Figure 5.1. In the methods and data section, the operational aspects of the four configurations are thoroughly discussed. The mathematical modelling section includes all the necessary equations for conducting the calculations. The design conditions and PX simulation flow chart section outlines the boundary conditions for numerical modelling and the flow chart for PX case calculations. The results and discussion section covers various aspects, including the PX efficiency curve, COP analysis for different configurations, PX work recovery potential, flash gas bypass, LP and HP ejectors, exergy efficiency, and temperatures around the PX, all presented through plotted data. The key points of Journal Article 1 are summarized as follows, emphasising the PX case.

PX efficiencies and COP: The PX efficiencies are determined through an iterative process, indicating that compression and expansion efficiencies fall within the range of 58 to 100%. However, moderate efficiencies were used for thermodynamic analysis. The COP analysis demonstrates that, under the investigated conditions, the PX case can surpass the ejector configuration by 2.4 to 5.5%.

PX work recovery and flash gas: The PX is good at recovering expansion work, and the recovered work falls within the range of 11.3 to 18.4% of the main compression work. However, under the investigated conditions, it is essential to implement a flash gas bypass since the PX cannot handle all the flash gas.

LP and HP ejectors: The efficiency of both LP and HP ejectors plays a crucial role in enhancing the COP of the PX case. Both ejectors are distinctive in their ability to provide only a 2-bar pressure lift. Notably, the LP ejector's entrainment ratio is significantly higher than the HP ejector, attributed to the substantial pressure difference between the motive and suction sides.

Temperatures: The LP ejector outlet temperature exhibits minor variations among various gas cooler cases with the same receiver pressure, given the low contribution of motive flow and the assumed constant ejector efficiency. The lower temperature of the LP ejector outlet is advantageous for PX compression, like the superheating effect for a compressor. Consequently, the PX compression temperature serves as an indicator for evaluating the PX compression process.

Exergy analysis: The exergy analysis reveals that the PX case exergy efficiency surpasses the ejector configuration by 7.2%. This disparity is primarily attributed to the superior exergy performance in the expansion process of the PX case.

5.2 Journal paper 2: Experimental investigation of a transcritical CO₂ refrigeration system incorporating rotary gas pressure exchanger and low lift ejectors

Abstract: *Natural refrigerants like CO₂ are playing a significant role in making refrigeration and heat pump systems climate-friendly by slowly phasing out the high global warming refrigerants like hydrofluorocarbons (HFCs). However, the efficiency of a transcritical CO₂ refrigeration system declines significantly when the ambient temperature increases, primarily attributed to the high-pressure lift and the losses incurred during expansion. To remedy this issue, this paper presents a novel rotary gas pressure exchanger (PXG) device, which simultaneously achieves high differential pressure expansion work recovery and the "free compression" of the portion of the flash gas in a compact, rotary machine. For this, a PXG device is designed, fabricated, and tested to achieve free compression of CO₂ over the entire differential pressure of approximately 70 bar between a receiver and a gas cooler. This is one of the highest free-pressure lift provided by any device to date in CO₂ refrigeration. However, there is a small pressure loss of approximately 1-2 bar in the system due to viscous and inertia losses in the piping and in the PXG itself, which needs to be overcome by an external booster device. Results on a baseline PXG integrated system with two low lift booster compressors are presented, which show up to 60 bar free pressure lift and up to 18.2% COP improvement provided by PXG. Additionally, key performance characteristics of the PXG, like the expansion work recovery, the mass boost ratio, direct fluid-to-fluid contact, and no pass-through operation are experimentally quantified. This work also presents a novel method to integrate two low lift ejectors with PXG to eliminate the need for separate low lift compressors. The low lift ejectors are designed, fabricated, and tested in-house, followed by their integration with the PXG device. A new type of transcritical CO₂ refrigeration system is designed to integrate these low lift ejectors with PXG, and experiments are conducted at various evaporator thermal duties and gas cooler exit temperatures, simulating varying ambient temperature conditions. A novel control system to control the gas cooler pressure to optimal thermodynamic levels using PXG rotational speed is demonstrated experimentally. Further, automated control of high-pressure low lift ejector mass flow using an in-built needle design has been successfully demonstrated to optimise PXG mass boost performance. The LP low lift ejector achieved a successful pressure lift of 3.8 bar, and the HP low lift ejector showed a lift of 5.7 bar on the top of 42 bar free pressure lift provided by PXG for up to 5.8 kg/min mass flow delivered by free PXG compression. The results from this study demonstrate that the PXG device provides a significant energy efficiency improvement to the transcritical CO₂ refrigeration system, and the novel low lift ejectors, when integrated with PXG, provide a successful method to maximise PXG's thermodynamic potential.*

This article is specifically dedicated to the experimental investigation of the PX integration concept with two low-lift ejectors (LP and HP). The study is complemented by discussing the experimental results of the PX integration with two booster compressors.

The article's introduction section discusses the performance of three generations of CO₂ transcritical systems. Subsequently, the PX is introduced with detailed explanations of its working mechanism, focusing on the four stages of compression, expansion, and heat transfer. The experimental test facility section provides a comprehensive overview of the SuperSmart CO₂ transcritical facility at the NTNU/SINTEF laboratory, excluding components not involved in the experiments. The PX mode control strategy is explained in this section. The data acquisition and uncertainty section details the accuracy of measuring instruments and the data acquisition method. The important conclusions of the journal article 2 are as follows.

Mass flows around PX: The flow meters were mounted on three ports, and it was observed that there was a minor mixing of flows from HP_{in} to HP_{out}. The various investigated cases show that the mixing ranges from 0.18 to 0.35 kg/min.

Pressure difference between compressor and gas cooler: The pressure difference between the gas cooler and compressor drives the HP ejector to lift the flash gas from the PX compression outlet to the gas cooler. It is observed that the average pressure difference for the investigated cases is in the range of 7.9 to 8.6 bar.

LP and HP ejectors: The LP ejector exhibited a pressure lift in the range of 3.5 to 4.1 bar, an entrainment ratio of around 2, and an efficiency of approximately 17%. In contrast, the HP ejector demonstrated a pressure lift in the 5.2 to 6 bar range, an entrainment ratio of around 0.16, and an ejector efficiency of around 5%. While both ejectors served the purpose of verifying the PX integration concept, the efficiency of the HP ejector impacted the overall performance.

PX pressure lift: The PX successfully lifted the pressure of flash gas. It is observed that the pressure lift of different cases is in the range of 30 to 42 bar.

PX temperatures: The temperatures at the three ports aligned with theoretical expectations, but the temperature at the PX compression outlet deviated significantly. On average, it was 5 °C higher than the GC temperature, emphasizing the existence of flow imbalance and heat transfer within the four streams of PX.

PX system with two booster compressors: The system with two booster compressors at ERI's test facility has a higher evaporation capacity (120 kW), resulting in a lower fraction of leakage/imbalance through the micro axial and radial gaps between the PX rotor and stators. The outcomes demonstrate a PX pressure lift of 40+ bar, reduced compression work, and improved expansion quality. The reported COP lift is 18% compared to a system with a high-pressure valve.

5.3 Journal paper 3: Ultra-Low-Temperature Refrigeration Systems: A Review and Performance Comparison of Refrigerants and Configurations

Abstract: *During the last decade, many industrial and medical applications have shown a requirement for low-temperature-cooling usage (from -40 to -80 °C), which cannot be efficiently obtained via the conventional refrigeration systems usually employed for medium-temperature applications (from 0 to -40 °C). A proper ultra-low-temperature (ULT) refrigeration system design is essential to achieve the desired output. The performance can be maximised via the suitable selection of the configuration and refrigerant for a specific temperature range. This work contributes a detailed overview of the different systems and refrigerants used in ultra-low-temperature applications. Different systems, such as single-stage vapour compression, multi-stage, cascade, auto-cascade, and air refrigeration cycles, are presented and discussed. An energy analysis is then carried out for these systems identifying the optimal system design and refrigerant selection to achieve the highest performance. This paper aims to provide the reader with a comprehensive background through an exhaustive review of refrigeration systems suitable for ultra-low-temperature applications. The effectiveness of these systems is proven numerically, mainly based on the temperature level and purpose of the application.*

This article forms the basis of refrigeration knowledge and behaviour of different natural working fluids. In this article, CO₂ refrigerant work is prominent and can be extended for potential PX integration for low-temperature applications. The main context is dedicated to the literature review and performance comparison of natural refrigerants and hydrocarbons. The different system configurations that can be used for cooling applications in the range of -40 to -80 °C are discussed in this article. The introduction chapter gives a brief review of the refrigerants and configurations. The second chapter performs a detailed study of natural refrigerants, hydrocarbons, and mixtures. Chapter 3 discusses different configurations (multistage, cascade, auto-cascade, and air refrigeration cycle) and their system performances. Their working mechanism is also discussed in that chapter. Chapter 4 comprehensively includes application-targeted system analysis, numerical model validation, and the investigated systems boundary conditions with COP analysis. The systemized outcome of the work is shown in Figure 5.2.

Refrigerants: The suitability of refrigerants is contingent upon the desired cooling temperature. Ammonia and CO₂ exhibit significant potential to address a broad range of applications without the risk of flammability. Propane proves suitable for the high circuit of a cascade system, provided safety standards permit its usage. Ethane, Ethylene, and air emerge as advantageous options for ultra-low temperature cooling, depending on specific criteria.

Compressor efficiency equations: The analysis shows the significance of real compressors' efficiencies equations, considering various factors such as refrigerant, superheat and pressure ratio.

Configurations: The cascade system exhibits remarkable capability to accommodate a broad spectrum of temperatures, ranging from medium to ultra-low applications. Additionally, a two-stage CO₂ system proves suitable for temperatures up to -50 °C. The air refrigeration cycle surpasses other configurations in addressing challenges related to ultra-low temperatures and flammability.

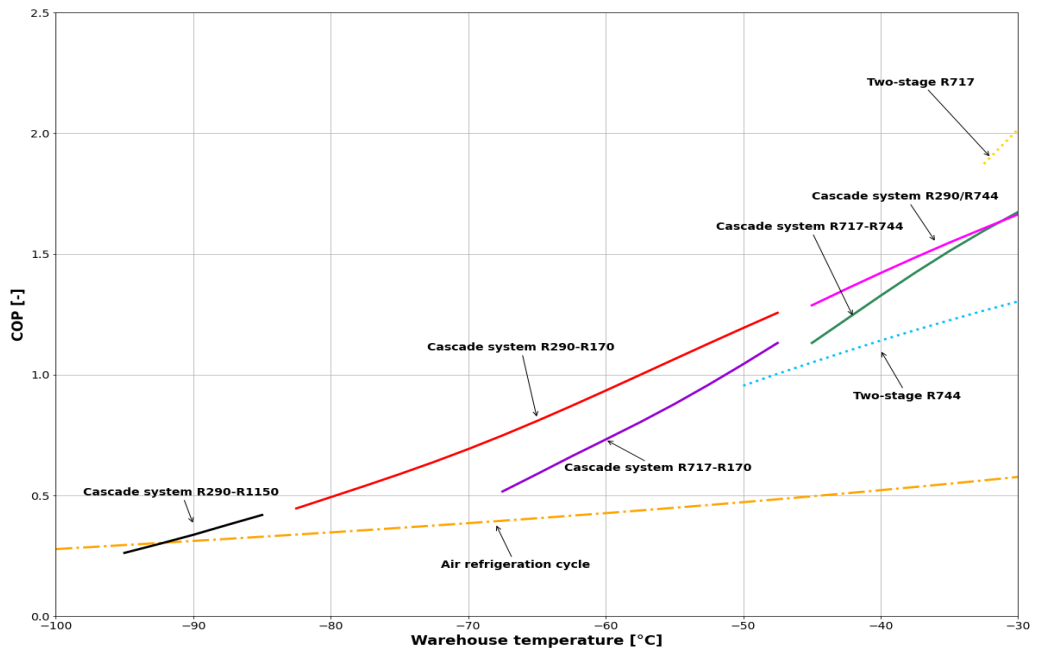


Figure 5.2: COP comparison between air refrigeration cycle, two-stage refrigeration system, cascade refrigeration system using different refrigerants

6 Conclusion and suggestions for further work

6.1 Conclusions

The primary aim of this thesis is to develop and experimentally validate the pressure exchanger integration concept tailored for a CO₂ transcritical system operating in high ambient temperatures. In conjunction with the primary objectives, a literature study was conducted on refrigerants and configurations suitable for low-temperature cooling. This additional effort enhanced the author's understanding of the refrigeration sector. To fulfil the research objectives, numerical investigations were conducted to assess the potential of the PX and formulate an integration concept. This numerical work utilized the Engineering Equation Solver, supplemented by Modelica, particularly in developing two novel ejectors. Following conceptualization, efforts were initiated to retrofit the SuperSmart facility in the NTNU Varmeteknisk laboratory and to fabricate new ejectors. Upon completing the test facility, experiments were conducted to validate the proposed concept. The acquired experimental results underwent meticulous evaluation using Python, and an additional script was devised for ejector uncertainty calculations.

The numerical simulation model, developed using Engineering Equation Solver (EES), was based on the pressure exchanger integration concept. This model helped to predict the system behaviour and anticipate the parameters of different components. Alongside evaluating the PX integration concept, a performance comparison involving standard booster, parallel, and ejector configurations was conducted. The analysis indicated that the PX concept could achieve a 2% to 6% higher performance than the ejector configuration, with the improved Coefficient of Performance (COP) primarily attributed to free flash gas compression. The recovered expansion work increased with a higher-pressure difference between the gas cooler and the receiver, amounting to 11% to 18% of the main compression work. The PX, capable of lifting a portion of the flash gas, necessitated bypassing the remaining amount using a flash gas bypass valve. The role of two booster ejectors within the PX configuration was discussed, emphasizing their impact on flash gas compression. Notably, the LP ejector's entrainment ratio was significantly higher than typical CO₂ ejectors. Exergy analysis revealed a performance estimate approximately 7.2% higher than the ejector configuration. The insights gained from the numerical work proved helpful in establishing the experimental system.

The experimental phase successfully validated the pressure exchanger integration concept employing two booster ejectors. Notably, a flow imbalance, equivalent to an average of 0.25 kg/min, emerged due to differences in travel distance between high-pressure and low-pressure ports. The compressor discharge and gas cooler pressure difference, on average, was 8.3 bar. This successfully confirmed the viability of the concept. However, the high-pressure difference contributed to increased compression work, subsequently impacting overall

performance. Both LP and HP ejectors demonstrated the capability to lift flash gas, achieving averages of 5.7 bar and 3.8 bar, respectively. The efficiencies of LP and HP ejectors were recorded at 17.2% and 5.3%, respectively. Challenges were encountered in the case of HP ejectors, emphasizing the need for precise design enhancements to optimize overall performance. While adjustments could be made to the motive side, the diffuser design posed a significant constraint. The PX exhibited excellent performance in lifting flash gas, with average lifts recorded at 30.4 bar, 35.9 bar, 40.3 bar, and 42.5 bar in four distinct cases. Despite the PX compression temperature registering 5 °C higher than the gas cooler, contrary to higher temperatures in numerical estimations, this discrepancy can be attributed to leakage flow through the bearing and flow imbalances resulting from unmatched travel distances.

The experimental findings from a 120 kW Pressure Exchanger (PX) system featuring two booster compressors at ERI's test facility indicate the PX's superior performance in higher capacity systems. The PX showcases its effectiveness by demonstrating an ability to deliver a pressure lift of 50+ bar and operate with a pressure boost of 1-2 bar. The results underscore the significance of maintaining the desired travel distance between high- and low-pressure streams, ensuring a no-pass-through operation. This optimization contributes to improved vapour quality and higher compression temperatures. Notably, the test results suggest a potential increase in the COP by up to 18% compared to a standard booster system.

6.2 Suggestions for further work

The thesis successfully conducted numerical investigations, developed an experimental setup, and verified the pressure exchanger integration concept for CO₂ transcritical systems. Upon analysing the results, suggestions for the further scope of this work are categorized as follows:

Evaporation capacity: The experimental results from ERI's test facility indicate that the PX operates more effectively at higher capacities. While experiments at NTNU lab were conducted with a 70 kW capacity, there is potential to increase capacity through specific alterations. The limitation on lower capacity was not due to compression capacity or evaporator heat exchanger size; instead, it stemmed from an insufficient heat source. Existing connections of the SuperSmart facility were predominantly utilized to minimize additional costs and time, leading to the bypassing of GC₁ in PX mode. GC₁ dissipates heat in the glycol tanks, and its inclusion in the PX mode could potentially increase evaporation capacity to approximately 85 kW. The glycol tanks are equipped with electric heaters of 48 kW, and enhancing the electric heat capacity could facilitate testing at 85 kW. However, it seems the more cost-effective option is to incorporate GC₁.

PX PID controller: The PID controller, responsible for maintaining gas cooler pressure by adjusting the PX rotor speed, was initially set 2 bar lower than the optimized setpoint of the

HPV. This adjustment guaranteed that the entire GC flow passes through the PX. However, it was observed that the HPV could be manually turned off from the Danfoss controller, allowing the PX to function effectively and safely without the HPV. As a recommendation for further study, the PX setpoint should be modified to match the optimized GC pressure.

PX compression temperature: It is suggested that more research be conducted on the PX design, mainly the rotor dynamics, to address the comparatively low compression temperature issue.

PX integration concepts: The recommendation is to analyse additional PX integration concepts to utilise the existing infrastructure fully.

HP ejector: Various motive nozzles were tested for the HP ejector. The recommendation is to adopt a wider motive nozzle, ideally ranging between 6.5 and 7 mm, as it can potentially diminish the pressure difference between the compressor discharge and the gas cooler for 70 kW capacity. However, it is crucial to design the diffuser correspondingly to prevent flow reversal. Notably, a large motive nozzle may make motive needle control ineffective, necessitating careful consideration in the design process. Currently, the HP ejector represents a compromise in its design. Even it was assembled using components characterized as 'off the shelf.' This compromise significantly impacts its performance, as it was never initially designed for such working conditions. The most substantial enhancement in performance could be achieved through a dedicated CFD-supported design. In this approach, all geometry components, particularly the flow channels, would be specifically tailored to the unique conditions imposed by the system, notably the very low difference between the motive nozzle's inlet and outlet pressures.

LP ejector: The LP ejector demonstrated excellent performance for the purpose of PX testing. Nevertheless, there is room for further optimization by leveraging the insights gained from experimental results.

References

- [1] Miljø Direktoratet, Proposes banning all perfluorinated substances, in, 2023. <https://www.miljodirektoratet.no/aktuelt/nyheter/2023/februar-2023/foeslar-a-forby-alle-perfluorerte-stoffer/>.
- [2] Norsk Varmepumpeforening, Will ban all PFASs – including R134a and HFO media, in, 2023. <https://www.novap.no/artikler/vil-forby-alle-pfas-er-deriblant-r134a-og-hfo-medier>.
- [3] IMO, Revised GHG reduction strategy for global shipping adopted, 7th July, in, 2023. <https://www.imo.org/en/MediaCentre/PressBriefings/Pages/Revised-GHG-reduction-strategy-for-global-shipping-adopted-.aspx>.
- [4] C.H. Gabriellii, CruizE - Cruising towards Zero Emissions. Development of innovative and integrated cooling and heating concepts onboard cruise ships, in, 2020. <https://www.sintef.no/en/projects/2020/cruize-cruising-towards-zero-emissions/>.
- [5] C.H. Gabriellii, Á.Á. Pardinás, Heat pumps and refrigeration systems on board, naturally!, in, 2023. <https://blog.sintef.com/sintefenergy/energy-efficiency/heat-pumps-and-refrigeration-systems-on-board-naturally/>.
- [6] A. Hafner, C.H. Gabriellii, K.N. Widell, Refrigeration units in marine vessels : Alternatives to HCFCs and high GWP HFCs. Nordisk Ministerråd. Copenhagen, in, 2019. <https://norden.diva-portal.org/smash/record.jsf?pid=diva2%3A1301641&dsid=9818>.
- [7] European Council press release, Fluorinated gases and ozone-depleting substances: Council and Parliament reach agreement, in, 2023. <https://www.consilium.europa.eu/en/press/press-releases/2023/10/05/fluorinated-gases-and-ozone-depleting-substances-council-and-parliament-reach-agreement/>.
- [8] European Commission, EU legislation to control F-gases. Review of the EU F-gas Regulation and the new Commission proposal, in, 2022. https://climate.ec.europa.eu/eu-action/fluorinated-greenhouse-gases/eu-legislation-control-f-gases_en.
- [9] E. Lemmon, Huber, M., and McLinden, M., NIST standard reference database 23: Reference Fluid Thermodynamic and Transport Properties-REFPROP, Version 10.0, (2018). in.

- [10] E. Söylemez, K.N. Widell, C.H. Gabriell, Y. Ladam, T. Lund, A. Hafner, Overview of the development and status of carbon dioxide (R-744) refrigeration systems onboard fishing vessels, *International Journal of Refrigeration*, 140 (2022) 198-212. <https://doi.org/10.1016/j.ijrefrig.2022.05.007>.
- [11] M. Bond, P&O Cruises and GEA embrace transcritical CO2 technology, in, 2018. <https://www.seatrade-cruise.com/news-headlines/po-cruises-and-gea-embrace-transcritical-co2-technology>.
- [12] P. NEKSÅ, H.T. WALNUM, A. HAFNER, CO2 - A REFRIGERANT FROM THE PAST WITH PROSPECTS OF BEING ONE OF THE MAIN REFRIGERANTS IN THE FUTURE, in: 9th IIR-Gustav Lorentzen Conference on Natural Working Fluids (GL2010), Sydney, Australia, 2010. <https://iifir.org/en/fridoc/co2-a-refrigerant-from-the-past-with-prospects-of-being-one-of-the-27229>.
- [13] P. Nekså, H. Rekstad, G.R. Zakeri, P.A. Schiefloe, CO2-heat pump water heater: characteristics, system design and experimental results, *International Journal of Refrigeration*, 21 (1998) 172-179. [https://doi.org/10.1016/S0140-7007\(98\)00017-6](https://doi.org/10.1016/S0140-7007(98)00017-6).
- [14] Y.-S. Gao, Z.-R. Peng, X.-R. Zhang, CO2 Refrigeration Cycle and Systems, in: X.-R. Zhang, T.M. Eikevik (eds.) *CO2 Refrigeration Cycle and Systems*, Springer International Publishing, Cham, 2023, pp. 1-8. https://doi.org/10.1007/978-3-031-22512-3_1.
- [15] G.J.M. Velders, S.O. Andersen, J.S. Daniel, D.W. Fahey, M. McFarland, The importance of the Montreal Protocol in protecting climate, *Proceedings of the National Academy of Sciences*, 104 (2007) 4814-4819. <https://doi.org/10.1073/pnas.0610328104>.
- [16] D. Fleet, D.J. Hanlon, D.K. Osborne, M.L. Vedrine, P. Ashford, Study on environmental and health effects of HFO refrigerants by Norwegian Environment Agency., in, 2017. <https://www.miljodirektoratet.no/globalassets/publikasjoner/M917/M917.pdf>.
- [17] European Chemicals Agency (ECHA), Per- and polyfluoroalkyl substances (PFAS), in, 2023. <https://echa.europa.eu/hot-topics/perfluoroalkyl-chemicals-pfas#:~:text=They%20submitted%20their%20proposal%20to,opinions%20finalised%20in%20June%202023>.
- [18] European Chemicals Agency (ECHA), ECHA publishes PFAS restriction proposal, in, 2023. <https://echa.europa.eu/-/echa-publishes-pfas-restriction-proposal>.
- [19] G. Lorentzen, Trans-critical vapour compression cycle device. International patent publication. Patent number WO 90/07683, in, 1990.
- [20] G. Lorentzen, Revival of carbon dioxide as a refrigerant, *International Journal of Refrigeration*, 17 (1994) 292-301. [https://doi.org/10.1016/0140-7007\(94\)90059-0](https://doi.org/10.1016/0140-7007(94)90059-0).

- [21] G. Lorentzen, The use of natural refrigerants: a complete solution to the CFC/HCFC predicament, *International Journal of Refrigeration*, 18 (1995) 190-197. [https://doi.org/10.1016/0140-7007\(94\)00001-E](https://doi.org/10.1016/0140-7007(94)00001-E).
- [22] P. Gullo, K. Tsamos, A. Hafner, Y. Ge, S.A. Tassou, State-of-the-art technologies for transcritical R744 refrigeration systems – a theoretical assessment of energy advantages for European food retail industry, *Energy Procedia*, 123 (2017) 46-53. <https://doi.org/10.1016/j.egypro.2017.07.283>.
- [23] E. Bellos, C. Tzivanidis, A comparative study of CO₂ refrigeration systems, *Energy Conversion and Management*: X, 1 (2019) 100002. <https://doi.org/10.1016/j.ecmx.2018.100002>.
- [24] M. Karampour, S. Sawalha, State-of-the-art integrated CO₂ refrigeration system for supermarkets: A comparative analysis, *International Journal of Refrigeration*, 86 (2018) 239-257. <https://doi.org/10.1016/j.ijrefrig.2017.11.006>.
- [25] G. Besagni, R. Mereu, F. Inzoli, Ejector refrigeration: A comprehensive review, *Renewable and Sustainable Energy Reviews*, 53 (2016) 373-407. <https://doi.org/10.1016/j.rser.2015.08.059>.
- [26] K. Pianthong, W. Seehanam, M. Behnia, T. Sriveerakul, S. Aphornratana, Investigation and improvement of ejector refrigeration system using computational fluid dynamics technique, *Energy conversion and Management*, 48 (2007) 2556-2564. <https://doi.org/10.1016/j.enconman.2007.03.021>.
- [27] E.F. Kranakis, The French Connection: Giffard's Injector and the Nature of Heat, *Technology and Culture*, 23 (1982) 3-38. <https://doi.org/10.2307/3104441>.
- [28] S. Elbel, Historical and present developments of ejector refrigeration systems with emphasis on transcritical carbon dioxide air-conditioning applications, *International Journal of Refrigeration*, 34 (2011) 1545-1561. <https://doi.org/10.1016/j.ijrefrig.2010.11.011>.
- [29] S. Elbel, N. Lawrence, Review of recent developments in advanced ejector technology, *International Journal of Refrigeration*, 62 (2016) 1-18. <https://doi.org/10.1016/j.ijrefrig.2015.10.031>.
- [30] P. Gullo, A. Hafner, K. Banasiak, S. Minetto, E.E. Kriezi, Multi-ejector concept: A comprehensive review on its latest technological developments, *Energies*, 12 (2019) 406. <https://doi.org/10.3390/en12030406>.

- [31] B.M. Tashtoush, M.d.A. Al-Nimr, M.A. Khasawneh, A comprehensive review of ejector design, performance, and applications, *Applied Energy*, 240 (2019) 138-172. <https://doi.org/10.1016/j.apenergy.2019.01.185>.
- [32] G. Besagni, Ejectors on the cutting edge: The past, the present and the perspective, *Energy*, 170 (2019) 998-1003. <https://doi.org/10.1016/j.energy.2018.12.214>.
- [33] P. Gullo, M.R. Kærn, M. Haida, J. Smolka, S. Elbel, A review on current status of capacity control techniques for two-phase ejectors, *International Journal of Refrigeration*, 119 (2020) 64-79. <https://doi.org/10.1016/j.iirefrig.2020.07.014>.
- [34] K.E. Ringstad, Y. Allouche, P. Gullo, Å. Ervik, K. Banasiak, A. Hafner, A detailed review on CO₂ two-phase ejector flow modeling, *Thermal Science and Engineering Progress*, 20 (2020) 100647. <https://doi.org/10.1016/j.tsep.2020.100647>.
- [35] Y. Song, Y. Ma, H. Wang, X. Yin, F. Cao, Review on the simulation models of the two-phase-ejector used in the transcritical carbon dioxide systems, *International Journal of Refrigeration*, 119 (2020) 434-447. <https://doi.org/10.1016/j.ijrefrig.2020.04.029>.
- [36] R.B. Barta, E.A. Groll, D. Ziviani, Review of stationary and transport CO₂ refrigeration and air conditioning technologies, *Applied thermal engineering*, 185 (2021) 116422. <https://doi.org/10.1016/j.applthermaleng.2020.116422>.
- [37] L. Zheng, Y. Zhang, L. Hao, H. Lian, J. Deng, W. Lu, Modelling, Optimization, and Experimental Studies of Refrigeration CO₂ Ejectors: A Review, *Mathematics*, 10 (2022) 4325. <https://doi.org/10.3390/math10224325>.
- [38] K. Banasiak, A. Hafner, 1D Computational model of a two-phase R744 ejector for expansion work recovery, *International Journal of Thermal Sciences*, 50 (2011) 2235-2247. <https://doi.org/10.1016/j.ijthermalsci.2011.06.007>.
- [39] K. Banasiak, A. Hafner, T. Andresen, Experimental and numerical investigation of the influence of the two-phase ejector geometry on the performance of the R744 heat pump, *International Journal of Refrigeration*, 35 (2012) 1617-1625. <https://doi.org/10.1016/j.ijrefrig.2012.04.012>.
- [40] K. Banasiak, A. Hafner, Mathematical modelling of supersonic two-phase R744 flows through converging-diverging nozzles: The effects of phase transition models, *Applied thermal engineering*, 51 (2013) 635-643. <https://doi.org/10.1016/j.applthermaleng.2012.10.005>.
- [41] N. Lawrence, S. Elbel, Theoretical and practical comparison of two-phase ejector refrigeration cycles including First and Second Law analysis, *International Journal of Refrigeration*, 36 (2013) 1220-1232. <https://doi.org/10.1016/j.ijrefrig.2013.03.007>.

- [42] A. Hafner, S. Försterling, K. Banasiak, Multi-ejector concept for R-744 supermarket refrigeration, *International Journal of Refrigeration*, 43 (2014) 1-13.<https://doi.org/10.1016/j.ijrefrig.2013.10.015>.
- [43] K. Banasiak, M. Palacz, A. Hafner, Z. Buliński, J. Smółka, A.J. Nowak, A. Fic, A CFD-based investigation of the energy performance of two-phase R744 ejectors to recover the expansion work in refrigeration systems: An irreversibility analysis, *International Journal of Refrigeration*, 40 (2014) 328-337.<https://doi.org/10.1016/j.ijrefrig.2013.12.002>.
- [44] N. Lawrence, S. Elbel, Experimental investigation of a two-phase ejector cycle suitable for use with low-pressure refrigerants R134a and R1234yf, *International Journal of Refrigeration*, 38 (2014) 310-322.<https://doi.org/10.1016/j.ijrefrig.2013.08.009>.
- [45] M. Haida, K. Banasiak, J. Smolka, A. Hafner, T.M. Eikevik, Experimental analysis of the R744 vapour compression rack equipped with the multi-ejector expansion work recovery module, *International Journal of Refrigeration*, 64 (2016) 93-107.<https://doi.org/10.1016/j.ijrefrig.2016.01.017>.
- [46] K.E. Ringstad, K. Banasiak, Å. Ervik, A. Hafner, Machine learning and CFD for mapping and optimization of CO₂ ejectors, *Applied thermal engineering*, 199 (2021) 117604.<https://doi.org/10.1016/j.applthermaleng.2021.117604>.
- [47] S. Elbel, P. Hrnjak, Experimental validation of a prototype ejector designed to reduce throttling losses encountered in transcritical R744 system operation, *International Journal of Refrigeration*, 31 (2008) 411-422.<https://doi.org/10.1016/j.ijrefrig.2007.07.013>.
- [48] M.Z. Saeed, Thatte, A., Hafner, A., Gabriellii, H.C., Simultaneous implementation of rotary pressure exchanger and ejectors for CO₂ refrigeration system, in: 15th IIR-Gustav Lorentzen Conference on Natural Refrigerants, Trondheim, Norway, 2022.<http://dx.doi.org/10.18462/iir.gl2022.0130>.
- [49] A. Thatte, A New Type of Rotary Liquid Piston Pump for Multi-Phase CO₂ Compression, in: ASME Turbo Expo 2018: Turbomachinery Technical Conference and Exposition, Vol. Volume 9: Oil and Gas Applications; Supercritical CO₂ Power Cycles; Wind Energy, 2018.<https://doi.org/10.1115/gt2018-77011>.
- [50] A. Thatte, Transcritical / Supercritical CO₂ Recompression Brayton Cycle Using a Novel Rotary Liquid Piston Compressor, in: ASME Turbo Expo 2019: Turbomachinery Technical Conference and Exposition, Vol. Volume 9: Oil and Gas Applications; Supercritical CO₂ Power Cycles; Wind Energy, 2019.<https://doi.org/10.1115/GT2019-91088>.

- [51] A. Thatte, B. Fricke, K. Nawaz, Novel rotary pressure exchanger for highly efficient trans-critical CO₂ refrigeration cycle, in: 15th IIR-Gustav Lorentzen Conference on Natural Refrigerants, 2022.<http://dx.doi.org/10.18462/iir.gl2022.0056>.
- [52] A. Elatar, B. Fricke, V. Sharma, K. Nawaz, Pressure Exchanger for Energy Recovery in a Trans-Critical CO₂ Refrigeration System, *Energies*, 14 (2021) 1754.<https://doi.org/10.3390/en14061754>.
- [53] P. Geisler, F.U. Hahnenstein, W. Krumm, T. Peters, Pressure exchange system for energy recovery in reverse osmosis plants, *Desalination*, 122 (1999) 151-156.[https://doi.org/10.1016/S0011-9164\(99\)00036-3](https://doi.org/10.1016/S0011-9164(99)00036-3).
- [54] L.J. Hauge, The pressure exchanger — A key to substantial lower desalination cost, *Desalination*, 102 (1995) 219-223.[https://doi.org/10.1016/0011-9164\(95\)00057-9](https://doi.org/10.1016/0011-9164(95)00057-9).
- [55] P. Geisler, W. Krumm, T.A. Peters, Reduction of the energy demand for seawater RO with the pressure exchange systems PES, *Desalination*, 135 (2001) 205-210.[https://doi.org/10.1016/S0011-9164\(01\)00151-5](https://doi.org/10.1016/S0011-9164(01)00151-5).
- [56] I. Costiuc, A. Chiru, L. Costiuc, A Review of Engine's Performance When Supercharging by a Pressure Wave Supercharger, *Energies*, 15 (2022) 2721.<https://doi.org/10.3390/en15082721>.
- [57] Y. Lei, D.S. Zhou, H.G. Zhang, Investigation on performance of a compression-ignition engine with pressure-wave supercharger, *Energy*, 35 (2010) 85-93.<https://doi.org/10.1016/j.energy.2009.08.035>.
- [58] Á.Á. Pardiñas, H. Selvnes, K. Banasiak, A. Hafner, Next generation of ejector-supported R744 booster systems for commercial refrigeration at all climates, *International Journal of Refrigeration*, 148 (2023) 168-178.<https://doi.org/10.1016/j.ijrefrig.2022.10.027>.
- [59] C. Aprea, F. de Rossi, R. Mastrullo, The uncertainties in measuring vapour compression plant performances, *Measurement*, 21 (1997) 65-70.[https://doi.org/10.1016/S0263-2241\(97\)00040-7](https://doi.org/10.1016/S0263-2241(97)00040-7).

Appendix

A.1: PX case simulation code, EES

```
$REFERENCE R744 IIR
$UnitSystem SI C bar
$ConvertEESREFPROPUnits
```

"input data"

```
T_gc_out = 35 [C] "Gas cooler outlet temperature"
p_cond=89 [bar] "Gas cooler optimized pressure"
p_hp_com=91,5 [bar]"Compressor discharge pressure found by iteration"
T_evap_LT = 0 [C] "Evaporating temperature"
Q_evap_LT=60 [kW] "Evaporation capacity"
```

```
Tamb1=T_gc_out-3 "ambient temperature C"
Tamb=Tamb1+273,15 [K] "ambient temperature in K"
T_source_evaporator=5 [C] "Source temperature exergy part"
T_sink_gascooler=Tamb1 "sink temperature exergy part"
```

"Liquid receiver"

```
p_rec = 40 [bar] "Liquid receiver pressure"
h_liq = enthalpy(R744;x=0;P=p_rec) "Liquid enthalpy receiver"
h_vap = enthalpy(R744;x=1;P=p_rec) "Vapour enthalpy receiver"
T_rec = temperature(R744;P=p_rec;x=1) "receiver temperature"
```

"Energy balance"

```
s_gascooler_out= entropy(R744;T=T_gc_out;P=p_cond) "entropy at gas cooler outletttt"
h_ec_in_i=enthalpy(R744;P=p_rec;s=s_gascooler_out) "enthalpy with constant entropy"
x_ec=(h_dis_px2-h_liq)/(h_vap-h_liq) "vapour quality using the real enthalpy at PX expansion"
```

```
m_gas_cooler=m_evap/(1-x_ec) "gas cooler flow rate"
m_vap=m_gas_cooler-m_evap "total vapour flow in the system"
```

"Evaporator"

```
p_evap_LT = pressure(R744;T=T_evap_LT;x=0) "evaporator pressure"
h_evap=enthalpy(R744;x=1;P=p_evap_LT) "enthalpy at evaporator outlet, no superheat"
T_evap_out=5 "assumed superheat of 5K at IHX outlet"
h_out_evap=enthalpy(R744;T=T_evap_out;P=p_evap_LT) "enthalpy after IHX"
```

"Energy balance for IHX"

```
m_evap_n=m_add_LT+m_evap "adding evaporator flow plus FGV"
```

$m_{add_LT} \cdot h_{vap} + m_{evap} \cdot h_{evap} = m_{evap_n} \cdot h_{in_hx}$ "energy balance to find enthalpy before IHX"
 $dh = h_{out_evap} - h_{in_hx}$ "enthalpy change in IHX with 5K superheat"
 $m_{evap_n} \cdot dh = m_{evap} \cdot h_{liq} - m_{evap} \cdot h_{out}$ "subcooling on the IHX other side"
 $h_{in_evap_LT} = h_{out}$ "evaporator inlet enthalpy with subcooling"
 $Q_{evap_LT} = m_{evap} \cdot (h_{evap} - h_{in_evap_LT})$ "evaporator flow rate using evaporation capacity"

"compressor"

$r_{main} = p_{cond} / p_{evap_LT}$ "compressor pressure ratio"
 $\eta_{is_com_LT} = (-0,0021 \cdot (r_{main})^2) - (0,0155 \cdot (r_{main})) + 0,7325$ "CO2 compressor efficiency equation"

$s_{suction_LT} = \text{entropy}(R744; h = h_{out_evap}; P = p_{evap_LT})$ "entropy at the compressor suction"
 $h_{dis_is_com_LT} = \text{enthalpy}(R744; P = p_{hp_com}; s = s_{suction_LT})$ "isentropic enthalpy at compressor discharge"
 $\eta_{is_com_LT} = (h_{dis_is_com_LT} - h_{out_evap}) / (h_{dis_com_LT} - h_{out_evap})$ "real enthalpy using compressor efficiency"
 $T_{dis_com_LT} = \text{temperature}(R744; P = p_{cond}; h = h_{dis_com_LT})$ "compressor discharge temperature"
 $Q_{com_LT} = m_{evap_n} \cdot (h_{dis_com_LT} - h_{out_evap})$ "compressor electricity power"
 $h_{gc_out} = \text{enthalpy}(R744; T = T_{gc_out}; P = p_{cond})$

"PX expansion side"

$s_{suction_px2} = \text{entropy}(R744; h = h_{gc_out}; P = p_{cond})$ "entropy at gas cooler outlet"
 $h_{dis_is_px2} = \text{enthalpy}(R744; P = p_{rec}; s = s_{suction_px2})$ "isentropic enthalpy at PX expansion"
 $\eta_{is_px2} = 0,8236$ "PX expansion efficiency"
 $\eta_{is_px2} = (h_{gc_out} - h_{dis_px2}) / (h_{gc_out} - h_{dis_is_px2})$ "real PX expansion enthalpy"
 $T_{dis_px2} = \text{temperature}(R744; P = p_{rec}; h = h_{dis_px2})$ "temperature, same as receiver temperature"
 $Q_{px2} = m_{gas_cooler} \cdot (h_{gc_out} - h_{dis_px2})$

"Ejector LP"

$m_{ejector_si} = m_{vap}$ {LP ejector suction start process}
 $m_{add_LT} = ((54,71 \cdot m_{ejector_si}) / 100)$ {% removal of flash gas from ejector suction line}
 $m_{ejector_s} = m_{ejector_si} - m_{add_LT}$ {LP Ejector suction flow}
 $p_{eject_out} = 42$ {predifined Lp ejector lift}
 $LP_{ej_s_entropy} = \text{entropy}(R744; h = h_{vap}; P = p_{rec})$ {suction entropy LP ejector}
 $LP_{ej_m_entropy} = \text{entropy}(R744; h = h_{dis_com_LT}; P = p_{hp_com})$ {motive entropy}
 $LP_{ej_s_out_enthalpy} = \text{enthalpy}(R744; P = p_{eject_out}; s = LP_{ej_s_entropy})$ {enthalpy suction to out}
 $LP_{ej_m_out_enthalpy} = \text{enthalpy}(R744; P = p_{eject_out}; s = LP_{ej_m_entropy})$ {enthalpy motive to out}
 $LP_{eject_eff} = 0,20$ {predefined ejector efficiency}
 $m_{ejector_m} = (m_{ejector_s} \cdot (LP_{ej_s_out_enthalpy} - h_{vap})) / (LP_{eject_eff} \cdot (h_{dis_com_LT} - LP_{ej_m_out_enthalpy}))$ {LP ejector required motive flow}
 $m_{ejector_out} = m_{ejector_s} + m_{ejector_m}$ {Lp ejector outlet flow}
 $h_{eject_out} = ((m_{ejector_s} \cdot h_{vap}) + (m_{ejector_m} \cdot h_{dis_com_LT})) / m_{ejector_out}$ {LP ejector outlet enthalpy}

$T_{\text{eject_out}} = \text{temperature}(R744; P=p_{\text{eject_out}}; h=h_{\text{eject_out}})$ {LP ejector outlet temperature}

{PX mass boost ratio}

$\text{density_HP_in} = \text{density}(R744; P=p_{\text{cond}}; h=h_{\text{gc_out}})$

$\text{density_LP_in} = \text{density}(R744; P=p_{\text{eject_out}}; h=h_{\text{eject_out}})$

$m_{\text{boost}} = \text{density_LP_in} / \text{density_HP_in}$

"PX part compression side"

$P_{\text{out_px}} = p_{\text{cond}} - 2$ "PX compression outlet fixed so it will decide compression flow"

$s_{\text{suction_px}} = \text{entropy}(R744; h=h_{\text{eject_out}}; P=p_{\text{eject_out}})$ "PX compression suction entropy"

$h_{\text{dis_is_PX}} = \text{enthalpy}(R744; P=P_{\text{out_px}}; s=s_{\text{suction_px}})$ "PX isentropic discharge enthalpy"

$\eta_{\text{is_px}} = 0,7041$ "PX compression efficiency"

$\eta_{\text{is_px}} = (h_{\text{dis_is_PX}} - h_{\text{eject_out}}) / (h_{\text{dis_px}} - h_{\text{eject_out}})$ "real enthalpy PX compression"

$T_{\text{dis_px}} = \text{temperature}(R744; P=P_{\text{out_px}}; h=h_{\text{dis_px}})$ "Discharge temperature PX compression"

$Q_{\text{px}} = m_{\text{ejector_out}} * (h_{\text{dis_px}} - h_{\text{eject_out}})$ "PX compression work in kW"

"Ejector HP"

$m_{\text{ejector_s2}} = m_{\text{ejector_out}}$ "LP ejector outlet flow equal HP ejector suction, no mixing in PX"

$p_{\text{eject_out2}} = 89$ "predined HP ejector lift"

$HP_{\text{ej_s_entropy}} = \text{entropy}(R744; h=h_{\text{dis_px}}; P=P_{\text{out_px}})$ "HP ejector suction entropy"

$HP_{\text{ej_m_entropy}} = \text{entropy}(R744; h=h_{\text{dis_com_LT}}; P=p_{\text{hp_com}})$ "HP ejector motive entropy same as LP"

$HP_{\text{ej_s_out_enthalpy}} = \text{enthalpy}(R744; P=p_{\text{eject_out2}}; s=HP_{\text{ej_s_entropy}})$ "HP suction to outlet enthalpy"

$HP_{\text{ej_m_out_enthalpy}} = \text{enthalpy}(R744; P=p_{\text{eject_out2}}; s=HP_{\text{ej_m_entropy}})$ "HP ejector motive to outlet enthalpy"

$HP_{\text{eject_eff}} = 0,20$ "Predined HP ejector efficiency"

$m_{\text{ejector_m2}} = (m_{\text{ejector_s2}} * (HP_{\text{ej_s_out_enthalpy}} - h_{\text{dis_px}})) / (HP_{\text{eject_eff}} * (h_{\text{dis_com_LT}} - HP_{\text{ej_m_out_enthalpy}}))$

$m_{\text{ejector_out2}} = m_{\text{ejector_s2}} + m_{\text{ejector_m2}}$ "mass flow HP ejector outlet"

$h_{\text{eject_out2}} = ((m_{\text{ejector_s2}} * h_{\text{dis_px}}) + (m_{\text{ejector_m2}} * h_{\text{dis_com_LT}})) / m_{\text{ejector_out2}}$

"enthalpy HP ejector outlet"

$T_{\text{eject_out2}} = \text{temperature}(R744; P=p_{\text{eject_out2}}; h=h_{\text{eject_out2}})$ "temperature HP ejector outlet"

"before gas cooler"

$m_{\text{before_valve}} = m_{\text{evap_n}} - (m_{\text{ejector_m}} + m_{\text{ejector_m2}})$ "to verify no flow is passing through metering valve"

$h_{\text{before_valve}} = h_{\text{dis_com_LT}}$

"Energy balance"

$m_{\text{gas_cooler}} * h_{\text{before_gascooler}} = m_{\text{before_valve}} * h_{\text{before_valve}} + m_{\text{ejector_out2}} * h_{\text{eject_out2}}$

$T_{\text{before_gascooler}} = \text{temperature}(R744; P=p_{\text{cond}}; h=h_{\text{before_gascooler}})$ "temperature before gas cooler same as Hp ejector outlet"

"Condenser/gas cooler section"

$Q_{rej} = m_{gas_cooler} * (h_{before_gascooler} - h_{gc_out})$ "gas cooler heat rejection"
 $COP = Q_{evap_LT} / Q_{com_LT}$ "COP of the system"

"Exergy analysis" "All variables used are defined in COP analysis"

$T_{e_s} = T_{source_evaporator} + 273,15$

$T_{c_s} = T_{sink_gascooler} + 273,15$

"Ejectors"

$s_{motive_ejectors} = \text{entropy}(R744; h=h_{dis_com_LT}; P=p_{hp_com})$

$s_{LPejector_suction} = \text{entropy}(R744; h=h_{vap}; P=p_{rec})$

$s_{LPejector_out} = \text{entropy}(R744; h=h_{eject_out}; P=p_{eject_out})$

$I_{ejector_LP} = Tamb * ((m_{ejector_s} + m_{ejector_m}) * s_{LPejector_out} - m_{ejector_s} * s_{LPejector_suction} - m_{ejector_m} * s_{motive_ejectors})$

$s_{HPejector_suction} = \text{entropy}(R744; h=h_{dis_px}; P=P_{out_px})$

$s_{HPejector_out} = \text{entropy}(R744; h=h_{eject_out2}; P=p_{eject_out2})$

$I_{ejector_HP} = Tamb * ((m_{ejector_s2} + m_{ejector_m2}) * s_{HPejector_out} - m_{ejector_s2} * s_{HPejector_suction} - m_{ejector_m2} * s_{motive_ejectors})$

$I_{ejector} = I_{ejector_LP} + I_{ejector_HP}$

"compressor"

$s_{compressor_out} = \text{entropy}(R744; h=h_{dis_com_LT}; P=p_{hp_com})$

$I_{compressor} = m_{evap_n} * Tamb * (s_{compressor_out} - s_{suction_LT})$

"Evaporator"

$s_{evaporator_in} = \text{entropy}(R744; h=h_{in_evap_LT}; P=p_{evap_LT})$

$s_{evaporator_out} = \text{entropy}(R744; h=h_{evap}; P=p_{evap_LT})$

$I_{evap} = Q_{evap_LT} * (1 - (Tamb / T_{e_s})) - m_{evap} * ((h_{evap} - h_{in_evap_LT}) - Tamb * (s_{evaporator_out} - s_{evaporator_in}))$

"Gas cooler"

$s_{gascooler_in} = \text{entropy}(R744; h=h_{before_gascooler}; P=p_{cond})$

$I_{gascooler} = m_{gas_cooler} * ((h_{before_gascooler} - h_{gc_out}) - Tamb * (s_{gascooler_in} - s_{gascooler_out}) - Q_{rej} * (1 - (Tamb / T_{c_s})))$

"IHX"

$s_{IHX_in_upper} = \text{entropy}(R744; h=h_{in_hx}; P=p_{evap_LT})$

$s_{IHX_in_lower} = \text{entropy}(R744; h=h_{liq}; P=p_{rec})$

$s_{IHX_out_lower} = \text{entropy}(R744; h=h_{in_evap_LT}; P=p_{rec})$

$I_{IHX} = Tamb * (m_{evap_n} * (s_{suction_LT} - s_{IHX_in_upper}) + m_{evap} * (s_{IHX_out_lower} - s_{IHX_in_lower}))$

"Expansion valves"

```
l_exp1=m_evap*Tamb*(s_evaporator_in-s_IHX_out_lower)
s_exp2_out=entropy(R744;h=h_vap;P=p_evap_LT)
l_exp2=m_add_LT*Tamb*(s_exp2_out-s_LPejector_suction)
l_exp=l_exp1+l_exp2
```

"PX"

```
s_PX_exp_out=entropy(R744;h=h_dis_px2;P=p_rec)
l_PX_expansion=Tamb*m_gas_cooler*(s_PX_exp_out-s_gascooler_out)
l_PX_compression=Tamb*m_ejector_out*(s_HPjector_suction-s_LPejector_out)
l_PX=l_PX_expansion+l_PX_compression
l_total=l_ejector+l_compressor+l_evap+l_gascooler+l_IHX+l_exp+l_PX
```

```
eta_ex=1-(l_total/Q_com_LT) "Exergy efficiency"
```

A.2: Python script for Ejector efficiency uncertainty calculation

```
fluid='CarbonDioxide'  
data=pd.read_csv('70kW_35C_40bar.csv',delimiter=';',skiprows=[1])
```

“Gathering data and variables from experiment”

```
GC_temperature=data['TI-I-622']  
Average_GC_temperature=sum(GC_temperature)/len(GC_temperature)
```

```
Temperature_after_IHX=data['TI-I-662']  
Average_Temperature_after_IHX=sum(Temperature_after_IHX)/len(Temperature_after_IHX)
```

```
PX_HP_in_flow=data['FI-I-815-MF']  
Average_PX_HP_in_flow=sum(PX_HP_in_flow)/len(PX_HP_in_flow)  
PX_HP_in_std_1=st.stdev(PX_HP_in_flow)
```

```
Receiver_pressure=data['PI-I-624']  
Average_Receiver_pressure=sum(Receiver_pressure)/len(Receiver_pressure)
```

```
com_suction_flow=data['FI-I-812-MF']  
Average_com_suction_flow=sum(com_suction_flow)/len(com_suction_flow)  
Com_s_flow_std_1=st.stdev(com_suction_flow)
```

```
HP_ejector_out_temp=data['PX.TC1']  
Average_HP_ejector_out_temp=sum(HP_ejector_out_temp)/len(HP_ejector_out_temp)  
Ej_HP_out_temp_std_1=st.stdev(HP_ejector_out_temp)
```

```
T_s_LP_temp=data['PX.T2']  
Average_T_s_LP_temp=sum(T_s_LP_temp)/len(T_s_LP_temp)  
Ej_LP_s_temp_std_1=st.stdev(T_s_LP_temp)
```

```
Motive_temperature=data['PX.T6']  
Average_Motive_temperature=sum(Motive_temperature)/len(Motive_temperature)  
Ej_motive_temp_std_1=st.stdev(Motive_temperature)
```

```
Lp_ejector_motive=data['PX.F2.flow']  
Average_Lp_ejector_motive=sum(Lp_ejector_motive)/len(Lp_ejector_motive)  
LP_ejec_m_std_1=st.stdev(Lp_ejector_motive)
```

```
Compressor_pressure=data['PI-I-612A']  
Average_Compressor_pressure=sum(Compressor_pressure)/len(Compressor_pressure)  
PX_com_P_std_1=st.stdev(Compressor_pressure)
```

```
Gascooler_pressure=data['PI-I-621']  
Average_Gascooler_pressure=sum(Gascooler_pressure)/len(Gascooler_pressure)  
PX_GC_P_std_1=st.stdev(Gascooler_pressure)
```

HP_ejector_out_enthalpy=PropsSI('H','P',Average_Gascooler_pressure*10e4,'T',Average_HP_ejector_out_temp+273.15,fluid)/1000

compressor_discharge_temp=data['TI-I-612A']

Average_compressor_discharge_temp=sum(compressor_discharge_temp)/len(compressor_discharge_temp)

compressor_suction=data['TI-I-643']

Average_compressor_suction=sum(compressor_suction)/len(compressor_suction)

Lp_ejector_outlet=data['PX.F1.flow']

Average_Lp_ejector_outlet=sum(Lp_ejector_outlet)/len(Lp_ejector_outlet)

Hp_ejector_suction=data['PX.F3.flow']

Average_Hp_ejector_suction=sum(Hp_ejector_suction)/len(Hp_ejector_suction)

PX_HP_out_std_1=st.stdev(Hp_ejector_suction)

HP_in_PX=data['PX.T5']

Average_HP_in_PX=sum(HP_in_PX)/len(HP_in_PX)

PX_HP_in_temp_std_1=st.stdev(HP_in_PX)

HP_out_PX=data['PX.T4']

Average_HP_out_PX=sum(HP_out_PX)/len(HP_out_PX)

PX_HP_out_temp_std_1=st.stdev(HP_out_PX)

LP_in_PX=data['PX.T3']

Average_LP_in_PX=sum(LP_in_PX)/len(LP_in_PX)

PX_LP_in_temp_std_1=st.stdev(LP_in_PX)

LP_out_PX=data['PX.T1']

Average_LP_out_PX=sum(LP_out_PX)/len(LP_out_PX)

PX_LP_out_temp_std_1=st.stdev(LP_out_PX)

LP_ejector_dp=data['PX.P1']

Average_LP_ejector_dp=sum(LP_ejector_dp)/len(LP_ejector_dp)

PX_LP_ej_dp_std_1=st.stdev(LP_ejector_dp)

LPe_out_pressure_c=Receiver_pressure+LP_ejector_dp

Average_LPe_out_pressure_c=sum(LPe_out_pressure_c)/len(LPe_out_pressure_c)

PX_LP_in_flow=data['PX.F1.flow']

Average_PX_LP_in_flow=sum(PX_LP_in_flow)/len(PX_LP_in_flow)

PX_LP_in_std_1=st.stdev(PX_LP_in_flow)

LP_eject_suction=Lp_ejector_outlet-Lp_ejector_motive

Average_LP_eject_suction=sum(LP_eject_suction)/len(LP_eject_suction)

HP_ejector_dp=data['PX.P2']

Average_HP_ejector_dp=sum(HP_ejector_dp)/len(HP_ejector_dp)

PX_HP_ej_dp_std_1=st.stdev(HP_ejector_dp)

PX_HP_out_press=Gascooler_pressure-HP_ejector_dp
Average_PX_HP_out_press=sum(PX_HP_out_press)/len(PX_HP_out_press)

"Ejector efficiency and uncertainty HP"

Motive_temperature=data['PX.T6']
Average_Motive_temperature=sum(Motive_temperature)/len(Motive_temperature)
suction_temperature_HP=data['PX.T4']

Average_suction_temperature_HP=sum(suction_temperature_HP)/len(suction_temperature_HP)
HP_outlet_temp=Average_HP_ejector_out_temp
m_motive_HP=Average_com_suction_flow/60

P_motive_HP_LP=Average_Compressor_pressure
T_motive_HP_LP=Average_Motive_temperature
P_suction_HP=Average_PX_HP_out_press

"Following the procedure from Apera et al to calculate uncertainty"

T_suction_HP=Average_suction_temperature_HP
P_HP_out=Average_Gascooler_pressure
h_motive_HP_LP=PropsSI('H','P',P_motive_HP_LP*10e4,'T',T_motive_HP_LP+273.15,fluid)/1000
IP_mo_pr_plus_HP_h=PropsSI('H','P',(P_motive_HP_LP+0.354)*10e4,'T',T_motive_HP_LP+273.15,fluid)/1000
IP_mo_pr_minus_HP_h=PropsSI('H','P',(P_motive_HP_LP-0.354)*10e4,'T',T_motive_HP_LP+273.15,fluid)/1000
IP_mot_HP_h=((IP_mo_pr_plus_HP_h-h_motive_HP_LP)+(IP_mo_pr_minus_HP_h-h_motive_HP_LP))/2
IT_mo_t_plus_HP_h=PropsSI('H','P',P_motive_HP_LP*10e4,'T',(T_motive_HP_LP+0.41)+273.15,fluid)/1000
IT_mo_t_minus_HP_h=PropsSI('H','P',P_motive_HP_LP*10e4,'T',(T_motive_HP_LP-0.41)+273.15,fluid)/1000
IT_mot_HP_h=((IT_mo_t_plus_HP_h-h_motive_HP_LP)+(IT_mo_t_minus_HP_h-h_motive_HP_LP))/2
Ah_mot_HP_h=np.sqrt(np.power(IP_mot_HP_h,2)+np.power(IT_mot_HP_h,2)) #1
s_motive_HP_LP=PropsSI('S','P',P_motive_HP_LP*10e4,'T',T_motive_HP_LP+273.15,fluid)/1000
IP_mo_pr_plus_HP_s=PropsSI('S','P',(P_motive_HP_LP+0.354)*10e4,'T',T_motive_HP_LP+273.15,fluid)/1000
IP_mo_pr_minus_HP_s=PropsSI('S','P',(P_motive_HP_LP-0.354)*10e4,'T',T_motive_HP_LP+273.15,fluid)/1000
IP_mo_HP_s=((IP_mo_pr_plus_HP_s-s_motive_HP_LP)+(IP_mo_pr_minus_HP_s-s_motive_HP_LP))/2
IT_mo_t_plus_HP_s=PropsSI('S','P',P_motive_HP_LP*10e4,'T',(T_motive_HP_LP+0.41)+273.15,fluid)/1000
IT_mo_t_minus_HP_s=PropsSI('S','P',P_motive_HP_LP*10e4,'T',(T_motive_HP_LP-0.41)+273.15,fluid)/1000
IT_mo_HP_s=((IT_mo_t_plus_HP_s-s_motive_HP_LP)+(IT_mo_t_minus_HP_s-s_motive_HP_LP))/2
Ah_mot_HP_s=np.sqrt(np.power(IP_mo_HP_s,2)+np.power(IT_mo_HP_s,2)) #2
h_motive_out_isentropic_HP=PropsSI('H','P',P_HP_out*10e4,'S',s_motive_HP_LP*1000,fluid)/1000
IP_mo_out_pr_plus_HP_h=PropsSI('H','P',(P_HP_out+0.371)*10e4,'S',s_motive_HP_LP*1000,fluid)/1000
000

```

IP_mo_out_pr_minus_HP_h=PropsSI('H','P',(P_HP_out-
0.371)*10e4,'S',s_motive_HP_LP*1000,fluid)/1000
IP_mo_out_HP_h=((IP_mo_out_pr_plus_HP_h-
h_motive_out_isentropic_HP)+(IP_mo_out_pr_minus_HP_h-h_motive_out_isentropic_HP))/2
IS_mo_out_s_plus_HP_h=PropsSI('H','P',P_HP_out*10e4,'S',(s_motive_HP_LP+Ah_mot_HP_s)*1000,
fluid)/1000
IS_mo_out_s_minus_HP_h=PropsSI('H','P',P_HP_out*10e4,'S',(s_motive_HP_LP-
Ah_mot_HP_s)*1000,fluid)/1000
IS_mo_out_HP_h=((IS_mo_out_s_plus_HP_h-
h_motive_out_isentropic_HP)+(IS_mo_out_s_minus_HP_h-h_motive_out_isentropic_HP))/2
Ah_mo_out_HP_h=np.sqrt(np.power(IP_mo_out_HP_h,2)+np.power(IS_mo_out_HP_h,2))

h_suction_HP=PropsSI('H','P',P_suction_HP*10e4,'T',T_suction_HP+273.15,fluid)/1000
IP_su_pr_plus_HP_h=PropsSI('H','P',(P_suction_HP+0.058)*10e4,'T',T_suction_HP+273.15,fluid)/100
0
IP_su_pr_minus_HP_h=PropsSI('H','P',(P_suction_HP-
0.058)*10e4,'T',T_suction_HP+273.15,fluid)/1000
IP_su_HP_h=((IP_su_pr_plus_HP_h-h_suction_HP)+(IP_su_pr_minus_HP_h-h_suction_HP))/2
IT_su_t_plus_HP_h=PropsSI('H','P',P_suction_HP*10e4,'T',(T_suction_HP+0.315)+273.15,fluid)/1000
#large difference
IT_su_t_minus_HP_h=PropsSI('H','P',P_suction_HP*10e4,'T',(T_suction_HP-
0.315)+273.15,fluid)/1000 #large difference
IT_su_HP_h=((IT_su_t_plus_HP_h-h_suction_HP)+(IT_su_t_minus_HP_h-h_suction_HP))/2
Ah_su_HP_h=np.sqrt(np.power(IP_su_HP_h,2)+np.power(IT_su_HP_h,2))

s_suction_HP=PropsSI('S','P',P_suction_HP*10e4,'T',T_suction_HP+273.15,fluid)/1000
IP_su_pr_plus_HP_s=PropsSI('S','P',(P_suction_HP+0.058)*10e4,'T',T_suction_HP+273.15,fluid)/1000
IP_su_pr_minus_HP_s=PropsSI('S','P',(P_suction_HP-
0.058)*10e4,'T',T_suction_HP+273.15,fluid)/1000
IP_su_HP_s=((IP_su_pr_plus_HP_s-s_suction_HP)+(IP_su_pr_minus_HP_s-s_suction_HP))/2
IT_su_t_plus_HP_s=PropsSI('S','P',P_suction_HP*10e4,'T',(T_suction_HP+0.315)+273.15,fluid)/1000
IT_su_t_minus_HP_s=PropsSI('S','P',P_suction_HP*10e4,'T',(T_suction_HP-
0.315)+273.15,fluid)/1000
IT_su_HP_s=((IT_su_t_plus_HP_s-s_suction_HP)+(IT_su_t_minus_HP_s-s_suction_HP))/2
Ah_su_HP_s=np.sqrt(np.power(IP_su_HP_s,2)+np.power(IT_su_HP_s,2))

h_suction_out_isentropic_HP=PropsSI('H','P',P_HP_out*10e4,'S',s_suction_HP*1000,fluid)/1000
IP_su_out_pr_plus_HP_h=PropsSI('H','P',(P_HP_out+0.371)*10e4,'S',s_suction_HP*1000,fluid)/1000
IP_su_out_pr_minus_HP_h=PropsSI('H','P',(P_HP_out-
0.371)*10e4,'S',s_suction_HP*1000,fluid)/1000
IP_su_out_HP_h=((IP_su_out_pr_plus_HP_h-
h_suction_out_isentropic_HP)+(IP_su_out_pr_minus_HP_h-h_suction_out_isentropic_HP))/2
IT_su_out_t_plus_HP_h=PropsSI('H','P',P_HP_out*10e4,'S',(s_suction_HP+Ah_su_HP_s)*1000,fluid)/
1000
IT_su_out_t_minus_HP_h=PropsSI('H','P',P_HP_out*10e4,'S',(s_suction_HP-
Ah_su_HP_s)*1000,fluid)/1000
IT_su_out_HP_h=((IT_su_out_t_plus_HP_h-
h_suction_out_isentropic_HP)+(IT_su_out_t_minus_HP_h-h_suction_out_isentropic_HP))/2
Ah_su_out_HP_s=np.sqrt(np.power(IP_su_out_HP_h,2)+np.power(IT_su_out_HP_h,2))

m_suction_HP=(Average_Hp_ejector_suction/60)

```

```

Entrainment_ratio_HP=m_suction_HP/m_motive_HP
ej_eff=(Entrainment_ratio_HP)*((h_suction_out_isentropic_HP-h_suction_HP)/(h_motive_HP_LP-
h_motive_out_isentropic_HP))
print(ej_eff)

```

"Calculating the uncertainty using derivatives"

```

Ah_mdot_motive = -m_suction_HP / np.power(m_motive_HP,2)
Ah_mdot_suction = 1/m_motive_HP
u_me_ratio_HP = np.sqrt(np.power(Ah_mdot_motive*9.25e-
3,2)+np.power(Ah_mdot_suction*1.081e-3,2)) #uncertainty flow in kg/s

```

"A, B, C, D values according to Elbel et al <https://doi.org/10.1016/j.ijrefrig.2007.07.013>"

```

u_h_A_HP=Ah_mot_HP_h
u_h_B_HP=Ah_mo_out_HP_h
u_h_C_HP=Ah_su_out_HP_s
u_h_D_HP=Ah_su_HP_h

```

```

h_A_HP=h_motive_HP_LP
h_B_HP=h_motive_out_isentropic_HP
h_C_HP=h_suction_out_isentropic_HP
h_D_HP=h_suction_HP
me_ratio_HP=Entrainment_ratio_HP

```

```

SC_eta_me_ratio_HP = (h_C_HP - h_D_HP)/(h_A_HP - h_B_HP)
SC_eta_h_C_HP = me_ratio_HP/(h_A_HP - h_B_HP)
SC_eta_h_D_HP = me_ratio_HP/(h_A_HP - h_B_HP)
SC_eta_h_A_HP = me_ratio_HP*(h_C_HP - h_D_HP)/np.power((h_A_HP - h_B_HP),2)
SC_eta_h_B_HP = me_ratio_HP*(h_C_HP - h_D_HP)/np.power((h_A_HP - h_B_HP),2)

```

"Final equation ejector uncertainty"

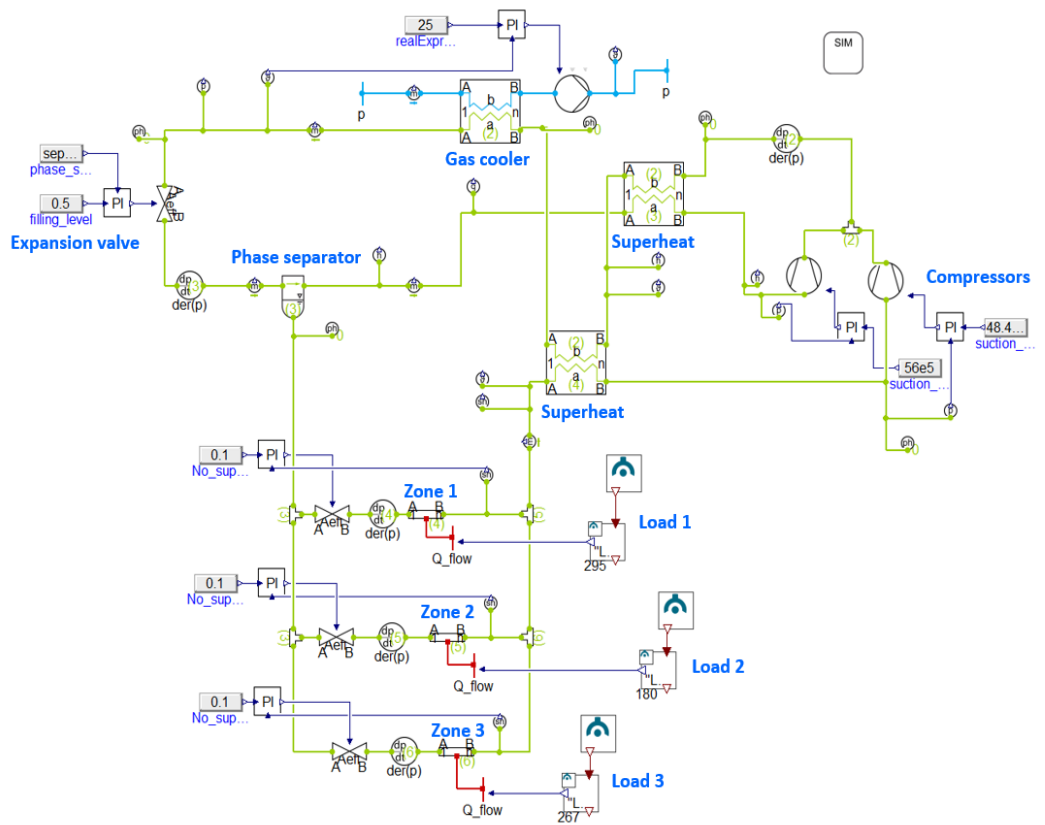
```

u_eta_ejector_HP =
np.sqrt(np.power(SC_eta_me_ratio_HP*u_me_ratio_HP,2)+np.power(SC_eta_h_C_HP*u_h_C_HP,2)
+np.power(SC_eta_h_D_HP*u_h_D_HP,2)+np.power(SC_eta_h_A_HP*u_h_A_HP,2)+np.power(SC_e
ta_h_B_HP*u_h_B_HP,2))
print(u_eta_ejector_HP)

```


A.3: Simulation model to analyze direct evaporation in HVAC system of ship

The work of this dynamic simulation is reported in conference paper 1.



A.4: Experimental results of booster and parallel compression mode

The following figure (Figure B.1) is the experimental results of the SuperSmart rack with standard booster and parallel compression mode conducted by the author of this thesis. The evaporation temperature was 0 °C, capacity 70 kW, and the GC pressure at the optimized pressure curves. According to the previous experiments performed on the SuperSmart test facility, the COP relative uncertainty is 4.99% and 5.17% for Booster and parallel compression mode, respectively.

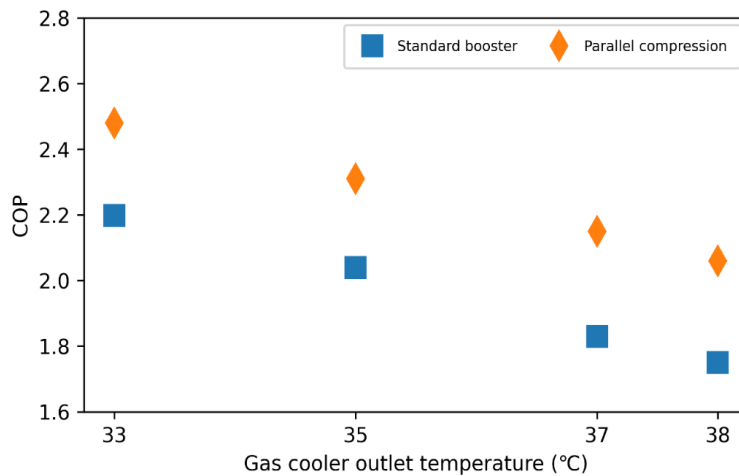


Figure B.1: Experimental results of evaporation capacity 70 kW at 0 °C

A.5: Experimental results of PX cases

Each experiment was performed for 10 minutes and only 100 seconds of results are attached in Appendix A5

Table A5.1: Experimental results of PX 33 °C case for 100 Seconds

Time Seconds	Ejectors motive pressure bar	GC pressure bar	LP ejector DP bar	HP ejector DP bar	PX DP bar	PX HP _{out} C	PX LP _{in} flow kg/min	PX HP _{out} flow kg/min	PX RPM RPM
1	89.76	81.76	3.50	5.58	31.06	36.44	5.08	5.29	708.72
2	89.76	81.72	3.51	5.57	31.02	36.44	5.09	5.29	706.48
3	89.76	81.72	3.51	5.57	31.02	36.44	5.09	5.29	706.48
4	89.78	81.76	3.53	5.57	31.05	36.44	5.13	5.29	708.45
5	89.76	81.73	3.53	5.57	31.03	36.45	5.11	5.27	708.15
6	89.79	81.74	3.52	5.57	31.05	36.34	5.09	5.27	708.21
7	89.74	81.76	3.53	5.57	31.05	36.44	5.12	5.27	709.09
8	89.76	81.71	3.54	5.57	31.01	36.45	5.13	5.27	709.46
9	89.78	81.72	3.53	5.57	31.01	36.34	5.08	5.31	711.30
10	89.78	81.72	3.53	5.57	31.01	36.34	5.08	5.31	711.30
11	89.74	81.69	3.54	5.58	30.98	36.44	5.09	5.31	712.50
12	89.75	81.68	3.54	5.58	30.96	36.34	5.13	5.31	712.59
13	89.75	81.68	3.54	5.58	30.96	36.34	5.13	5.31	712.59
14	89.72	81.69	3.54	5.58	30.97	36.34	5.07	5.30	712.31
15	89.71	81.66	3.54	5.58	30.95	36.34	5.10	5.29	711.99
16	89.71	81.64	3.55	5.58	30.94	36.34	5.14	5.27	711.90
17	89.70	81.66	3.54	5.58	30.96	36.34	5.11	5.31	712.08
18	89.70	81.66	3.54	5.58	30.96	36.34	5.11	5.31	712.08
19	89.69	81.60	3.54	5.59	30.89	36.34	5.15	5.29	711.72
20	89.68	81.62	3.54	5.59	30.91	36.34	5.15	5.29	711.43
21	89.68	81.60	3.54	5.59	30.88	36.34	5.10	5.30	711.97
22	89.66	81.58	3.53	5.59	30.88	36.34	5.08	5.33	711.59
23	89.63	81.58	3.53	5.59	30.88	36.34	5.05	5.32	711.87
24	89.63	81.58	3.53	5.59	30.88	36.34	5.09	5.31	711.79
25	89.63	81.56	3.53	5.59	30.87	36.34	5.13	5.31	712.30
26	89.60	81.56	3.52	5.59	30.87	36.34	5.11	5.32	712.14
27	89.62	81.56	3.53	5.59	30.87	36.34	5.11	5.31	711.72
28	89.60	81.53	3.53	5.59	30.83	36.34	5.09	5.30	711.55
29	89.60	81.55	3.54	5.59	30.85	36.34	5.16	5.30	712.12
30	89.60	81.52	3.54	5.59	30.83	36.23	5.08	5.30	712.27
31	89.59	81.51	3.53	5.59	30.83	36.23	5.15	5.29	711.50
32	89.57	81.51	3.52	5.59	30.84	36.23	5.08	5.29	711.64
33	89.56	81.51	3.53	5.59	30.83	36.23	5.10	5.30	711.51
34	89.56	81.49	3.53	5.60	30.80	36.33	5.09	5.31	711.38
35	89.55	81.47	3.54	5.60	30.77	36.23	5.07	5.32	711.73

36	89.54	81.47	3.54	5.60	30.77	36.23	5.13	5.33	712.34
37	89.52	81.47	3.53	5.59	30.78	36.23	5.13	5.31	712.12
38	89.53	81.48	3.52	5.59	30.80	36.23	5.09	5.31	711.45
39	89.51	81.46	3.53	5.59	30.76	36.23	5.11	5.31	712.12
40	89.49	81.43	3.52	5.59	30.75	36.23	5.08	5.32	711.96
41	89.49	81.43	3.52	5.59	30.75	36.23	5.08	5.32	711.96
42	89.51	81.42	3.52	5.59	30.74	36.23	5.07	5.32	712.01
43	89.52	81.43	3.53	5.59	30.75	36.23	5.10	5.31	711.79
44	89.51	81.43	3.53	5.59	30.75	36.23	5.11	5.31	713.47
45	89.49	81.44	3.52	5.59	30.76	36.23	5.09	5.31	713.41
46	89.50	81.41	3.52	5.59	30.73	36.13	5.10	5.30	712.84
47	89.48	81.39	3.53	5.59	30.71	36.13	5.07	5.29	713.65
48	89.47	81.40	3.53	5.60	30.71	36.13	5.10	5.33	714.27
49	89.47	81.40	3.53	5.60	30.71	36.13	5.10	5.33	714.27
50	89.48	81.37	3.53	5.60	30.67	36.13	5.09	5.30	714.85
51	89.48	81.37	3.53	5.60	30.67	36.13	5.09	5.30	714.85
52	89.46	81.38	3.53	5.60	30.70	36.13	5.08	5.29	713.51
53	89.48	81.39	3.53	5.60	30.70	36.13	5.08	5.29	715.02
54	89.48	81.38	3.53	5.60	30.69	36.13	5.12	5.29	714.25
55	89.48	81.38	3.54	5.61	30.68	36.13	5.12	5.31	714.11
56	89.48	81.39	3.53	5.60	30.71	36.13	5.08	5.33	714.33
57	89.46	81.39	3.54	5.60	30.69	36.13	5.11	5.32	715.72
58	89.46	81.39	3.55	5.60	30.69	36.13	5.12	5.30	715.44
59	89.47	81.39	3.55	5.61	30.68	36.13	5.08	5.30	715.52
60	89.47	81.38	3.54	5.61	30.68	36.13	5.11	5.32	715.67
61	89.46	81.40	3.54	5.61	30.70	36.13	5.08	5.32	716.20
62	89.47	81.40	3.53	5.61	30.71	36.05	5.09	5.32	716.22
63	89.45	81.39	3.53	5.61	30.70	36.13	5.03	5.32	715.66
64	89.47	81.37	3.53	5.61	30.68	36.04	5.05	5.33	715.60
65	89.45	81.37	3.54	5.61	30.66	36.05	5.10	5.33	715.60
66	89.47	81.40	3.55	5.61	30.69	36.05	5.10	5.32	715.80
67	89.45	81.42	3.55	5.61	30.71	36.05	5.11	5.30	715.33
68	89.46	81.36	3.55	5.60	30.66	36.05	5.08	5.30	715.73
69	89.44	81.37	3.54	5.60	30.68	36.05	5.12	5.31	715.59
70	89.44	81.37	3.55	5.60	30.68	36.05	5.09	5.30	714.97
71	89.45	81.39	3.54	5.60	30.69	36.05	5.09	5.31	715.58
72	89.44	81.39	3.53	5.60	30.70	36.05	5.06	5.31	716.51
73	89.45	81.34	3.53	5.61	30.65	36.13	5.06	5.33	715.24
74	89.44	81.38	3.53	5.61	30.69	36.13	5.03	5.34	715.24
75	89.43	81.38	3.53	5.61	30.69	36.13	5.10	5.33	715.46
76	89.44	81.36	3.54	5.60	30.68	36.13	5.13	5.32	715.87
77	89.44	81.35	3.54	5.60	30.67	36.05	5.02	5.29	716.06
78	89.43	81.35	3.54	5.60	30.67	36.13	5.03	5.29	715.61
79	89.44	81.35	3.53	5.60	30.67	36.13	5.03	5.30	715.55
80	89.42	81.34	3.53	5.60	30.67	36.13	5.02	5.31	715.30
81	89.40	81.36	3.53	5.60	30.69	36.13	5.07	5.31	715.74
82	89.41	81.32	3.53	5.60	30.65	36.13	5.07	5.32	715.38
83	89.43	81.33	3.53	5.61	30.66	36.13	5.13	5.31	715.97

84	89.43	81.33	3.54	5.61	30.65	36.13	5.12	5.32	715.40
85	89.40	81.32	3.54	5.61	30.63	36.13	5.07	5.32	715.65
86	89.43	81.30	3.55	5.61	30.60	36.13	5.05	5.32	714.85
87	89.41	81.29	3.54	5.61	30.60	36.13	5.08	5.30	715.91
88	89.40	81.30	3.55	5.62	30.60	36.05	5.11	5.32	715.24
89	89.40	81.31	3.54	5.62	30.61	36.05	5.10	5.34	715.15
90	89.36	81.29	3.54	5.62	30.59	36.05	5.11	5.33	714.76
91	89.37	81.27	3.54	5.62	30.58	36.05	5.09	5.32	715.56
92	89.38	81.27	3.52	5.62	30.58	36.05	5.05	5.33	715.91
93	89.37	81.27	3.52	5.62	30.58	36.05	5.08	5.34	716.87
94	89.37	81.29	3.53	5.62	30.59	36.05	5.07	5.34	716.77
95	89.36	81.27	3.53	5.62	30.58	36.05	5.08	5.35	716.86
96	89.34	81.26	3.53	5.62	30.56	36.13	5.13	5.34	716.58
97	89.37	81.29	3.54	5.62	30.59	36.04	5.12	5.34	716.99
98	89.39	81.34	3.54	5.61	30.65	36.05	5.10	5.30	718.01
99	89.39	81.34	3.54	5.61	30.65	36.05	5.10	5.30	718.01
100	89.35	81.34	3.55	5.60	30.64	36.05	5.09	5.29	717.91

Table A5.2: Experimental results of PX 35 °C case for 100 Seconds

Time Seconds	Ejectors motive pressure bar	GC pressure bar	LP ejector DP bar	HP ejector DP bar	PX DP bar	PX HP _{out} C	PX LP _{in} flow kg/min	PX HP _{out} flow kg/min	PX RPM RPM
1	95.39	87.09	3.80	5.74	36.00	39.72	5.36	5.62	696.85
2	95.38	87.12	3.81	5.75	36.02	39.72	5.31	5.65	696.77
3	95.35	87.08	3.80	5.75	35.98	39.72	5.31	5.66	696.87
4	95.36	87.11	3.80	5.75	36.01	39.71	5.29	5.65	696.99
5	95.36	87.11	3.80	5.75	36.01	39.71	5.29	5.65	696.99
6	95.39	87.11	3.81	5.75	36.02	39.65	5.38	5.67	697.17
7	95.39	87.10	3.81	5.75	36.00	39.65	5.36	5.66	695.82
8	95.37	87.10	3.81	5.75	36.00	39.65	5.36	5.66	695.82
9	95.39	87.10	3.80	5.75	36.01	39.65	5.26	5.66	695.72
10	95.38	87.12	3.80	5.76	36.02	39.65	5.29	5.67	696.09
11	95.38	87.11	3.80	5.75	36.02	39.65	5.29	5.67	696.06
12	95.36	87.10	3.80	5.75	36.01	39.65	5.29	5.67	696.32
13	95.37	87.11	3.80	5.75	36.01	39.65	5.38	5.65	695.66
14	95.37	87.09	3.81	5.75	36.00	39.65	5.29	5.67	696.06
15	95.36	87.11	3.81	5.75	36.02	39.65	5.27	5.68	695.41
16	95.38	87.11	3.80	5.75	36.02	39.65	5.22	5.66	696.30
17	95.36	87.09	3.80	5.75	36.01	39.65	5.23	5.63	696.02
18	95.35	87.08	3.80	5.75	36.00	39.65	5.26	5.65	695.79
19	95.37	87.12	3.81	5.75	36.03	39.65	5.22	5.66	695.26
20	95.36	87.14	3.80	5.74	36.07	39.65	5.29	5.61	695.47

21	95.34	87.13	3.80	5.74	36.06	39.65	5.29	5.61	695.72
22	95.34	87.13	3.80	5.73	36.07	39.65	5.33	5.58	695.72
23	95.34	87.15	3.81	5.72	36.09	39.65	5.31	5.58	695.26
24	95.35	87.15	3.81	5.71	36.10	39.65	5.36	5.56	695.66
25	95.35	87.15	3.81	5.70	36.11	39.65	5.31	5.55	695.42
26	95.34	87.18	3.81	5.69	36.14	39.65	5.26	5.53	695.79
27	95.36	87.17	3.81	5.69	36.15	39.65	5.31	5.52	695.48
28	95.37	87.21	3.81	5.69	36.17	39.65	5.31	5.54	695.75
29	95.37	87.15	3.81	5.69	36.11	39.65	5.31	5.55	695.80
30	95.35	87.18	3.81	5.69	36.15	39.65	5.26	5.53	695.94
31	95.35	87.13	3.81	5.69	36.09	39.65	5.29	5.55	695.97
32	95.33	87.13	3.81	5.69	36.09	39.65	5.29	5.55	695.97
33	95.31	87.11	3.81	5.70	36.07	39.65	5.29	5.58	696.85
34	95.30	87.12	3.81	5.70	36.07	39.65	5.29	5.59	697.01
35	95.28	87.07	3.81	5.71	36.01	39.65	5.27	5.62	696.75
36	95.28	87.07	3.81	5.71	36.01	39.65	5.27	5.62	696.75
37	95.28	87.06	3.81	5.71	36.01	39.65	5.27	5.59	696.52
38	95.27	87.05	3.81	5.70	36.00	39.65	5.24	5.58	697.04
39	95.25	87.08	3.80	5.70	36.03	39.65	5.30	5.59	697.09
40	95.24	87.05	3.80	5.70	36.01	39.65	5.31	5.59	697.55
41	95.22	87.04	3.80	5.70	35.99	39.65	5.29	5.59	696.63
42	95.25	87.04	3.80	5.70	36.00	39.65	5.29	5.57	696.72
43	95.23	87.01	3.80	5.70	35.97	39.65	5.31	5.57	697.29
44	95.22	87.02	3.80	5.70	35.98	39.65	5.29	5.60	695.83
45	95.22	87.03	3.80	5.70	35.99	39.72	5.31	5.59	696.85
46	95.21	87.00	3.80	5.70	35.97	39.65	5.36	5.58	696.95
47	95.24	87.00	3.80	5.70	35.96	39.65	5.31	5.58	696.58
48	95.22	86.98	3.80	5.70	35.94	39.65	5.29	5.57	697.05
49	95.21	86.99	3.80	5.71	35.95	39.65	5.26	5.59	697.30
50	95.18	86.97	3.80	5.71	35.93	39.65	5.27	5.59	697.15
51	95.18	86.97	3.80	5.71	35.92	39.65	5.25	5.61	697.20
52	95.17	86.97	3.80	5.70	35.93	39.65	5.25	5.60	696.83
53	95.16	86.95	3.80	5.70	35.91	39.65	5.29	5.59	696.57
54	95.16	86.95	3.80	5.70	35.91	39.65	5.29	5.59	696.57
55	95.14	86.94	3.80	5.70	35.90	39.72	5.31	5.59	697.26
56	95.14	86.94	3.80	5.70	35.90	39.72	5.31	5.59	697.26
57	95.16	86.94	3.80	5.71	35.90	39.72	5.33	5.62	695.72
58	95.15	86.91	3.79	5.71	35.87	39.69	5.31	5.61	695.72
59	95.16	86.92	3.79	5.71	35.87	39.71	5.29	5.62	695.78
60	95.15	86.92	3.79	5.72	35.88	39.71	5.31	5.63	695.71
61	95.15	86.92	3.79	5.72	35.87	39.65	5.24	5.63	695.91
62	95.15	86.91	3.79	5.72	35.87	39.71	5.28	5.62	695.57
63	95.15	86.94	3.79	5.72	35.88	39.65	5.27	5.62	695.67
64	95.16	86.95	3.80	5.72	35.90	39.65	5.25	5.63	695.65
65	95.18	86.93	3.80	5.71	35.88	39.65	5.29	5.63	695.59
66	95.19	86.94	3.80	5.71	35.89	39.71	5.31	5.62	694.31
67	95.19	86.93	3.80	5.72	35.87	39.65	5.29	5.61	695.81
68	95.17	86.94	3.80	5.72	35.89	39.65	5.31	5.61	694.86

69	95.20	86.97	3.80	5.72	35.91	39.65	5.21	5.61	694.68
70	95.20	86.96	3.80	5.72	35.90	39.65	5.26	5.62	694.07
71	95.21	86.98	3.80	5.72	35.94	39.65	5.31	5.61	694.35
72	95.19	86.95	3.80	5.72	35.91	39.65	5.31	5.61	694.39
73	95.18	86.95	3.79	5.71	35.91	39.65	5.33	5.62	693.91
74	95.18	86.94	3.79	5.71	35.90	39.65	5.24	5.61	694.62
75	95.19	86.97	3.80	5.71	35.93	39.65	5.26	5.61	694.60
76	95.19	86.96	3.80	5.71	35.92	39.65	5.29	5.60	694.28
77	95.21	86.98	3.80	5.71	35.93	39.65	5.26	5.62	694.88
78	95.20	86.96	3.80	5.71	35.92	39.65	5.17	5.61	694.44
79	95.20	86.98	3.80	5.71	35.93	39.65	5.26	5.61	694.14
80	95.20	86.96	3.80	5.71	35.91	39.65	5.27	5.60	694.77
81	95.19	86.96	3.80	5.71	35.91	39.65	5.29	5.62	694.56
82	95.22	86.98	3.80	5.71	35.94	39.65	5.33	5.61	694.14
83	95.19	86.95	3.80	5.71	35.90	39.65	5.29	5.61	694.77
84	95.18	86.98	3.80	5.72	35.94	39.65	5.31	5.61	694.56
85	95.19	86.95	3.79	5.71	35.91	39.71	5.20	5.61	694.83
86	95.16	86.97	3.79	5.72	35.92	39.65	5.29	5.62	694.10
87	95.16	86.97	3.79	5.72	35.92	39.65	5.29	5.62	694.10
88	95.18	86.95	3.80	5.71	35.91	39.72	5.33	5.62	694.44
89	95.20	86.98	3.80	5.71	35.93	39.71	5.31	5.62	694.45
90	95.19	86.98	3.80	5.71	35.93	39.66	5.29	5.61	693.54
91	95.19	86.98	3.80	5.71	35.93	39.66	5.29	5.61	693.54
92	95.19	86.97	3.79	5.72	35.93	39.65	5.27	5.63	694.78
93	95.19	86.98	3.79	5.72	35.94	39.65	5.23	5.62	694.59
94	95.20	86.98	3.79	5.73	35.93	39.65	5.29	5.61	694.30
95	95.20	86.98	3.79	5.73	35.93	39.65	5.29	5.61	694.30
96	95.21	86.94	3.79	5.72	35.89	39.65	5.19	5.63	694.16
97	95.20	86.95	3.79	5.72	35.91	39.65	5.31	5.63	694.55
98	95.21	86.97	3.79	5.72	35.92	39.65	5.29	5.64	694.71
99	95.21	86.97	3.79	5.72	35.92	39.65	5.29	5.64	694.71
100	95.20	86.96	3.79	5.72	35.91	39.65	5.33	5.61	694.92

Table A5.3: Experimental results of PX 37 °C case for 100 Seconds

Time Seconds	Ejectors motive pressure bar	GC pressure bar	LP ejector DP bar	HP ejector DP bar	PX DP bar	PX HP _{out} C	PX LP _{in} flow kg/min	PX HP _{out} flow kg/min	PX RPM
1	100.99	92.32	4.02	6.07	40.72	42.13	5.46	5.59	624.22
2	101.01	92.31	4.02	6.07	40.71	42.03	5.41	5.59	624.33
3	100.98	92.32	4.02	6.07	40.72	42.03	5.43	5.59	624.24
4	100.96	92.28	4.02	6.07	40.68	42.03	5.39	5.60	624.32
5	100.96	92.28	4.02	6.07	40.68	42.03	5.39	5.60	624.32
6	100.95	92.28	4.02	6.06	40.70	42.02	5.41	5.59	624.40
7	100.96	92.28	4.02	6.07	40.69	41.94	5.40	5.59	623.96
8	100.96	92.27	4.02	6.07	40.68	41.94	5.44	5.61	624.23
9	100.95	92.25	4.02	6.07	40.66	41.94	5.46	5.60	624.58
10	100.94	92.25	4.02	6.07	40.66	41.94	5.45	5.60	624.21
11	100.93	92.27	4.02	6.06	40.68	42.03	5.42	5.59	623.95
12	100.92	92.27	4.02	6.06	40.68	42.03	5.42	5.59	623.95
13	100.89	92.22	4.02	6.06	40.63	42.03	5.46	5.60	624.81
14	100.88	92.22	4.02	6.06	40.63	42.02	5.43	5.59	624.80
15	100.84	92.23	4.02	6.06	40.64	42.03	5.46	5.55	623.98
16	100.86	92.20	4.02	6.05	40.61	41.94	5.40	5.57	624.33
17	100.83	92.19	4.01	6.05	40.61	41.94	5.39	5.57	623.83
18	100.79	92.17	4.01	6.05	40.60	41.94	5.42	5.58	623.99
19	100.80	92.14	4.01	6.05	40.56	41.94	5.41	5.57	622.72
20	100.78	92.13	4.01	6.05	40.56	41.94	5.41	5.56	622.77
21	100.76	92.12	4.01	6.05	40.54	41.94	5.42	5.59	624.62
22	100.77	92.12	4.01	6.05	40.54	41.94	5.42	5.60	624.62
23	100.74	92.10	4.01	6.05	40.51	41.94	5.49	5.58	624.57
24	100.74	92.09	4.01	6.05	40.50	41.94	5.45	5.59	624.25
25	100.74	92.09	4.01	6.05	40.50	41.84	5.44	5.59	624.45
26	100.70	92.08	4.01	6.05	40.50	41.84	5.40	5.60	624.63
27	100.70	92.05	4.01	6.05	40.47	41.83	5.40	5.61	624.50
28	100.71	92.05	4.01	6.05	40.47	41.83	5.40	5.61	624.50
29	100.68	92.05	4.01	6.05	40.47	41.84	5.40	5.60	624.30
30	100.70	92.02	4.01	6.05	40.43	41.84	5.44	5.60	624.05
31	100.67	92.01	4.01	6.05	40.43	41.84	5.43	5.60	624.35
32	100.67	92.04	4.01	6.05	40.46	41.84	5.43	5.60	624.21
33	100.68	92.01	4.01	6.05	40.42	41.84	5.41	5.60	623.23
34	100.64	92.00	4.01	6.04	40.43	41.83	5.36	5.58	623.90
35	100.63	91.98	4.01	6.04	40.40	41.73	5.42	5.57	624.46
36	100.64	91.99	4.01	6.04	40.42	41.73	5.43	5.59	624.50
37	100.62	91.99	4.01	6.04	40.42	41.73	5.38	5.59	624.41
38	100.62	91.99	4.01	6.04	40.41	41.73	5.38	5.60	624.41
39	100.62	91.99	4.00	6.04	40.42	41.73	5.44	5.59	623.88
40	100.63	91.99	4.00	6.04	40.42	41.73	5.44	5.61	624.14
41	100.61	92.00	4.00	6.04	40.43	41.73	5.38	5.59	624.12

42	100.60	91.96	4.00	6.04	40.40	41.73	5.42	5.60	624.06
43	100.60	91.95	4.00	6.04	40.39	41.73	5.40	5.60	623.87
44	100.61	91.95	4.00	6.04	40.39	41.73	5.40	5.60	623.87
45	100.60	91.99	4.00	6.04	40.43	41.73	5.41	5.60	624.42
46	100.59	91.96	4.00	6.04	40.39	41.73	5.42	5.60	623.80
47	100.60	91.94	4.00	6.04	40.36	41.73	5.37	5.60	624.86
48	100.62	91.95	4.00	6.04	40.38	41.73	5.39	5.60	623.77
49	100.59	91.93	4.00	6.04	40.36	41.73	5.43	5.61	624.38
50	100.58	91.95	4.00	6.04	40.38	41.72	5.42	5.61	623.68
51	100.61	91.94	4.00	6.04	40.37	41.72	5.38	5.62	624.25
52	100.53	91.96	4.00	6.05	40.39	41.73	5.41	5.62	623.95
53	100.17	91.89	4.00	6.04	40.33	41.73	5.40	5.61	623.96
54	100.00	91.75	4.00	5.98	40.24	41.73	5.42	5.54	624.38
55	99.85	91.59	3.99	5.92	40.14	41.67	5.39	5.42	624.44
56	99.70	91.32	3.98	5.86	39.94	41.71	5.31	5.37	624.43
57	99.39	91.16	3.97	5.83	39.81	41.73	5.33	5.37	624.31
58	99.63	91.08	3.96	5.82	39.74	41.73	5.33	5.34	624.78
59	99.73	91.13	3.96	5.87	39.74	41.73	5.31	5.42	624.51
60	99.82	91.18	3.96	5.93	39.73	41.72	5.33	5.55	624.12
61	99.88	91.22	3.96	5.96	39.74	41.73	5.36	5.60	624.26
62	99.96	91.28	3.96	6.00	39.77	41.73	5.39	5.62	624.86
63	100.02	91.36	3.96	6.03	39.82	41.63	5.33	5.63	624.23
64	100.05	91.38	3.97	6.03	39.82	41.63	5.39	5.63	623.91
65	100.11	91.41	3.97	6.03	39.85	41.63	5.41	5.63	624.01
66	100.11	91.45	3.97	6.04	39.88	41.63	5.41	5.61	623.82
67	100.17	91.50	3.97	6.05	39.93	41.63	5.41	5.62	624.74
68	100.23	91.56	3.98	6.05	39.98	41.63	5.40	5.64	624.56
69	100.26	91.56	3.98	6.05	39.97	41.63	5.38	5.65	624.01
70	100.30	91.62	3.98	6.05	40.04	41.63	5.39	5.64	623.84
71	100.33	91.63	3.98	6.06	40.04	41.63	5.41	5.63	624.42
72	100.40	91.69	3.99	6.05	40.10	41.63	5.46	5.66	624.08
73	100.43	91.73	3.99	6.06	40.13	41.63	5.41	5.66	625.10
74	100.46	91.76	3.99	6.06	40.16	41.52	5.43	5.67	625.63
75	100.46	91.77	3.99	6.07	40.16	41.52	5.43	5.68	623.67
76	100.50	91.83	3.99	6.07	40.22	41.52	5.38	5.67	624.30
77	100.52	91.82	3.99	6.07	40.21	41.52	5.40	5.65	624.28
78	100.54	91.85	3.99	6.07	40.24	41.52	5.40	5.66	624.44
79	100.54	91.88	4.00	6.07	40.27	41.52	5.43	5.66	624.08
80	100.56	91.92	4.00	6.07	40.32	41.63	5.39	5.64	624.01
81	100.56	91.92	4.00	6.07	40.32	41.63	5.42	5.64	624.31
82	100.59	91.95	4.00	6.06	40.34	41.63	5.41	5.65	624.49
83	100.62	91.97	4.00	6.06	40.37	41.63	5.45	5.63	623.99
84	100.64	91.96	4.00	6.06	40.35	41.63	5.46	5.62	623.92
85	100.65	92.00	4.00	6.06	40.40	41.63	5.46	5.63	623.84
86	100.67	92.01	4.00	6.06	40.41	41.63	5.44	5.63	624.46
87	100.67	92.00	4.00	6.06	40.40	41.63	5.43	5.63	624.73
88	100.67	92.02	4.01	6.06	40.43	41.63	5.44	5.61	623.98
89	100.67	92.02	4.00	6.06	40.42	41.63	5.41	5.64	624.27

90	100.68	92.04	4.00	6.06	40.45	41.63	5.36	5.63	623.99
91	100.67	92.02	4.00	6.06	40.44	41.63	5.36	5.62	624.75
92	100.68	92.02	4.00	6.06	40.44	41.63	5.42	5.61	624.86
93	100.68	91.99	4.00	6.06	40.40	41.52	5.44	5.61	624.82
94	100.67	92.01	4.00	6.06	40.43	41.63	5.42	5.63	624.38
95	100.68	92.02	4.00	6.06	40.43	41.63	5.43	5.63	624.24
96	100.68	92.02	4.00	6.06	40.43	41.63	5.43	5.63	624.24
97	100.69	92.01	4.01	6.06	40.42	41.63	5.43	5.63	624.39
98	100.65	91.99	4.01	6.07	40.39	41.63	5.44	5.63	624.21
99	100.62	91.99	4.00	6.07	40.40	41.63	5.43	5.65	624.38
100	100.62	91.99	4.00	6.07	40.40	41.63	5.43	5.65	624.38

Table A5.4: Experimental results of PX 38 °C case for 100 Seconds

Time Seconds	Ejectors motive pressure bar	GC pressure bar	LP ejector DP bar	HP ejector DP bar	PX DP bar	PX HP _{out} C	PX LP _{in} flow kg/min	PX HP _{out} flow kg/min	PX RPM
1	103.26	94.64	4.12	6.06	42.96	43.01	5.52	5.75	617.18
2	103.27	94.63	4.12	6.05	42.94	43.02	5.48	5.70	618.13
3	103.27	94.63	4.12	6.05	42.94	43.02	5.48	5.70	618.13
4	103.25	94.65	4.12	6.06	42.96	43.01	5.46	5.69	617.76
5	103.24	94.60	4.12	6.06	42.92	43.01	5.46	5.71	618.40
6	103.27	94.61	4.12	6.06	42.92	43.01	5.48	5.70	618.27
7	103.27	94.61	4.12	6.06	42.92	43.01	5.48	5.70	618.27
8	103.28	94.63	4.12	6.06	42.94	43.01	5.46	5.73	618.68
9	103.29	94.66	4.12	6.06	42.96	43.01	5.48	5.76	618.13
10	103.29	94.65	4.12	6.06	42.96	43.14	5.43	5.73	618.05
11	103.28	94.63	4.12	6.06	42.94	43.13	5.48	5.73	618.04
12	103.29	94.66	4.11	6.06	42.97	43.14	5.48	5.73	617.89
13	103.29	94.66	4.11	6.06	42.97	43.14	5.48	5.73	617.89
14	103.28	94.64	4.12	6.06	42.95	43.01	5.46	5.70	618.28
15	103.28	94.64	4.12	6.07	42.93	43.13	5.45	5.73	618.47
16	103.27	94.61	4.11	6.07	42.90	43.13	5.52	5.77	618.08
17	103.26	94.58	4.11	6.07	42.87	43.01	5.47	5.76	618.12
18	103.21	94.55	4.11	6.07	42.84	43.13	5.46	5.76	617.76
19	103.21	94.53	4.11	6.08	42.81	43.10	5.46	5.78	618.28
20	103.21	94.53	4.11	6.08	42.82	43.14	5.48	5.80	618.18
21	103.17	94.53	4.11	6.08	42.82	43.01	5.51	5.80	617.92
22	103.18	94.50	4.11	6.08	42.79	43.01	5.48	5.78	618.33
23	103.19	94.50	4.11	6.08	42.79	43.02	5.46	5.78	618.04
24	103.19	94.52	4.11	6.08	42.80	43.02	5.41	5.78	618.12
25	103.18	94.49	4.11	6.08	42.78	43.14	5.46	5.79	617.95
26	103.19	94.51	4.11	6.08	42.80	43.01	5.44	5.77	618.34

27	103.14	94.50	4.11	6.07	42.79	43.14	5.50	5.76	618.27
28	103.12	94.48	4.11	6.07	42.77	43.01	5.45	5.75	617.61
29	103.15	94.48	4.11	6.08	42.77	43.01	5.45	5.76	617.64
30	103.13	94.49	4.11	6.08	42.77	43.01	5.44	5.75	618.11
31	103.11	94.46	4.11	6.08	42.74	43.01	5.43	5.75	618.43
32	103.12	94.45	4.11	6.08	42.73	43.02	5.47	5.74	617.73
33	103.11	94.45	4.11	6.07	42.74	43.01	5.50	5.74	617.80
34	103.09	94.45	4.11	6.07	42.73	43.02	5.45	5.74	618.36
35	103.10	94.45	4.11	6.07	42.73	43.02	5.51	5.73	619.17
36	103.10	94.46	4.11	6.07	42.75	43.02	5.51	5.72	619.20
37	103.11	94.52	4.11	6.06	42.82	43.02	5.48	5.70	618.85
38	103.14	94.52	4.11	6.05	42.82	43.01	5.46	5.65	619.61
39	103.12	94.53	4.11	6.04	42.85	43.02	5.50	5.63	618.86
40	103.12	94.53	4.12	6.04	42.84	43.02	5.52	5.61	620.52
41	103.11	94.53	4.11	6.04	42.84	43.01	5.47	5.65	620.28
42	103.12	94.51	4.12	6.05	42.81	43.01	5.50	5.67	620.16
43	103.10	94.53	4.12	6.05	42.82	43.01	5.41	5.67	621.56
44	103.11	94.52	4.12	6.05	42.81	43.01	5.42	5.64	621.87
45	103.07	94.48	4.12	6.05	42.78	43.02	5.46	5.63	621.96
46	103.08	94.48	4.12	6.05	42.78	43.01	5.47	5.65	621.37
47	103.09	94.49	4.12	6.04	42.79	43.01	5.40	5.66	622.04
48	103.07	94.47	4.12	6.05	42.78	43.01	5.46	5.62	621.45
49	103.03	94.46	4.12	6.04	42.78	42.94	5.50	5.65	621.57
50	103.03	94.46	4.12	6.04	42.78	42.94	5.50	5.65	621.57
51	103.03	94.45	4.12	6.04	42.76	43.01	5.42	5.64	621.66
52	103.02	94.46	4.11	6.04	42.77	43.01	5.42	5.62	621.60
53	103.00	94.43	4.11	6.04	42.74	43.02	5.43	5.61	621.58
54	103.01	94.47	4.11	6.03	42.79	43.01	5.43	5.62	621.45
55	103.03	94.43	4.11	6.03	42.77	43.01	5.44	5.60	621.67
56	103.02	94.44	4.11	6.03	42.76	43.01	5.52	5.58	621.78
57	102.98	94.39	4.11	6.03	42.70	43.01	5.45	5.62	622.52
58	102.98	94.39	4.11	6.03	42.70	43.01	5.45	5.62	622.52
59	102.92	94.33	4.11	6.04	42.63	43.01	5.46	5.63	622.90
60	102.92	94.33	4.11	6.04	42.63	43.01	5.46	5.63	622.90
61	102.90	94.28	4.11	6.04	42.58	43.01	5.46	5.65	621.35
62	102.87	94.28	4.11	6.05	42.58	43.01	5.44	5.67	623.10
63	102.83	94.24	4.11	6.05	42.54	43.01	5.44	5.65	622.97
64	102.84	94.22	4.11	6.05	42.52	43.01	5.47	5.65	622.56
65	102.84	94.22	4.11	6.05	42.52	43.01	5.47	5.65	622.56
66	102.81	94.20	4.11	6.05	42.51	43.02	5.39	5.63	621.70
67	102.80	94.19	4.10	6.05	42.50	43.01	5.44	5.67	621.99
68	102.75	94.19	4.11	6.05	42.49	43.02	5.52	5.66	621.63
69	102.77	94.17	4.11	6.05	42.47	43.13	5.48	5.65	621.76
70	102.77	94.17	4.10	6.05	42.48	43.13	5.38	5.63	623.22
71	102.76	94.16	4.10	6.05	42.48	43.13	5.41	5.63	622.60
72	102.77	94.15	4.10	6.05	42.46	43.14	5.45	5.64	623.46
73	102.74	94.18	4.10	6.05	42.49	43.14	5.43	5.63	622.90
74	102.73	94.13	4.10	6.05	42.45	43.13	5.46	5.65	622.78

75	102.75	94.14	4.11	6.06	42.45	43.13	5.42	5.67	623.01
76	102.75	94.14	4.11	6.06	42.45	43.13	5.42	5.67	623.01
77	102.74	94.12	4.11	6.06	42.44	43.13	5.50	5.66	623.02
78	102.74	94.12	4.11	6.06	42.43	43.14	5.50	5.66	623.02
79	102.73	94.14	4.10	6.06	42.46	43.13	5.42	5.65	622.31
80	102.73	94.14	4.10	6.06	42.46	43.13	5.42	5.65	622.31
81	102.77	94.19	4.11	6.05	42.52	43.01	5.46	5.63	621.93
82	102.79	94.19	4.11	6.04	42.51	43.01	5.44	5.60	621.40
83	102.79	94.21	4.11	6.04	42.55	43.01	5.46	5.59	622.05
84	102.81	94.25	4.11	6.03	42.58	43.02	5.50	5.60	622.68
85	102.81	94.25	4.11	6.03	42.58	43.02	5.50	5.60	622.68
86	102.83	94.23	4.11	6.03	42.56	42.94	5.51	5.59	623.25
87	102.83	94.24	4.11	6.03	42.57	43.02	5.50	5.57	622.69
88	102.82	94.23	4.11	6.03	42.55	43.01	5.48	5.60	622.72
89	102.82	94.22	4.11	6.03	42.54	43.01	5.50	5.59	622.35
90	102.84	94.23	4.11	6.03	42.56	43.01	5.47	5.59	622.58
91	102.82	94.23	4.11	6.03	42.55	43.01	5.44	5.61	623.08
92	102.83	94.24	4.11	6.03	42.55	43.01	5.46	5.61	623.31
93	102.81	94.29	4.11	6.03	42.62	43.01	5.43	5.58	623.15
94	102.81	94.26	4.11	6.03	42.58	43.02	5.44	5.58	622.88
95	102.84	94.29	4.11	6.02	42.62	43.02	5.44	5.60	622.02
96	102.84	94.28	4.11	6.02	42.61	43.01	5.41	5.61	623.22
97	102.86	94.29	4.11	6.03	42.62	43.01	5.44	5.62	621.95
98	102.90	94.29	4.11	6.03	42.62	43.01	5.44	5.62	621.95
99	102.90	94.29	4.11	6.03	42.61	43.02	5.50	5.59	622.75
100	102.90	94.32	4.11	6.03	42.64	42.94	5.46	5.59	621.23

Appendix B

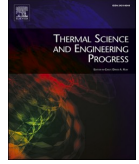
Journal article 1

M.Z. Saeed, Á.Á. Pardiñas, K. Banasiak, A. Hafner, A. Thatte, Thermodynamic analysis of rotary pressure exchanger and ejectors for CO₂ refrigeration system, *Thermal Science and Engineering Progress*, 51 (2024) 102643. <https://doi.org/10.1016/j.tsep.2024.102643>.



Contents lists available at ScienceDirect

Thermal Science and Engineering Progress

journal homepage: www.sciencedirect.com/journal/thermal-science-and-engineering-progressThermodynamic analysis of rotary pressure exchanger and ejectors for CO₂ refrigeration system[☆]Muhammad Zahid Saeed^{a,*}, Ángel Álvarez Pardiñas^b, Krzysztof Banasiak^c, Armin Hafner^a, Azam Thatte^d^a NTNU, Department of Energy and Process Engineering, Kolbjørn Hejes vei 1B, 7491 Trondheim, Norway^b Energy Division, Galicia Institute of Technology ITG, 15003 A Coruña, Spain^c SINTEF Energy Research, Sem Sælands vei 11, 7034 Trondheim, Norway^d Energy Recovery, San Leandro, CA 94577, USA

ARTICLE INFO

Keywords:

Refrigeration
Carbon Dioxide
Transcritical
Pressure Exchanger
Ejectors
Energy Efficiency

ABSTRACT

Natural refrigerant CO₂ has become a viable choice for refrigeration units for land-based and offshore applications due to its environment-friendly nature and compactness. The CO₂ transcritical cycle allows operating in colder climates and in elevated ambient temperature conditions and with significant heat recovery. However, the energy efficiency of the system suffers at higher heat rejection conditions mainly due to expansion losses. This work theoretically investigates and proposes the implementation of a new expansion work recovery device, a pressure exchanger (CO₂-PX), for the transcritical CO₂ cycle. The numerical models are developed in the Engineering Equation solver (EES) to compare the performance of CO₂-PX configuration with standard booster-, parallel-, and ejector- configurations for various conditions. The analysis is carried out for the evaporation temperature of 0 °C and the gas cooler outlet temperature of 33 °C to 37 °C. The results indicate that the coefficient of performance (COP) is improved by 17.7–23.5%, 16.3–20.3%, and 2.4–5.5% to the standard booster, parallel and ejector configurations, respectively, at the investigated conditions.

1. Introduction

High GWP (Global Warming Potential) refrigerants are being phased out due to different international and national regulations. The EU F-gas Regulation regulates a phase-down of HFCs throughout the EU, which began in 2015 [1]. Its goal is to reduce EU HFC emissions by two-thirds by 2030 compared to 2014 [2]. According to the F-gas regulation, stationary refrigeration equipment that includes, or whose operation is dependent on, HFCs with a GWP of 2500 or more is currently prohibited as of January 2020, with the exception of equipment meant to cool items to temperatures below –50 °C [3]. On January 1, 2019, the Kigali Amendment to the Montreal Protocol for the Phase down of HFCs was adopted at the global level. By 2047, the objective is to reduce HFC use by more than 80 %. The amendment's influence will prevent a global temperature rise of up to 0.5 °C by the end of the century [4]. As a consequence, ammonia (NH₃), carbon dioxide (CO₂), hydrocarbons and water as working fluids have gained a lot of attention [1]. However, NH₃

and hydrocarbons are restricted for some applications due to toxicity, flammability, and additional safety requirements, which increase the complexity and cost of units. CO₂ as a refrigerant is accepted as a long-term solution for onshore and offshore commercial applications due to its suitable thermodynamic properties, non-flammability, non-toxicity, natural existence, and global availability in the market. This gives wide application possibilities to CO₂ compared to other natural and synthetic refrigerants [5,6].

In the past, the low critical point of CO₂ made operation difficult, especially in regions with high temperatures. This issue was successfully addressed by Lorentzen [7], who re-evaluated the use of CO₂ in transcritical mode as a potential substitute refrigerant to mitigate the adverse effect of global warming and ozone depletion. In transcritical operation, a substantial energy loss occurs in the expansion valve due to the significant pressure difference between the gas cooler and liquid receiver. As a result, there is much interest in adopting alternate expansion devices to reduce the throttling losses and improve the coefficient of performance (COP) of CO₂ systems. Due to the distinctive

[☆] PX concept of this paper has previously been introduced in the 15th IIR Gustav Lorentzen conference. Saeed et al., 2022. Simultaneous implementation of rotary pressure exchanger and ejectors for CO₂ refrigeration system. Pg 790–797. <http://dx.doi.org/10.18462/iir.gl2022.0130>.

* Corresponding author.

E-mail addresses: muhammad.z.saeed@ntnu.no (M.Z. Saeed), athatte@energyrecovery.com (A. Thatte).

<https://doi.org/10.1016/j.tsep.2024.102643>

Received 18 October 2023; Received in revised form 28 April 2024; Accepted 17 May 2024

Available online 20 May 2024

2451-9049/© 2024 The Author(s). Published by Elsevier Ltd. This is an open access article under the CC BY license (<http://creativecommons.org/licenses/by/4.0/>).

Nomenclature		W	power (kW)
CFD	computation fluid dynamics	x	vapour quality
COP	coefficient of performance	<i>Subscripts</i>	
EES	engineering equation solver	b	booster case
Ejec	ejector	BR	boost ratio
EU	European union	com	compressor
evap	evaporator	D	destruction
exp	expansion	e	evaporator
FGBV	flash gas bypass valve	ej	ejector
GC	gascooler	exp	expansion
GWP	global warming potential	g	generation
HFC	hydrofluorocarbon	GC	gascooler
HP	high pressure	HP	high pressure
HX	heat exchanger	in	inlet
LP	low pressure	is	isentropic
MBR	mass boost ratio	LP	low pressure
N	no	m	motive
PX	pressure exchanger	o	ambient
PWS	Pressure wave supercharger	out	outlet
RO	reverse osmosis	par	parallel
SHX	suction gas HX	px	pressure exchanger
Y	yes	rec	liquid receiver
<i>Variables</i>		s	suction
E	exergy (kW)	SHX	suction gas HX
h	specific enthalpy (kJ/kg)	tot	total
m	mass flow (kg/s)	<i>Greek symbols</i>	
P	pressure (bar)	ρ	density (kg/m ³)
Q	heat load (kW)	η	efficiency
s	specific entropy (kJ/kg K)	\emptyset	Entrainment ratio
T	temperature (°C)		

properties of carbon dioxide, a feasible option is to recuperate the expansion work by means of expansion turbine. The utilisation of expansion turbine has the potential to result in a COP enhancement ranging from 14 % to 17 % [8]. Ejectors are a well-known method for enhancing the efficiency of the CO₂ cycle [9]. The efficacy of incorporating ejectors in transcritical CO₂ refrigeration systems has been substantiated both through theoretical and empirical means. Based on the outcomes of the simulation, it can be inferred that the coefficient of performance of the ejector expansion transcritical CO₂ cycle exhibits an approximate increase of 20 % in comparison to that of a basic transcritical cycle [10–12]. Two key innovation techniques are pushing and expanding the CO₂ system's uses further for warmer climates. The first is consolidating all thermal functions into a single compact unit. The second strategy is to improve the energy efficiency of conventional CO₂ systems at warm climate operations. Some of the most recently implemented innovations in the supermarket refrigeration industry include ejectors, parallel compression, mechanical sub-cooling, and gas cooler evaporative cooling. Mechanical sub-cooling and evaporative cooling are two modification choices that enhance the gas cooling process and give greater energy efficiency in hotter regions. In contrast, flooding evaporation increases system energy efficiency in any climate [13]. The CO₂ refrigerant has also been affected in the past by high operating and installation costs [14]. The growing demand for CO₂ systems has reduced the components' cost, and the price is becoming competitive, which encourages manufacturers to introduce more sustainable components in the market [15].

The present study investigates a novel work recovery device for CO₂ systems, namely a pressure exchanger [16]. A pressure exchanger consists of a cylindrical rotor with several channels arranged around its axis. The rotor is supported by two fixed-end plates on either side of which

there are ports for directing fluid flow into and out of the rotor channels. As the rotor turns, the channel ends are periodically exposed to a range of port pressures, resulting in compression and expansion inside the rotor channels.

As a consequence, a high-pressure stream's pressure can be transferred to a low-pressure stream, increasing its pressure while decreasing the high-pressure stream's [16]. The detailed working principle of pressure exchangers is explained in the literature [17–19]. A 2D CFD model to show the CO₂ inlet and outlet flows in the PX is reported by Elatar et al. [20]. PX has already been used in reverse osmosis (RO) desalination units for many years to recover pressure work from the high-pressure reject concentrate and transfer it to a low-pressure feed. The PX device was designed for direct pressure transmission from HP to LP stream of RO unit to improve performance [21]. The early research development of PX for desalination units predicted power savings higher than 60 % [22]. The results obtained from the desalination plant equipped with PX proved that the energy demand of the RO unit can decrease by 25 to 30 % compared to other energy recovery devices [23]. PX also works on the same working principle as a pressure-wave supercharger (PWS). In compression ignition engines, PWS increase the pressure of fresh air intake by extracting the pressure from exhaust gas through PWS rotor. As a result, the air intake gets compression and exhaust gas gets expansion. PWS works on the fact that pressure equalization is faster than the mixing of streams [24,25]. The working principle of CO₂-PX and PWS is same, but CO₂-PX is unique in few ways. A CO₂-PX can expand high pressure and high-density supercritical CO₂ gas into two-phase fluid, but PWS deals with low pressure, low density and only one-phase fluid. In contrast to RO-PX, the only difference is two-phase fluid as the RO-PX can manage high pressure and high density.

A new version of PX is adapted for work recovery in CO₂ systems (CO₂-PX) to recover the expansion work and compress the flash gas directly, as shown schematically in Fig. 1. High-pressure CO₂ enters from the bottom right port (HP_{in}) and, after decrementing in pressure, goes through the bottom-left port (LP_{out}). The flash gas from the phase separator enters from the top left port (LP_{in}) and, after getting compressed inside the PX, leaves through the top right port (HP_{out}). The energy required for this compression is extracted through the expansion work recovered released during the expansion of HP_{in} fluid stream to LP_{out} pressure. The proposed CO₂-PX integration concept using ejectors (Fig. 5) is an evolution of a previous approach where two booster compressors [18] were implemented to overcome small pressure lifts of flash gas. The use of novel ejectors gives an innovative approach to integrate the PX without complexity and boosting the system performance. This work aims to theoretically investigate the performance of CO₂-PX and ejectors integration and the comparison with existing configurations of CO₂, i.e., standard booster, parallel and ejector configuration. The thermodynamic models are made in EES [26] to study and compare the energy and exergy performance of the PX-based architecture as well as of other configurations.

2. Methods and data

2.1. Evaluated systems

This work compares three system configurations of CO₂ with the newly proposed pressure exchanger integrated concept for CO₂ systems. The different system configurations are presented in Figs. 2–5, including their p-h diagrams.

The first system is the standard booster system which is one of the three comparison configurations, and it is depicted in Fig. 2. The standard booster system includes an evaporator, suction gas HX, compressor, gas cooler, throttling valve, liquid receiver, and flash gas bypass valve (FGBV). The refrigerant in the evaporator absorbs heat, and the suction gas HX then superheats the refrigerant. The compressor lifts the pressure from the evaporator to the gas cooler and maintains the required suction pressure. The gas cooler rejects heat, and then the refrigerant expands to the liquid receiver pressure in the throttling valve. The throttling valve also controls the gas cooler pressure. The FGBV removes the vapour from the receiver and bypasses it to the suction gas HX. The liquid

refrigerant flows from the receiver, and the second throttling valve expands it to the evaporator pressure, which maintains the required cooling capacity, and the cycle repeats. The second comparison system is illustrated in Fig. 3, which is a parallel compression system. In this system, the addition is the parallel compressor, which removes the flash gas from the liquid receiver and lifts it to the gas cooler pressure. The second addition is another suction gas HX, which assures the superheating of flash gas before parallel compressor suction. The third system is the ejector configuration presented in Fig. 4. The ejector provides the free pressure lift of the refrigerant stream from the evaporator back to the liquid receiver pressure. The compressor lifts the vapour from receiver pressure to the gas cooler pressure, and the superheat of vapours is added in the suction gas HX.

The novel concept of an integrated pressure exchanger is presented in Fig. 5. In this configuration, the addition is the PX, and the two ejectors compared to the standard booster system. The expansion work of high-pressure gas compresses the flash gas, thus reducing the energy required by the main compressor and thereby enhancing the system's efficiency. The flash gas from the liquid receiver needs a pressure boost before entering the PX. According to the PX manufacturer, this small pressure boost is essential to push the two-phase stream out of PX [18]. The flash gas from the liquid receiver is slightly (around 2 bar) lifted with the ejector (LP), flows into the PX, and is lifted to 2 bar below the gas cooler pressure. This 2-bar pressure loss arises from flow friction losses in the piping and in the gas cooler as well as due to a small pressure loss in the PX. The second ejector (HP) provides this lift of 2 bar to the gas cooler pressure. If PX cannot handle all the available flash gas alone, it partially bypasses it to the evaporator pressure using FGBV. The amount of flash gas bypass can be determined using mass boost ratio. The other side of the PX expands the high-pressure gas from the gas cooler exit into a low-pressure two-phase fluid which then proceeds to the liquid receiver. It is important to note that the compressor discharge and gas cooler pressures differ by around 2–3 bar to entrain the flash gas with the HP ejector from the exit of PX to the gas cooler pressure. All the systems are evaluated under the exact same boundary conditions so as to accurately compare their coefficient of performance.

2.2. Mathematical modelling

The primary equations for the developed PX concept and other

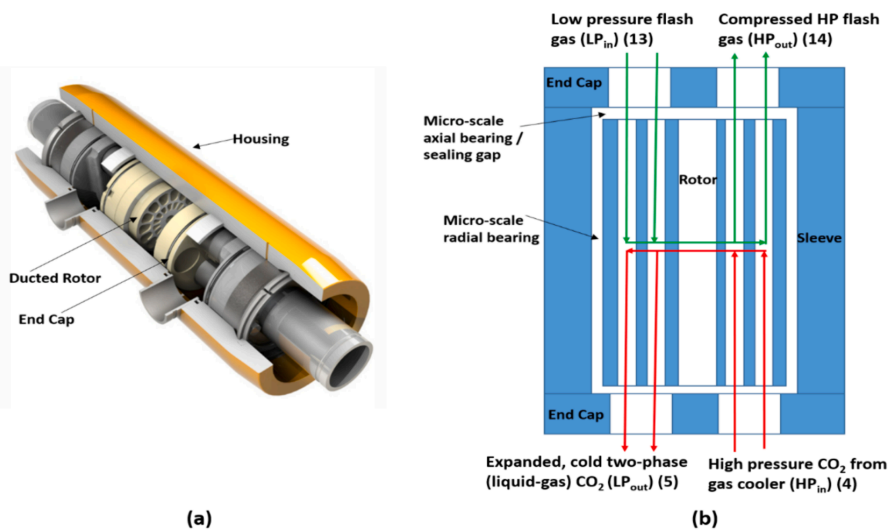


Fig. 1. PX internal mechanism (a) Cut section (b) Four ports of the PX.

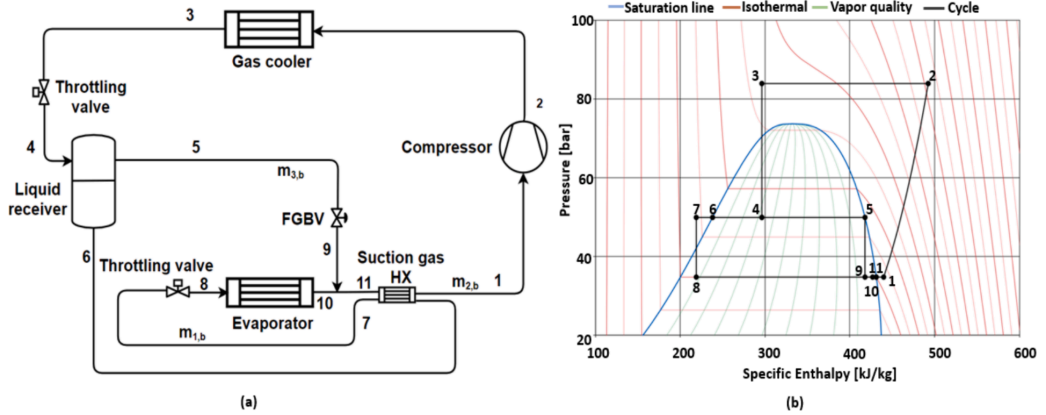


Fig. 2. High stage of standard booster CO₂ system (a) Schematic (b) Ph diagram.

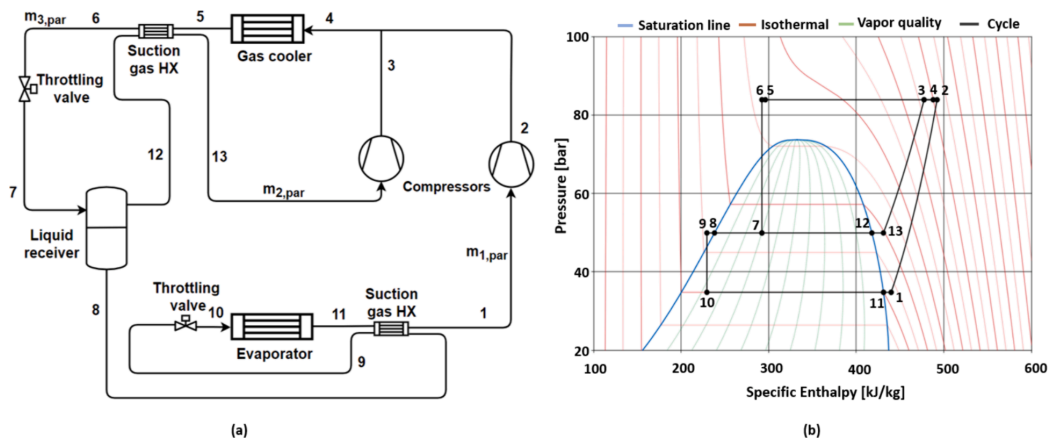


Fig. 3. Parallel compression CO₂ system (a) Schematic (b) Ph diagram.

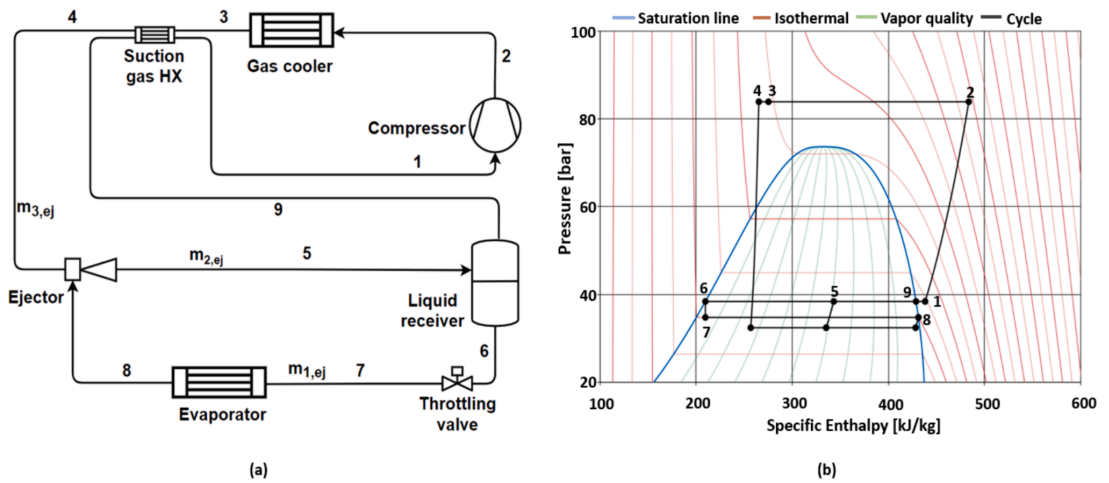
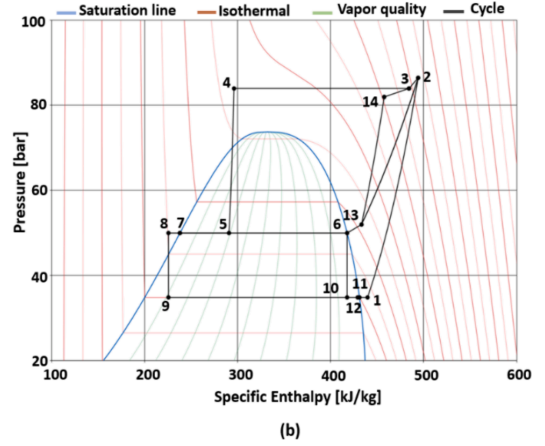
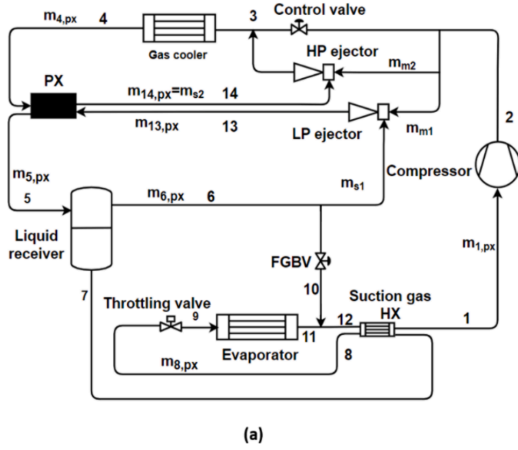


Fig. 4. Ejector configuration CO₂ system (a) Schematic (b) Ph diagram.



(MBR) for the PX is defined as the ratio of low-pressure inlet mass flow that can be compressed per unit mass flow entering the high-pressure inlet for expansion, which is shown in Eq. (15). The MBR can also be written in terms of their density ratio as shown in Eq. (16).

$$\text{MBR} = \frac{m_{13,\text{px}}}{m_{4,\text{px}}} \quad (15)$$

$$\text{MBR} = \frac{\rho_{13}}{\rho_4} \quad (16)$$

In the ideal operation of PX, it is assumed that no mixing of fluids between the expansion and compression sides takes place. Thus, the relationship between mass flow rates becomes

$$m_{4,\text{px}} = m_{5,\text{px}} \quad (17)$$

$$m_{13,\text{px}} = m_{14,\text{px}} \quad (18)$$

The compression and expansion efficiency can be formulated as:

$$\eta_{\text{com,px}} = \frac{h_{14,\text{is}} - h_{13}}{h_{14} - h_{13}} \quad (19)$$

$$\eta_{\text{exp,px}} = \frac{h_4 - h_5}{h_4 - h_{5,\text{is}}} \quad (20)$$

The efficiencies guessed for Eq. (19) and Eq. (20) must satisfy the mass boost ratio of Eq. (15) to get the real enthalpies.

$$\text{MBR} = \frac{h_5 - h_4}{h_{13} - h_{14}} = \frac{h_4 - h_5}{h_{14} - h_{13}} \quad (21)$$

To calculate the entropy generation in the PX device, Eq. (22) can be utilised.

$$s_g = (\text{MBR} \cdot (s_{14} - s_{13}) + (s_5 - s_4)) * m_{4,\text{px}} \geq 0 \quad (22)$$

2.3.1. PX integrated modelling

In this subsection, the modelling and the numbers correspond to Fig. 5. It is to be noted that $h_4 \neq h_5$. The expansion work recovery of the PX is formulated as follows:

$$W_{\text{exp,px}} = m_{4,\text{px}} \cdot (h_4 - h_5) \quad (23)$$

The PX compression mass flow ($m_{13,\text{px}} = m_{s2}$) is the sum of LP ejector suction and motive mass flow (m_{m1}). The PX compression can be written as:

$$W_{\text{com,px}} = m_{13,\text{px}} \cdot (h_{14} - h_{13}) \quad (24)$$

The entrainment ratio of the LP and HP ejectors are as follows:

$$\phi_{\text{LP}} = \frac{m_{s1}}{m_{m1}} \quad (25)$$

$$\phi_{\text{HP}} = \frac{m_{s2}}{m_{m2}} \quad (26)$$

2.3.2. Exergy analysis method

Exergy analysis is used to assess the irreversibility of heat pump cycles. Improving the heat pump cycle curtails exergy degradation. An exergy analysis allows to evaluate the potential improvements in each component and the cycle [29,30]. The following equations describe the framework for exergy calculation according to the state points and variables of PX configuration as described in Fig. 5 and section 2.3.1. The ambient temperature (reference condition), T_0 , is linked to the gas cooler outlet temperature, T_{GCout} , according to the relation $T_0 = T_{\text{GCout}} - 3$. Thus the heat sink temperature $T_{s1} = T_0$, and the heat source temperature is $T_{s2} = T_e + 5$ [31]. The temperature unit for exergy analysis is Kelvin (K). The same equations are utilised for the exergy analysis of

other configurations with their corresponding state points.

$$E_{\text{D,com}} = W_{\text{com,px}} - m_{1,\text{px}} \cdot [(h_2 - h_1) - T_0 \cdot (s_2 - s_1)] \quad (27)$$

$$E_{\text{D,GC}} = m_{4,\text{px}} \cdot [(h_3 - h_4) - T_0 \cdot (s_3 - s_4)] - Q_c \cdot \left(1 - \frac{T_0}{T_{s1}}\right) \quad (28)$$

$$E_{\text{D,exp}} = (m_{e,\text{px}} - m_{s1}) \cdot T_0 \cdot (s_{10} - s_6) + m_{8,\text{px}} \cdot T_0 \cdot (s_9 - s_8) \quad (29)$$

$$E_{\text{D,e}} = Q_{e,\text{px}} \cdot \left(1 - \frac{T_0}{T_{s2}}\right) - m_{8,\text{px}} \cdot [(h_{11} - h_9) - T_0 \cdot (s_{11} - s_9)] \quad (30)$$

$$E_{\text{D,ej}} = T_0 \cdot [(m_{m1} + m_{s1}) \cdot s_{13} - m_{s1} \cdot s_6 - m_{m1} \cdot s_2] + T_0 \cdot [(m_{m2} + m_{s2}) \cdot s_3 - m_{s2} \cdot s_{14} - m_{m2} \cdot s_2] \quad (31)$$

$$E_{\text{D,px}} = m_{4,\text{px}} \cdot T_0 \cdot (s_5 - s_4) + m_{13,\text{px}} \cdot T_0 \cdot (s_{14} - s_{13}) \quad (32)$$

$$E_{\text{D,SHX}} = m_{1,\text{px}} \cdot T_0 \cdot (s_1 - s_{12}) + m_{8,\text{px}} \cdot T_0 \cdot (s_8 - s_7) \quad (33)$$

$$E_{\text{D,tot}} = E_{\text{D,com}} + E_{\text{D,GC}} + E_{\text{D,exp}} + E_{\text{D,e}} + E_{\text{D,ej}} + E_{\text{D,px}} + E_{\text{D,SHX}} \quad (34)$$

$$\eta_{\text{exergy}} = 1 - \frac{E_{\text{D,tot}}}{W_{\text{com,px}}} \quad (35)$$

2.4. Design conditions and PX simulation flow chart

The boundary conditions are identical for the different investigated cases. The evaporation capacity of 60 kW is kept constant for an evaporating temperature (T_e) of 0 °C for all cases to accurately compare the results of different configurations. The gas cooler outlet temperatures are varied from 33 °C to 37 °C with a step size of 1 °C to evaluate the performance of this temperature range. The optimised gas cooler pressures [32] are used, corresponding to the gas cooler outlet temperature for each case. The compressor outlet pressure differs from the gas cooler pressure for the CO₂-PX case, which is unique and essential for this configuration. The difference between the compressor and gas cooler pressure entrains the flash gas from the PX outlet to the gas cooler pressure through the HP ejector. Other investigated cases have the same gascooler and compressor outlet pressures. The calculation models are established on the EES [26]. The calculation flow chart of the PX case is shown in Fig. 6. The compressor discharge pressure is calculated in a way to provide the required motive flow for both ejectors, which directly depends on the flash gas handling capacity of PX and the ejectors efficiencies. Higher ejector efficiencies will reduce the required motive flow, which can reduce the discharge pressure. If the compressor discharge pressure is reduced below the reported value, the refrigerant flow is not enough for the motive flow of both ejectors. This will reduce suction flow for both ejectors and ultimately affect the performance. If the discharge pressure increases, the refrigerant flow is more than the required motive flow, which will decrease the COP. The increased compressor discharge pressure will lead to unnecessary bypassing of flow through control valve (between gas cooler and compressor). The main role of this control valve is to assist in reaching the desired compressor discharge pressure in real system and in this work the objective is to have zero flow through this valve. Iterations were performed to find the compressor discharge pressure and flash gas bypassing percentage through FGBV that satisfy the ejectors motive flows and PX flash gas compression ability with the objective of high COP.

The LP and HP ejector efficiencies are also critical for overall COP improvement, and it is assumed constant for calculation models. The assumed ejector efficiencies are in the range discussed in the literature [33,34]. For the standard booster case, the liquid receiver pressure has no influence on the performance because all the flash gas is expanded to the evaporator pressure. For parallel configuration, the EES min–max function is used to find the receiver pressure, which gives maximum

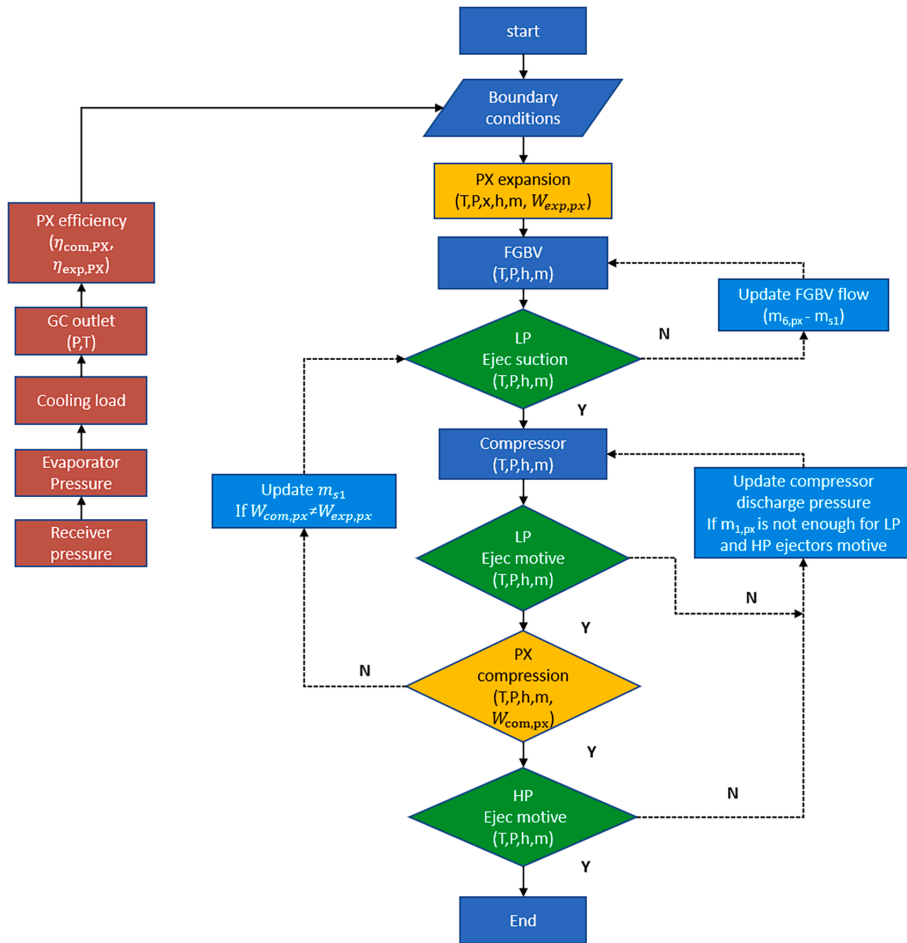


Fig. 6. PX case simulation flow chart.

COP. The liquid receiver pressure in the ejector configuration differs depending upon the pressure lift by the ejector at the given efficiency. Some assumptions have been made in this work to develop the calculation models for energy and exergy analysis:

- All investigated cases are in steady state condition.
- There is no pressure drop and heat loss in the heat exchangers and pipes.
- Superheating of 5 K for compressor suction is used for numerical models.
- The outlets of the liquid receiver are considered saturated liquid and vapour.
- Expansion valve processes are considered as isenthalpic.
- For the ejector configuration case, the ejector efficiency is assumed to be 25 %.
- LP and HP ejectors efficiency is assumed to be 20 % for the CO₂-PX concept.

3. Results and discussions

3.1. PX efficiencies

The PX case is investigated for three different efficiency curves at the

liquid receiver pressure of 40, 45 and 50 bar. Fig. 7 presents the compression and expansion efficiencies of these scenarios of the PX case. The PX compression and expansion efficiencies combination is computed in such a way that gives a constant mass boost ratio, and the entropy generation is minimum at the maximum expansion efficiency. The efficiencies are found by iterative process and then used as boundary conditions specified in Table 2 to the PX case calculation model.

The liquid receiver pressure has some influence on the efficiency curve. By decreasing the receiver pressure, the compression efficiency will decrease at the maximum expansion efficiency. Similarly, the expansion efficiency will also decline at the maximum compression efficiency. However, changing the gas cooler temperature at the optimised pressure makes the change in compression and expansion efficiency curve minimal. For each liquid receiver pressure, similar efficiency curves can be achieved by altering the gas cooler pressure. When the GC outlet temperature increases, GC pressure also increases to an optimised value, and the density change at the GC outlet will be small. The effect on the PX LP_{in} density will also be small as the contribution of LP ejector motive flow is low. So, density is the main parameter effecting the mass boost ratio. Thus, the mass boost ratio for a given receiver pressure will remain almost constant but will change for various receiver pressures.

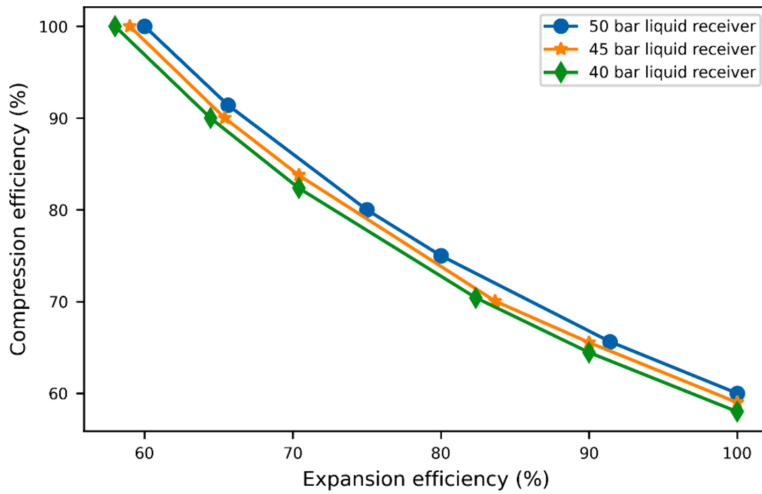


Fig. 7. Compression and expansion efficiency curves of PX at GC outlet 35 °C.

The average mass boost ratios of the 40, 45, and 50 bar receiver cases are 0.169, 0.194 and 0.222, respectively. The compression and expansion efficiencies assumed for the calculation models from Fig. 7 are presented in Table 1.

3.2. Performance analysis

All the results depicted in Fig. 8 are computed at the operating conditions and GC pressures specified in Table 2 corresponding to the GC outlet temperatures. The results indicate that the highest COP difference is obtained for the PX case at 40 bar receiver pressure and GC outlet 37 °C compared to other configurations at 37 °C. It is 23.5 % higher than the standard booster case and 5.5 % enhancement compared to the ejector configuration at the maximum difference. The COP difference between PX cases of 40 and 50 bar is within 1.2–1.4 %. The parallel compressor configuration has a COP of 1.2–2.6 % higher than the standard booster case but 13.5–13.9 % lower than the ejector configuration. The higher COP of the PX case is mainly due to the free pressure lift of flash gas by the PX.

Compressor efficiency is a critical parameter of the COP analysis, which plays a significant role in the system’s overall performance. The COP results in Fig. 8 are according to compressor efficiency equations presented in sections 2.2.1 and 2.2.2. The PX efficiencies can also affect the overall performance. At the maximum compression efficiency, more flash gas can be removed. However, at the same time, due to low expansion efficiency, recovered work will be low, and the expansion process will move towards isenthalpic expansion. The outcome will be low performance but still higher than the Standard booster. However, at the maximum expansion efficiency, vapour quality will be much lower (more liquid), and the recovered work will increase. Even though the compression efficiency is low, it will significantly increase the performance. The COP of the PX case will continue to increase by decreasing

Table 1
PX expansion and compression efficiencies for modelling.

	40 bar receiver case	45 bar receiver case	50 bar receiver case
PX expansion efficiency (%)	82.4	83.7	80
PX compression efficiency (%)	70.4	70.5	75

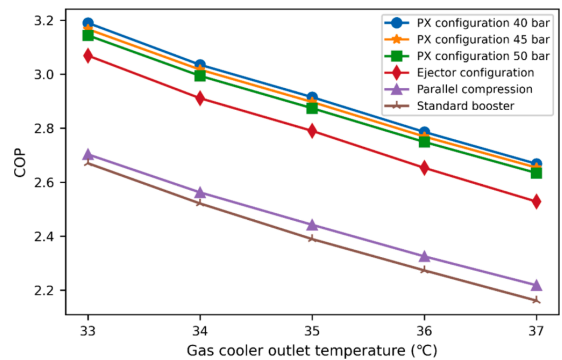


Fig. 8. COP comparison between PX and other configurations.

receiver pressure (50 to 40 bar) compared to booster case because PX is doing expansion with some isentropic efficiency. According to the phase envelop diagram of CO₂, as the receiver pressure decreases, the isentropic line moves towards the left inside the two-phase region, reducing the vapour quality (more liquid after expansion). Thus, by decreasing receiver pressure, the performance will increase compared to the booster case, which follows isenthalpic expansion. A minimum 2 bar pressure difference is required between receiver and evaporator to be able to supply liquid through expansion valve but typically 4–5 bar is indicated.

The PX efficiency values are theoretical, and the potential losses are not included, which can give an advantage to the reported PX performance. The losses could arise from flow imbalance (PX 4 streams) and heat transfer within PX. In the ideal scenario, a loss-free PX would eliminate the need for two booster ejectors for the discussed PX configuration. There will not be any performance difference between the ideal PX and ejector configuration. The PX applicability is more suited for higher GC outlet temperatures as the potential benefit is limited for low temperatures. An economic analysis is important to include in future work for PX and ejector configuration to conclude the real benefits. The operating conditions of the various configurations are shown in Table 2.

The compression power for all the investigated cases is shown in

Table 2
Operating conditions of the Various configurations.

Parameters	GC outlet (33 °C)	GC outlet (34 °C)	GC outlet (35 °C)	GC outlet (36 °C)	GC outlet (37 °C)
Compressor outlet pressure, PX cases (bar)	86.5	89.5	91.5	94.5	97.5
GC pressure all cases (bar)	84	87	89	92	95
Evaporator pressure all cases (bar)	34.85	34.85	34.85	34.85	34.85
Receiver pressure PX cases (bar)	40,45,50	40,45,50	40,45,50	40,45,50	40,45,50
Receiver pressure Ejector cases (bar)	38.48	38.70	38.93	39.19	39.45
Receiver pressure Booster cases (bar)	40	40	40	40	40
Receiver pressure Parallel cases (bar)	51.32	51.2	51.16	51.12	51.1
Booster cases, $m_{2,b}$ (kg/s)	0.418	0.422	0.430	0.436	0.441
Parallel cases, $m_{3,par}$ (kg/s)	0.426	0.431	0.441	0.446	0.451
Ejector cases, $m_{3,ej}$ (kg/s)	0.424	0.428	0.437	0.443	0.449
PX cases, $m_{4,px}$ 40 bar (kg/s)	0.402	0.405	0.412	0.415	0.418
PX cases, $m_{4,px}$ 45 bar (kg/s)	0.408	0.410	0.418	0.421	0.424
PX cases, $m_{4,px}$ 50 bar (kg/s)	0.414	0.418	0.426	0.429	0.433

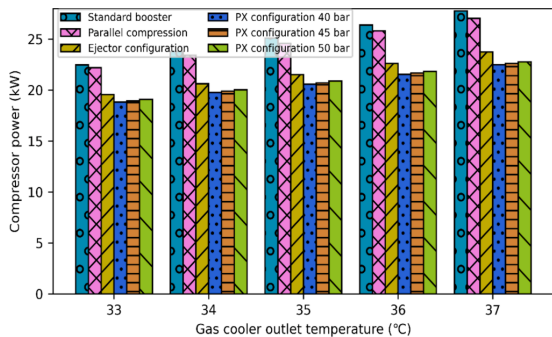


Fig. 9. Compression power comparison for 60 kW and 0 °C evaporation.

Fig. 9. As the GC outlet temperature increased, the pressure ratio increased to reach the GC pressure, which directly increased compression power. The highest power consumption is for the standard booster case, and the lowest is for the PX 40 bar receiver case. This indicates that the combination of ejectors and PX subsequently reduces the compression power, increasing the system’s performance.

3.3. PX work recovery and flash gas

Fig. 10 indicates the expansion work recovery of the PX device at the specified expansion efficiency (Table 2). It shows that the recovered expansion work increased with lower receiver pressure and higher GC

outlet temperature. With higher GC outlet temperature (corresponding to optimized GC pressure), the pressure difference between receiver and GC increased which led to more expansion work recovery. The recovered work is then used to compress the flash gas at the specified compression efficiency. The recovered work from the PX expansion is in the range of 11.3–18.4 % of the total compression work for all cases.

Fig. 11 indicates the flash gas bypass comparison between PX cases and the standard booster case. It shows that the flash gas bypass amount is increasing for both configurations from GC outlet of 33 °C to 37 °C which is due to the generation of more flash gas at elevated GC outlet temperatures. However, for PX cases the increased amount of flash gas bypass is small. At a liquid receiver pressure of 40 bar, the amount of flash gas is highest compared to 45 bar and 50 bar due to the phase envelope shape of the CO₂. When the flash gas quantity exceeds the PX handling capacity at the given receiver pressure, bypassing is necessary. This trend can be observed in Fig. 11. In the standard booster case, all the flash gas is bypassed, but a reduced amount is bypassed for the PX cases.

3.4. LP and HP ejectors

Fig. 12 presents the entrainment ratio of the LP and HP ejectors of the PX case. Both ejectors provide a pressure lift of 2 bar. The LP ejector is lifting 2 bars from the receiver pressure, and the HP ejector is lifting 2 bars from the PX HP_{out} to the GC cooler pressure. The entrainment ratio of the LP ejector is much higher than the HP ejector due to the high-pressure difference between the suction and motive side (Compressor discharge) of the LP ejector. Additionally, the motive flow has high pressure and temperature, which leads to reduced amount of motive flow. As the entrainment ratio is the ratio between suction and motive flow, a lower motive flow compared to suction flow will give higher entrainment ratio and better COP. As the GC outlet temperature increases, the entrainment ratio difference between PX cases is reduced due to the small difference in motive flow in these cases. The motive flow of the HP ejector is much higher than the LP ejector and gives a relatively lower entrainment ratio.

Fig. 13 presents the suction and motive temperatures of LP and HP ejectors. The suction temperature of the LP ejector is the saturation temperature of the receiver pressure, which is not plotted in Fig. 13. The LP ejector outlet temperature is almost constant for the various GC outlet temperature for the given receiver pressure. The reason is the motive flow of the LP ejector, which is very small, and its variation with the GC outlet has a minor effect on the LP ejector outlet temperature. However, the LP ejector outlet temperature difference for various receiver pressure is mainly due to its saturation temperature.

HP ejector suction temperature is the outlet temperature of the PX compression, and it is highest for 40 bar cases and lowest for 50 bar. The trend is mainly due to more recovered expansion work in the case of 40 bar to compress flash gas than in the 50 bar case. The trend of the HP ejector suction is the same for the HP ejector outlet for various receiver pressures. The ejector motive temperature is identical for all cases at the given GC outlet temperature, increasing with the GC outlet temperature due to the increased compressor discharge pressure. The LP and HP ejector efficiencies are critical for the performance of the PX configuration. The higher efficiency of the LP ejector will reduce the LP ejector outlet temperature and eventually increase the density. Due to higher density, more flash gas can be compressed through the PX. The higher efficiency of both ejectors will reduce the required compressor discharge pressure and increase system performance. However, lower ejector efficiencies will decrease the performance. In general ejector efficiencies are critical, operation at off-design conditions mostly deteriorate the ejector efficiencies.

3.5. Exergy analysis

The exergy analysis of the PX and other configurations is presented in

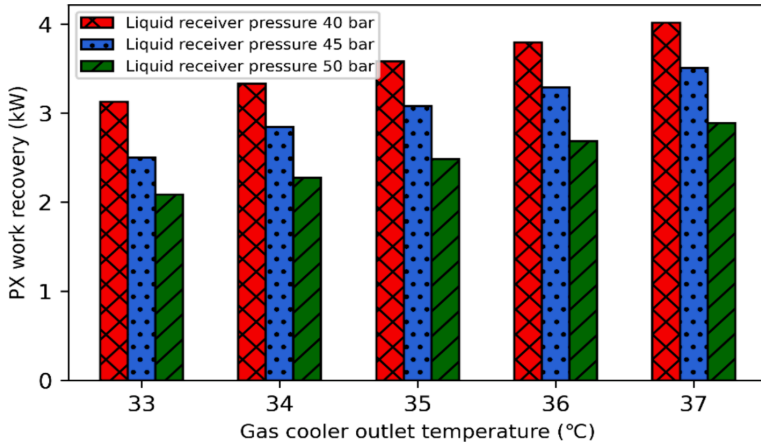


Fig. 10. PX work recovery to compress flash gas.

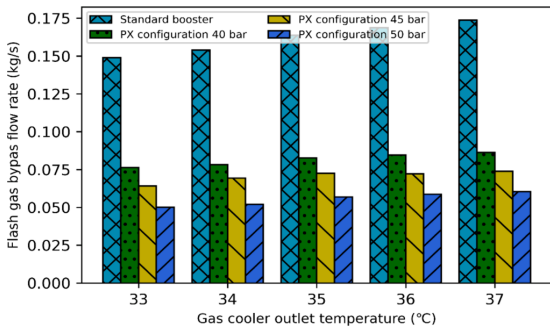


Fig. 11. Flash gas bypass comparison between PX and standard booster configurations.

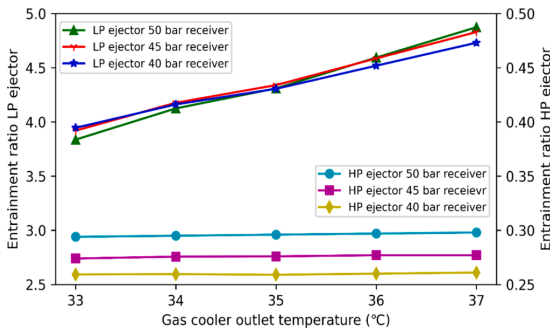


Fig. 12. Entrapment ratio of LP and HP ejectors of PX configuration.

Fig. 14. It is performed for the same conditions as discussed for COP analysis. The results show the improvement of exergy efficiency in the PX integrated cycle. The exergy efficiency of the PX system, on average, is 21.5 %, 18.3 %, and 7.2 % higher than the standard booster, parallel and ejector configuration, respectively. The exergy efficiency is decreasing with cases moving from 33 °C to 37 °C. As the total flow in the system is increasing (33 °C to 37 °C) due to higher expanded vapour flow, the exergy destruction in each component is increasing leading to

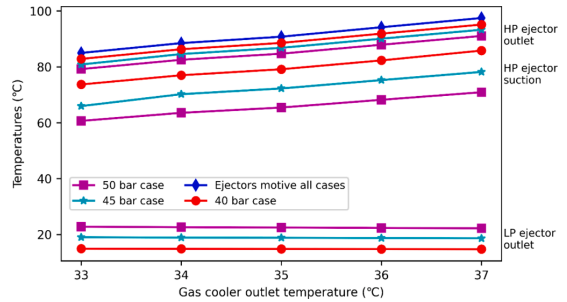


Fig. 13. Temperatures of LP and HP ejectors for different receiver pressures.

reduced exergy efficiency. The higher exergy efficiency of the PX case is mainly due to the less exergy destruction in the expansion process. The exergy destruction trend of different components is presented in Table 3. The exergy destruction of identical components with multiple uses is summed together and presented as one in Table 3. For example, in a parallel compression configuration case, two compressors' exergy destruction is presented as one value. It can be observed that the expansion exergy destruction (exp, Ej, and PX) in the PX configuration is lower compared to other configurations. In the GC and evap, the exergy destruction is similar in various configurations due to identical boundaries at the outlet of GC and evap. The small difference is due to the variation in inlet conditions. In SHX, the highest exergy destruction is in the ejector configuration, which is due to the large temperature difference between the two sides. However, in the parallel case, the flow is less in the SHX, which has a larger temperature difference compared to the ejector configuration. The exergy destruction in SHX of the PX case is lower as compared to the booster case because some of the flash gas is handled by PX.

4. Conclusion

In this work, a new expansion work recovery device, PX, is investigated to quantify the impact it has on CO₂ system performance by a theoretical approach. The thermodynamic analysis has been performed for the PX integration and compared with the standard booster, parallel and ejector configurations. The numerical models for this purpose are established on EES. The boundary conditions for the analysis are GC outlet temperature of 33 °C to 37 °C, evaporator 0 °C and cooling

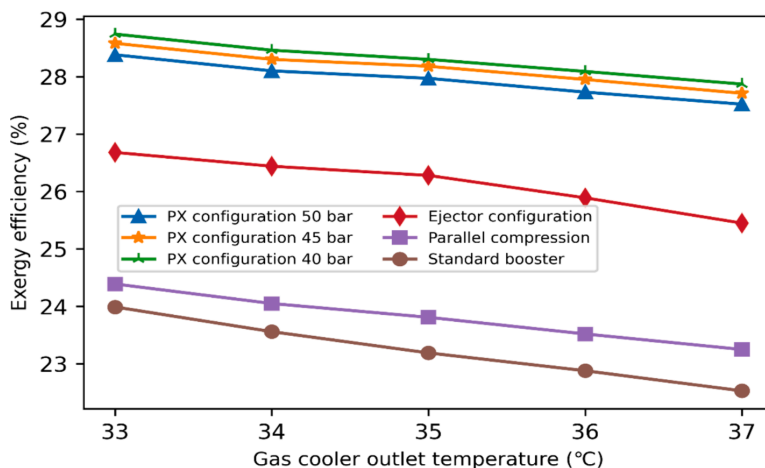


Fig. 14. Exergy efficiency comparison between PX and other configurations.

Table 3

Exergy destruction of various configurations at GC outlet of 35 °C.

Exergy destruction configurations	com	exp	Ejec	GC	evap	PX	SHX
Standard booster (kW)	6.97	6.26	–	4.76	1.19	–	0.0895
Parallel configuration (kW)	8.58	3.92	–	4.78	1.12	–	0.236
Ejector configuration (kW)	5.87	0.256	3.69	4.41	1.20	–	0.409
PX configuration 40 bar case (kW)	5.61	0.601	0.829	4.73	1.20	1.768	0.010

capacity of 60 kW. The important conclusions are summarised as:

- The highest COP is for the PX case at 40 bar receiver pressure, which is 19.4–23.5 % higher than the standard booster case but only 3.9–5.5 % higher than the ejector configuration. The higher COP of the PX case is due to the free pressure lift of flash gas from the receiver pressure to the gas cooler pressure.
- The maximum recovered PX expansion work is for the 40-bar receiver case and 37 °C GC outlet temperature. The PX recovered work is in the range of 11.3–18.4 % of the main compression work for all cases.
- At lower liquid receiver pressures, the amount of flash gas is higher than the PX handling capacity (recovered expansion work) and is necessary to bypass.
- The entrainment ratio of the LP ejector is higher than the traditionally employed ejectors for CO₂ systems. This is due to the high-pressure difference between the motive and suction stream and with only 2 bar lift for the suction stream. The entrainment ratio of the HP ejector is relatively low because of the small pressure difference and higher motive flow than suction flow. The LP ejector outlet temperature is relatively less than the HP ejector outlet due to the high entrainment ratio.
- The exergy efficiency of the PX system shows improvement, and it is 21.5 %, 18.3 %, and 7.2 % higher than a standard booster, parallel and ejector configurations, respectively. The higher exergy efficiency of PX is mainly due to improvement in the exergy destruction in the expansion process.

- An economic analysis is important to include in future work for PX and other configurations to conclude the real benefits.

CRedit authorship contribution statement

Muhammad Zahid Saeed: Conceptualization, Formal analysis, Investigation, Methodology, Software, Validation, Visualization, Writing – original draft, Writing – review & editing. **Ángel Álvarez Pardiñas:** Supervision, Writing – review & editing. **Krzysztof Banasiak:** Supervision, Visualization. **Armin Hafner:** Conceptualization, Funding acquisition, Project administration, Resources, Supervision. **Azam Thatte:** Supervision, Writing – review & editing.

Declaration of competing interest

The authors declare that they have no known competing financial interests or personal relationships that could have appeared to influence the work reported in this paper.

Data availability

Data will be made available on request.

Acknowledgements and Funding

The authors gratefully acknowledge the Research Council of Norway for the financial support for carrying out the present research [Project No. 308779 CruizE and Project No. 257632 HighEFF] and Energy Recovery International for technical support.

References

- [1] E. Bellos, C. Tzivanidis, A comparative study of CO₂ refrigeration systems, *Energy Conversion and Management*: X, 1 (2019) 100002. <https://doi.org/10.1016/j.ecmx.2018.100002>.
- [2] European Environment Agency, Fluorinated greenhouse gases, in, 2021. <https://www.eea.europa.eu/publications/fluorinated-greenhouse-gases-2021> (accessed May 9, 2023).
- [3] European commission, Regulation (EU) No 517/2014 of the European Parliament and of the Council of 16 April 2014 on fluorinated greenhouse gases and repealing Regulation (EC) No 842/2006 Text with EEA relevance, in: E. L.-. 32014R0517 (ed.), 2014. <https://eur-lex.europa.eu/legal-content/EN/TXT/?uri=celex%3A32014R0517> (accessed May 9, 2023).
- [4] K.Z. Skačanová, M. Battesti, Global market and policy trends for CO₂ in refrigeration, *Int. J. Refrig.* 107 (2019) 98–104, <https://doi.org/10.1016/j.jrefrig.2019.08.010>.

- [5] P. Gullo, K. Tsamos, A. Hafner, Y. Ge, S.A. Tassou, State-of-the-art technologies for transcritical R744 refrigeration systems – a theoretical assessment of energy advantages for European food retail industry, *Energy Procedia* 123 (2017) 46–53, <https://doi.org/10.1016/j.egypro.2017.07.283>.
- [6] K.E. Ringstad, Y. Allouche, P. Gullo, Å. Ervik, K. Banasiak, A. Hafner, A detailed review on CO₂ two-phase ejector flow modeling, *Thermal Science and Engineering Progress* 20 (2020), <https://doi.org/10.1016/j.tsep.2020.100647>.
- [7] G. Lorentzen, The use of natural refrigerants: a complete solution to the CFC/HCFC predicament, *Int. J. Refrig* 18 (1995) 190–197, [https://doi.org/10.1016/0140-7007\(94\)00001-E](https://doi.org/10.1016/0140-7007(94)00001-E).
- [8] E.A. Groll, J.-H. Kim, Review Article: Review of Recent Advances toward Transcritical CO₂ Cycle Technology, *HVAC&R Research* 13 (2007) 499–520, <https://doi.org/10.1080/10789669.2007.10390968>.
- [9] S. Singh, P.M. Maiya, A. Hafner, K. Banasiak, P. Neksa, Energy efficient multiejector CO₂ cooling system for high ambient temperature, *Thermal Science and Engineering Progress* 19 (2020), <https://doi.org/10.1016/j.tsep.2020.100590>.
- [10] M.E. Ahammed, S. Bhattacharyya, M. Ramgopal, Thermodynamic design and simulation of a CO₂ based transcritical vapour compression refrigeration system with an ejector, *Int. J. Refrig* 45 (2014) 177–188, <https://doi.org/10.1016/j.jrefrig.2014.06.010>.
- [11] S. Fangtian, M. Yitai, Thermodynamic analysis of transcritical CO₂ refrigeration cycle with an ejector, *Appl. Therm. Eng.* 31 (2011) 1184–1189, <https://doi.org/10.1016/j.applthermaleng.2010.12.018>.
- [12] D. Li, E.A. Groll, Transcritical CO₂ refrigeration cycle with ejector-expansion device, *Int. J. Refrig* 28 (2005) 766–773, <https://doi.org/10.1016/j.jrefrig.2004.10.008>.
- [13] M. Karampour, S. Sawalha, State-of-the-art integrated CO₂ refrigeration system for supermarkets: A comparative analysis, *International Journal of Refrigeration* 86 (2018) 239–257, <https://doi.org/10.1016/j.jrefrig.2017.11.006>.
- [14] P. Maina, Z. Huan, A review of carbon dioxide as a refrigerant in refrigeration technology, *S. Afr. J. Sci.* 111 (2015) 01–10, <https://doi.org/10.17159/SAJS.2015/20140258>.
- [15] P. Neksä, H.T. Walnum, A. Hafner, CO₂ - A refrigerant from the past with prospects of being one of the main refrigerants in the future, in: 9th IIR-Gustav Lorentzen Conference on Natural Working Fluids, 2010. <https://iifir.org/en/fridoc/co2-a-refrigerant-from-the-past-with-prospects-of-being-one-of-the-27229>.
- [16] M.Z. Saeed, A. Thatte, A. Hafner, H.C. Gabriellii, Simultaneous implementation of rotary pressure exchanger and ejectors for CO₂ refrigeration system, in: 15th IIR-Gustav Lorentzen Conference on Natural Refrigerants, 2022. <https://doi.org/10.18462/iir.gl2022.0130>.
- [17] A. Thatte, A New Type of Rotary Liquid Piston Pump for Multi-Phase CO₂ Compression, in: ASME Turbo Expo: Turbomachinery Technical Conference and Exposition, Vol. 9: Oil and Gas Applications; Supercritical CO₂ Power Cycles; Wind Energy, 2018. doi: 10.1115/gt2018-77011.
- [18] A. Thatte, B. Fricke, K. Nawaz, Novel rotary pressure exchanger for highly efficient transcritical CO₂ refrigeration cycle, in: 15th IIR-Gustav Lorentzen Conference on Natural Refrigerants, 2022. doi: 10.18462/iir.gl2022.0056.
- [19] A. Thatte, Transcritical / Supercritical CO₂ Recompression Brayton Cycle Using a Novel Rotary Liquid Piston Compressor, in: ASME Turbo Expo: Turbomachinery Technical Conference and Exposition, Vol. 9: Oil and Gas Applications; Supercritical CO₂ Power Cycles; Wind Energy, 2019. doi: 10.1115/GT2019-91088.
- [20] A. Elatar, B. Fricke, V. Sharma, K. Nawaz, Pressure Exchanger for Energy Recovery in a Trans-Critical CO₂ Refrigeration System, *Energies*, 14 (2021) 1754. doi: 10.3390/en14061754.
- [21] P. Geisler, F.U. Hahnenstein, W. Krumm, T. Peters, Pressure exchange system for energy recovery in reverse osmosis plants, *Desalination* 122 (1999) 151–156, [https://doi.org/10.1016/S0011-9164\(99\)00036-3](https://doi.org/10.1016/S0011-9164(99)00036-3).
- [22] L.J. Hauge, The pressure exchanger — A key to substantial lower desalination cost, *Desalination* 102 (1995) 219–223, [https://doi.org/10.1016/0011-9164\(95\)00057-9](https://doi.org/10.1016/0011-9164(95)00057-9).
- [23] P. Geisler, W. Krumm, T.A. Peters, Reduction of the energy demand for seawater RO with the pressure exchange systems PES, *Desalination* 135 (2001) 205–210, [https://doi.org/10.1016/S0011-9164\(01\)00151-5](https://doi.org/10.1016/S0011-9164(01)00151-5).
- [24] Y. Lei, D.S. Zhou, H.G. Zhang, Investigation on performance of a compression-ignition engine with pressure-wave supercharger, *Energy* 35 (2010) 85–93, <https://doi.org/10.1016/j.energy.2009.08.035>.
- [25] I. Costiuc, A. Chiru, L. Costiuc, A Review of Engine's Performance When Supercharging by a Pressure Wave Supercharger, *Energies* 15 (2022) 2721, <https://doi.org/10.3390/en15082721>.
- [26] S.A. Klein, Engineering equation solver (EES), F-Chart software, Madison, USA, in, 2020. <https://fchartsoftware.com/ees/>.
- [27] P. Gullo, B. Elmegaard, G. Cortella, Energy and environmental performance assessment of R744 booster supermarket refrigeration systems operating in warm climates, *Int. J. Refrig* 64 (2016) 61–79, <https://doi.org/10.1016/j.jrefrig.2015.12.016>.
- [28] C. Lucas, J. Koehler, Experimental investigation of the COP improvement of a refrigeration cycle by use of an ejector, *Int. J. Refrig* 35 (2012) 1595–1603, <https://doi.org/10.1016/j.jrefrig.2012.05.010>.
- [29] P. Byrne, R. Ghouballi, Exergy analysis of heat pumps for simultaneous heating and cooling, *Appl. Therm. Eng.* 149 (2019) 414–424, <https://doi.org/10.1016/j.applthermaleng.2018.12.069>.
- [30] F. Li, Z. Chang, X. Li, Q. Tian, Energy and exergy analyses of a solar-driven ejector-cascade heat pump cycle, *Energy* 165 (2018) 419–431, <https://doi.org/10.1016/j.energy.2018.09.173>.
- [31] S. Singh, N. Purohit, M.S. Dasgupta, Comparative study of cycle modification strategies for trans-critical CO₂ refrigeration cycle for warm climatic conditions, *Case Studies in Thermal Engineering* 7 (2016) 78–91, <https://doi.org/10.1016/j.csite.2016.03.002>.
- [32] J. Wronski, Winter, M., Kærn, M. R., IPU software, Simple one stage CO₂ version 3.0, in, 2022. <https://www.ipu.dk/products/simple-one-stage-co2/> (accessed April 15, 2023).
- [33] L. Zheng, J. Deng, Research on CO₂ ejector component efficiencies by experiment measurement and distributed-parameter modeling, *Energ. Convers. Manage.* 142 (2017) 244–256, <https://doi.org/10.1016/j.enconman.2017.03.017>.
- [34] K. Banasiak, A. Hafner, E.E. Kriezci, K.B. Madsen, M. Birkelund, K. Fredslund, R. Olsson, Development and performance mapping of a multi-ejector expansion work recovery pack for R744 vapour compression units, *Int. J. Refrig* 57 (2015) 265–276, <https://doi.org/10.1016/j.jrefrig.2015.05.016>.

Journal article 2

M.Z. Saeed, A. Thatte, K. Banasiak, A. Hafner, Á.Á. Pardiñas. Experimental Investigation of Transcritical CO₂ Refrigeration System incorporating Rotary Gas Pressure Exchanger and Low Lift Ejectors. Applied Thermal Engineering. 2024. (In review process)



This paper is submitted for publication and is therefore not included.

Journal article 3

M.Z. Saeed, L. Contiero, S. Blust, Y. Allouche, A. Hafner, T.M. Eikevik. Ultra-Low-Temperature Refrigeration Systems: A Review and Performance Comparison of Refrigerants and Configurations. *Energies* **2023**, *16*, 7274. <https://doi.org/10.3390/en16217274>

Review

Ultra-Low-Temperature Refrigeration Systems: A Review and Performance Comparison of Refrigerants and Configurations

Muhammad Zahid Saeed ^{*,†} , Luca Contiero [†], Stefanie Blust, Yosr Allouche, Armin Hafner ^{*} and Trygve Magne Eikevik 

Department of Energy and Process Engineering, Norwegian University of Science and Technology (NTNU), 7491 Trondheim, Norway; luca.contiero@ntnu.no (L.C.); stefanie.blust@ntnu.no (S.B.); yosr.allouche@ntnu.no (Y.A.); trygve.m.eikevik@ntnu.no (T.M.E.)

^{*} Correspondence: muhammad.z.saeed@ntnu.no (M.Z.S.); armin.hafner@ntnu.no (A.H.)

[†] These authors contributed equally this work.

Abstract: During the last decade, many industrial and medical applications have shown a requirement for low-temperature-cooling usage (from -40 to -80 °C), which cannot be efficiently obtained via the conventional refrigeration systems usually employed for medium-temperature applications (from 0 to -40 °C). A proper ultra-low-temperature (ULT) refrigeration system design is essential to achieve the desired output. The performance can be maximised via the suitable selection of the configuration and refrigerant for a specific temperature range. This work contributes a detailed overview of the different systems and refrigerants used in ultra-low-temperature applications. Different systems, such as single-stage vapour compression, multi-stage, cascade, auto-cascade, and air refrigeration cycles, are presented and discussed. An energy analysis is then carried out for these systems identifying the optimal system design and refrigerant selection to achieve the highest performance. This paper aims to provide the reader with a comprehensive background through an exhaustive review of refrigeration systems suitable for ultra-low-temperature applications. The effectiveness of these systems is proven numerically, mainly based on the temperature level and purpose of the application.

Keywords: ultra-low-temperature refrigeration; natural refrigerants; COP; freezing fish; storing fish; air refrigeration system; auto-cascade system; cascade system; multi-stage refrigeration system



Citation: Saeed, M.Z.; Contiero, L.; Blust, S.; Allouche, Y.; Hafner, A.; Eikevik, T.M. Ultra-Low-Temperature Refrigeration Systems: A Review and Performance Comparison of Refrigerants and Configurations. *Energies* **2023**, *16*, 7274. <https://doi.org/10.3390/en16217274>

Academic Editor: Fabio Polonara

Received: 20 September 2023

Revised: 23 October 2023

Accepted: 24 October 2023

Published: 26 October 2023



Copyright: © 2023 by the authors. Licensee MDPI, Basel, Switzerland. This article is an open access article distributed under the terms and conditions of the Creative Commons Attribution (CC BY) license (<https://creativecommons.org/licenses/by/4.0/>).

1. Introduction

ULT systems are gaining significant interest, and researchers are putting great effort into developing and identifying the most reliable and efficient solutions. The application of ULT technology is quite diverse, such as in the medical, industrial, and food sectors. According to the American Society of Heating, Refrigeration and Air-Conditioning Engineers (ASHRAE), ULT refrigeration systems are those that operate below -50 °C [1]. There are options available for ULT systems. However, the high cost of synthetic refrigerants and the new policy towards sustainable development have created a huge interest in natural, hydrocarbon, and mixture refrigerants. The F-Gas Regulation (EU 517/2014) aims to reduce the fluorinated greenhouse gas (F-gas) emissions in Europe by two-thirds by 2030 compared to 2014. Hydrofluorocarbons (HFCs) are refrigerants that are responsible for most F-gas emissions. The European Union has therefore set priorities to phase down HFCs following a reduction schedule that started in 2015 [2] and will continue to 2030 and beyond. HFC producers and consumers have been provided with HFC quotas for a progressive HFC phasedown. The F-Gas Regulation intends to cut F-gas emissions by two-thirds of the 2010 levels by 2030 by enhancing equipment leak-tightness, promoting more ecologically friendly gases, and restricting EU HFC sales through an HFC phasedown [3]. The F-Gas Regulation excludes the regulations pertaining to refrigeration below -50 °C in its low-GWP Alternative Refrigerants Evaluation Program (AREP), which can be explained by the limited number of units in use (in comparison to other applications) and

the slower pace of development [4]. The target temperature of the product/environment and the application constitute the main influencing parameters to consider when selecting a refrigerant to achieve an optimal system performance. The flammability and toxicity of the refrigerant are also important to account for safety considerations. A limited number of natural refrigerants can be used for low-temperature applications as an alternative to HFC refrigerants, such as carbon dioxide, ammonia, air, nitrogen, hydrocarbons, and their mixtures. For instance, at $-33\text{ }^{\circ}\text{C}$, ammonia (R717) evaporates at atmospheric pressure ($p = 1.013\text{ bar}$). The refrigerant's pressure should be further reduced to achieve lower evaporation temperatures. This allows the refrigeration unit to work under atmospheric-pressure conditions, making the process challenging to implement [5]. Carbon dioxide (R744) is a natural fluid with a high volumetric refrigerating capacity of 22.545 kJ/m^3 at $0\text{ }^{\circ}\text{C}$ (from 3 to 10 times higher than CFC, HCFC, HFC, and HC refrigerants), allowing for a compact system. However, its high triple point of $-56.6\text{ }^{\circ}\text{C}$ is a constraint [6].

Different refrigeration cycles can be utilised for ULT refrigeration, but limitations exist. For example, a single-stage system is limited for ULT refrigeration due to a high compression ratio and an excessive compressor discharge temperature [7]. One of the solutions is the two-stage system, which utilises a single refrigerant with two compression stages. The pressure lift from the evaporator to the condenser is divided into two compressors. The key optimised parameter is the intermediate pressure. It is generally taken as the geometric mean of the evaporator and condenser pressures, providing maximum efficiency within the allowable discharge temperature [8]. Several studies [8–11] have been performed to optimise the vapour compression two-stage system. Another alternative is the cascade system, in which two refrigeration cycles with the same or different working fluids interact in the cascade heat exchanger. In the cascade heat exchanger, the lower-cycle refrigerant condenses with the evaporation of the upper cycle. Pan et al. (2020) [12], Singh et al. (2020) [13], and Udriou et al. (2023) [14] performed a recent review and comparative analysis of the cascade system. The literature also suggests using an auto-cascade system for cost reduction and simplicity. In an auto-cascade system, a refrigerant mixture of two fluids with different boiling points is used for ULT applications. Due to the difference in the boiling points, it is possible to separate the two refrigerants in the condenser and expand them to the different pressures. This provides substantially lower evaporation temperatures than standard single-stage cycles [7]. The investigation of auto-cascade systems with mixtures has been performed by several researchers, such as Du et al. (2009) [15], Yan et al. (2015) [16], Hao et al. (2018) [17], Qin et al. (2021) [18], Aprea and Maiorina (2009) [19], Asgari et al. (2017) [20], and Rodríguez-Jara et al. (2022) [7]. The air refrigeration cycle (ARC) is another solution for ULT refrigeration. The ARC is widely used for airplane air conditioning but can also be used for ULT applications [21]. However, the research on the ARC is limited; some of it is reported by Zhang et al. (2011) [22], Gigiel et al. (2006) [23], and Kikuchi et al. (2005) [24]. The two commercially available ARC machines were developed by Mirai [25] and Mayekawa (Pascal air) [26], and they can operate on an open or closed cycle. The open cycle eliminates the need for an evaporator, auxiliary fan, and secondary circuits, and the air is directly supplied to the cold room. Even though several promising studies have been performed for ULT refrigeration, their targeted application investigations are not well addressed. Very few studies have focused on combined studies of natural refrigerants, hydrocarbons, mixtures, and their applications. Therefore, evaluating and finding the optimum choice of refrigerant and cycle for ULT applications are important. This paper concerns these issues and will help in finding the best selection.

The primary motivation of this work is to evaluate and identify various options for low-temperature applications (from -40 to $-80\text{ }^{\circ}\text{C}$). The different refrigerant cycles, namely the multi-stage (MRS), cascade (CRS), auto-cascade (ACR), and air (ARC) refrigeration systems, are numerically investigated by applying natural working fluids, hydrocarbons, and mixtures to find the optimum options using the coefficient of performance (COP) as the key performance indicator. The numerical models are developed in Engineering Equation Solver (EES) [27]. The main target applications are fish freezing and storage, natural-gas

cooling, vaccine storage, and CERN detector cooling. For each case, the practical challenges and dominance over other systems are thoroughly discussed to give a decisive overview of the best options.

2. Refrigerants for Ultra-Low-Temperature Applications

A large selection of refrigerants is available for refrigeration systems operating at evaporation temperatures above $-40\text{ }^{\circ}\text{C}$. This list is found to be larger than that available for ULT refrigeration applications. At very low temperatures (below $-40\text{ }^{\circ}\text{C}$), the physical properties of some refrigerants are found to challenge the application operating conditions: a pressure below 1 bar at the required evaporation temperature, low density at the inlet of the compressor, and a high normal boiling point (NBP)/freezing point. The selection criteria for the operating refrigerant are based on the NBP and freezing point, which must be low enough so that the liquid refrigerant can turn into gas when it absorbs heat and without freezing at the given pressure. Refrigerants suitable for such temperature levels are usually known as low-temperature refrigerants. A list of these refrigerants following the EU F-Gas Regulation 517/2014 is given in the sections below.

2.1. Natural Working Fluids

Within the context of the increasing awareness about the impact of HFC and HCFC refrigerants on global warming and ozone depletion, there has been a transition from the old-generation refrigerants towards environmentally friendly ones. Several natural refrigerants, such as R744, R717, R744A, and air, have been studied over the years to promote their application in the refrigeration industry [6,28]. Their characteristics are illustrated in Table 1.

Table 1. Natural refrigerant properties for ULT application.

Refrigerant	Molecular Mass (kg/kmol)	NBP ($^{\circ}\text{C}$)	Critical Temperature ($^{\circ}\text{C}$)	Critical Pressure (bar)	ODP	GWP (100 Years)
R-717	17	-33.1	132.3	113.5	0	0
R-744	44	-78.5 (-56.6 *)	31.1	73.8	0	1
Air	28.9	-213.4	-140.7	38	0	0
R-744A	44	-88.7	36.4	72.5	0	240

* Triple point.

R717 and R744 are the most common refrigerants employed in cascade refrigeration systems. A cascade system consists of two refrigerants, utilising one refrigerant to condense the other primary refrigerant, operating at the desired evaporator temperature. Ammonia provides the best performance when applied in the high-temperature circuit (HTC) thanks to its favourable thermodynamic properties [29]. Operating conditions at sub-atmospheric pressure increase the risk of air leakage into the evaporator, limiting the use of ammonia in some applications. However, using R744, the triple point is the main issue in achieving ultra-low temperatures. At $-56\text{ }^{\circ}\text{C}$, dry ice is formed, requiring a specific design of the evaporator (sublimation cycles) [30]. As an alternative, R744 can be applied in the ACR system with another refrigerant (i.e., hydrocarbons) to produce a refrigerant mixture that preserves favourable thermodynamic properties and low levels of toxicity and flammability [31]. It can be seen from Table 1 that nitrous oxide (R744A) has similar properties to R744 and would be a valid substitute for it. Another alternative could be to use a mixture of R744A and R744 in the LTC. Air as a refrigerant has significant advantages, with its critical temperature at $-140.7\text{ }^{\circ}\text{C}$. Thus, when air is used in a higher temperature range, it becomes a gas cycle without phase transition (supercritical cycle) [32]. Safety regulations are not required due to the low operating pressure and there is zero cost for the working fluid [32].

2.2. Hydrocarbons

Within the phase-out process of HCFC and HFC refrigerants due to their high greenhouse effect, hydrocarbons (HCs) are gaining increasing interest from the refrigeration sectors. Compared to HFC refrigerants, HCs have lower refrigerant charges and better miscibility with oil. The latter particularity ensured an effective oil return to the compressors and was found to enhance the evaporator's heat transfer process, yielding a better performance [33]. Several oils are typically employed in HC systems, such as PAO (polyalphaolefin), POE (polyolester), and PAG (polyalkylene). Their adoption in the context of the ULT region must be considered carefully due to the low solubility and high viscosity of ULT systems. Another advantage of working with HCs is the ability to retrofit the existing HFC and HCFC systems without any significant modifications to the system components. This has been found to limit the installation CAPEX costs [33].

Depending on the refrigerant cycle (MRS, CRS, ACR, ARC), one or more HCs or a mixture can be used. The most common HCs used in ULT applications are R-290, R-1270, R-170, and R-1150 [4]. Their properties are depicted in Table 2. Although characterised by low toxicity, these refrigerants have high flammability (A3 refrigerants). Therefore, the refrigerant charge should be kept as low as possible for safety reasons.

Table 2. HC properties for ULT applications.

Refrigerant	Name	Molecular Mass (kg/kmol)	NBP (°C)	Critical Temperature (°C)	Critical Pressure (bar)	ODP	GWP (100 Years)
R-290	Propane	44.1	−42.1	96.7	42.5	0	3.3
R-1270	Propylene	42.1	−47.6	92.4	46.7	0	1.8
R-170	Ethane	30.1	−88.58	32.2	48.7	0	5.5
R-1150	Ethylene	28.05	−103.77	9.2	50.4	0	4

2.3. Mixtures

Refrigerant mixtures are blends of two or more pure refrigerant fluids. These mixtures offer customised properties to meet the various temperature requirements and constitute a competitive substitute to the existing high-ODP and -GWP refrigerants. The thermophysical properties and NBP, critical point, freezing point, oil miscibility, toxicity, and flammability levels of each refrigerant mixture vary depending on the compositions of the individual refrigerants. Thus, the best refrigerant mixture profile can be obtained for the desired application [34]. However, issues can appear when the system is running, like changes in the composition during leakage and heat transfer degradation in the mixture. Refrigerant mixtures are divided into three types: zeotropic, azeotropic, and near azeotropic.

Azeotropic mixtures follow constant-temperature condensation and evaporation, behaving as a pure fluid (the stable equilibrium of one liquid state with one vapour state). However, the properties of the mixture are different from those of either of its pure refrigerant components. They are further classified into positive and negative azeotropes. Positive azeotropes have a lower boiling point than their constituents, whereas negative azeotropes have a higher boiling point [35].

Near-azeotrope mixtures behave more like azeotrope mixtures, but they do not need additional system design considerations compared to azeotrope mixtures. These mixtures have very low temperature glides ranging between 0.2 and 0.6 °C. However, under leakage conditions, they may alter their properties and compositions [36]. Zeotropic mixtures diverge from the pure fluid and do not follow isothermal evaporation and condensation. Their temperature glides can exceed 50 K based on the refrigerants, composition, and pressure [37]. The mixtures can match the temperature load profile well depending on the temperature glide. In the cooling process, a particular temperature glide allows the load temperature profile to be followed better and decreases the exergy losses [36].

3. System Configurations

The refrigeration system used in ULT refrigeration is a vapour compression system. For ultra-low (below $-50\text{ }^{\circ}\text{C}$), low (from -25 to $-50\text{ }^{\circ}\text{C}$), and medium (from 0 to $-25\text{ }^{\circ}\text{C}$) temperatures [38], the performances of these systems depend on the refrigerant properties and the efficiency of the components. Five different system layouts are identified depending on the desired temperature level and temperature difference in the secondary fluid.

3.1. Single-Stage Vapour Compression Systems

The single-stage vapour compression system is widely used in refrigeration (Figure 1), covering most typical commercial and industrial applications, except ULT applications.

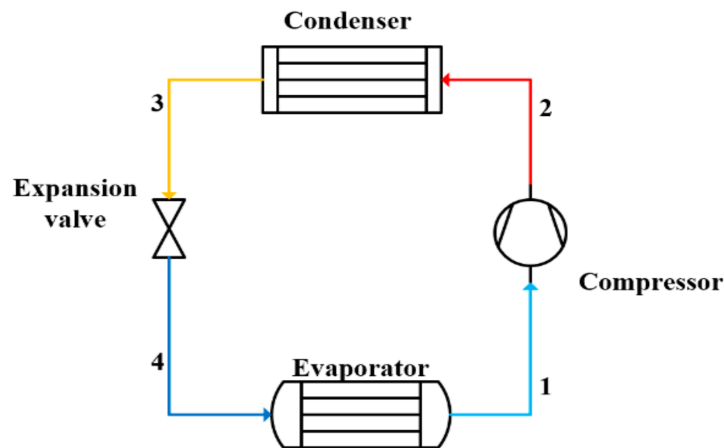


Figure 1. Single-stage vapour compression system.

The wide choice of refrigerants, simplicity of the operation, and easy maintenance represent the advantages to its application. However, its applicability in the ULT region is limited. The pressure ratio is too high for the available compressor technology, leading to a limited system performance and lower volumetric capacity. Moreover, the refrigerant properties deteriorate when the compressor discharge temperature exceeds limits. The minimum temperature that can be achieved using single-stage vapour compression systems and pure refrigerant is $-40\text{ }^{\circ}\text{C}$, depending on the condensing temperature. A further reduction would require operating under vacuum conditions for most refrigerants and increases the risk of air infiltration into the system and performance degradation. Alternatively, a low-NBP refrigerant would require a heat rejection at high pressure, increasing the compression work. Therefore, a single-stage system is not included in the numerical modelling comparison. However, a mixture of refrigerants can be used in a single-stage system to cool at very low temperatures, but at a performance cost [39]. The use of ejectors can provide significant cycle performance improvements, which can be from 16 to 20% higher than the normal cycle (Figure 1) [40,41]. The COP can also be enhanced by up to 20% using a sub-cooler and suction gas heat exchanger [42].

3.2. Multi-Stage Refrigeration Systems

A multi-stage refrigeration system, represented in Figure 2, is usually the solution to limit the high-temperature difference between the condenser and the evaporator encountered when using a single-stage refrigeration system. The two-stage system allows for reaching lower evaporation temperatures, with a COP improvement of around 8% compared to a single-stage system [43]. The system operates with a single refrigerant with one cooling cycle at two different pressure levels connected through a separator.

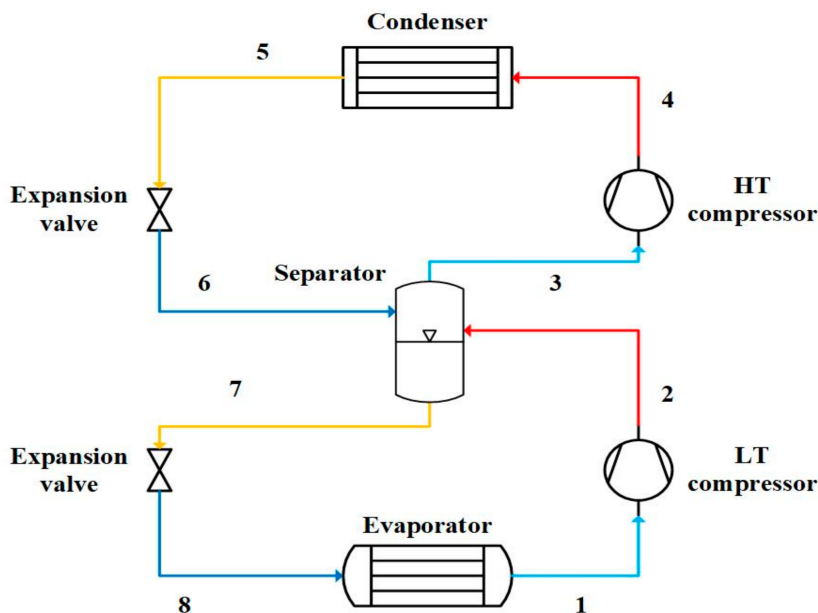


Figure 2. Two-stage system with separator.

A phase separator cools the refrigerant between the two compression stages, reducing its compression losses (increasing its compression efficiency). It also ensures that the vapours are directed into the suction of the HT compressor, and that only liquid is flowing towards the second expansion. A two-stage system can use several configurations, each giving a different performance output. Jiang et al. (2015) [44] and Torrella et al. (2011) [8] discuss the various optimised two-stage configurations and their performances. In the present study, a two-stage cycle with a phase separator [28] for nitrous oxide, carbon dioxide, and ammonia was studied (Figure 2). However, special attention was given to the ammonia system because of the challenges associated with high compression discharge temperatures.

3.3. Cascade Refrigeration Systems

This system is one of the most common technologies used to produce cooling and heating. A cascade refrigeration unit (Figure 3) consists of two separate circuits, a high-temperature cycle (HTC) and a low-temperature cycle (LTC), connected through a cascade heat exchanger, which acts as a condenser for the LTC and as an evaporator for the HTC [45]. The two cycles can apply the same or different refrigerants for an improved system performance. The HTC ensures an evaporating temperature as low as $-30\text{ }^{\circ}\text{C}$, while the LTC can achieve an evaporating temperature lower than $-80\text{ }^{\circ}\text{C}$. Several cascade configurations have been investigated by Singh et al. (2020) [13], Pan et al. (2020) [12], and Udroui et al. (2023) [14]. The CRS produces a higher efficiency than the MRS. An ejector expansion CRS is the best option, and the inclusion of an ejector in the transcritical R744 cycle results in a performance enhancement of 38% compared to the same system without an ejector [14]. The oil-handling system in the CRS is simpler than in the MRS, as both cycles in the CRS have independent oil management systems.

Pure refrigerants have limitations, like poor performances at ULTs, and mixed refrigerants are an alternative to improve the performance and overcome such issues. Azeotropic refrigerants are an acceptable solution for ULT refrigeration for a better performance compared to pure refrigerants [12]. In recent years, there has also been considerable interest in

using refrigerant mixtures in the LTC to reduce the risk of the flammability or toxicity of some pure refrigerants (i.e., HCs).

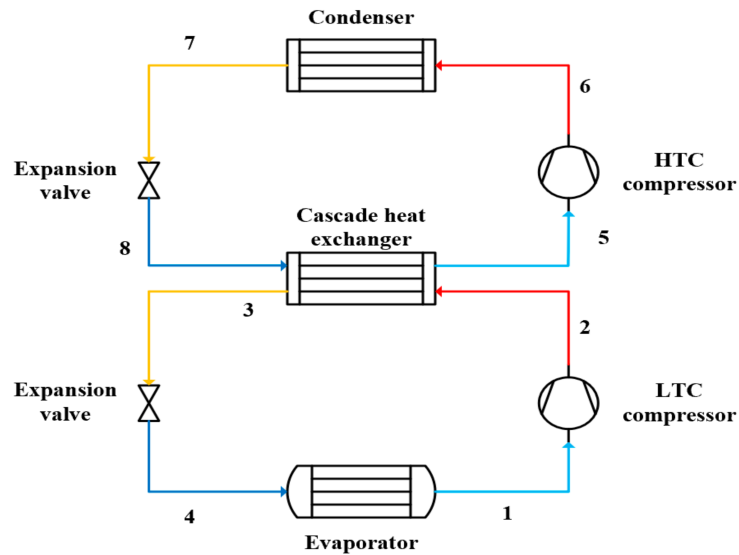


Figure 3. Cascade refrigeration system.

3.4. Auto-Cascade Refrigeration Systems

The auto-cascade system employs mixed refrigerants with different NBPs. These systems are driven by a single-stage compressor and can achieve very low temperatures (from $-200\text{ }^{\circ}\text{C}$ to $-40\text{ }^{\circ}\text{C}$) [46] with pressure ratios from 5 to 21 [16,47], without excessive discharge temperatures. The refrigerant mixture is an important parameter influencing the system performance, including the efficiency of the heat exchanger and the compressor pressure ratio. Several research studies have been performed on binary refrigerant mixtures for ULTs. Applying a binary refrigerant mixture in an auto-cascade system is an attractive solution, as it is characterised by a lower cost and simpler construction due to there being only one compressor. Yan et al. (2015) [16] reported a COP improvement of 7.8–13.3% for the zeotropic mixture of R290/R600a at an evaporation temperature of $-28\text{ }^{\circ}\text{C}$ compared to the domestic refrigerator freezer. Bai et al. (2018) [48] investigated R134a/R23 in an ejector-enhanced auto-cascade system for an evaporation temperature of $-50\text{ }^{\circ}\text{C}$ and reported a COP of 9.6% more than the conventional auto-cascade system of Figure 4. Recently, Liu et al. (2022) [49] proposed another configuration of the auto-cascade system with the mixture R290/R170 and reported a 42.85% higher COP than the typical auto-cascade refrigeration cycle (Figure 4).

An auto-cascade refrigeration system is represented in Figure 4. The vapour mixture is first compressed (1–2) and is then directed to the condenser to reject heat (2–3). The heat sink temperature should be selected properly in the condenser to avoid a pinch point due to temperature glide. Only the refrigerant with the highest NBP condenses as it flows through the condenser. At the condenser outlet, the refrigerant mixture flows through a separator where the high (liquid) NBP is separated from the low (vapour) NBP. The high NBP is expanded (4–5) through the expansion valve to the operating pressure of the cascade condenser. Its temperature increases while exchanging heat with the low-NBP refrigerant. The low-NBP refrigerant is then condensed (7–8) and flows through the evaporator, providing the required refrigeration effect (9–10). However, in real systems, it is not possible to completely separate the pure refrigerants in the condenser because some of the low-NBP refrigerant condenses and some of the high-NBP refrigerant leaves

the condenser in vapour form. The phase separation process significantly impacts the system's performance. It should be carefully handled to guarantee the required refrigerant mixture concentration in the appropriate parts of the system. [31,41]. The compressor isentropic efficiency equation used for auto-cascade investigation is adapted from Yan et al. (2015) [16].

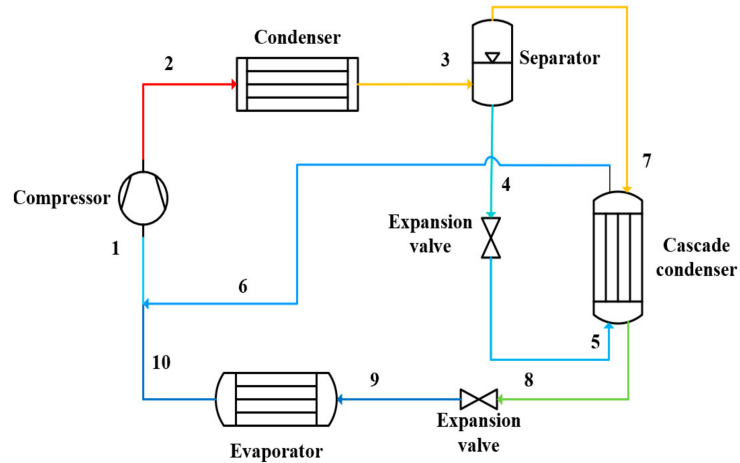


Figure 4. Auto-cascade refrigeration system.

3.5. Air Refrigeration Cycle

An air refrigeration cycle consists of four processes: two isentropic processes (i.e., compression and expansion) and two isobaric processes (i.e., cooling and heating). The refrigeration unit is described in Figure 5. It comprises three main parts: an integrated turbo compressor and expander, a primary cooler, and a cold recovery heat exchanger. The combined turbo compressor–expander is connected in the same shaft through a motor. The work generated by the expander is used as an auxiliary power input to the compressor, achieving energy savings.

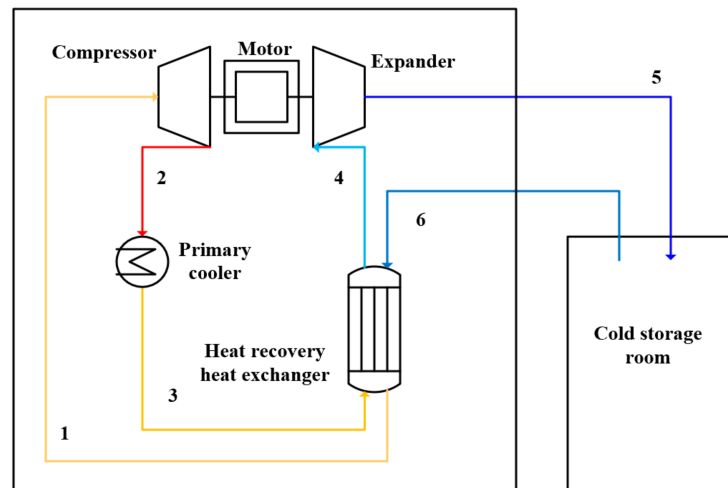


Figure 5. Air refrigeration cycle.

Moreover, the refrigerant does not need to be refilled or recovered. Thus, the maintenance costs are reduced [32]. The air from the cold-storage room is compressed (1–2) and then cooled down (2–3) in the primary cooler by air or water. The energy is then recovered in the heat recovery heat exchanger, where the warmer air heats the intake air (1) and, consequently, the air cools down further (3–4). The air is then expanded (4–5) and sent to the cold-storage room, where it is taken in, and the cycle starts again.

Air is used as the working fluid. The use of these systems represents an attractive solution for refrigeration operators. Using air as the working fluid in an open arrangement, the air of the space to be cooled can be used directly in the cycle to avoid the installation of evaporators, air coolers, and fans and thus avoid additional exergy losses in such heat exchangers. Because there is no secondary refrigerant, defrost cycles are not required, and the pipe dimensions are drastically reduced. This can reduce power usage by up to 40% compared to the CRC [26]. Very limited literature is available on the ARC, and it is reported in the Introduction section.

The COP is extremely sensitive to the machine's efficiencies. The thermal performance of the air cycle is improved when applying cold storage at low temperatures, which makes the air a suitable working fluid at very low temperatures (down to $-100\text{ }^{\circ}\text{C}$), which outperforms traditional refrigeration systems. It should be noted that, as the system operates at low temperatures (from -60 to $-100\text{ }^{\circ}\text{C}$), the formation of ice due to humidity could affect the system's performance. Therefore, it is necessary to install a humidity extraction device inside the refrigerating chamber to reduce the humidity ratio.

4. Performance Analysis of the Different ULT Refrigeration System Configurations for Various Applications

In this study, different scenarios were investigated, focusing mainly on three aspects: the temperature requirements, reliability of the system, and system performance. Different applications operating at temperature levels ranging from -80 to $0\text{ }^{\circ}\text{C}$ were explored (Table 3), including detector-cooling technology; fish processing, including the freezing and storage processes for different types of fish; medicine and biomedical applications; and the pre-stage cooling process of the liquefaction of LNG. In this study, the food-freezing and storage processes are related to the different types of fish caught on board ships, as the temperature requirements are within the investigated ULT range.

Table 3. Classifications of the different cases investigated in the study.

Application	Temperature Level	System Requirements	Configurations Investigated
Freezing fish (mackerel, cod)	From -0 to $-40\text{ }^{\circ}\text{C}$	Space limited, quick freezer, refrigerants according to the country regulations	VRC, MRS, CRS
Storage of fish (mackerel, cod)	$-40\text{ }^{\circ}\text{C}$	Proper insulation, stable cooling load, good air flow characteristics	VRC, MRS, CRS, ARC
Detector cooling	From -40 to $-50\text{ }^{\circ}\text{C}$	Slow cooling process, limited to refrigerants with resistance to radiation and without any risk in case of leakage	CRS, ARC
Freezing fish (tuna)	From -50 to $-70\text{ }^{\circ}\text{C}$	Quick freezing, limited space	MRS, CRS
Storage of tuna	$-60/-70\text{ }^{\circ}\text{C}$	Proper insulation, stable cooling load, good air flow characteristics	CRS, ARC
Medical applications, vaccine storage	From -60 to $-80\text{ }^{\circ}\text{C}$	Effective cooling process, minimised exposure to external loads, no air infiltrations	ACR, CRS, ARC
Cooling of gas	From -30 to $-70\text{ }^{\circ}\text{C}$	Optimisation of the heat transfer process	CRS

Thermodynamic analysis of different configurations was performed for the energy analysis. The numerical models were also validated with the existing literature. Figure 6 presents a classification of the different types of systems according to their operating

temperature ranges. It can be seen that the ACR system and CRS are commonly applied in ULT applications ranging from -40 to -80 °C. The VRC and MRS are those applied in the range from 0 to -50 °C.

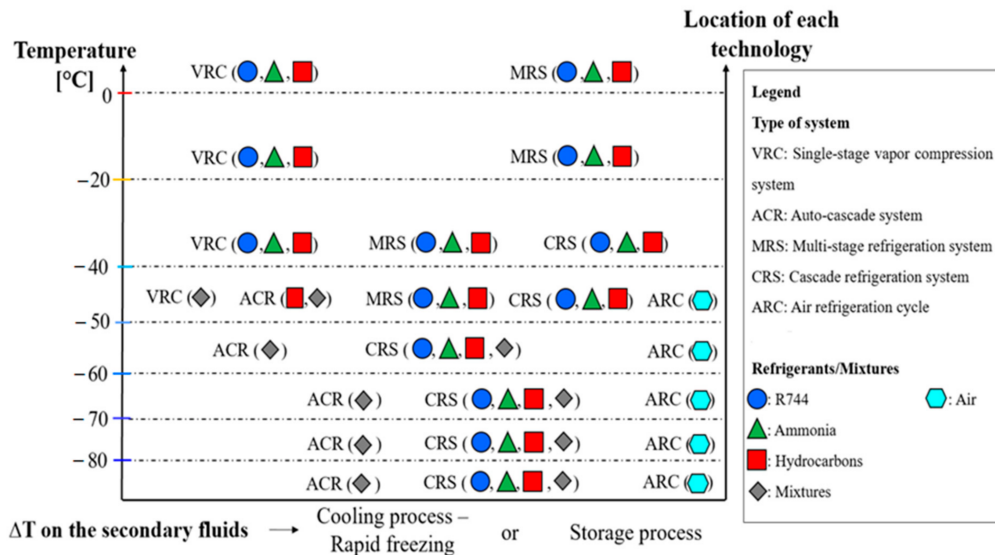


Figure 6. System configurations for different temperature levels.

The COPs of systems operating in the temperature range of from -40 to -80 °C were analysed for the MRS, CRS, ACR, and ARC. The general assumptions for the numerical models are listed below:

- The heat losses and pressure drops in the pipes and system components are neglected;
- Steady-state and steady-flow processes are assumed in all components;
- Heat leakages to the external environment are neglected;
- Expansion processes are treated as isenthalpic;
- The power consumption of the pumps is neglected;
- The compressors are non-isentropic, and their efficiencies are expressed as a function of the pressure ratio;
- No superheating or subcooling, and saturated conditions at the heat exchanger outlet;
- The temperature difference in the cascade heat exchanger (CHX) is set to 5 K.

4.1. Model Validation

In this sub-section, the thermodynamic models simulated in EES are validated using the data published by Bellos et al. (2019a) [50] and Lee et al. (2016) [29] for the CRS and by Bellos et al. (2019b) [51] for the MRS with the same compressor efficiency equations. For the MRS operating with R744, a double optimisation (intermediate and high pressure) was performed to obtain the highest COP. The system energy efficiency strongly depends on the intermediate and high pressure (transcritical conditions). The obtained COPs are shown in Figure 7. These are in good agreement with those obtained by Bellos et al. (2019b) [51]. The highest COP deviation is recorded to be around 3%, and the lowest is around 0.6%. Regarding the CRS design, the validation was only performed for R717/R744 (Figure 8).

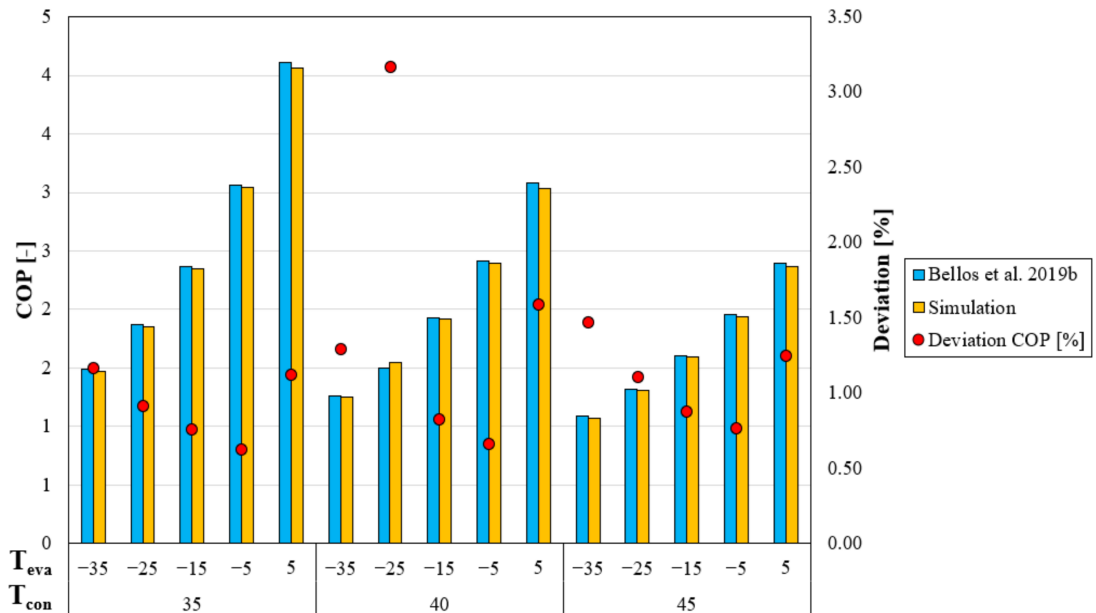


Figure 7. COP comparison between developed model and literature data for MRS operating with R744 [51].

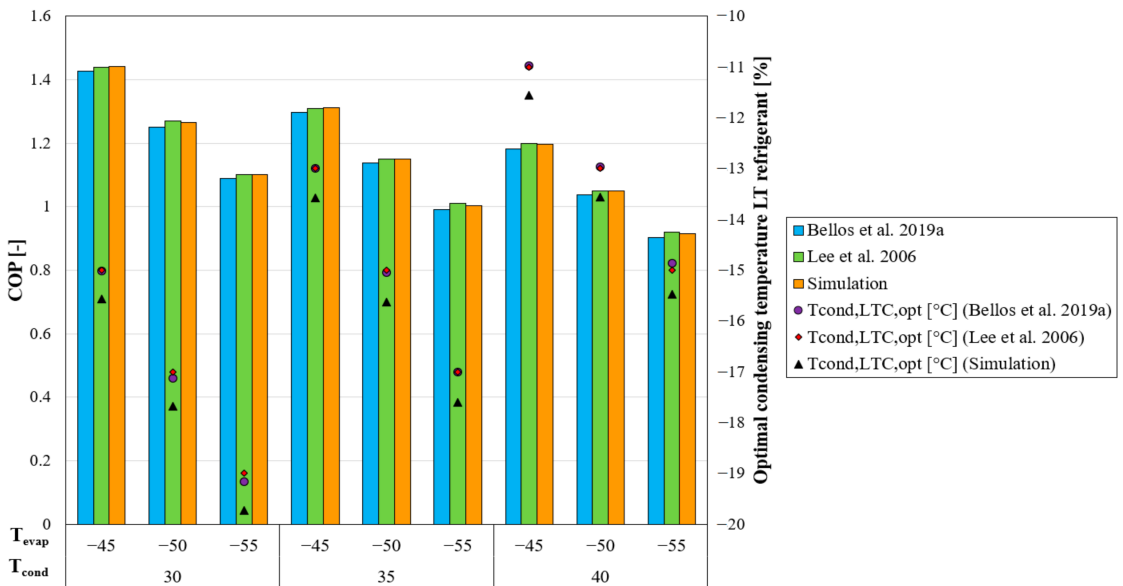


Figure 8. Comparison in terms of COPs and optimal condensing temperatures for the LTC between developed model and literature data [29,50].

As described in [52], the correlations for the isentropic efficiency of the HT and LT compressors should be determined as accurately as possible, as they all strongly influence the maximum COP and optimal condensing temperature of the LTC. This is understandable, considering the logic behind the optimisation process. The highest COP value is inversely

proportional to the total power consumption, which is directly influenced by the isentropic efficiency of the HT and LT compressors. The calculation program uses the pressure ratio values in both cycles with the highest possible efficiencies, impacting the optimal condensing temperature.

4.2. Fish Freezing of Mackerel and Cod

A brief overview of the onboard freezing systems is presented. There are many possible system architectures for the process applications, and centralised or independent systems may fulfil their needs. Usually, a larger vessel tends to have a centralised system that serves all the refrigeration demands (RSW, cooling, and freezing). Refrigerated seawater (RSW) is used for chilling fish before it is processed or frozen. Here, focusing only on the freezing process, the choice of the refrigerant and freezing system strongly depends on two factors: Firstly, it must conform to the national regulations and insurance requirements for fishing vessels. Many countries do not allow toxic refrigerants such as ammonia in storage, for instance. The second factor is the type and size of the fish species to be frozen. An additional factor would be the quality target of the food, which is generally described through the freezing time, as will be highlighted later. All the other additional requirements are reported in the article [53]. Three large families of refrigerating systems are considered here:

- Air blast freezers, which are generally small rooms or tunnels where cold air is blown to freeze the whole fish. Air-cooling coils cool the air;
- Plate freezers, which are typically used for small fish sizes. These consist of hollow plates cooled by refrigerant evaporating inside them, ensuring good contact between the cold surface of the plate and the food. Contrary to air blast freezers, they can only be used to freeze regular-shaped blocks of fish;
- Brine immersion freezing, which can use liquid nitrogen or liquid CO₂ and is usually used to quickly freeze a tremendous number of fish by spraying or dipping the fish in the liquid. As a result, the fish quickly cool down to lower temperatures. Extra care is required to protect the fish surface from thermal cracking [54].

The choice of one of the systems presented above depends on the amount and size of the fish and the space available on board. Furthermore, although R-22 is still the dominant refrigerant in marine offshore refrigerated vessels [55], ammonia and carbon dioxide have begun to enter the fishing refrigeration market. Ammonia is the refrigerant choice for modern, environmentally friendly refrigeration systems across the cold fisheries in Europe. With the increased restrictive measures aimed at the safety on board, and the lower temperatures required, R717 is also applied with R744 in indirect and cascade systems in new refrigerated ships. The cases investigated are listed below in Table 4, in which the condenser is assumed to be cooled with seawater, and the target temperature for freezing is set to $-30\text{ }^{\circ}\text{C}$.

Table 4. Cases investigated for fish freezing of mackerel and cod.

Application		Fish Freezing (Mackerel, Cod)				
System	Primary Refrigerant	Secondary Refrigerant	Evaporating Temperature ($^{\circ}\text{C}$)	$\Delta T_{\text{refrigerant-air}}$ $\Delta T_{\text{air-fish}}$ or $\Delta T_{\text{refrigerant-fish}}$ (K)	Condensing Temperature ($^{\circ}\text{C}$)	Type of Freezing System
MRS		R717	-38	$4-4$	15	Air blast freezer
MRS		R744	-50	20	15	Plate freezer
MRS		R744A	-50	20	15	Plate freezer
CRS	R717	R744	-50	20	15	Plate freezer
CRS	R290	R744	-50	20	15	Plate freezer

The design temperature of the plate freezers/air blast freezers should be related to the temperature of the cold-storage room to which the product is transferred after freezing. It is worth remembering that below $-33\text{ }^{\circ}\text{C}$, the ammonia refrigeration plant is working under sub-atmospheric conditions, as already declared in Section 2.1, and a VRC would be infeasible due to the high discharge temperature at the compressor outlet.

Figure 9 illustrates the COPs of the systems presented above. The COP cannot be the only criterion for the selection of the refrigeration unit.

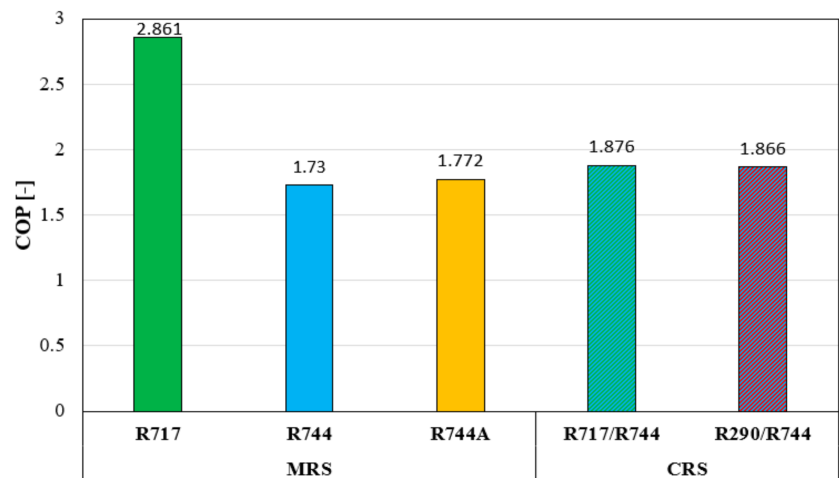


Figure 9. COPs of the different systems analysed.

The freezing time is one of the most important aspects to account for during the design of an onboard refrigeration system. The colder the freezer, the faster the fish will freeze; however, the cost of the freezing unit increases as the freezing temperature decreases. Different factors can be observed. The MRS simulated operating with ammonia works in sub-atmospheric conditions, with related concerns about the non-condensable build-up and moisture infiltrations due to vacuum leakages. In addition to this, the temperature difference between the air and fish can only be reduced by increasing the air velocity to freeze the products fast. However, this measure and a reduction in the air temperature harm the efficiency. Evaporating temperatures for R717 systems are seldom lower than $-35\text{ }^{\circ}\text{C}$.

Regarding plate freezers, without considering the dependence of the freezing time on the food water content and thickness of the product, faster freezing can be achieved by using R744 or R744A as the working fluid. The lower NBP of CO_2 allows for reducing the evaporating temperature, while its environmentally friendly properties agree with the heat transfer process occurring through direct contact between the fish surface and refrigerant plates. The investigation of R744A is purely theoretical, as possible exothermal decomposition calls for safety devices and intensive refrigerant charge monitoring [6]. From a COP point of view, an increment of about 8% can be recorded independently using the HT refrigerant. In real applications, R717 refrigeration systems suffer from a high discharge temperature at the compressor's discharge. Therefore, the CRS can be used under some operating conditions if the system works far away from the optimal condensing temperature of the LTC. Additional considerations can be made: the CRS with R744 as the LT refrigerant has different advantages over the MRS operating with R717 [53], such as follows:

- A much higher volumetric refrigeration capacity;
- It always works with positive pressure above the atmospheric one;

- The use of R744 allows for the design of the HTC with a reduced refrigerant charge and, consequently, with a reduction in the costs related to the safety management process;
- Flammable or toxic refrigerants can be used in the primary circuit isolated from the cooling process and storage areas, aiding safety.

4.3. Storage of Mackerel and Cod

As described above, fast freezing to ensure a high-quality product and an environmentally friendly solution are the primary targets for onboard freezing and storage systems. Therefore, considering the freezing target temperature as the temperature at which the products must be stored, the following cases were evaluated (Table 5).

Table 5. Cases investigated for storage of mackerel and cod.

Application	Fish Storage (Mackerel, Cod)				
System	Primary Refrigerant	Secondary Refrigerant	Evaporating Temperature (°C)	($\Delta T_{\text{refrigerant-R744}}$) $-\Delta T_{\text{refrigerant-air}}$ (K)	Condensing Temperature (°C)
MRS	R717	R744	−40	5–5	15, 40
MRS		R744	−35	5	
CRS	R290	R744	−35	5	
CRS	R717	R744	−35	5	
CRS	R744	R744	−35	5	
ARC (open cycle)		Air	Simulation result	~20	

In most low-temperature applications, an R744 cascade system would be able to fill the bill, if the local health and safety regulations influence the use of R717. In that case, secondary refrigerants, such as R744, which may satisfy the regulations with a lower risk of leakage, are necessary. Here, the flammable or toxic refrigerant is isolated to the machine room. R744, a volatile secondary refrigerant, is cost-effective thanks to the reduced pumping and pipework costs. If a secondary fluid, and therefore a heat exchanger, is involved, an additional temperature difference is required to allow heat transfer in the evaporator and to compensate for the pressure losses on the secondary loop [56]. In this simulation, the target temperature is too low to use an R717 indirect system because of the sub-atmospheric pressure. Only five systems with different heat-rejecting temperatures were investigated.

On board, once the fish is caught and frozen, it is stored through the MRS or CRS and transported to the onshore storage system. The thermodynamic analysis reported the following results for condensing temperatures of 15 and 40 °C, as the intermediate cases at 25 and 30 °C reflect the same trend (Figure 10).

As is already well known, when the temperature difference between the condenser and evaporator increases, the COP of the MRS is strongly penalised by the adoption of one single refrigerant. Vice versa, the CRS obtains a higher COP compared to the MRS, as widely stated in the literature [57]. As described by Mumanachit et al. (2012) [28], the MRS presents a higher system efficiency at higher evaporating temperatures, while the CRS is more efficient at lower evaporating temperatures. The MRS operating with R717 degrades the COP more rapidly than the CRS because of the high vapour-specific volume. In comparison, the MRS with R744 is strongly influenced by the throttling losses that occur at high heat rejection temperatures and thus becomes uncompetitive with the CRS in terms of high condensing temperatures. The adoption of R717 as the HT refrigerant in the CRS is considered one of the best options thanks to its superior thermodynamic properties compared to traditional refrigerants, among them the high latent heat of the vaporisation. As for the freezing processes, using the optimal condensing temperature of the LTC leads to an excessive pressure ratio and, therefore, too-high discharge temperatures, making this layout infeasible in warmer climates. Using R744 in the HTC would lead to the worst

performance compared to any other refrigerant [50] because of the transcritical operating conditions. Therefore, R290 could be a valid option, considering its confinement in the machine room, critical temperature, and molecular weight, which would induce a much lower liquid curve slope than R717.

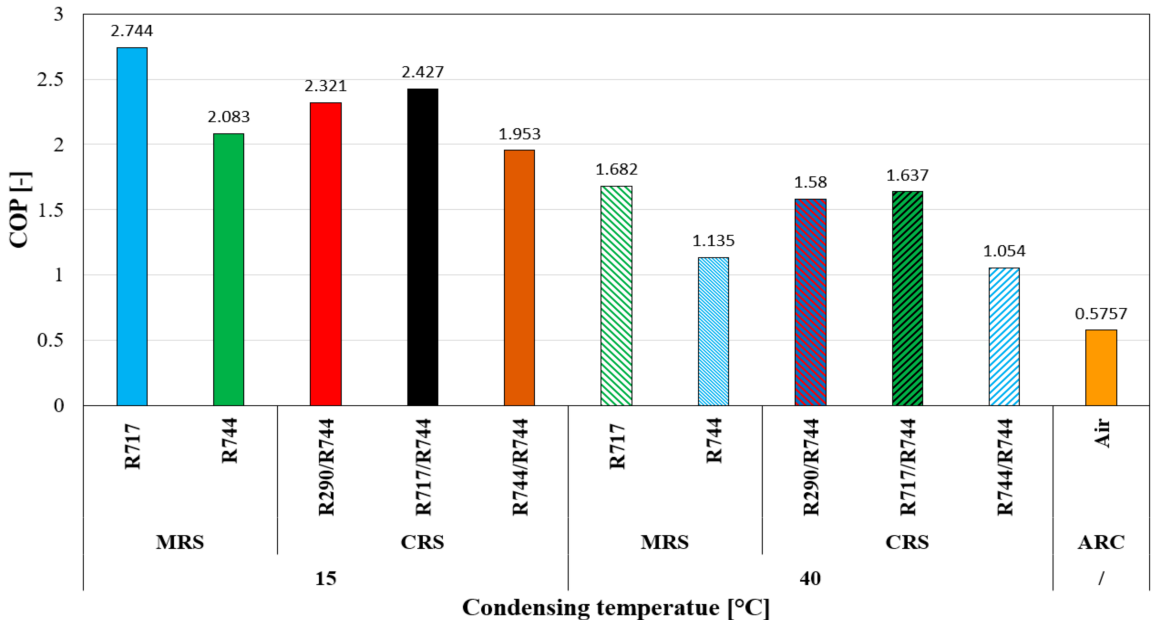


Figure 10. COPs of the different systems analysed for fish storage of mackerel and cod.

Different considerations are made for the ARC: a water-cooled heat exchanger (primary cooler) is used to decrease the compressor outlet's discharge temperature, resulting in a system independent of the external ambient air, being the heat losses neglected. Based on these points, only one COP value is calculated for a given cold-storage temperature. The further assumptions used for the calculations are listed below (according to Figure 5):

- The PAS-30R is used as a design reference for the simulations [32];
- The temperature at the primary cooler outlet is set to 40 °C;
- The turbine and compressor have the same efficiency, which is set to 0.76;
- The effectiveness of the recuperative heat exchanger is equal to 0.95;
- The high-pressure limit in the system is set to 2 bar;
- The circulating air is assumed to be dry;
- There is no air leakage from the system.

4.4. Fish Freezing of Tuna

The high-quality target for the consumption of raw tuna requires very low cooling and storage temperatures, namely in the range of from -50 to -70 °C. This temperature range does not allow any MRS to work with pure fluids; therefore, a suitable mixture should be found. Blends of R744 and HCs have been studied in the literature [58], and they have become very attractive from several points of view. The triple point of R744 holds back its use as an ultra-low-temperature refrigerant in the CRS. Pure refrigerants such as R170, R1150, and R744A are the only options available. R744A has not been deeply studied, and safety issues could occur, while R170 and R1150 are flammable refrigerants, and thus their implementation requires additional safety measures. Furthermore, the freezing process of tuna occurs after a pre-cooling process, and it usually starts around -20 / -30 °C. Consequently, azeotropic and zeotropic mixtures with small temperature glides could

match the needs very well. The different refrigerant pairs and mixtures investigated are listed below in Table 6 for a target freezing temperature of $-60\text{ }^{\circ}\text{C}$.

Table 6. Cases investigated for freezing of tuna.

Application		Fish Freezing (Tuna)				
System	Primary Refrigerant	Secondary Refrigerant	Evaporating Temperature ($^{\circ}\text{C}$)	Condensing Temperature ($^{\circ}\text{C}$)	$\Delta T_{\text{refrigerant-air}} - \Delta T_{\text{air-fish}}$ (K)	Type of Freezing Unit
CRS	R717, R744, R290, R1270	R170	-75	15	5–10	Vessel/cold chamber with cold air flow
CRS	R717, R744, R290, R1270	R1150	-75	15	5–10	
CRS	R717, R744, R290, R1270	R744A	-75	15	5–10	
CRS	R717	R744 + R170	-75	15	5–10	
CRS	R717	R744 + R1150	-75	15	5–10	

Figure 11 illustrates the COPs of the different refrigerant pairs used in a CRS. The use of R744 in the HTC is attractive from the environmental point of view, but in terms of the COP, it is inefficient compared to the other systems, as shown in the freezing process of mackerel. This discrepancy between R744 and HCs increases as the evaporating temperature decreases. R717 is still the best fluid for the HTC, but, in real applications, it would require working far away from the optimal point because of the excessively high discharge temperature (Figure 12), which is limited to 120 degrees [1]. It can be seen that the lower the NBP of the LT refrigerant considering the same HT refrigerant (Tables 1 and 2), the lower its optimal condensing temperature and the higher the pressure ratio.

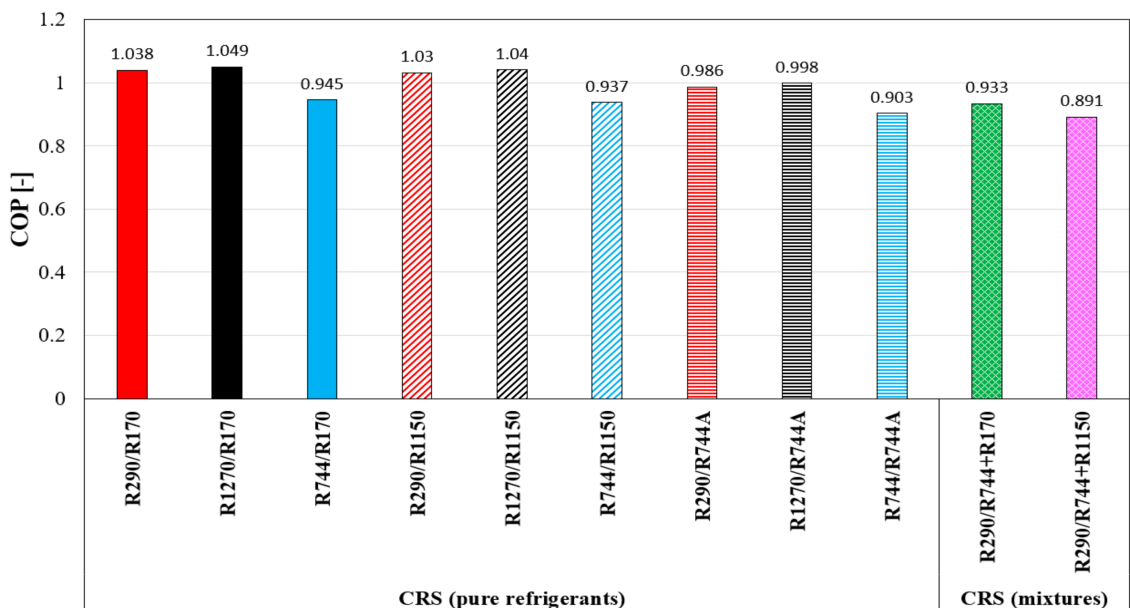


Figure 11. COPs of the CRS investigated with different refrigerant pairs.

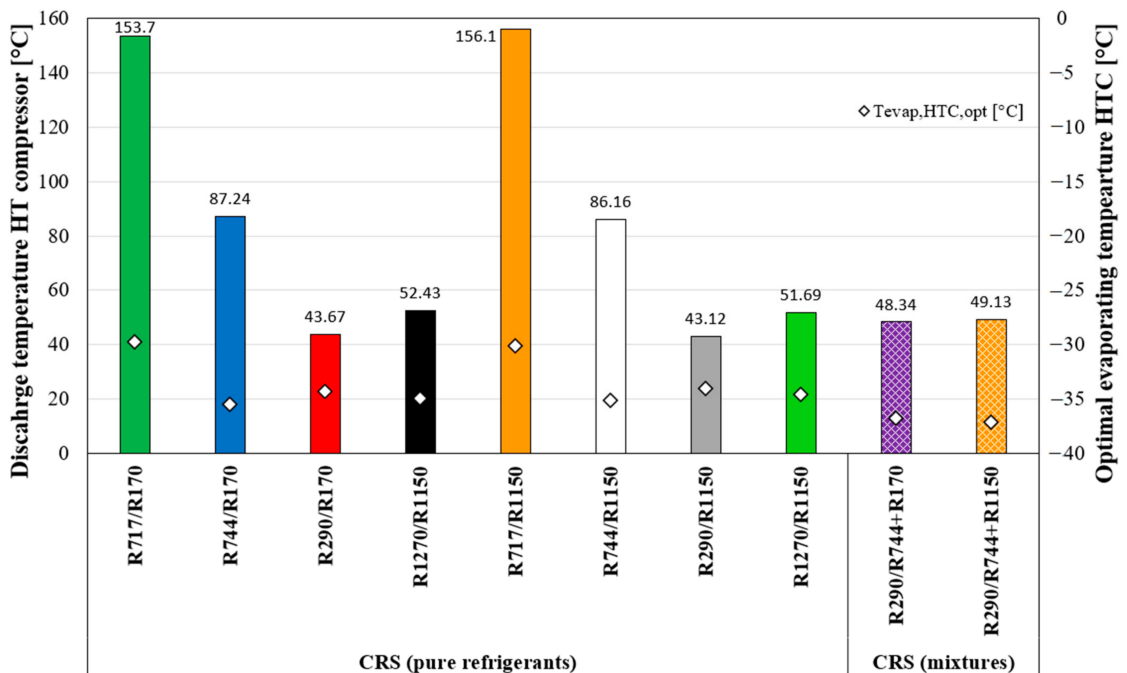


Figure 12. Discharge temperatures at the HT compressor outlet and optimal evaporating temperatures for the HTC.

After this consideration, the most performant cycles are the CRS with R1270 and R290 as the HT refrigerants and R170 and R1150 as the LT refrigerants. Similar COPs can be recorded using nitrous oxide in the LT stage, but this requires further studies on its stability when it is used as a working fluid in refrigeration systems. Considerable interest should be given to mixtures of R744 + R744A, which have very good volumetric refrigeration capacities and are almost climate-neutral. As stated by Kauffeld et al. (2020) [59], an alternative to the HFC substances or flammable mixtures used in applications below -50 °C has been found, and it is already in an advanced study stage. The mixtures simulated containing R744 and HCs (R170 and R1150) would lead to a worse performance compared to their pure counterparts. However, they can achieve non-flammability as long as the mass fraction of R744 is sufficient enough and does not vary throughout the cycle compared to the initially charged concentration. The exceptionally low temperatures used in these freezers (from about -60 to -70 °C) have increased the special precautions to be taken in fishing vessels.

4.5. Storage of Tuna

The same considerations presented above regarding the refrigerants employable in the CRS are valid for the storage process of tuna, except that PAS is an alternative and more environmentally friendly solution. Table 7 summarises the systems analysed, with a target storage temperature of -60 °C.

The option of having R717 as an HT refrigerant has not been considered, as the temperature difference between the condenser and evaporator leads to excessively high discharge temperatures at the compressor outlet. However, R717 may be an interesting option in some cases, such as in the cold chain, after the freezing process, and in the transportation of food to the warehouse. If the size of the warehouse is small enough to be confined in a larger room, then its external temperature can be reduced by using a traditional refrigeration system, minimising the losses and increasing the energy performance of the refrigeration

unit by decreasing the rejecting heat temperature on the HTC. However, the total costs will rise while the total energy efficiency will be reduced due to the additional refrigeration unit needed to pre-cool the room. Considering a warehouse in which the operating refrigeration unit rejects heat to the external environment, Figure 13 allows for the identification of the most promising refrigerant pair.

Table 7. Cases investigated for tuna storage.

Application	Fish Storage (Tuna)				
System	Primary Refrigerant	Secondary Refrigerant	Evaporating Temperature (°C)	$\Delta T_{\text{refrigerant-air}}$ (K)	Condensing Temperature (°C)
CRS	R744, R290, R1270	R170	−65	5	
CRS	R744, R290, R1270	R1150	−65	5	15, 40
CRS	R290, R744	R744+R170	−65	5	
CRS	R290, R744	R744+R1150	−65	5	
ARC (open cycle)	Air		Simulation result	~20	

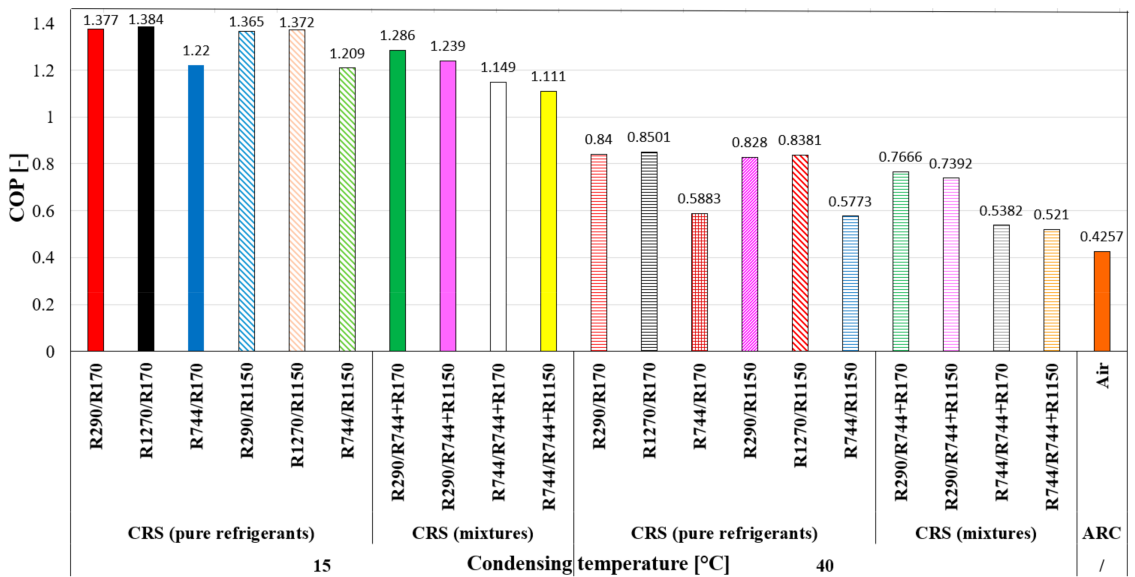


Figure 13. COPs of the ARC and CRSs investigated with different refrigerant pairs.

Once again, the inefficiency of using R744 as an HT refrigerant has been proven (Figure 13). The best refrigerant pairs are R290/R170 and R1270/R170 (even though R290 does not change the COP).

The use of a CRS for the offshore storage of tuna is encouraged, while the use of ARC is encouraged for onshore storage because of all its relative advantages. Dry ice is frequently used for transportation to the onshore warehouse, but with a relative time limit, which depends on the stored products’ temperature level and quality target.

From the numerical simulation, the COP of the ARC is much lower than the COP in a CRS, even with a condensing temperature of 40 degrees. The discrepancy between the simulation results and the data available in the literature [60] will be discussed later (Section 5).

4.6. Vaccine Storage/Medical Applications

Most traditional vaccines can be stored in standard refrigerators within a temperature range of from +2 to +8 °C. Storing enzymes, vaccines, or pharmaceutical products requires a temperature of −20 °C, while some vaccines are stored between −50 and −15 °C. The BNT162b2 (COVID-19) and Ervebo (Ebola) vaccines need to be stored at a temperature below −50 °C, ensuring their stability, efficacy, and safety all along the cold-chain terrain. The Pfizer vaccine, for instance, is stored at a temperature of −70 °C [61]. Currently, the most energy-efficient freezers use hydrocarbon refrigerants, such as R170 and R290. These units are popular in the European pharmacy industry but unavailable in other countries due to regulatory restrictions. Different systems have been analysed depending on the number of vaccines to be stored, such as the ACR system, CRS, and ARC.

Furthermore, the freezer location affects the lifetime and efficiency of the ULT freezer, namely the heat rejection temperature. When ULT freezers cannot meet the space requirements, an air-cooled condenser must be replaced with a water-cooled condenser. As stated by some manufacturers, such as Intarcon and PHCBI, the operator must follow a procedure for correctly preserving the vaccines. The refrigeration unit works in a cold room at around −20 °C, where the operator always works safely to insert the products in or remove them from the ULT freezers. The pre-cooling of the cold room minimises the losses and avoids humid-air infiltrations into the cabinet. This principle is applied depending on the location, climate, and cost analysis. For developed countries located in warmer climates, the ULT freezers work by rejecting the heat to the external ambient air, and therefore a degradation of the COP occurs. This degradation appears even in ULT freezers placed in pre-cooled rooms. The additional costs for the refrigeration unit aimed at the pre-cooling and its energy consumption could lead to a deterioration in the overall COP. Contrarily, in the opposite case, a well-insulated chamber/freezer must be designed to avoid excessive energy losses and relatively high energy consumption.

Small-sized refrigerators with cooling capacities below 1 kW typically use ACR. Recently, its use has drawn considerable interest because of its simpler structure and, by using a zeotropic mixture, it could realise one-stage compression. The CRS and ARC are viable options for larger cooling capacities (for instance, storing some containers containing vaccines). The ARC draws much attention at this temperature level thanks to its significant advantages compared to the conventional CRS. Table 8 summarises the cases investigated.

Table 8. Cases investigated for vaccine storage.

Application		Vaccine Storage (Pfizer)			
System	Primary Refrigerant	Secondary Refrigerant	Evaporating Temperature (°C)	$\Delta T_{\text{refrigerant-air}}$ (K)	Condensing Temperature (°C)
ACR	R1150/R600, R1150/R290		−80	5–10	15, 30
ACR	R170/R290, R170/R600, R744/R290		−80	5–10	
CRS	R744, R290	R170	−75	5	15, 30, 40
CRS	R744, R290	R1150	−75	5	
CRS	R290, R744	R744+R170	−75	5	
CRS	R290, R744	R744+R1150	−75	5	
ARC (open cycle)	Air		Simulation result	~20	/

The compositions of all the mixtures are adopted in such a way as to avoid sub-atmospheric conditions. The composition of the first refrigerant of all the mixtures in Table 8 is 0.8, except R1150/R290, which is 0.7. The vapour quality after the condenser was fixed to 0.4 and high pressure is the consequence of the vapour fraction. A higher vapour fraction after the condenser will reduce the pressure ratio, and a lower vapour fraction will increase the pressure ratio. As the zeotropic mixtures exhibit temperature

glide, lower evaporation temperatures are necessary compared to other cases. The COPs of the auto-cascade cycle with different refrigerant mixtures are shown in Figure 14.

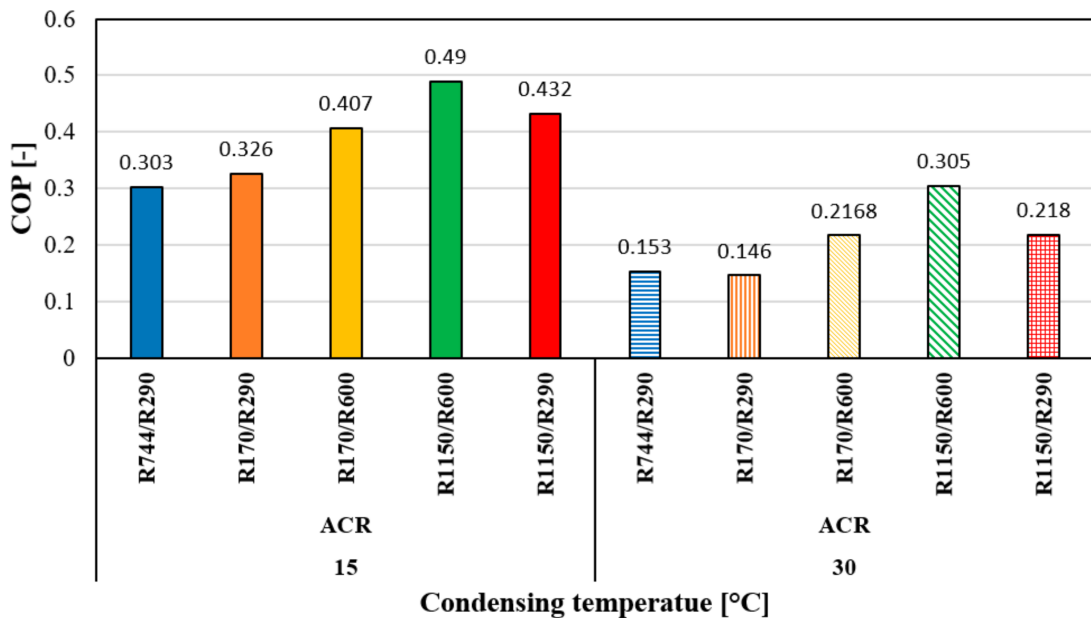


Figure 14. COPs of the ACR with mixtures for vaccine storage.

The COP is competitive with other systems, but the pressure ratio and temperature after the compressor are high, which can hinder the implementation of this system in some cases. However, modifications with a recuperator, an ejector, and an additional expansion valve were investigated by Yan et al. (2018) [62] to improve the pressure ratio and COP. They concluded that, by adopting the modifications, proposed ACR units could solve the challenges of small low-temperature storage.

For larger cooling capacities, Figure 15 shows the COP values for the CRSs investigated and the ARC. The use of HCs as HT refrigerants still leads to the best performance. Using mixtures in the LTC reduces the risks related to the flammability limits of such refrigerants but attains a lower performance. The use of zeotropic mixtures does not imply an increase in efficiency, and the reason is two-fold. First, the area between the two temperature profiles is representative of the losses. The exergy losses during the heat transfer can be reduced whenever a secondary fluid is cooled down. Second, because superheating is required in real applications to ensure that no liquid bubbles at the compressor suction port, if the glide temperature is too large, then the temperature profile is lifted and requires additional work for the compressors.

Furthermore, additional considerations can be drawn. The temperature difference required for having a heat transfer induces a change in the composition of a zeotropic mixture. The extra temperature difference associated with the difference in the concentration decreases the total heat transfer coefficient compared to a pure fluid. Resistance to mass transfer, which implies a resistance to heat transfer, is present due to the different compositions in the liquid and vapour bubbles.

Regarding the cases investigated, using a zeotropic mixture, such as R744 + R170, may present some issues in real applications: The choice of the R744 concentration must satisfy the need to minimise the flammability risk while working above the triple point. An oscillation of the evaporating pressure can cause the formation of solid particles to impact the refrigerant flow and the heat transfer performance.

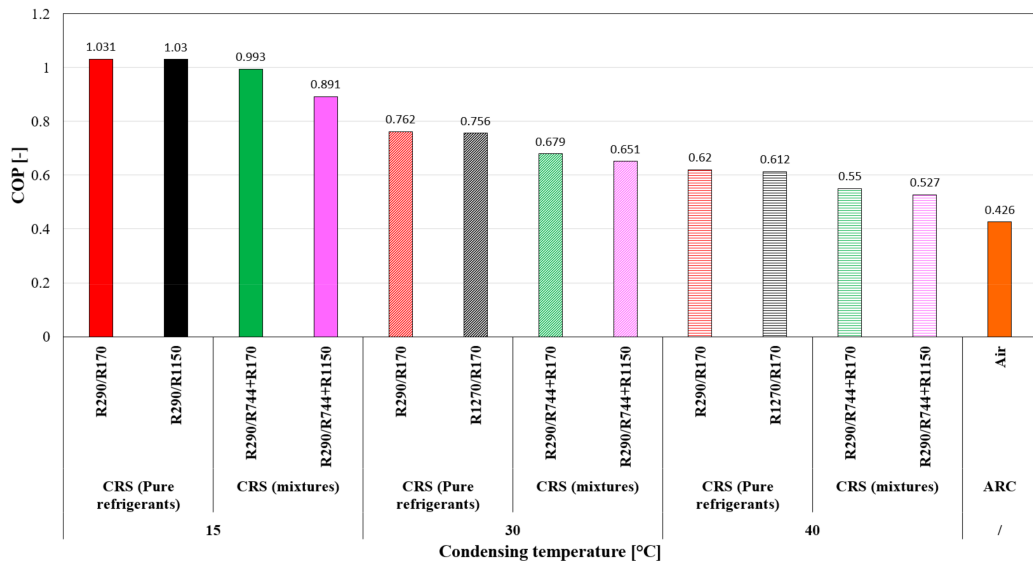


Figure 15. COPs of the different systems analysed for vaccine storage.

In warmer climates and at low storage temperatures, the ARC is becoming competitive with CRSs. The presence of recuperative heat exchangers is fundamental. Having the maximum allowable pressure at 2 bar, the recuperative heat exchanger achieves lower temperatures in the cold-storage room for a given pressure ratio by pre-cooling the air at point 6 thanks to the relatively cold air taken from the room (point 5, Figure 5)

4.7. Gas Pre-Cooling

Liquefied natural gas (LNG) is a liquid state of natural gas around $-162\text{ }^{\circ}\text{C}$ under atmospheric pressure and temperature. LNG has a volume 600 times smaller than gas under normal conditions, allowing enormous volumes of it to be carried by ships [63]. In the pre-cooling stage of LNG, the natural gas is cooled to a temperature ranging from $-30\text{ }^{\circ}\text{C}$ to $-50\text{ }^{\circ}\text{C}$ or even lower, depending on the pre-cooling method used. The outlet temperature of the pre-cooling stage is a critical design parameter influenced by technological and strategic factors [64]. The choice of technology is a consequence of many factors, including economic, environmental, financial, licensing, and technical concerns [63]. The scope of this part is dependent on the COP analysis of the cascade system because most of the economic data on liquefaction units are treated as confidential. Natural gas is cooled down in several processes, such as pre-cooling, liquefaction, and subcooling, for the method based on more than one refrigerant cycle [64]. Figure 16 shows the temperature glides of different zeotropic refrigerant mixtures at constant pressure, which was used for analysis.

The highest glide is with R1150/R600 and the lowest is with R170/R290. The temperature glides can be adjusted according to the requirements of the gas-processing unit by altering their compositions. The cascade system with mixtures can reduce the multiple pressure levels for cooling and improve the efficiency by matching the temperature glide. The cascade cycle with mixtures can reduce the existing one cycle of three-stage processes. Two refrigerants (R717 and R290) were investigated for the HTC with a condensing temperature of $15\text{ }^{\circ}\text{C}$ (Figure 17). The pressure ratio and temperature after compression are within their allowable range. For the HTC, R290 possesses more potential due to its better pressure ratio and temperature after compression. For the LTC, the evaporation temperature was kept at $-80\text{ }^{\circ}\text{C}$ for all cases. The highest COP is represented by the R170/R600 mixture, but the temperature glide is less than that of R1150/R600. In comparison, the cases with

propane have 4.5% higher COPs than R717. In addition, the cascade system with mixtures can also be used for the liquefaction of other gases (e.g., CO₂).

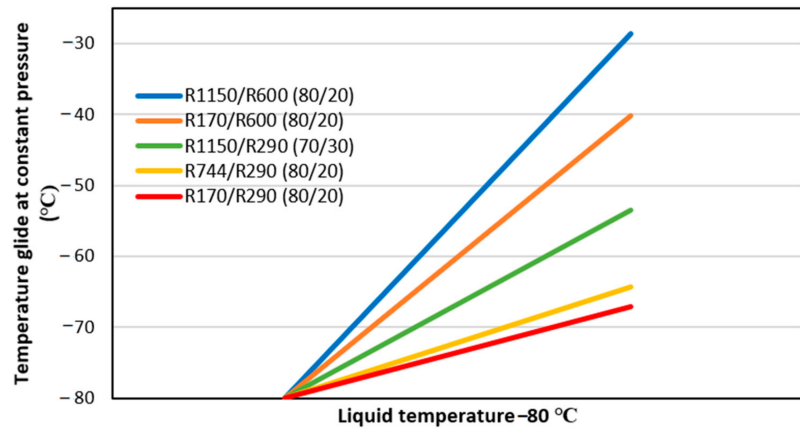


Figure 16. Temperature glides of zeotropic refrigerant mixtures.

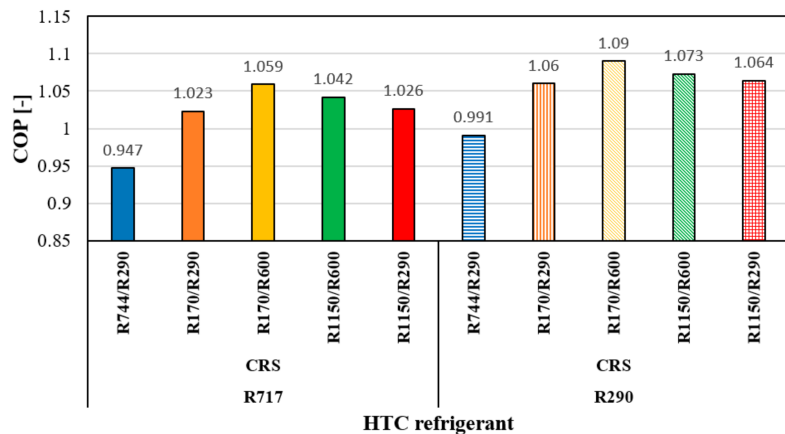


Figure 17. COP of the cascade system with refrigerant mixtures.

4.8. Detector Cooling

The Large Hadron Collider (LHC) detectors at CERN in Switzerland need to dissipate several hundred kilowatts of heat (300–600 kW). Therefore, a refrigeration system is needed, which cools down these detectors and keeps them below a temperature of -40 °C, leading to evaporation temperatures below -50 °C. Because the detectors are worth around NOK 1 billion, reliability and stability in the cooling are crucial, but the COP of the system is not. Furthermore, the detectors are highly sensitive, requiring an oil-free configuration. In this case, a cascade system is needed, which consists of a high-pressure side operating with piston compressors and an oil-free low-pressure loop on the evaporation side. The primary booster system is mainly located on the surface, providing the cooling for the oil-free cycle in the cavern 100 m underground, consisting of evaporators. The secondary loop circulates the refrigerant through the evaporators inside the detectors [65]. The space in the cavern is limited, and radiation occurs, making R744 an appropriate refrigerant on both the low- and high-pressure sides. Flammable refrigerants are not suitable, and neither are their mixtures. Radiation occurs in the machine rooms, resulting in another requirement regarding the

refrigerant choice. The ARC is not appropriate due to its space requirement, for instance. Moreover, due to the large cooling load, many machines in parallel would be involved, lowering the total system efficiency.

5. Further Considerations Regarding Storage Applications

Different products, such as food, antibiotics, and vaccines, require storage at different temperature levels. The temperature level and the constraints related to the product's storage indicate the most suitable system. However, further considerations must be made to assess the feasibility under certain operating conditions. An excessive discharge temperature at the compressor outlet, unachievable pressure ratio levels, and safety concerns are examples of those aspects that need to be controlled in real applications. This would change the results of the numerical analysis. Figure 18 illustrates the COPs of the three most common technologies (the ARC, MRS, CRS) generally used in the low- and ultra-low temperature region for different warehouse temperatures under the following assumptions:

- For the ARC, the assumptions previously presented are still valid;
- For the MRS and CRS, the same assumptions are used as before;
- The heat rejection temperature is set to 30 °C;
- The optimisation procedure of the high-pressure (ARC), intermediate-pressure (MRS), and gas-cooler-pressure (R744) condensing temperatures of the LTC (CRS) has been carried out;
- The temperature difference between the refrigerant evaporating and the air in the cold room is set to 5 K (MRS, CRS), while for the ARC, it is a result of the simulation;
- For the MRS, the refrigerants R717 and R744 have been considered, while for the CRS, different refrigerant pairs were included in the simulation, such as R717/R744, R290/R744, R717/R170, R290/R170, and R290/R1150.

R717, as a low-temperature refrigerant, has proven that the issue related to its implementation is the sub-atmospheric pressure in the evaporator. Consequently, the MRS with R744 would be a much better option from a real application point of view. However, the COP would be much lower due to the transcritical condition of the cycle. Therefore, for a warehouse temperature in the region from −30 to −45 °C, a CRS would supply the cooling load more efficiently than an MRS without any constraints because the pressure ratio limit in both the upper and lower cycles is never exceeded. Because of the triple point of R744, its use as an LT refrigerant is a holdback in real applications for warehouse temperatures below −50 °C. As illustrated before, only a few refrigerants can match these temperature requirements, all belonging to the hydrocarbon family. Ethane and ethylene may match the requirements because of their NBPs. For the couple R717/R170, the optimisation procedure has been performed for warehouse temperatures until −85 °C. The optimisation process shows a decrease in the optimal condensing temperature of the LTC as the evaporating temperature drops, deteriorating the R717 compressor's efficiency due to the relatively high compression ratio. The excellent thermodynamic properties of R717 cannot overcome the poor compressor efficiencies, and using R290 for low-evaporating-temperature storage is a better option.

Furthermore, in this specific case, the lower NBP of R290, with its thermodynamic features, is important for attaining good efficiencies. R1150 is the only pure refrigerant employed for deep storage temperatures in the LTC. In scenarios in which the evaporating temperature is below −95 °C, the optimisation procedure followed by the software would lead to infeasible pressure ratios in the low stage. Therefore, a different approach must be considered: the optimal condensing temperature of the LTC must be fixed as an input to maintain the pressure ratio below its upper limit.

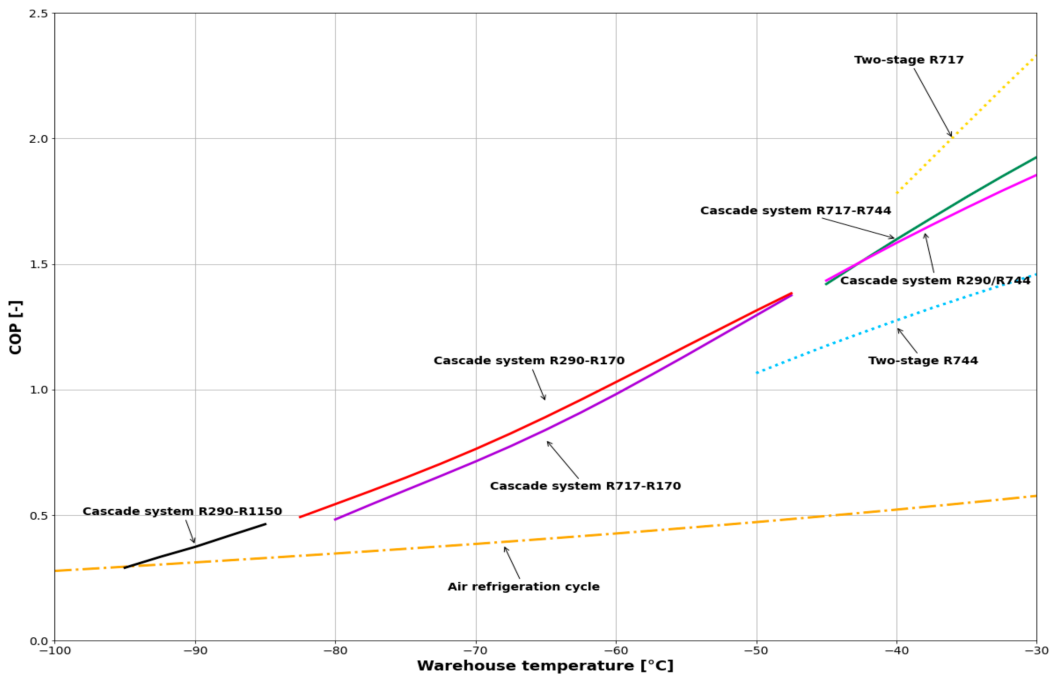


Figure 18. COP comparison between ARC, MRS, and CRS for different warehouse temperatures by using different refrigerants. Only pressure ratio limitation is considered (solid line: CRS; dotted line: MRS; dash-dot line: ARC).

It can be seen how the COP curve of the ARC is in agreement with the results of the report, while the COP curves of the CRS are quite different from those presented in the industrial report [60]. The reasons for this discrepancy can be found in several factors, including superheat at the suction port, a limited discharge temperature, pressure drops, the fan power, and a higher temperature difference in the heat exchangers. Figure 19 shows the superheating effect and the limited discharge temperature at the compressor outlet, which is set to 120 °C and should never be exceeded. The fan power is supposed to be 10% of the total power consumption.

Starting from the evaluation of the MRS, different aspects can be recorded:

- For an MRS operating with R717, only for an evaporating temperature of -35 °C is the discharge temperature limit not exceeded;
- For lower evaporating temperatures, the discharge temperature exceeds the limit, and therefore the optimal intermediate pressure obtained in the first simulation run is used as an input for subsequent simulations;
- The assumption above is valid for a small temperature range in the warehouse, as seen in the shortened curve (green dotted line). This is mainly linked to the following consideration: Keeping the discharge temperature of the HT compressor under control causes a deterioration in the discharge temperature in the LT stage. The discharge temperature limit is exceeded in the LT stage;
- For R744, the range of applicability remains unchanged, and only a deterioration in the COP has been noticed because of the negative effect of the superheat.
- For the CRS, the following conclusions are drawn:
- For the refrigerant pair R717/R744, one constant LT condensing temperature is used to limit the discharge temperature in the HTC. The superheat reduces the compressor's capacity and increases the discharge temperature, reducing the COP (Figure 20) due

to the constant condensing temperature in the LTC (around $-1.4\text{ }^{\circ}\text{C}$). A decreased evaporating temperature results in a decreased optimal condensing temperature, implying a further deterioration in the energy performance;

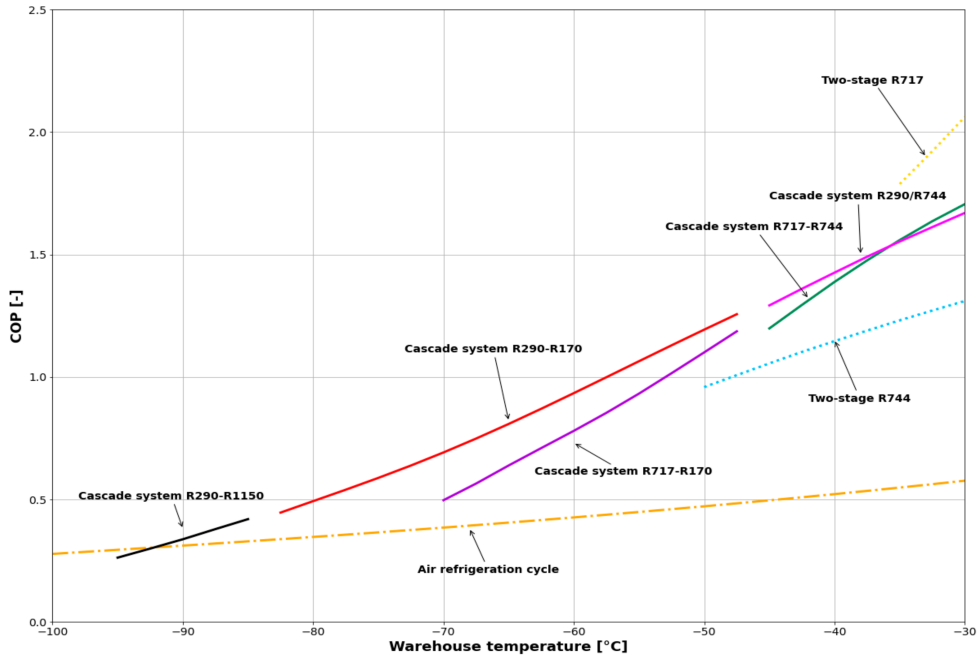


Figure 19. COP comparison between ARC, MRS, and CRS for different warehouse temperatures by using different refrigerants. Pressure ratio limitation, discharge temperature limit, superheat of 10 K, and fan power are considered.

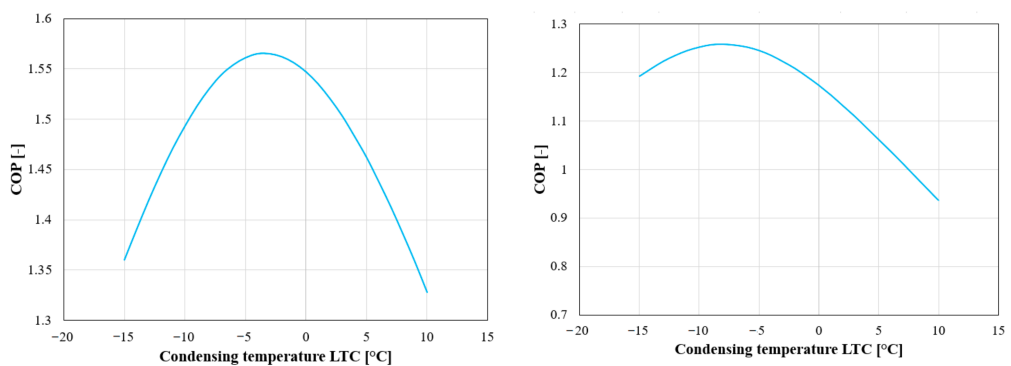


Figure 20. COP as a function of the condensing temperature in the LTC. On the left is an evaporating temperature of $-40\text{ }^{\circ}\text{C}$, and on the right is an evaporating temperature of $-50\text{ }^{\circ}\text{C}$.

- For R290/R744, no issues have been recorded, promoting its implementation in the evaporating temperature region between -35 and $-50\text{ }^{\circ}\text{C}$. It can also be noticed that the COP curve of the CRS working with the refrigerant pair R717/R744 starts to detach from the upper curve of R290/R744. This can be explained by the high energy losses

that occur in the ammonia circuit. The superheating losses strongly influence R717, and therefore including the superheating induces a faster deterioration of the COP;

- The optimisation procedure presents the same issues described above for the refrigerant pair R717/R170 used for storage purposes at lower temperatures. Thus, the condensing temperature has been defined to maintain the discharge temperature below the limit of 120 °C. Considering the superheating, the range of applicability of such a refrigerant pair is shortened, and where it can be used, the COP undergoes a sharp decrease. For lower evaporating temperatures (above the NBP of ethane), the use of R290 is recommended. Another choice may be an azeotropic mixture to attain the best heat transfer;
- For the pair R290/R1150, the condensing temperature has been chosen according to the limit in the pressure ratio on both sides. At extremely low temperatures, the LTC shows a pressure ratio close to 12, and the compressor efficiencies are excessively low, leading to poor COP values. In this scenario, a CRS with a two-stage layout on the upper cycle can solve these issues, attaining better efficiency and promoting the system, even in warmer climates. The disadvantages are the investment costs and the additional heat exchangers involved in the system.

Figure 21 shows the COP curves for a superheat of 15 K: the increment in the superheating degree leads to a further reduction in the applicability region for the refrigerant pair R717/R170. Furthermore, the drop in the COP for the remaining pair of refrigerants is not so evident: the lack of an accurate set of equations for defining the isentropic efficiencies of the different types of compressors as a function of the refrigerant, cooling load, and temperature levels, as well as the superheating effect, would enlarge the discrepancy between the simulation results and the energy performance calculation coming from the experimental measurements. Therefore, it appears that the necessity of evaluating, as accurately as possible, those efficiencies in the analysis of the MRS and CRS is understandable.

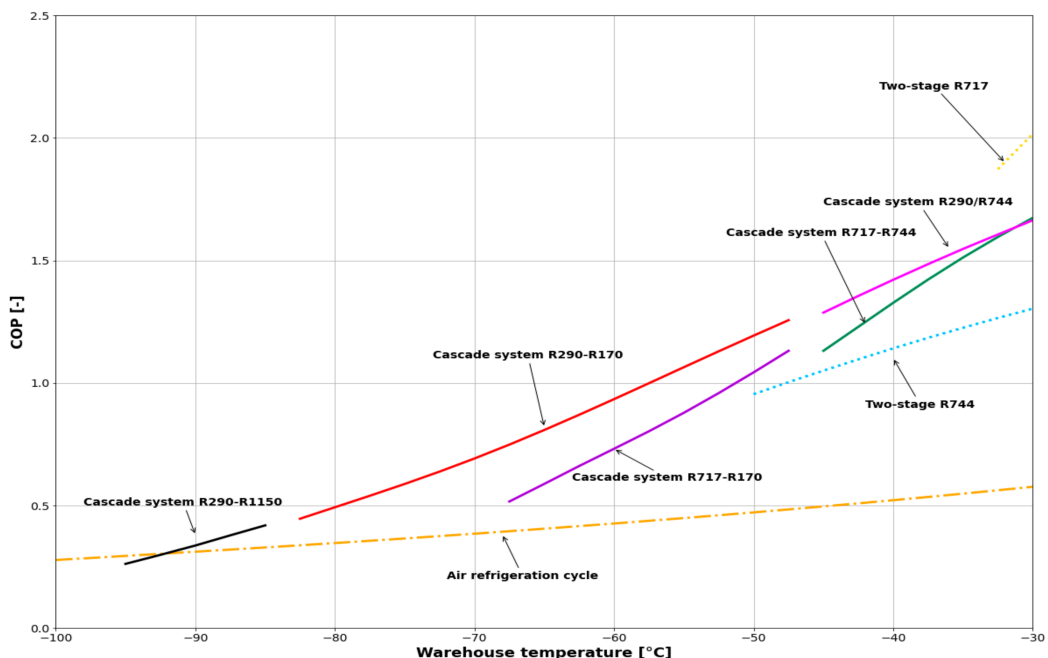


Figure 21. COP comparison between ARC, MRS, and CRS for different warehouse temperatures by using different refrigerants. Pressure ratio limitation, discharge temperature limit, superheat of 15 K, and fan power are considered.

6. Conclusions

In this paper, different refrigeration systems, namely single-stage compression, multi-stage compression, cascade, auto-cascade, and air refrigeration systems, are compared for various natural refrigerants, such as ammonia, carbon dioxide, nitrous oxide, air, propane, propylene, ethane, ethylene, as well as their mixtures in the ultra-low-temperature region. This comparison aims to find the system with the best performance in the required temperature range and application (namely freezing and storing cod/mackerel and tuna, vaccine storage, detector cooling, and the cooling of gas). The following conclusions are drawn in this work:

- For freezing mackerel/cod from 0 to -40 °C, a CRS working with R717 in the HTC and R744 in the LTC (COP ~ 1.9) is suggested, considering the applicability;
- For the onboard storage of cod/mackerel at -30 °C, an MRS or CRS is used. A good, non-flammable option is using a CRS with R717 in the HTC and R744 in the LTC with a COP of about 2.5 (a condensing temperature of 15 °C). An ARC was analysed, resulting in a COP of about 0.55. In this temperature area, ARCs are not competitive with other systems;
- The CRS is the most efficient system for freezing tuna from -20 to -60 °C using HCs in both cycles (the HTC and LTC). R290 or R1270 for the HTC and R170 or R1150 for the LTC are the best-performing solutions, with COPs of about 1, also taking the discharge temperature of the HTC into account. Similar COPs can be recorded using R744a in the LT stage, but its use requires further studies on its stability. Great interest should be given to the R744 and R744A pair (COP ~ 0.9), which has a very good volumetric refrigeration capacity and is almost climate-neutral;
- For storing tuna at -60 °C, a CRS with the refrigerant pair R1270 (HTC)/R170 (LTC) or R290 (HTC)/R170 (LTC) results in the best COP (COP ~ 1.4). A distinction is made whether it is on- or offshore storage that is needed. For onshore storage, the ARC is a good option (COP ~ 0.4). A CRS using R290 as the HTC refrigerant and R744/R1150 or R744/R170 as the LTC mixture gives a COP of 1.2/1.3. Using a mixture as the LTC refrigerant lowers the COP but shows beneficial properties, such as non-flammability, if the suitable composition is chosen;
- Pfizer vaccines are stored at -70 °C. A CRS (large capacities) or ACR (small capacities) is used, depending on the required cooling capacity. An ARC is also very interesting for large capacities due to its significant advantages at this temperature level. At a warehouse temperature of -70 °C, the COP of an ARC is about 0.4;
- LNG pre-cooling is performed via a CRS using mixtures as refrigerants. The cascade system with mixtures can improve the efficiency by matching the temperature glides, which can be adjusted according to the requirements of the gas-processing unit by altering their compositions. The highest glide is achieved with R1150/R600, and the lowest is achieved with R170/R290. For the HTC, R290 possesses the best potential, and for the LTC, the highest COP is achieved with the R170/R600 mixture;
- For the detector-cooling process, specific requirements, such as radiation, space limitation, and the absence of oil, are needed for the refrigerant and system configuration. This results in a CRS with R744 as a suitable refrigerant in both cycles;
- The deep analysis conducted on storage applications revealed the importance of defining the real compressors' efficiencies considering several aspects, such as the refrigerant, pressure ratio, and superheating degree at the suction port.

Author Contributions: Conceptualisation, M.Z.S., L.C., S.B., A.H. and T.M.E.; methodology, M.Z.S., L.C., S.B., A.H. and T.M.E.; formal analysis, M.Z.S., L.C. and S.B.; investigation, M.Z.S., L.C. and S.B.; writing—original draft preparation, M.Z.S., L.C. and S.B.; writing—review and editing, M.Z.S., L.C., S.B. and Y.A.; supervision, A.H., T.M.E. and Y.A.; project administration, A.H. and T.M.E.; funding acquisition, A.H. and T.M.E. All authors have read and agreed to the published version of the manuscript.

Funding: This research received funding from the Research Council of Norway (Project No. 308779 Cruize and Project No. 257632 FME HighEFF).

Data Availability Statement: Not applicable.

Conflicts of Interest: The authors declare no conflict of interest.

Nomenclatures

ACR	Auto-cascade refrigeration system
ARC	Air refrigeration cycle
AREP	Alternative Refrigerants Evaluation Program
ASHRAE	American Society of Heating, Refrigeration and Air-Conditioning Engineers
CAPEX	Capital expenditure
CERN	European Organisation for Nuclear Research
CFC	Chlorofluorocarbon
CHX	Cascade heat exchanger
COP	Coefficient of performance
cond	Condenser
CRS	Cascade refrigeration system
EES	Engineering Equation Solver
EU	European Union
evap	Evaporator
GWP	Global warming potential
HCFCs	Hydrochlorofluorocarbons
HCs	Hydrocarbons
HFCs	Hydrofluorocarbons
HT	High temperature
HTC	High-temperature circuit
LHC	Large Hadron Collider
LNG	Liquefied natural gas
LT	Low temperature
LTC	Low-temperature cycle
MRS	Multi-stage refrigeration system
NBP	Normal boiling point
ODP	Ozone depletion potential
PAG	Polyalkylene
PAO	Polyalphaolefin
POE	Polyolester
RSW	Refrigerated seawater
T	Temperature (°C)
ULT	Ultra-low temperature
VRC	Vapor compression refrigeration system

References

1. ASHRAE. *Handbook-Refrigeration*; American Society of Heating Refrigerating and Air-Conditioning Engineers: Atlanta, GA, USA, 2018.
2. European Commission EU Legislation to Control F-Gases. Available online: https://climate.ec.europa.eu/eu-action/fluorinated-greenhouse-gases/eu-legislation-control-f-gases_en (accessed on 10 May 2021).
3. European Environment Agency Hydrofluorocarbon Phase-Down in Europe. Available online: <https://www.eea.europa.eu/ims/hydrofluorocarbon-phase-down-in-europe> (accessed on 10 May 2021).
4. Mota-Babiloni, A.; Mastani Joybari, M.; Navarro-Esbri, J.; Mateu-Royo, C.; Barragán-Cervera, Á.; Amat-Albuixech, M.; Molés, F. Ultralow-temperature refrigeration systems: Configurations and refrigerants to reduce the environmental impact. *Int. J. Refrig.* **2020**, *111*, 147–158. [CrossRef]
5. Sharma, V.; Fricke, B.; Bansal, P. Comparative analysis of various CO₂ configurations in supermarket refrigeration systems. *Int. J. Refrig.* **2014**, *46*, 86–99. [CrossRef]
6. Kruse, H.; Rüssmann, H. The natural fluid nitrous oxide—An option as substitute for low temperature synthetic refrigerants. *Int. J. Refrig.* **2006**, *29*, 799–806. [CrossRef]

7. Rodríguez-Jara, E.Á.; Sánchez-de-la-Flor, F.J.; Expósito-Carrillo, J.A.; Salmerón-Lissén, J.M. Thermodynamic analysis of auto-cascade refrigeration cycles, with and without ejector, for ultra low temperature freezing using a mixture of refrigerants R600a and R1150. *Appl. Therm. Eng.* **2022**, *200*, 117598. [CrossRef]
8. Torrella, E.; Larumbe, J.A.; Cabello, R.; Llopis, R.; Sanchez, D. A general methodology for energy comparison of intermediate configurations in two-stage vapour compression refrigeration systems. *Energy* **2011**, *36*, 4119–4124. [CrossRef]
9. Baakeem, S.S.; Orfi, J.; Alabdulkarem, A. Optimization of a multistage vapor-compression refrigeration system for various refrigerants. *Appl. Therm. Eng.* **2018**, *136*, 84–96. [CrossRef]
10. Cabello, R.; Torrella, E.; Llopis, R.; Sánchez, D. Comparative evaluation of the intermediate systems employed in two-stage refrigeration cycles driven by compound compressors. *Energy* **2010**, *35*, 1274–1280. [CrossRef]
11. Agrawal, N.; Bhattacharyya, S. Studies on a two-stage transcritical carbon dioxide heat pump cycle with flash intercooling. *Appl. Therm. Eng.* **2007**, *27*, 299–305. [CrossRef]
12. Pan, M.; Zhao, H.; Liang, D.; Zhu, Y.; Liang, Y.; Bao, G. A Review of the Cascade Refrigeration System. *Energies* **2020**, *13*, 2254. [CrossRef]
13. Kumar Singh, K.; Kumar, R.; Gupta, A. Comparative energy, exergy and economic analysis of a cascade refrigeration system incorporated with flash tank (HTC) and a flash intercooler with indirect subcooler (LTC) using natural refrigerant couples. *Sustain. Energy Technol. Assess.* **2020**, *39*, 100716. [CrossRef]
14. Udroui, C.-M.; Mota-Babiloni, A.; Giménez-Prades, P.; Barragán-Cervera, Á.; Navarro-Esbri, J. Thermodynamic evaluation of CO₂ for ultra-low temperature refrigeration. *Energy Convers. Manag.* **2023**, *20*, 100446. [CrossRef]
15. Du, K.; Zhang, S.; Xu, W.; Niu, X. A study on the cycle characteristics of an auto-cascade refrigeration system. *Exp. Therm. Fluid Sci.* **2009**, *33*, 240–245. [CrossRef]
16. Yan, G.; Hu, H.; Yu, J. Performance evaluation on an internal auto-cascade refrigeration cycle with mixture refrigerant R290/R600a. *Appl. Therm. Eng.* **2015**, *75*, 994–1000. [CrossRef]
17. Hao, X.; Wang, L.; Wang, Z.; Tan, Y.; Yan, X. Hybrid auto-cascade refrigeration system coupled with a heat-driven ejector cooling cycle. *Energy* **2018**, *161*, 988–998. [CrossRef]
18. Qin, Y.; Li, N.; Zhang, H.; Liu, B. Energy and exergy performance evaluation of a three-stage auto-cascade refrigeration system using low-GWP alternative refrigerants. *Int. J. Refrig.* **2021**, *126*, 66–75. [CrossRef]
19. Aprea, C.; Maiorino, A. Autocascade refrigeration system: Experimental results in achieving ultra low temperature. *Int. J. Energy Res.* **2009**, *33*, 565–575. [CrossRef]
20. Asgari, S.; Noorpoor, A.R.; Boyaghchi, F.A. Parametric assessment and multi-objective optimization of an internal auto-cascade refrigeration cycle based on advanced exergy and exergoeconomic concepts. *Energy* **2017**, *125*, 576–590. [CrossRef]
21. Giannetti, N.; Milazzo, A. Thermodynamic analysis of regenerated air-cycle refrigeration in high and low pressure configuration. *Int. J. Refrig.* **2014**, *40*, 97–110. [CrossRef]
22. Zhang, Z.; Liu, S.; Tian, L. Thermodynamic analysis of air cycle refrigeration system for Chinese train air conditioning. *Syst. Eng. Procedia* **2011**, *1*, 16–22. [CrossRef]
23. Gigiel, A.; Giuliani, G.; Vitale, C.; Polonara, F. An open air cycle freezer. In Proceedings of the 7th IIR Gustav Lorentzen Conference on Natural Working Fluids, Trondheim, Norway, 29–31 May 2006; pp. 325–328.
24. Kikuchi, S.; Dore, M.P. Epidemiology of *Helicobacter pylori* Infection. *Helicobacter* **2005**, *10*, 1–4. [CrossRef]
25. Mirai Mirai Cold Products, Open and Closed Cycle for Air Refrigeration. Available online: <https://mirai-intex.com/products> (accessed on 8 September 2021).
26. Mayekawa Ultra-Low Temperature Air Refrigeration System Pascal-Air. Available online: <https://www.mayekawa.com.au/products/pascal-air/> (accessed on 8 September 2021).
27. Klein, S.A. Engineering Equation Solver (EES), F-Chart Software, Madison, USA. Available online: <https://fchartsoftware.com/ees/index.php/> (accessed on 7 April 2021).
28. Mumanachit, P.; Reindl, D.T.; Nellis, G.F. Comparative analysis of low temperature industrial refrigeration systems. *Int. J. Refrig.* **2012**, *35*, 1208–1221. [CrossRef]
29. Lee, T.-S.; Liu, C.-H.; Chen, T.-W. Thermodynamic analysis of optimal condensing temperature of cascade-condenser in CO₂/NH₃ cascade refrigeration systems. *Int. J. Refrig.* **2006**, *29*, 1100–1108. [CrossRef]
30. Niu, X.-D.; Yamaguchi, H.; Iwamoto, Y.; Neksá, P. Experimental study on a CO₂solid–gas–flow-based ultra-low temperature cascade refrigeration system. *Int. J. Low-Carbon Technol.* **2011**, *6*, 93–99. [CrossRef]
31. Sobieraj, M.; Rosiński, M. High phase-separation efficiency auto-cascade system working with a blend of carbon dioxide for low-temperature isothermal refrigeration. *Appl. Therm. Eng.* **2019**, *161*, 114149. [CrossRef]
32. Boone, J.; Machida, A. Development of air refrigeration system “Pascal Air”. In Proceedings of the 23rd International Congress of Refrigeration, Prague, Czech Republic, 21–26 August 2011; pp. 1597–1605.
33. Harby, K. Hydrocarbons and their mixtures as alternatives to environmental unfriendly halogenated refrigerants: An updated overview. *Renew. Sustain. Energy Rev.* **2017**, *73*, 1247–1264. [CrossRef]
34. Rajapaksha, L. Influence of special attributes of zeotropic refrigerant mixtures on design and operation of vapour compression refrigeration and heat pump systems. *Energy Convers. Manag.* **2007**, *48*, 539–545. [CrossRef]
35. Zhao, Y.; Li, Z.; Zhang, X.; Wang, X.; Dong, X.; Gao, B.; Gong, M.; Shen, J. Azeotropic refrigerants and its application in vapor compression refrigeration cycle. *Int. J. Refrig.* **2019**, *108*, 1–13. [CrossRef]

36. Mohanraj, M.; Muraleedharan, C.; Jayaraj, S. A review on recent developments in new refrigerant mixtures for vapour compression-based refrigeration, air-conditioning and heat pump units. *Int. J. Energy Res.* **2011**, *35*, 647–669. [CrossRef]
37. Lemmon, E.W.; Huber, M.L.; McLinden, M.O.; Bell, I. *NIST Standard Reference Database 23: Reference Fluid Thermodynamic and Transport Properties-REFPROP, Version 10.0*; National Institute of Standards and Technology: Gaithersburg, MD, USA, 2020.
38. Linde Refrigeration: Processes & Temperatures. Selecting the Best Refrigerant Gas for Your Process Temperature Requirements. Available online: https://www.linde-gas.com/en/processes/refrigeration_and_air_conditioning/refrigeration_processes_and_temperatures/index.html (accessed on 5 May 2021).
39. Bai, T.; Li, D.; Xie, H.; Yan, G.; Yu, J. Experimental research on a Joule-Thomson refrigeration cycle with mixture R170/R290 for -60 °C low-temperature freezer. *Appl. Therm. Eng.* **2021**, *186*, 116476. [CrossRef]
40. Ahammed, M.E.; Bhattacharyya, S.; Ramgopal, M. Thermodynamic design and simulation of a CO₂ based transcritical vapour compression refrigeration system with an ejector. *Int. J. Refrig.* **2014**, *45*, 177–188. [CrossRef]
41. Chakravarthy, V.S.; Shah, R.K.; Venkatarathnam, G. A Review of Refrigeration Methods in the Temperature Range 4–300 K. *J. Therm. Sci. Eng. Appl.* **2011**, *3*, 020801. [CrossRef]
42. Llopis, R.; Nebot-Andrés, L.; Sánchez, D.; Catalán-Gil, J.; Cabello, R. Subcooling methods for CO₂ refrigeration cycles: A review. *Int. J. Refrig.* **2018**, *93*, 85–107. [CrossRef]
43. Nasution, A.; Ambarita, H.; Sihombing, H.; Setiawan, E.; Kawai, H. *The Effect of Stage Number on the Performance of a Vapor Compression Refrigeration Cycle Using Refrigerant R32*; IOP Conference Series: Materials Science and Engineering; IOP Publishing: Bristol, UK, 2020.
44. Jiang, S.; Wang, S.; Jin, X.; Zhang, T. A general model for two-stage vapor compression heat pump systems. *Int. J. Refrig.* **2015**, *51*, 88–102. [CrossRef]
45. Adamson, B. Application of Hydrocarbon Refrigerants in Low Temperature Cascade Systems. In Proceedings of the 7th IIR Gustav Lorentzen Conference on Natural Working Fluids, Trondheim, Norway, 29–31 May 2006; Refrigeration Engineering Pty Ltd.: Unanderra, Australia, 2006.
46. Xu, X.; Liu, J.; Cao, L. Mixed refrigerant composition shift due to throttle valves opening in auto cascade refrigeration system. *Chin. J. Chem. Eng.* **2015**, *23*, 199–204. [CrossRef]
47. Liu, Y.; Yu, J. Performance evaluation of an ejector subcooling refrigeration cycle with zeotropic mixture R290/R170 for low-temperature freezer applications. *Appl. Therm. Eng.* **2019**, *161*, 114128. [CrossRef]
48. Bai, T.; Yan, G.; Yu, J. Experimental investigation of an ejector-enhanced auto-cascade refrigeration system. *Appl. Therm. Eng.* **2018**, *129*, 792–801. [CrossRef]
49. Liu, J.; Liu, Y.; Yu, J.; Yan, G. Thermodynamic analysis of a novel ejector-enhanced auto-cascade refrigeration cycle. *Appl. Therm. Eng.* **2022**, *200*, 117636. [CrossRef]
50. Bellos, E.; Tzivanidis, C. A Theoretical Comparative Study of CO₂ Cascade Refrigeration Systems. *Appl. Sci.* **2019**, *9*, 790. [CrossRef]
51. Bellos, E.; Tzivanidis, C. A comparative study of CO₂ refrigeration systems. *Energy Convers. Manag.* **2019**, *1*, 100002. [CrossRef]
52. Alberto Dopazo, J.; Fernández-Seara, J.; Sieres, J.; Uhiá, F.J. Theoretical analysis of a CO₂–NH₃ cascade refrigeration system for cooling applications at low temperatures. *Appl. Therm. Eng.* **2009**, *29*, 1577–1583. [CrossRef]
53. Hafner, I.A.; Gabriellii, C.; Widell, K. *Refrigeration Units in Marine Vessels: Alternatives to HCFCs and High GWP HFCs*; Nordic Council of Ministers: Copenhagen, Denmark, 2019.
54. Airah, M. Carbon Dioxide (CO₂) for the Food Processing and Cold Storage Industries. 2002. Available online: [https://www.semanticscholar.org/paper/CARBON-DIOXIDE-\(CO2\)-FOR-THE-FOOD-PROCESSING-AND-Airah/e29fe13c23eabeebedff039cc4fb906e30589f9#citing-papers](https://www.semanticscholar.org/paper/CARBON-DIOXIDE-(CO2)-FOR-THE-FOOD-PROCESSING-AND-Airah/e29fe13c23eabeebedff039cc4fb906e30589f9#citing-papers) (accessed on 6 October 2021).
55. Söylemez, E.; Widell, K.N.; Gabriellii, C.H.; Ladam, Y.; Lund, T.; Hafner, A. Overview of the development and status of carbon dioxide (R-744) refrigeration systems onboard fishing vessels. *Int. J. Refrig.* **2022**, *140*, 198–212. [CrossRef]
56. Sawalha, S. Carbon Dioxide in Supermarket Refrigeration. Ph.D. Thesis, KTH, Stockholm, Sweden, 2008.
57. Llopis, R.; Sánchez, D.; Sanz-Kock, C.; Cabello, R.; Torrella, E. Energy and environmental comparison of two-stage solutions for commercial refrigeration at low temperature: Fluids and systems. *Appl. Energy* **2015**, *138*, 133–142. [CrossRef]
58. Di Nicola, G.; Polonara, F.; Stryjek, R.; Artoni, A. Performance of cascade cycles working with blends of CO₂ + natural refrigerants. *Int. J. Refrig.* **2011**, *34*, 1436–1445. [CrossRef]
59. Kauffeld, M.; Maurath, T.; Germanus, J.; Askar, E. N₂O/CO₂-Mixtures as Refrigerants for Temperatures below -50 °C. *Int. J. Refrig.* **2020**, *117*, 316–327. [CrossRef]
60. Refolution Industriekalte Efficiency Comparison of Refrigeration Technologies for Ultra-Low Temperature (ULT) Applications between -40 °C and -110 °C. Available online: https://3f74e260-dfd4-47ca-9b8e-d224d67a4b12.filesusr.com/ugd/dc61a9_97e8adedbd4f43a5b0bfff1c800cc267.pdf?index=true (accessed on 6 June 2021).
61. Santos, A.F.; Gaspar, P.D.; de Souza, H.J.L. Refrigeration of COVID-19 Vaccines: Ideal Storage Characteristics, Energy Efficiency and Environmental Impacts of Various Vaccine Options. *Energies* **2021**, *14*, 1849. [CrossRef]
62. Yan, G.; He, C.; Yu, J. Theoretical investigation on the performance of a modified refrigeration cycle using binary zeotropic hydrocarbon mixture R170/R290. *Int. J. Refrig.* **2018**, *94*, 111–117. [CrossRef]
63. Castillo, L.; Majzoub Dahouk, M.; Di Scipio, S.; Dorao, C.A. Conceptual analysis of the precooling stage for LNG processes. *Energy Convers. Manag.* **2013**, *66*, 41–47. [CrossRef]

64. Castillo, L.; Dorao, C.A. On the conceptual design of pre-cooling stage of LNG plants using propane or an ethane/propane mixture. *Energy Convers. Manag.* **2013**, *65*, 140–146. [[CrossRef](#)]
65. Bhanot, V.; Dhumane, R.; Petagna, P.; Cioncolini, A.; Iacovides, H.; Ling, J.; Aute, V. Development of a Numerical Tool for Dynamic Simulations of Two-Phase Cooling Systems. *Int. J. Simul. Model.* **2019**, *18*, 302–313. [[CrossRef](#)]

Disclaimer/Publisher’s Note: The statements, opinions and data contained in all publications are solely those of the individual author(s) and contributor(s) and not of MDPI and/or the editor(s). MDPI and/or the editor(s) disclaim responsibility for any injury to people or property resulting from any ideas, methods, instructions or products referred to in the content.

Conference paper 1

M.Z. Saeed, A. Hafner, C.H. Gabrieli, I. Tolstorebrov, K.N. Widell. CO₂ refrigeration system design and optimization for LNG driven cruise ship. 9th IIR Conference on Ammonia and CO₂ Refrigeration Technologies. Proceedings: Ohrid, North Macedonia, 16-17 September 2021. <http://dx.doi.org/10.18462/iir.nh3-co2.2021.0015>

CO₂ refrigeration system design and optimization for LNG driven cruise ships

Muhammad Zahid SAEED^(a), Armin HAFNER^(a), Cecilia H. GABRIELII^(b),
Ignat TOLSTOREBROV^(a), Kristina N. WIDELL^(c)

^(a)Norwegian University of Science and Technology
Trondheim, 7491, Norway, muhammad.z.saeed@ntnu.no

^(b)SINTEF Energy Research
Trondheim, 7491, Norway, cecilia.gabriellii@sintef.no

^(c)SINTEF Ocean
Trondheim, 7465, Norway, kristina.widell@sintef.no

ABSTRACT

The cruise industry is in the evolution of eco-friendly technologies due to strict environmental regulations. Liquefied natural gas (LNG) is an alternative marine fuel. Compared to conventional diesel fuels, LNG offers a reduced environmental impact and can serve as a transition towards zero emission. LNG is stored in onboard cryogenic tanks at low temperatures. Various techniques can be applied to vaporize the LNG fuel before feeding it to the gas engine. The recovery of this vaporization energy with air conditioning as a heat source can enhance system performance. On a cruise ship, heating, cooling, and ventilation (HVAC) require an average 40 % of the ship's total energy demand. The natural refrigerant CO₂ is an attractive choice due to its compact units, non-toxic nature, and non-flammability, all being primary concerns on a cruise ship. The energy efficiency can be improved by utilizing LNG cold and reducing the need of indirect loops with CO₂ as a refrigerant. This work investigates the LNG cold, waste heat recovery potentials, and CO₂ refrigeration system for cruise ships.

Keywords: Refrigeration, Carbon Dioxide, Cruise Ships, Energy Efficiency, LNG, Cold Recovery

1. INTRODUCTION

The traditional heavy fuel oil (HFO) marine engines are associated with large amounts of sulphur oxides (SO_x), nitrogen oxides (NO_x), and greenhouse (GHG) emissions from exhaust gases (Zhang et al., 2021). The international maritime organization (IMO) leads the UN sustainable development goals of the shipping sector. It aims to reduce CO₂ emissions by 40 % by 2030 and 70 % by 2050 compared to 2008, and also to limit SO_x and NO_x pollution by setting different regulations (IMO, 2021). To comply with the new rules, alternative propulsion systems, fuels and exhaust gas cleaning technologies are under investigation. Among various options, liquefied natural gas (LNG) is a favorable marine fuel with 25 % less CO₂, 90 % less NO_x, and about no SO_x as compared to conventional fuel oils (Jafarzadeh et al., 2017). LNG is a reasonable choice to meet the current and upcoming environmental regulations without a significant technical modification.

LNG is stored under cryogenic temperatures between -165 °C and -138 °C, and vaporization/heating is essential before combustion in the gas engine. The recovery of vaporization energy ("cold recovery"), for onboard applications can reduce emissions and overall energy consumption to some extent (Baldasso et al., 2020). Prior studies have extensively investigated LNG cold recovery applications in regasification terminals, including power generation (Gomez et al., 2014), air separation, gas turbine suction air cooling and hydrocarbon liquefaction (Otsuka, 2006), freezing and refrigeration (Dispenza et al., 2009), production of liquid CO₂/dry ice (Hongyu et al., 2010), cryogenic comminution (Lian et al., 2015), seawater desalination (Dhameliya et al., 2015). Recently, the LNG cold recovery researched areas are broadened to transportation sector like LNG-driven refrigerated vehicles (Tan et al., 2010) and fishing vessels (Saeed et al., 2020). Few studies have investigated LNG-driven passenger ships. The common technology evaluated by most authors (Sung et al., 2016, Pasini et al., 2019, Han et al., 2019 and Koo et al., 2019) is the Organic Rankine cycle (ORC) for cold recovery and flue gases heat recovery. Baldasso et al., 2020 analyzed the cold recovery for ferry with 16030 kW engine for HVAC. They reported the primary engines fuel savings of 0.43 % to 0.84 %

with refrigeration system COP of 3 and 5, respectively. However, their work did not discuss the design of HVAC system.

For passenger ships, current refrigerants in use are R22 and HFCs (globally) and CO₂ for provision cooling and freezing (Hafner et al., 2019). Natural refrigerants are a long-term solution for the shipping industry due to numerous international and national regulations for the use of high GWP (Global warming potential) refrigerants. The usage of these refrigerants is already complicated due to the F-gas regulation and high environmental taxes. Due to such reasons, shipowner companies have a high interest in low GWP refrigerants (Pigani et al., 2016). Zhang et al., (2021) theoretically investigated an integrated trans-critical CO₂ cycle for onboard heating, cooling, engine waste heat recovery. The high-pressure side of CO₂ system was integrated with waste heat, and work was recovered by expansion turbine. Their findings showed operational flexibility and efficient performance, but they suggested more theoretical research and experimental studies. This paper aims to numerically investigate the direct expansion of CO₂ refrigerant in the air-handling units or air conditioning coils for summer mode and the energy-saving potential with LNG cold recovery.

2. METHODS AND DATA

2.1. Reference case

This paper's reference case is a hypothetical cruise ship with a passenger capacity of 330 (excluding crew members) and total engine power of around 8 MW. The operating parameters were adopted from two commercial ships (MS Spitsbergen 2021 and MS Fram 2021) and engine manufacturer (Wärtsilä, 2021) under the following assumptions. The engines were considered dual fuel and equipped with a low-pressure LNG fuel supply system. The fuel consumption of LNG was calculated from its lower heating value (LHV) and a constant engine efficiency. The fuel consumption can also be calculated by specific gas consumption (SGC), but SGC varies with engine load and the data is currently unavailable. So, LHV method was used for approximation. The flow rate of exhaust gases was calculated using a lean air-fuel ratio, and the exhaust temperature was assumed constant. The assumptions were validated by comparing them with the existing available data referred to in introduction of this paper. Table 1 shows the boundary conditions for the reference case.

Table1. Boundary conditions for the reference case

Parameters	Description	Parameters	Description
Engine type	4*dual fuel engines	LNG pressure (bar)	8
Engine rated power (kW)	1980	Lower heating value LNG (MJ/kg)	48.6
Average engine load (%)	85	Engine efficiency (%)	46
LNG supply system	Low pressure	LNG flow (kg/h)	1084
LNG tank	Type C	Exhaust flow (kg/s)	9.15
LNG temperature (°C)	-128.7	Exhaust gas temperature (°C)	365
Inlet temperature to engine (°C)	10		

2.2. LNG cold and exhaust heat recovery

The two standard methods of transferring LNG from the fuel tank to the engine are pressure build-up and cryogenic fuel pump systems. The system described in Fig. 1 is the fuel pump system. For safety reasons, two parallel fuel systems are common for ships with four engines. LNG in the tank (1 bar and -162 °C) is pressurized to 8 bar by the cryogenic pump and then vaporized in the cold box. The gas valve unit acts as a small storage tank and maintains a smooth flow of gas to the engine. A heat source is required to vaporize the LNG in a cold box. The cold recovery was calculated by the enthalpy difference of methane between -128 °C and 10 °C under adiabatic conditions. The superheating level of fuel gas was adopted from the engine

manufacturer data (Wärtsilä, 2021), which required gas temperature in the range of 0 to 60 °C before the engine. In traditional systems, the engine oil cooling circuit is used as a heat source, but it can be replaced by air conditioning system secondary loops. This can maximize the use of cold in an efficient way.

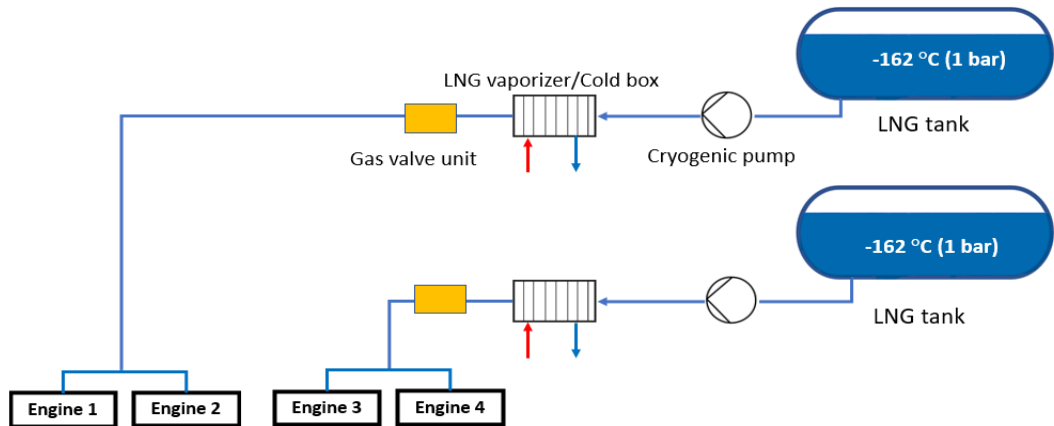


Figure 1: Cryogenic fuel pump system

The engine's exhaust gases contain a considerable amount of heat at high temperatures (at around 350 °C) that can cover heating demands onboard. The values were calculated by using constant specific heat capacity of air and cooling of gases from 365 °C to 120 °C. The LNG/gas has negligible sulphur content, and heat recovery can be made at lower temperatures without acid formation compared to diesel fuel. In warmer climatic conditions, the excess heat can be used to produce cooling by applying absorption cooling technology. Other heat recovery methods are electricity production with an Organic Rankine cycle, however, not included in the scope of this work.

2.3. Refrigeration system design

A CO₂ refrigeration system was investigated for summer conditions by using the dynamic modeling software Dymola with components and libraries from TLK Thermo. In summer, the required temperature in the cabins and the public areas is in the range of 18 °C to 24 °C, and the supply air temperature can be a maximum of 10 °C lower than the indoor temperature. The design cooling and heating load for the reference cruise ship was 1483 kW and 76 kW, respectively, and is distributed in three different zones. The concept evaluated is to circulate CO₂ refrigerant in the air handling unit and cooling fan coils, leading to high evaporation temperature and reducing energy consumption. In the case of other refrigerants, direct circulation in AC coils is not possible due to flammability, toxicity, and other safety issues, and they required low evaporation temperatures for indirect circuits. The reference case was simulated with load variations from 100 % to 50 % for each evaporation temperature of 13 °C to 17 °C with an assumption of only 5K temperature difference from indoor temperature. The high pressure was varied from 85 bar to 80 bar (load dependent), but the temperature before the high-pressure expansion valve was kept at 25 °C. The heat rejection in the condenser/gas cooler was made with in a single heat exchanger operating with a constant inlet seawater temperature of 20 °C.

The refrigeration system layout is presented in Fig. 2. Evaporation temperature was kept constant in the three zones for each simulation. Each zone can have multiple evaporators and coils for air-conditioning, but they were added together for simplicity of simulation effort. The cooling load was controlled by the expansion valves, which take superheat as an input to maintain the required refrigerant flow. The parallel compressor removes gas vapor from the liquid receiver to make sure only liquid flows to the expansion valves before evaporators. The suction gas of both main compressors and the parallel compressor was superheated by an internal heat exchanger for the safety of compressors. The compressor isentropic and volumetric efficiency was set to 0.7. The mechanical work of the gas cooler pump was neglected due to its small value compared to compression work.

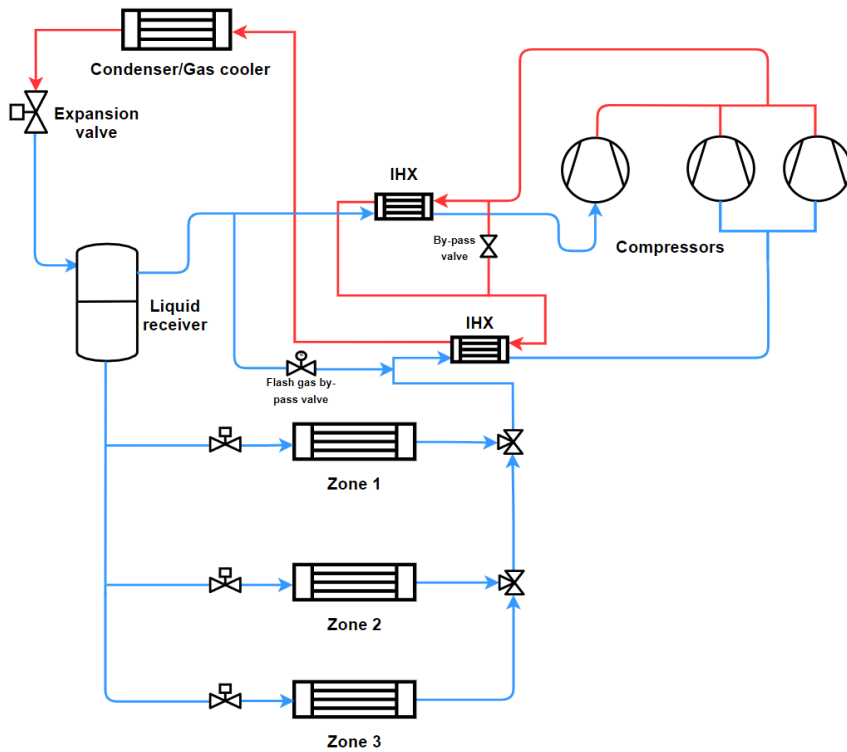


Figure 2: Refrigeration system layout

The cooling load profile of the reference ship for 24 hours is shown in Fig. 3. The load is minimum during the night, gradually increasing from 7 am, being at its maximum during midday when the sun is at its peak. The load is then decreasing in a polynomial way and reaches the lowest value at 24 hours.

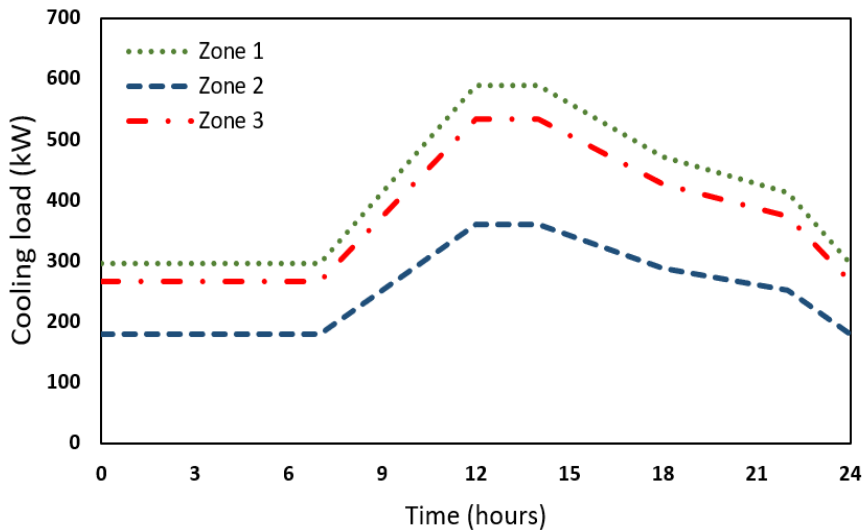


Figure 3: Cooling load of three different zones

3. RESULTS AND DISCUSSIONS

The cold recovery potential from the LNG fuel is shown in Fig. 4. As seen, the recovered cold energy is 265 kW at 100 % engine load and 106 kW at 40 % engine load. Possible heat sinks or applications for this cold were discussed by some researchers, as mentioned in the introduction, but utilizing it in an efficient way is the main challenge. Integration of the cold recovery with HVAC system possesses a more significant potential for energy efficiency compared to engine oil cooling. The LNG cold recovery at the average engine load of 85 % is 225 kW, and the maximum cooling load for the reference ship is 1483 kW. By utilizing cold recovery, the AC cooling system size can be reduced to 1258 kW. The engine load can be less than 85 % at peak cooling demand, but the integration of thermal energy storage can compensate for the reduced AC system size. If the COP of the refrigeration system is assumed to 5, the potential fuel savings will be 0.67 % at average engine load and 0.79 % at full load.

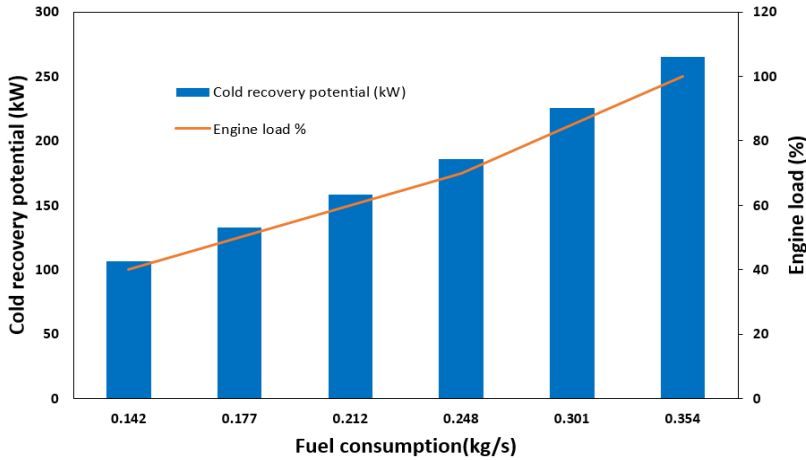


Figure 4: LNG cold recovery versus fuel consumption

The heat recovery from the exhaust gases of the engines is presented in Fig. 5. The heat recovery at 100 % engine load is 2715 kW and 1090 kW at 40 % engine load. This high-temperature heat recovery can be used for onboard hot water production, electricity production using ORC, heat to power production by thermoelectric effect, or the combination of different applications. The different applications will be analyzed in further work.

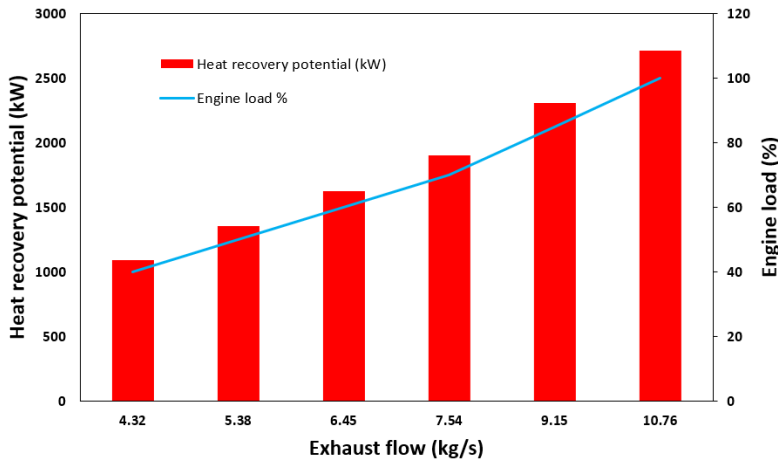


Figure 5: Heat recovery versus exhaust flow gases

The simulation model of the refrigeration system was run for the 24 h load profile shown in Fig. 3. Five different simulations were performed with evaporation temperatures of 13 °C to 17 °C. The power consumption presented in Fig. 6 is the sum of the main compressor and the parallel compressor. The maximum power consumption was in the 13 °C evaporation case due to the higher pressure ratio as compared to other cases, and the minimum was observed in 17 °C case. The maximum power consumption in 13 °C, 14 °C, 15 °C, 16 °C, and 17 °C cases was 256.3 kW, 242.7 kW, 229.3 kW, 216.1 kW, and 203.1 kW, respectively. It can be concluded that at the maximum cooling capacity, each °C increase in evaporation temperature will save an average 13 kW (and 65 kW for 5 °C increase).

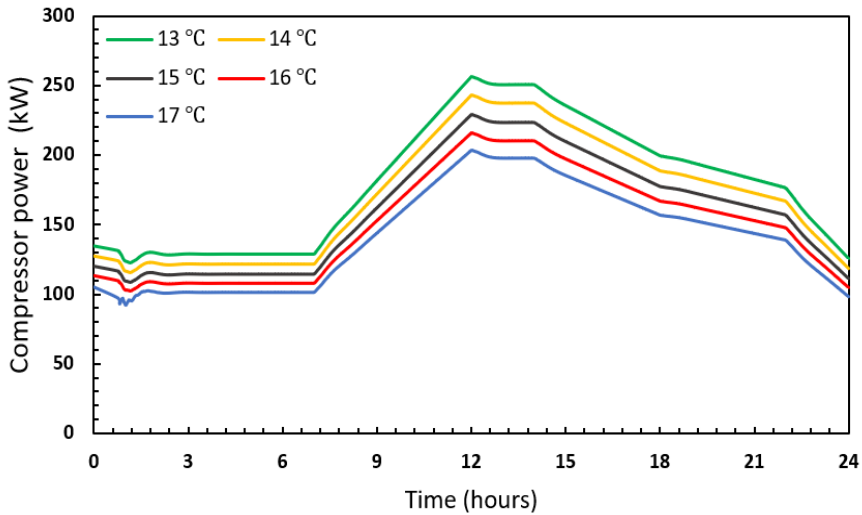


Figure 6: Cooling unit power consumption versus time

A general trend was observed for COP in all cases. High COP at low loads and low COP at high loads. At high loads, the pressure ratio slightly increased as the system had to dissipate more heat, and it reduced at lower loads. The COP at maximum load in 13 °C, 14 °C, 15 °C, 16 °C, and 17 °C cases was 5.5, 5.8, 6.2, 6.5 and 7.1, respectively. The average COP difference at maximum load for each °C rise in evaporation temperature is 0.4.

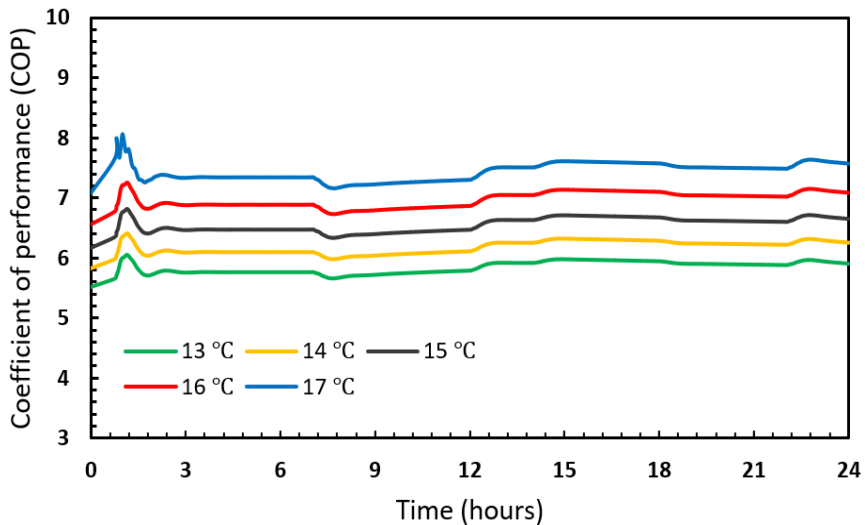


Figure 7: Coefficient of performance versus time

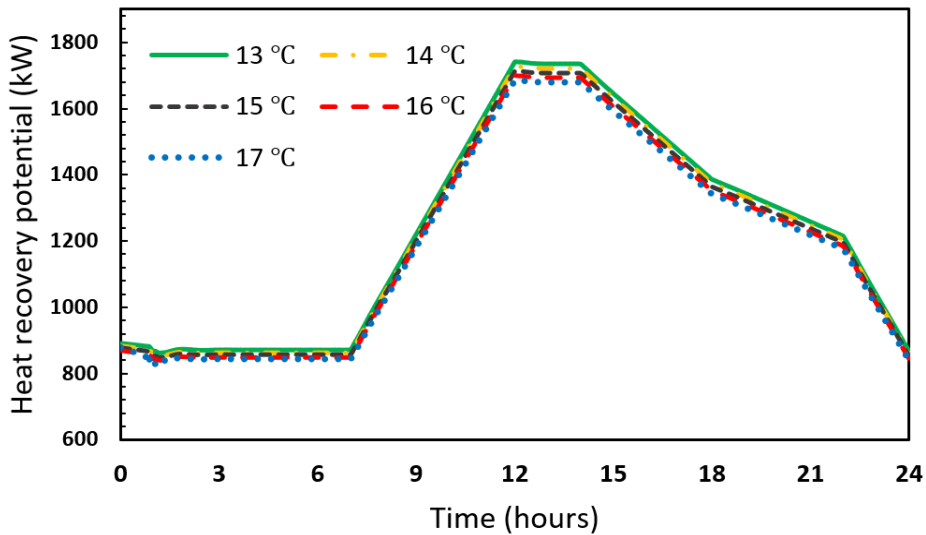


Figure 7: Refrigeration system heat recovery versus time

The temperature before the gas cooler varied from 58 °C to 55 °C. The heat recovery from the gas cooler is low temperature as compared to recovery from engine exhaust gases. The heat recovery at maximum load in 13 °C, 14 °C, 15 °C, 16 °C, and 17 °C cases was 1740 kW, 1726 kW, 1713 kW, 1700 kW, and 1687 kW, respectively. The average heat recovery difference for each evaporation case is 13 kW. Depending on the applications and temperature levels, heat recovery can be made in two heat exchangers.

4. CONCLUSION

In this paper, thermal system analysis of a reference cruise ship driven by LNG fuel was performed by calculations and simulations in Dymola. A cruise ship was investigated with a passenger capacity of 330, engine power around 8 MW, designed cooling load 1483 kW, and heating load of 76 kW, in summer mode. Results showed that 225 kW LNG cold could be recovered at the average engine load of 85 %. By utilizing this cold for air conditioning application, 0.67 % of fuel can be saved at maximum cooling capacity. The heat recovery from the exhaust gases of the engine at 85 % load was estimated at 2.3 MW. Evaluations of CO₂ refrigerant direct expansion in air handling units and coils showed impressive results for energy saving compared to indirect systems. Each °C increase in evaporation will save an average of 13 kW of the compressor power. Besides, the CO₂ system also provides flexibility for integrated cooling and heating. The work of this paper will extend to further development of CO₂ refrigeration system for cruise ships and integration with thermal energy storage. Other thermal systems will also evaluate further for the best possible optimization

ACKNOWLEDGEMENTS

The authors gratefully acknowledge the Research Council of Norway for the financial support for carrying out the present research [NFR Project No. 308779 Cruize]

REFERENCES

- Baldasso, E., Mondejar, M. E., Mazzoni, S., Romagnoli, A., Haglind, F., 2020. Potential of liquefied natural gas cold recovery on board ships. *Journal of Cleaner Production*, 271. 122519.
- Dispenza, C., Dispenza, G., La, V., Panno, G., 2009. Exergy recovery in regasification facilities cold utilization: a modular unit. *Appl. Therm. Eng.* 29, 3595-3608.

- Dhameliya, H., Agrawal, P., 2015. LNG cryogenic energy utilization. In: 5th International Conference on Advances in Energy Research, ICAER. Mumbai, India, pp. 660-665.
- Hongyu, S., Ning, M., Xiaoyan, W., 2010. Optimized utilization OF liquefied natural gas (LNG) cold energy. In: 14th International Heat Transfer Conference, ASME. Washington, DC, USA.
- Hafner, A., Gabriellii, C.A., Widell, K., 2019. Refrigeration units in marine vessels. Alternatives to HCFCs and high GWP HFCs, Nordic council of ministers, Team nord. <http://norden.diva-portal.org/smash/get/diva2:1301641/FULLTEXT01.pdf>
- Han, F., Wang, Z., Ji, Y., Li, W., Sunden, B., 2019. Energy analysis and multi-objective optimization of waste heat and cold energy recovery process in LNG-fueled vessels based on a triple organic Rankine cycle. *Energy Convers. Manag.* 195, 561-572.
- IMO, 2021. Reducing green house gas emissions from ships. Available: <https://www.imo.org/en/MediaCentre/HotTopics/Pages/Reducing-greenhouse-gas-emissions-from-ships.aspx>
- Jafarzadeh, S., Paltrinieri, N., Utne I. B., Ellingsen, H., 2017. LNG-fuelled fishing vessels. A systems engineering approach, *Transportation Research Part D* 50, 202–222.
- Koo, J., Oh, S.R., Choi, Y.U., Hung, J.H., Park, K., 2019. Optimization of an organic rankine cycle system for an LNG-powered ship. *Energies* 12.
- Lian, J., Xia, B., Yang, G., Yang, Y., Gou, X., Liu, L., Wu, J., 2015. Research on high efficient utilization of LNG cold energy. In: 4th International Conference on Computer, Mechatronics, Control and Electronic Engineering. Hangzhou, China, pp. 282-287.
- MS Fram, 2021. Technical information. <https://www.fincantieri.com/en/products-and-services/cruise-ships/fram/>
- MS Spitsbergen, 2021. About the ship. <https://global.hurtigruten.com/ships/ms-spitsbergen/>
- Otsuka, T., 2006. Evolution of an LNG terminal: senboku terminal of osaka gas. 23rd World Gas Conference. Amsterdam.
- Pigani, L., Boscolo, M., Pagan, N., 2016. Marine refrigeration plants for passenger ships: Low-GWP refrigerants and strategies to reduce environmental impact. *International journal of refrigeration* 64, 80-92.
- Pasini, G., Baccioli, A., Ferrari, L., Desideri, U., 2019. Potential energy recovery from regasification in LNG-fueled ships. In: *Sustainable Polyenergy Generation and Harvesting e SUPEHR 2019*. Savona, Italy, pp. 1-6.
- Romero Gomez, M., Ferreiro Garcia, R., Romero Gomez, J., Carbia Carril, J., 2014. Review of thermal cycles exploiting the exergy of liquefied natural gas in the regasification process. *Renew. Sustain. Energy Rev.* 38, 781- 795.
- Saeed, M. Z., Widell, K. N., Hafner, A., Nordtvedt, T. S., Svendsen, E. S., 2020. Cryogenic cold utilization and system integration possibilities for LNG-driven fishing vessels. 6th IIR conference on sustainability and the cold chain. Nantes, France. *ICCC/IIR*, 35-42.
- Sung, T., Kim, K.C., 2016. Thermodynamic analysis of a novel dual-loop organic Rankine cycle for engine waste heat and LNG cold. *Appl. Therm. Eng.* 100, 1031-1041.
- Tan, H., Li, Y., Tuo, H., Zhou, M., Tian, B., 2010. Experimental study on liquid/solid phase change for cold energy storage of Liquefied Natural Gas (LNG) refrigerated vehicle, *Energy*, 35, 1927-1935.
- Wärtsilä, 2021. Wärtsilä 20 DF, Wärtsilä 50 DF, Wärtsilä 46 DF. <https://www.wartsila.com/marine/build/engines-and-generating-sets/dual-fuel-engines>
- Zhang, Q., Luo, Z., Zhao, Y., Pavel, S., 2021. Thermodynamic analysis and multi-objective optimization of a transcritical CO₂ waste heat recovery system for cruise ship application. *Energy conversion and management* 227, 113612.

Conference paper 2

M.Z. Saeed, A. Hafner, A. Thatte, C.H. Gabriellii. Simultaneous implementation of rotary pressure exchanger and ejectors for CO₂ refrigeration system. 15th IIR-Gustav Lorentzen Conference on Natural Refrigerants. Proceedings. Trondheim, Norway, June 13-15th 2022. <http://dx.doi.org/10.18462/iir.gl2022.0130>

Simultaneous implementation of rotary pressure exchanger and ejectors for CO₂ refrigeration system

Muhammad Zahid SAEED^(a), Armin HAFNER^(a), Azam THATTE^(b), Cecilia H. GABRIELII^(c)

^(a)Norwegian University of Science and Technology
Trondheim, 7491, Norway, muhammad.z.saeed@ntnu.no

^(b)Energy Recovery
San Leandro, 94577, USA, Athatte@energyrecovery.com

^(c)SINTEF Energy Research
Trondheim, 7491, Norway, cecilia.gabrielii@sintef.no

ABSTRACT

Natural refrigerant CO₂ has become a viable choice for refrigeration units. The CO₂ systems are working efficiently on land-based facilities, and their demand is increasing for offshore applications, e.g., cruise ships and fishing vessels, due to their environment-friendly nature and compactness. The investigated application of the CO₂ system in this work is a single-stage system for air conditioning and a two-stage system for provision refrigeration at high heat rejection temperatures. The CO₂ transcritical cycle allows operating in higher ambient temperatures and in a colder climate with significant heat recovery. However, the system efficiency decreases in higher ambient conditions due to the high-pressure ratio and expansion losses. Therefore, ejectors are implemented to boost the cycle efficiency at high heat rejection temperature conditions. The pressure exchanger (PX) device recently came up and claimed to be an option to recover expansion work in CO₂ systems. PX is already in use for reverse osmosis (RO) desalination units to recover pressure work from the high pressure reject concentrate to low-pressure seawater. This work theoretically investigates the implementation of a CO₂-PX for transcritical CO₂ systems combined with ejectors and compressors. The energy efficiency of alternative system configurations is evaluated for various operating conditions.

Keywords: Refrigeration, Carbon Dioxide, Transcritical, Pressure Exchanger, Ejector, Energy Efficiency.

1. INTRODUCTION

High GWP (Global Warming Potential) refrigerants are prohibited under different international and national regulations. As a result, instead of searching for new synthetic refrigerants, there has been a surge of interest in natural working fluids, such as hydrocarbons, water, carbon dioxide (CO₂), and ammonia. CO₂ has been used as a working fluid in the past, but the low critical point made operation difficult, particularly in hot climates. Lorentzen et al. (1994) reconsider CO₂ in a transcritical mode as a possible alternative refrigerant to combat global warming and ozone depletion. Today, such systems operate successfully in a transcritical mode.

However, a transcritical operation's heat absorption and rejection sides have a high-pressure difference. In addition, a traditional vapor compression cycle results in a significant energy loss in the expansion valve. As a result, there is a lot of interest in adopting alternate expansion devices to make a CO₂ system's Coefficient of Performance (COP) comparable with systems employing standard fluorinated working fluids.

The simple transcritical cycle can be improved by reducing the throttling losses of the transcritical CO₂ cycle (Elatar et al., 2021). Because of the characteristics of CO₂, one viable alternative is to recover the expansion work directly using an expansion machine. The COP may increase between 14% to 17% (Groll et al., 2007) by employing an expansion turbine. Another renowned way to improve CO₂ cycle efficiency is by ejectors. Both theoretically and empirically, the benefit of utilizing ejectors in transcritical CO₂ refrigeration systems has

been verified. According to several simulation assessments, the COP of the ejector expansion transcritical CO₂ cycle can be about 20% greater than that of a basic transcritical cycle (Zhu et al., 2017).

This work investigates a new work recovery device for CO₂ systems, a pressure exchanger (PX). A pressure exchanger is made up of a cylindrical rotor with a series of channels positioned around the rotor's axis. The rotor rotates between two fixed end plates with ports for directing fluid flow into and out of the rotor channels on either side. The channel ends are regularly exposed to varying port pressures as the rotor rotates, causing compression and expansion inside the rotor channels. As a result, the pressure of a high-pressure stream can be transferred to a low-pressure stream, boosting the low-pressure stream's pressure while lowering that of the high-pressure stream (Fricke et al., 2019, Energy Recovery, 2017). The detailed working principle of pressure exchangers is explained in Thatte (2018) and Thatte (2019). The internal mechanism of the device is shown in Figure 1.

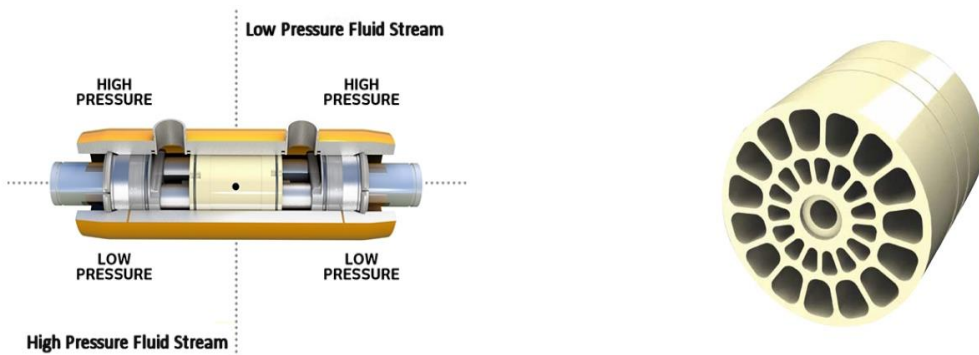


Figure 1: Cut section of PX and rotor (Fricke et al., 2019, Thatte 2018, Thatte 2019).

Figure 2 shows the four ports of the PX. High-pressure CO₂ enters from the top left port and, after decrementing in pressure, goes through the bottom-left port. The flash gas from the phase separator enters from the bottom right port and, after gaining pressure, leaves through the top right port. This work theoretically investigates different layouts for CO₂ systems to implement PX, including ejectors, and this will be verified experimentally in further work.

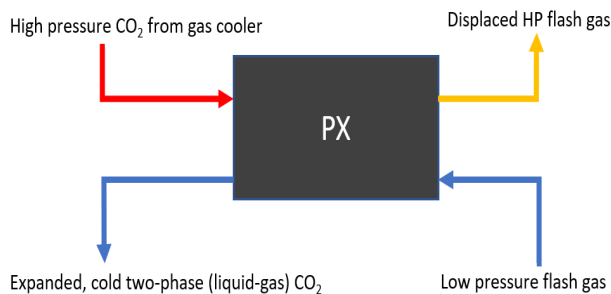


Figure 2: Two inlets and outlets of PX

2. METHODS AND DATA

The PX device can be implemented in the single-stage and two-stage refrigeration system, and the application can be an offshore or onshore installation. These two different layouts are analysed (Figure 4 and Figure 5). Figure 4 is a single-stage system producing chilled water at 5 °C for air conditioning purpose. Figure 5 shows

a typical refrigeration system for supermarket/onboard provision with LT evaporator at -25 °C and MT evaporator 0 °C. The focus of this work is on PX and how it can best integrate into the proposed layouts. The flash gas from the phase separator needs a pressure boost before entering the PX. For this purpose, an ejector is used to lift the pressure of flash gas, and then the PX further increases the pressure. A second ejector is implemented to further boost the flash gas pressure at the PX outlet to the gas cooler pressure. The efficiencies for both ejectors were fixed to 30%. The PX's mass boost ratio can be calculated using Eq. 1 and Eq. 2. For calculation purposes, some simplifications were made, shown in Eq. 3 and Eq. 4. The entropy generation can be calculated using Eq. 6.

$$m_{BR} = \frac{\rho_{LP_{in}}}{\rho_{HP_{in}}} \quad \text{Eq. (1)}$$

$$m_{BR} = \frac{m_{LP_{in}}}{m_{HP_{in}}} \quad \text{Eq. (2)}$$

$$m_{LP_{out}} = m_{HP_{in}} \quad \text{Eq. (3)}$$

$$m_{HP_{out}} = m_{LP_{in}} \quad \text{Eq. (4)}$$

$$m_{BR} = \frac{h_{LP_{out}} - h_{HP_{in}}}{h_{LP_{in}} - h_{HP_{out}}} = \frac{h_{HP_{in}} - h_{LP_{out}}}{h_{HP_{out}} - h_{LP_{in}}} \quad \text{Eq. (5)}$$

$$E_g = m_{BR} \cdot (S_{HP_{out}} - S_{LP_{in}}) + (S_{LP_{out}} - S_{HP_{in}}) \cdot m_{HP_{in}} \geq 0 \quad \text{Eq. (6)}$$

Where m is mass flow rate (kg/s), ρ is density (kg/m³), h is enthalpy (kJ/kg), S is entropy (J/kg. K), and E_g is entropy generation (J/kg. K). The calculation models were established on an Engineering equation solver (EES) under various boundary conditions. Using Eq. 1 to Eq. 6, different combinations of compression and expansion efficiencies were found that satisfied the mass boost ratio. The mass boost ratios for both cases are presented in Table 3 and Table 4. Figure 3 shows the efficiency curves of PX for single stage and two stage. Each case is analysed with two temperatures of 33 °C and 35 °C (outlet temperature of gas cooler). Although 100% compression or expansion efficiency is not practically possible, the median efficiencies were used as an input for modelling.

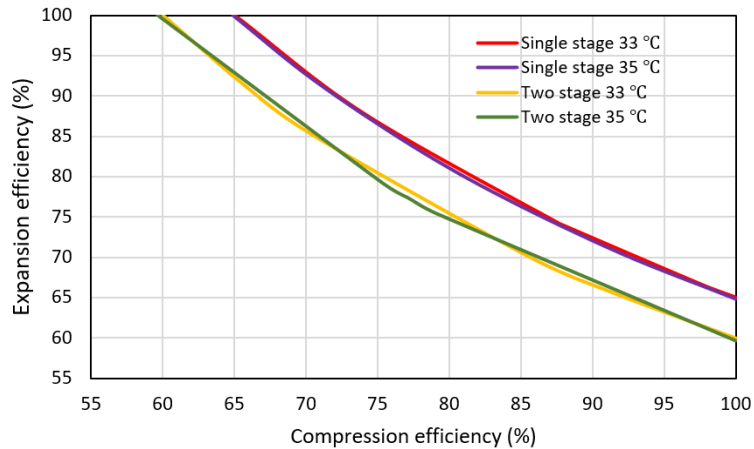


Figure 3: Efficiency curves for different operating conditions

The boundary conditions for the single-stage system with PX is tabulated in Table 1, and the corresponding system layout is shown in Figure 4. The PX system layouts are compared with parallel compression to evaluate the efficiency of the system. Due to system's flow resistance (pressure losses in piping, and a small pressure loss in PX (~ 1 bar) etc.), the high-pressure outlet of the PX is ~ 2 bar lower than the gas cooler pressure. The value of 2 bar is selected based on the discussions with PX manufacturer. To overcome this small pressure loss, an ejector is used in conjunction with PX to boost the PX exit flow by additional 2 bar. Another ejector is implemented between the separator and PX to raise the flash gas pressure by 2 bar. After the gas cooler, the mass flow rate was kept constant in all cases, but two different temperatures were investigated. The temperature range will extend in further work. A suction gas heat exchanger is used to superheat the refrigerant gas by 5 K coming from the evaporator and by-pass valve. The compressor efficiency was kept constant.

Table 1. Boundary conditions for the single stage system

Parameters	Single stage (33 °C)	Parallel compression (33 °C)	Single stage (35 °C)	Parallel compression (35 °C)
Compressor outlet (bar)	86	84	91	89
Gas cooler pressure (bar)	84	84	89	89
Mass flow gas cooler (kg/s)	0.5	0.5	0.5	0.5
Liquid receiver pressure (bar)	55	55	55	55
Gas cooler outlet temperature (°C)	33	33	35	35
Compressor efficiency (%)	70	70	70	70
PX compression efficiency (%)	74.14	-	77.44	-
PX expansion efficiency (%)	87.7	-	83.78	-

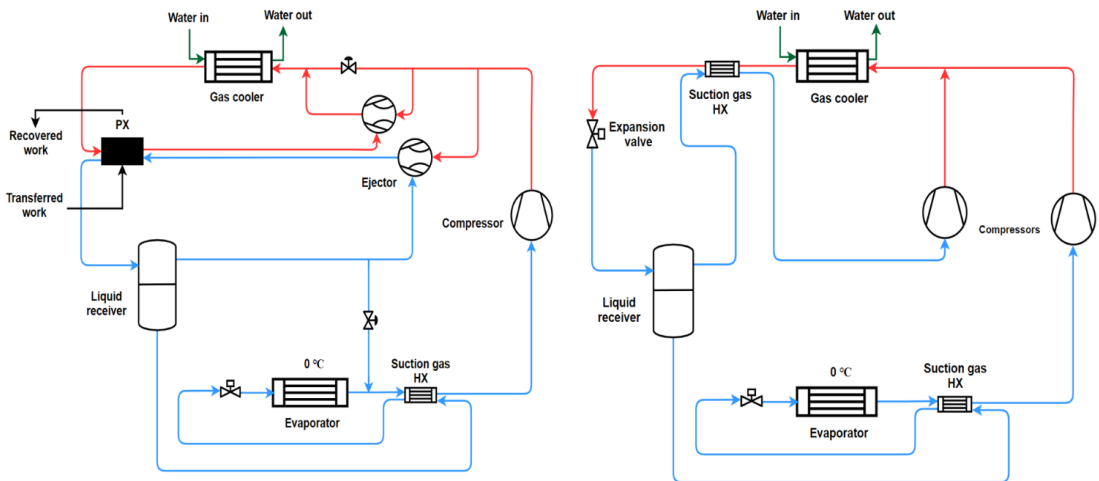


Figure 4: System layouts for single stage modelling, PX integration (left), Parallel compression (right)

The optimal (max COP) gas cooler pressure with their corresponding temperature was used in the models. The optimal pressure was also followed for the flash tank pressure. In the two-stage model, the flash tank

pressure is 5 bar lower than in the single-stage system. The by-pass valve is also implemented in both layouts to ensure the removal of remaining gas that cannot handle by PX or ejector. The two-stage system layout with PX and ejectors is shown in Figure 5. All the parameters that were used for the two-stage modelling purpose are tabulated in Table 2.

Table 2. Boundary conditions for the two-stage system

Parameters	Two stage (33 °C)	Parallel compression (33 °C)	Two stage (35 °C)	Parallel compression (35 °C)
Compressor outlet (bar)	86	84	91	89
Gas cooler pressure (bar)	84	84	89	89
Mass flow gas cooler (kg/s)	0.5	0.5	0.5	0.5
Liquid receiver pressure (bar)	50	50	50	50
Gas cooler outlet temperature (°C)	33	33	35	35
Compressor efficiency (%)	70	70	70	70
PX compression efficiency (%)	70.41	-	75.42	-
PX expansion efficiency (%)	85.21	-	79.09	-

The refrigerant gas from the LT evaporator was superheated by 5 K, by exchanging heat in the liquid receiver. The refrigerant flow from the liquid line of the receiver is equally divided between the LT and MT evaporator. The LT compressor lifts the pressure to 34.85 bar, which is the same pressure as for the MT evaporator. The MT compressor lifts the gas from LT evaporator, by-pass valve, and MT evaporator to the designed outlet pressure of the MT compressor.

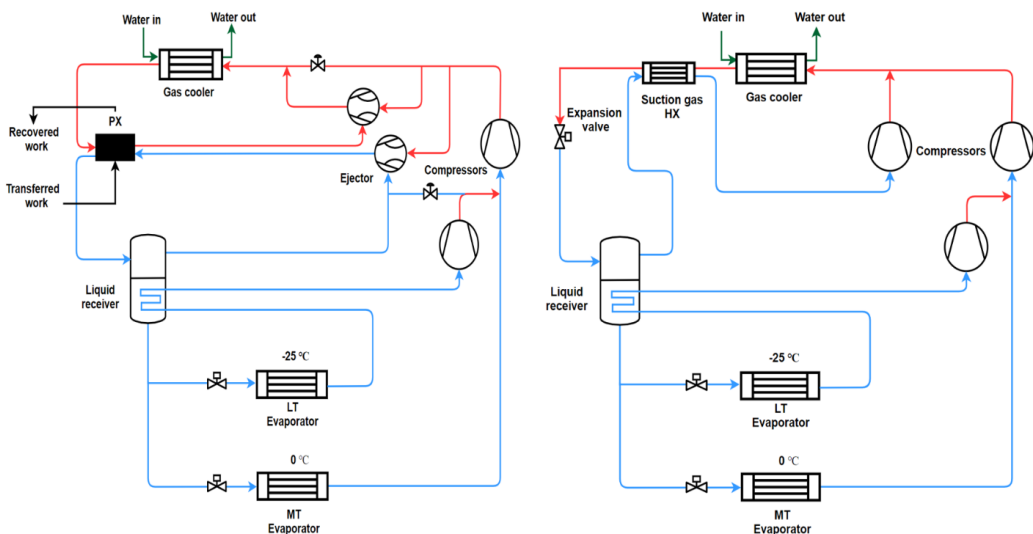


Figure 5: System layouts for two stage modelling, PX integration (left), Parallel compression (right)

3. RESULTS AND DISCUSSIONS

Figure 6 shows the COP analysis of the single-stage system. The comparison of different system layouts indicates that COP of the PX system is 6% higher compared to parallel compression with 33 °C gas cooler outlet temperature. The COP difference increased to 7.5% when the gas cooler outlet temperature was 35 °C.

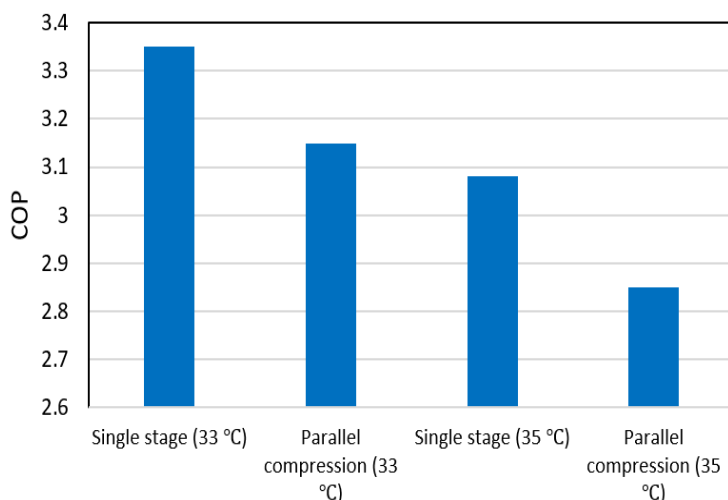


Figure 6: COP comparison between single-stage PX layout and parallel compression

The remaining modelling results for the single-stage system is presented in Table 3. The evaporation capacity in the PX case is higher than in the parallel compression case due to the less vapor fraction in the liquid receiver. An average 4.9% higher evaporation capacity was achieved in both PX cases. The recovered work from the PX expansion equals 10.4% of the compression work, but it is not enough to completely remove the flash gas. As a result, 15.5% of the flash gas is by-passed in the 33 °C case and 19.7% in 35 °C case.

Table 3. Modelling results for the single-stage system

Parameters	Single stage (33 °C)	Parallel compression (33 °C)	Single stage (35 °C)	Parallel compression (35 °C)
Evaporator load (kW)	70.93	67.77	68.85	65.11
Compression work (kW)	21.15	18.77	22.37	19.36
Parallel compressor (kW)	-	2.752	-	3.465
PX expansion (kW)	2.208	-	2.508	-
PX expansion theoretical (kW)	2.517	-	2.993	-
PX compression (kW)	2.205	-	2.504	-
Vapor quality	0.257	0.284	0.282	0.313
Mass boost ratio	0.258	-	0.263	-
Flash gas by-pass (%)	15.5	-	19.7	-

Figure 7 shows the COP results of the two-stage system. In these scenarios, the COP of the PX system (33 °C) case is 14.2% higher than the parallel compression under similar conditions. The COP takes further lead to 16.5% in the 35 °C case. The increase in COP is mainly due to the removal of flash gas by the free expansion work of PX.

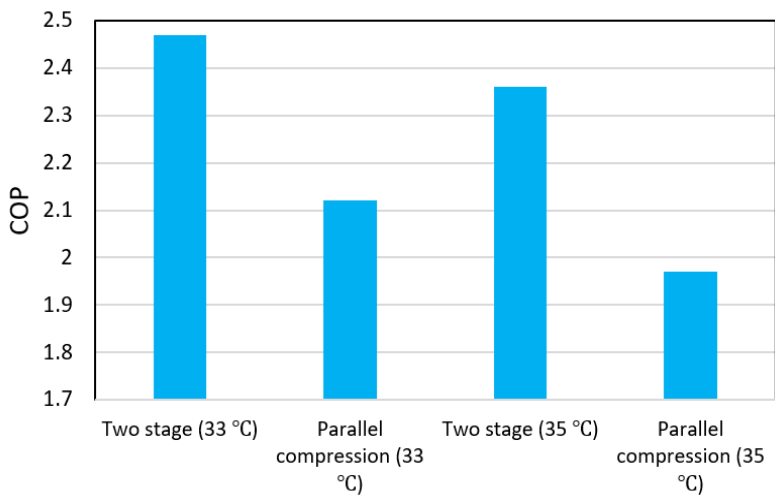


Figure 7: COP comparison between two stage PX layout and parallel compression

The modelling results for the two-stage system is presented in Table 4. In addition to the increased COP, the average evaporation capacity of both cases with PX is 4.4% higher than the parallel compression. The average vapor fraction difference between PX and parallel compression cases is 9.2%. The expansion follows the entropy lines in the PX cases, resulting in less vapor fraction than the isenthalpic process. The recovered work from the PX expansion equals 9.3% of the total compression work.

The results of this modelling work depend on the compression and expansion efficiency of the PX device. In further work, the experiments will be performed according to the system layouts highlighted in this work, which will act as a benchmark for extended applications of PX.

Table 4. Modelling results for the two-stage system

Parameters	Two stage (33 °C)	Parallel compression (33 °C)	Two stage (35 °C)	Parallel compression (35 °C)
Evaporator load LT (kW)	35.64	34.2	34.55	32.93
Evaporator load MT (kW)	34.56	33.16	33.5	31.92
Compression LT (kW)	7.91	7.59	7.667	7.307
Compression MT (kW)	20.42	20.08	21.13	20.75
Parallel compressor (kW)	-	4.068	-	4.911
PX expansion (kW)	2.68	-	2.884	-
PX expansion theoretical (kW)	3.146	-	3.646	-
PX compression (kW)	2.679	-	2.883	-
Vapor quality	0.2934	0.3232	0.3163	0.3484
Mass boost ratio	0.2243	-	0.2283	-
Flash gas by-pass (%)	34.4	-	37.1	-

4. CONCLUSION

In this work, thermodynamic analysis has been performed to investigate the integration of a pressure exchanger device into the CO₂ transcritical refrigeration system. The numerical models were established on Engineering Equation Solver to evaluate the potential of PX to enhance the energy efficiency of the CO₂ system. Two different layouts were investigated, including PX and ejectors: a single stage, and a two-stage system. Comparison of the systems was made with a system based on parallel compression. The refrigerant flow was constant after the gas cooler in all cases, but two temperatures, 33 °C and 35 °C, were analyzed. Results for the single-stage system show that COP could improve by 6% to 7.5% under investigated conditions. In addition, the evaporation capacity was 4.9 % higher than the parallel compression case. The investigation of the two-stage system shows that COP could improve by 14 % to 16.5 % and with an increased evaporation capacity of 4.4%. In further work, experiments will be performed with the proposed layouts to verify the efficiency of PX.

ACKNOWLEDGEMENTS

The authors gratefully acknowledge the Research Council of Norway for the financial support for carrying out the present research [NFR Project No. 308779 CruIZE] and Energy Recovery for technical support.

NOMENCLATURE

<i>LP</i>	Low pressure	<i>PX</i>	Pressure exchanger
<i>HP</i>	High pressure	<i>h</i>	Enthalpy (KJ/kg)
<i>E_g</i>	Entropy generation (J/kg. K)	<i>S</i>	Entropy (J/kg. K)
<i>BR</i>	Boost ratio	<i>in</i>	Inlet
<i>out</i>	Outlet	<i>LT</i>	Low temperature
<i>MT</i>	Medium temperature		

REFERENCES

- Elatar, A., Fricke, B., Sharma, V., Nawaz, K., 2021. Pressure Exchanger for Energy Recovery in a Trans-Critical CO₂ Refrigeration System. *Energies* 14, 1754.
- Energy Recovery. 2017. <http://www.energyrecovery.com> Energy Recovery, Inc., San Leandro, California.
- Fricke, B. A., Nawaz, K., Elatar, A., Sharma, V., 2019. Increasing the efficiency of a carbon dioxide refrigeration system using a pressure exchanger. 25th IIR international congress of refrigeration. Montreal, Canada. ICR/IIR, 1775-1781.
- Groll, E., Kim, J.-H., 2007. Review Article: Review of Recent Advances toward Transcritical CO₂ Cycle Technology. *HVAC&R Research* 13, 499–520.
- Lorentzen, G., 1994. The use of natural refrigerants: a complete solution to the CFC/HCFC predicament. *International journal of refrigeration*. 18,3, 190-197.
- Thatte A., 2018, "A New Type of Rotary Liquid Piston Pump for Multi-Phase CO₂ Compression", *Proceedings of ASME Turbo Expo 2018*, GT2018-77011.
- Thatte A., 2019, "Transcritical / Supercritical CO₂ Recompression Brayton Cycle using A Novel Rotary Liquid Piston Compressor", *Proceedings of ASME Turbo Expo 2020*, GT2019-91088.
- Zhu, Y., Li, C., Zhang, F., Jiang, P.-X., 2017. Comprehensive experimental study on a transcritical CO₂ ejector-expansion refrigeration system. *Energy Conversion and Management* 151, 98–106.